Simultaneous nitrification, denitrification, and phosphorus removal at low temperatures

by

Xuanye Bai

A thesis

presented to the University of Waterloo

in fulfillment of the

thesis requirement for the degree of

Doctor of Philosophy

in

Civil Engineering

Waterloo, Ontario, Canada, 2022

Examining Committee Membership

The following served on the Examining Committee for this thesis. The decision of the Examining Committee is by majority vote.

Supervisor	Dr. Wayne J. Parker Professor
Internal Members	Dr. Peter Huck Professor Dr. Jose Bicudo Adjunct Professor
Internal-external Member	Dr. Trevor Charles Professor
External Examiner	Dr. Sheng Chang Professor

Author's Declaration

This thesis consists of material all of which I authored or co-authored: see Statement of Contributions included in the thesis. This is a true copy of the thesis, including any required final revisions, as accepted by my examiners.

I understand that my thesis may be made electronically available to the public.

Statement of Contributions

Chapter 3 of this thesis consists of a paper that was co-authored by myself, a PhD student, Michelle M. McKnight, a professor, Dr. Josh D. Neufeld, and my supervisor, Dr. Wayne J. Parker. Michelle M. McKnight and Dr. Josh D. Neufeld were responsible for microbial analysis and review the analysis results from me. I conducted the other tasks. This section has been published in Bioresource Technology on April 2022 with the title of "Nitrogen removal pathways during simultaneous nitrification, denitrification, and phosphorus removal under low temperature and dissolved oxygen conditions".

Chapter 4 of this thesis was co-authored by myself, a PhD student, Michelle M. McKnight, a professor, Dr. Josh D. Neufeld, and my supervisor, Dr. Wayne J. Parker. Michelle M. McKnight and Dr. Josh D. Neufeld were responsible for microbial analysis and review the analysis results from me. I conducted the other tasks. This chapter will be submitted to Bioresource Technology later.

Chapter 5 of this thesis was co-authored by myself, Ferenc Hazi, Dr. Imre Takacs, Dr. Tanush Wadhawan, and my supervisor, Dr. Wayne J. Parker. Ferenc Hazi, Dr. Imre Takacs, and Dr. Tanush Wadhawan were responsible to develop the floc model in Sumo. I conducted the other tasks. This chapter will be submitted to a journal later.

Abstract

Simultaneous nitrification, denitrification, and phosphorus removal (SNDPR) has been demonstrated to be a promising technology for carbon, nitrogen, and phosphorus removal. However, SNDPR has not been fully studied at low temperatures. This study was the first to investigate the performance of SNDPR at 10℃ to treat a complex synthetic wastewater and real municipal wastewater. A comprehensive floc model was developed, calibrated, and validated to quantitatively understand the transformation of carbon, nitrogen, and phosphorus in the SNDPR system at 10 ℃.

Nitrogen removal pathways of SNDPR at low dissolved oxygen (0.3 mg/L) and temperature (10℃) were explored to understand nitrogen removal mechanisms. Biological nitrogen and phosphorus removal were sustained with total inorganic nitrogen removal, phosphorus removal, and simultaneous nitrification and denitrification (SND) efficiencies of 62.6%, 97%, and 31%, respectively. The SND was observed in the first 2 h of the aerobic phase and was attributed to denitrifying ordinary heterotrophic organisms (OHOs) using readily biodegradable chemical oxygen demand and denitrifying phosphorus accumulating organisms (DPAOs), which removed 15% and 12% of influent nitrogen, respectively. A phosphorus accumulating organism (PAO)-rich community was indicated by stoichiometric ratios and supported by 16S rRNA gene analysis, with *Dechloromonas*, *Zoogloea*, and *Paracoccus* as DPAOs, and *Ca.* Accumulibacter and *Tetrasphaera* as PAOs. Even though *Ca.* Competibacter (10.4%) was detected, limited denitrifying glycogen accumulating organism (DGAO) denitrification was observed, which might be due to low temperatures. This research was the few researches that investigated the SNDPR process at 10℃ by using a complex synthetic wastewater, investigated the nitrogen removal pathways in the aerobic phase using an experimental method, and integrated microbial community analysis with experimental findings.

The feasibility of SNDPR at a low temperature (10℃) when treating real municipal wastewater was explored by implementing two process configurations (anaerobic/aerobic (AO) and anaerobic/aerobic/anoxic (AOA)). It was found that SNDPR in the AO configuration failed, however,

SNDPR in the AOA configuration was achieved with total nitrogen removal, phosphorus removal, and SND efficiencies of 91.1%, 92.4%, and 28.5%, respectively. The main nitrogen removal pathways were denitrification by DPAOs in the aerobic phase and denitrifying OHOs using hydrolyzed carbon in the anoxic phase, which accounted for 16% and 56% of influent nitrogen, respectively. A PAO-rich system was indicated by stoichiometric ratios and supported by 16S rRNA gene analysis, with *Dechloromonas* and *Ca.* Accumulibacter as dominant DPAOs and PAOs. *Ca.* Competibacter was detected, whereas limited denitrifying GAO denitrification was observed, which might be due to low temperatures. This research was the first to 1) investigate the performance of SNDPR when real municipal wastewater was treated under low temperature conditions (10℃); 2) investigate whether operational conditions that have been successfully employed to treat synthetic wastewaters can also be applied to real municipal wastewaters; 3) compare the performance of SNDPR when operated in different process configurations (AO and AOA).

A comprehensive floc model was designed to investigate SNDPR at 10℃. Results show that only boundary layer thickness in the floc-related parameters established a minor impact on nitrite, and seven new incorporated parameters ($f_{P,VFA}$, $f_{PP,PHA,ox}$, and intrinsic half-saturation coefficients of oxygen of ammonia oxidizing bacteria (AOB), nitrite oxidizing bacteria (NOB), OHOs, PAOs, and GAOs) were deemed as sensitive parameters. The model calibration and validation were demonstrated successful based on R^2, mean square relative error, and residual analysis. After model validation, intrinsic K_O values of AOB, NOB, OHOs, PAOs, and GAOs were estimated to be 0.08, 0.18, 0.03, 0.1, and 0.07 mg/L, respectively. Based on model analysis, 87% of volatile fatty acids were stored by PAOs and GAOs, leading to successful PO_4-P uptake through PAO aerobic growth (85%) and PAO denitrification via nitrite (12%). In the aerobic phase, 93% and 5% of consumed readily biodegradable chemical oxygen demand were used for OHO aerobic growth and OHO denitrification via nitrite, respectively. Regarding to SND, nitrite was the dominant electron acceptor for denitrification by PAOs (75%) and OHOs (25%), indicating NO_2-N was easier to be used by PAOs and OHOs for denitrification than by NOB for nitrification. This study was the first to design a comprehensive floc model that incorporated PAOs and GAOs, intrinsic half-saturation coefficients of

each microorganism, external mass transfer terms, internal diffusion, and intra-floc movement, to simulate SNDPR. A set of intrinsic half-saturation coefficients of oxygen of each microorganism was estimated for the first time.

Acknowledgements

During the period of my PhD, there were many obstacles, but my heart was full of love with the help from the people surrounding me. I was touched by the selfless help from my supervisor, the technical support from collaborators, the help from lab technicians, the emotional support from friends, and of course, the selfless love from my family. It is because of your presence I can finish this degree strongly.

To my supervisor, Dr. Wayne Parker, I am extremely grateful to be your student. With your guidance, I have learned how to approach a research question, critical thinking, how to organize and present a paper, how to conduct a presentation, etc. These are the key skills for a qualified researcher. I appreciate your encouragement, your professional advice, and your tireless effort in editing my thesis. Without your guidance, I can not finish this degree.

To the committee, I would like to thank Dr. Peter Huck, Dr. Jose Bicudo, Dr. Trevor Charles, and Dr. Sheng Chang for your time to review my thesis and provide valuable feedback. Your contributions make my thesis more informative and complete.

To the collaborators, I would like to thank Dr. Josh D. Neufeld, Michelle McKnight, Dr. Imre Takacs, Ferenc Hazi, Dr. Tanush Wadhawan for their contributions during the research. Dr. Josh D. Neufeld and Michelle McKnight are the co-authors of the Chapters 3 and 4. Their contributions on microbial community analysis make the discussion sounder and more comprehensive. Dr. Imre Takacs, Ferenc Hazi, and Dr. Tanush Wadhawan provided more insights in design the floc model. Thank you for your critical thinking and technical support.

To lab technicians, I would like to thank Mark Merlau, Mark Sobon, Peter Volcic, Shirley Chatten, and Marianne Vandergriendt for their help with experimental setup, quick response to equipment failure, and sample testing. I also would like to thank Jane Russwurm from writing center for her friendship and writing support. I am grateful to them who facilitate my study.

To friends, I appreciate the friendship from my friends in China, Canada, and Maylasia. It is because of your company that I do not feel lonely. It is also your support that helps me through the dark period and comes to the finish line. May our friendship endure!

To my beloved family, your love, patient, company, understanding, and financial support are essential for me during the journey. It is not easy for me, but it is even harder for you. Wish you all healthy and joyful every day!

Finally, I would like to thank myself for not giving up during the dark time, hardworking, and focusing. I wish in the future I can use the research skills I learned to develop cutting-edge technologies to promote the progress of society.

Table of Contents

List of Figures

List of Tables

Nomenclature

AO: anaerobic/aerobic

AOA: anaerobic/aerobic/anoxic

AOB: ammonia oxidizing bacteria

AS: activated sludge

ASMs: activated sludge models

BNPR: biological nitrogen and phosphorus removal

C/N: carbon to nitrogen

CV: coefficients of variation

DGAOs: denitrifying glycogen accumulating organisms

DO: dissolved oxygen

DOHOs: denitrifying ordinary heterotrophic organisms

DPAOs: denitrifying phosphorus accumulating organisms

EBPR: enhanced biological phosphorus removal

FAPROTAX: functional annotation of prokaryotic taxa

HRT: hydraulic retention time

IWA: international Water Association

MDL: method detection limit

MLSS: mixed liquor suspended solids

MLVSS: mixed liquor volatile suspended solids

MSRE: mean square relative error

NOB: nitrite oxidizing bacteria

OHOs: ordinary heterotrophic organisms

PAOs: phosphorus accumulating organisms

PH2MV: poly-β-hydroxy-2-methylvalerate

PHA: poly-β-hydroxyalkanoate

PHB: poly-β-hydroxybutyrate

PHV: poly-β-hydroxyvalerate

rbCOD: readily biodegradable chemical oxygen demand

SBR: sequencing batch reactor

sCOD: soluble COD

SCRR: specific sCOD reduction rate

SNDPR: simultaneous nitrification, denitrification, and phosphorus removal

SNRR: specific nitrate removal rate

SPRR: specific phosphorus removal/release rate

STINRR: specific total inorganic nitrogen removal rate

sTKN: soluble total Kjeldahl nitrogen

sTN: soluble total nitrogen

TIN: total inorganic nitrogen

TN: total nitrogen

TP: total phosphorus

VFAs: volatile fatty acids

WWTPs: wastewater treatment plants

Chapter 1 Introduction

1.1. Problem statement

Modern wastewater treatment plants (WWTPs) are designed to reduce organic carbon, nitrogen, and phosphorus discharges to the environment (Conley et al., 2009). Historically this has been achieved with conventional biological nitrogen and phosphorus removal (BNPR) processes. In conventional processes ammonia (NH_4^+) is fully oxidized to nitrate (NO_3^-) in an aerobic tank, and nitrate is denitrified to nitrogen gas (N_2) in an anoxic tank when biodegradable organic matter is available. In conventional biological phosphorus removal, phosphorus is released in the anaerobic stage and phosphorus uptake takes place in the subsequent aerobic stage by phosphorus accumulating organisms (PAOs). The difference between the phosphorus release and uptake amounts represents the amount of total phosphorus removed.

In conventional BNPR energy consumption can be significant. A high amount of energy is consumed by the aeration system for both nitrification and phosphorus uptake. The latter can account for 40%-60% of the total energy cost of WWTPs (Barnard & Meiring, 1988). Processes with low energy requirements have been developed in recent years. Simultaneous nitrification, denitrification, and phosphorus removal (SNDPR) has been proposed as an alternative to conventional BNPR. Many studies have shown that full-scale WWTPs have implemented SNDPR with different configurations including sequencing batch reactor (SBR) (Jia et al., 2016), anoxic/oxic-membrane bioreactor (MBR), University of Cape Town-MBR (UCT-MBR) (Sarioglu et al., 2017), step-feed UCT (Ge et al., 2013), and anoxic-oxic biofilter (Tian et al., 2017a) flowsheets. Given that, SNDPR has been proved to be a feasible and promising process to remove nitrogen and phosphorus at a low cost.

The reported benefits of the SNDPR process over conventional BNPR processes include (Abeling & Seyfried, 1993; do Canto et al., 2008; Jia et al., 2016; Li et al., 2008; Sun et al., 2010):

1. 33-45% of aeration reduction is achieved by suppressing nitrite oxidizing bacteria (NOB) (Dotro et al., 2011).
2. 22-40% less organic matter is required since denitrification in SNDPR is from nitrite instead of nitrate, which means that a low carbon to nitrogen (C/N) ratio wastewater can be treated by the SNDPR process without adding external carbon, therefore saving the operational costs.
3. Less sludge processing costs are required since SNDPR can reduce 30% of sludge production compared to conventional BNPR.
4. Less alkalinity is required in SNDPR since nitrification and denitrification can take place in a single tank instead of two or more that are required for conventional nitrogen removal.
5. The SNDPR process can reduce capital costs since denitrification can happen in the aerobic tank with low DO concentrations, eliminating/reducing the need of the anoxic tank.
6. Influent carbon can be more efficiently used to remove both nitrogen and phosphorus, especially in carbon-limited wastewater.
7. More nitrogen can be removed through SNDPR under low DO conditions, which is conducted by denitrifying ordinary heterotrophic organisms (DOHOs), denitrifying phosphorus accumulating organisms (DPAOs), and denitrifying glycogen accumulating organisms (DGAOs) using organic carbon and intracellular carbon (PHA).

Even though SNDPR has been employed in a number of full-scale projects, it still has several associated challenges. At low temperatures, all the biological reaction rates are reduced, especially the hydrolysis and fermentation rates, which might cause the deterioration of nitrogen and phosphorus removal due to lack of available carbon (Henze et al., 2000). Long sludge retention time (SRT) and aerobic hydraulic retention time (HRT) are required for SNDPR when compared to conventional BNPR systems since the nitrification rate in SNDPR is low due to low DO concentrations, especially at low temperatures (Li & Irvin, 2007). At low temperatures, optimization of SNDPR is challenging since various classes of functional bacteria with different optimal growth environments must function in a limited number of zones (Paredes et al., 2007).

Therefore, this study focuses on developing an improved understanding of SNDPR at low temperatures such that operation and design can optimally address these challenges.

Wastewater characteristics can significantly impact on the performance of SNDPR at low temperatures. Many studies have achieved SNDPR when treating simple synthetic wastewater with acetic acid as the carbon source (Li et al., 2019; Salehi et al., 2019). However, limited studies have employed carbon sources that require hydrolysis and fermentation in the treatment although at low temperatures hydrolysis and fermentation might be the rate-limiting processes in SNDPR (Yuan et al., 2011). When complex wastewater that includes readily biodegradable chemical oxygen demand (rbCOD) and soluble organic nitrogen, rbCOD is treated, organic matter needs to be fermented to volatile fatty acids (VFAs) to be used for biological phosphorus removal, and soluble organic nitrogen will be hydrolyzed to ammonia prior to removal. Therefore, there is a need to study the treatment of complex wastewaters by SNDPR at low temperatures (around 10°C) to elucidate performance limiting processes.

The composition difference between synthetic wastewaters and real municipal wastewaters may cause different SNDPR performance under the same operational conditions. Compared with synthetic wastewaters that do not account for unbiodegradable and particulate fractions, real municipal wastewaters have a lower biodegradable carbon fraction, which could make SNDPR unfeasible (He et al., 2016; Zaman et al., 2021). The lack of particulate biodegradable COD and particulate unbiodegradable COD in synthetic wastewaters reduces the need for hydrolysis and reduces the presence of particulate unbiodegradable COD in the sludge, which can alter the sludge composition (Melcer, 2004). Therefore, there is a need to study whether the operational conditions employed to treat synthetic wastewaters to achieve SNDPR can also be used for real municipal wastewater at low temperatures.

The microbial community in SNDPR processes has been found to be complex and includes OHOs, ammonia oxidizing bacteria (AOB), NOB, PAOs, DPAOs, GAOs, and DGAOs (Wang et al., 2015). Such complexity is caused by the multiple carbon, nitrogen, and phosphorus conversions that occur in different

redox zones. Several studies have illustrated the microbial community in SNDPR systems at room temperatures (Chen et al., 2020; Wang et al., 2015). However, limited studies have studied the microbial community in SNDPR at low temperatures. In addition, the temperature dependencies of each bacteria are different, leading to different microbial ecology at different temperatures (Henze et al., 2000). Therefore, there is a need to understand of the microbial community in the SNDPR system to help understand and improve the performance of SNDPR at low temperatures.

Simulation is a widely used method to study biological processes and extend the information for design purposes. The activated sludge models (ASMs) developed by the International Water Association (IWA) have been widely used to study traditional BNPR processes, however, traditional ASMs can not accurately simulate SNDPR since the half-saturation coefficients in ASMs are extant values that do not describe systems where diffusion limitations are present. Several studies have developed floc models that include intrinsic half-saturation coefficients and molecular diffusion terms to simulate diffusion-limiting processes (Pochana et al., 1999; Wang et al., 2007). However, the assumptions in these floc models are too simple to reflect SNDPR. For example, the assumptions of the absence of the external boundary layer, uniform distribution of microbes, and limited movement of solids within a floc make it challenging to reflect SNDPR conditions. Ignoring the boundary layer can result in lack of consideration of low mixing intensity, which might occur in SNDPR systems (Nogueira et al., 2015). The assumption of uniform distribution of microbes is unrealistic due to different redox conditions within flocs under low dissolved oxygen (DO) conditions (Baeten et al., 2019). The assumption of limited movement of solids within flocs is also inaccurate since inert components can accumulate in the inner of flocs, conflicting with the observations in SNDPR systems (Baeten et al., 2019). In addition, prior floc models did not incorporate phosphorus removal processes. Therefore, there is a need to develop a comprehensive floc model that includes these aspects to simulate SNDPR.

1.2. Objectives and scope

The primary objective of this research is to identify SNDPR design and operating conditions that could be employed under low temperature conditions that are typical of Canadian winters. The average temperature of influent wastewater in most WWTPs in Ontario during the winter is around 10°C (Lishman et al., 2006). Therefore, in this study, 10°C was chosen as a representative low temperature.

The research is intended to:

- Assess the performance of SNDPR under low temperature (e.g., 10°C) and DO (e.g., 0.3 mg/L) conditions when treating a complex synthetic wastewater.
- Assess whether the same operational conditions that have been used to treat a complex synthetic wastewater in this study can also be used to treat real municipal wastewater under low temperature (e.g., 10°C) and DO (e.g., 0.3 mg/L) conditions, and the potential operational conditions to achieve SNDPR when treating real municipal wastewater under low temperature (e.g., 10°C) and DO (e.g., 0.3 mg/L) conditions.
- Identify organism groups that are responsible for SNDPR at 10°C when treating a complex wastewater and real municipal wastewater, and critically examine linkages between indicators of microbial activity and microbial community composition.
- Develop a comprehensive floc model that can simulate the SNDPR performance when using the complex synthetic wastewater, and quantitatively assess the nutrient removal pathways in SNDPR by using the floc model.

1.3. Significance

The operational strategies developed can be used to inform wastewater treatment plants regarding how to efficiently and cost-effectively operate in the winter season in Canada. The microbial community results can be used to understand the SNDPR system in order to develop specific control strategies to maintain SNDPR in the winter season. The validated floc model can be used to understand the nutrient removal mechanisms and develop different strategies to improve nutrient removal performance at low DO and temperatures.

1.4. Thesis structure

This thesis is divided into six chapters. Chapter 1 presents an introduction to the problem under investigation and illustrates the main objectives of the research. Chapter 2 provides a literature review on SNDPR, including the mechanisms of SNDPR, the bacteria involved in SNDPR, the impact of temperature and oxygen concentration on SNDPR performance, SNDPR simulation, and prior studies of the application of SNDPR to treat real municipal wastewaters. Chapter 3 describes a study of nitrogen removal pathways during SNDPR under low temperature and dissolved oxygen conditions. Chapter 4 presents the results of a study that addresses the performance of SNDPR when treating municipal wastewater at a low temperature. Chapter 5 presents a comprehensive innovative floc model with explicit external mass transfer terms to simulate SNDPR in activate sludge systems. Chapter 6 sums up the conclusions as well as recommendations for further research.

Chapter 2 Literature review

2.1. SNDPR overview

2.1.1. SNDPR mechanisms

The SNDPR process includes two parallel and connected activities, which are SND and enhanced biological phosphorus removal (EBPR). In this section, detailed descriptions of the mechanisms responsible for SND are illustrated. In brief, depending on oxygen diffusion within sludge flocs, the activated sludge flocs can form two zones — the aerobic zone at the outer layer of the floc and the anoxic zone within the core of the floc, as shown in Figure 2-1 (Sun et al., 2010). In the aerobic zone, nitrifying bacteria such as AOB and NOB use oxygen as an electron acceptor for nitrification. Heterotrophic bacteria also consume oxygen and organic carbon for growth. In the anoxic zone, denitrifying heterotrophic bacteria use NO_2-N or NO_3-N generated from the aerobic zone, and organic carbon diffused from the bulk liquid to achieve denitrification (He et al., 2020a). In addition, denitrification in the anoxic zone can be conducted by DPAOs and DGAOs using intracellular storage (Poly-β-hydroxyalkanoate (PHA) and glycogen) (He et al., 2020a). Hence, fully understanding the SND mechanisms can help with design of sampling campaigns that are intended to assess whether SND is occurring in a reactor.

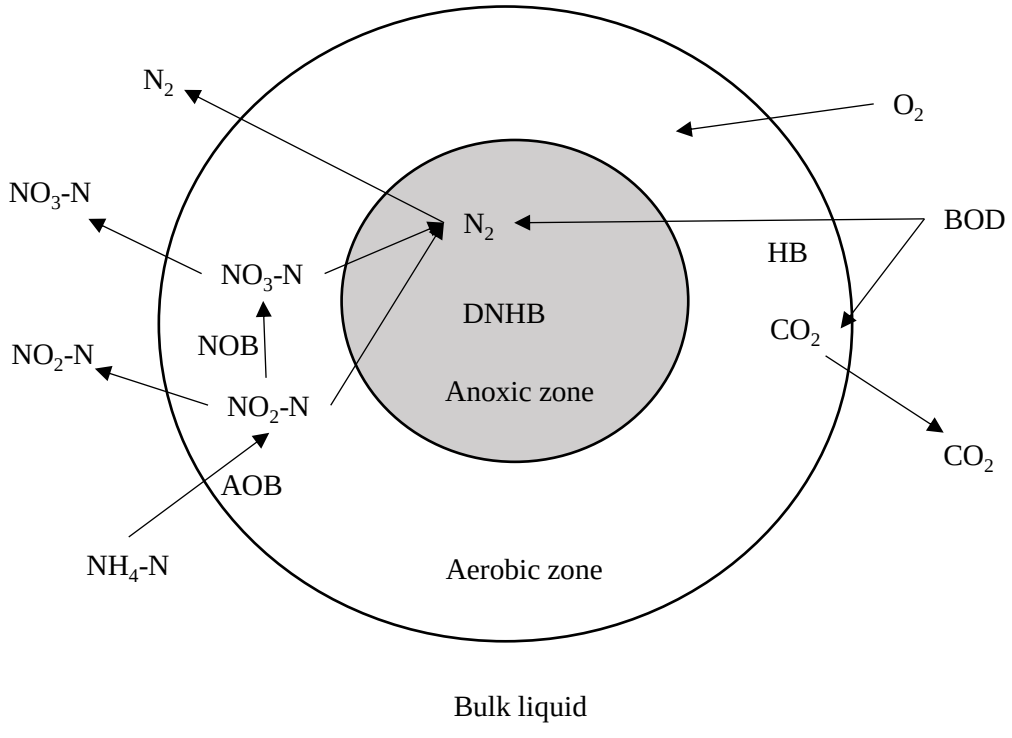

Figure 2-1. Theoretical explanation of simultaneous nitrification and denitrification in an activated sludge floc; Modified from Sun et al. (2010).

The specific processes related to phosphorus removal are illustrated in Figure 2-2. Alternating environmental conditions from anaerobic to aerobic conditions are required to remove phosphorus (Metcalf et al., 2014). In the anaerobic stage, VFAs are generated through fermentation using readily biodegradable substrates, which are hydrolyzed from slowly biodegradable organic carbon. Afterwards, polyphosphate hydrolysis in the PAOs releases both phosphorus and energy. The energy is used to take up VFAs and store them as PHA in the PAOs. In the aerobic stage, energy generated through PHA oxidation is used to take up phosphorus in the bulk and store it as polyphosphate in the PAOs. By understanding the mechanisms of EBPR, it is possible to identify and adjust factors that may cause the failure of EBPR.

In summary, nitrogen and phosphorus removal are achieved based on different types of microbial species and associated metabolisms. Nitrogen removal can be achieved in an aerobic zone with low oxygen concentration, where partial nitrification and denitrification occur. Phosphorus removal is performed

through phosphorus release in the anaerobic zone and phosphorus uptake in the aerobic zone by PAOs. The understanding of these mechanisms was employed to guide the design of SBR operating configurations and dynamic tests that were used to probe the activities in the SBR and which are described in the following chapters.

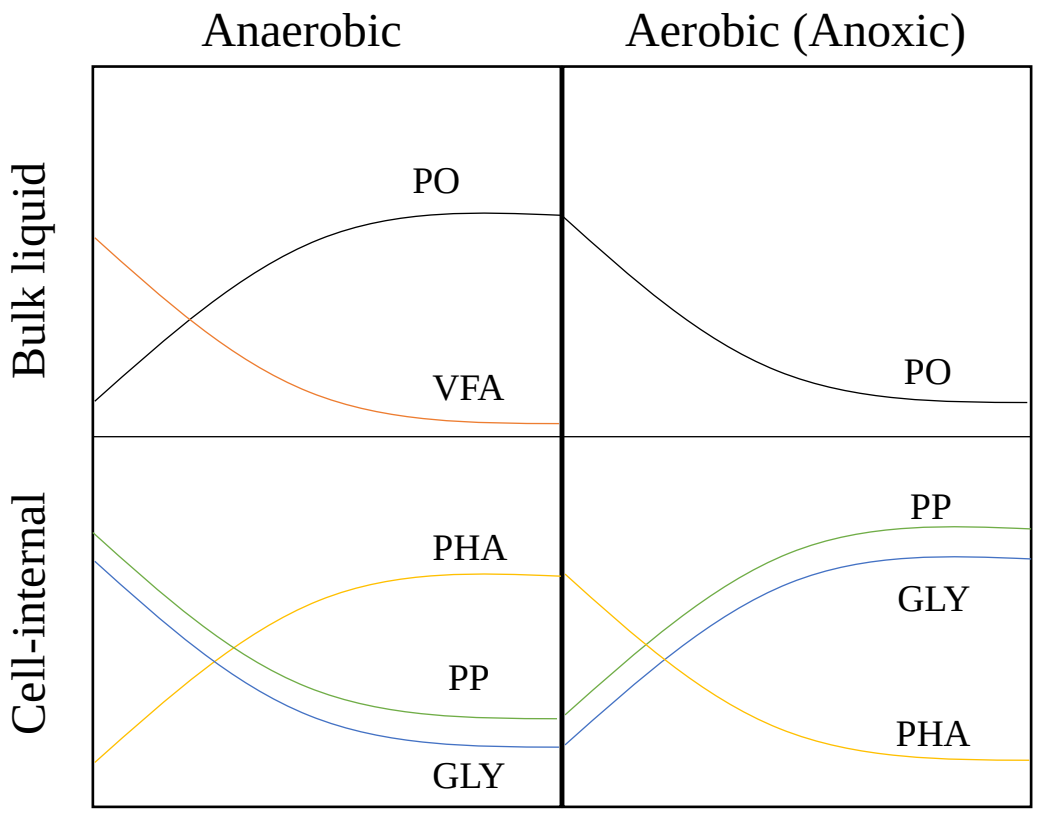

Figure 2-2. Schematic representation of the biological phosphorus removal process; Modified from (Meijer, 2004)

2.1.2. The functional bacteria involved in each process

As previously discussed SNDPR incorporates carbon, nitrogen, and phosphorus removal by all the common bacterial groups employed in wastewater treatment. These include OHOs, AOB, NOB, PAOs, DPAOs, GAOs, and DGAOs. Table 2-1 shows different biological reactions that take place under the different

environmental conditions. The understanding of the biological reactions was employed in subsequent experimental design and analysis.

Table 2-1. Functional bacteria for different processes

Process	Functional bacteria
Anaerobic	
Polyphosphate hydrolysis	PAOs, DPAOs
VFA uptake	PAOs, DPAOs, GAOs, DGAOs
Anoxic	
Nitrate denitrification	DOHOs, DPAOs, DGAOs
Nitrite denitrification	DOHOs, DPAOs, DGAOs
Phosphorus uptake	DPAOs
Glycogen uptake	DPAOs, DGAOs
Aerobic	
COD oxidation	OHOs
Nitrification	AOB, NOB
Phosphorus uptake	PAOs
Glycogen uptake	PAOs, GAOs

Table 2-1 shows different functional bacteria are expected to be active in the different redox zones. In the anaerobic zone, polyphosphate hydrolysis takes place by PAOs and DPAOs to release energy, which is used for VFA uptake (Metcalf et al., 2014). In addition, VFAs can be stored by GAOs and DGAOs as PHA (Wang et al., 2016b). VFAs are regarded as the substrates for growth of all the phosphorus removal-related bacteria (PAOs, DPAOs, GAOs, and DGAOs). In anoxic zones, nitrogen is removed either from nitrate or nitrite by DOHOs, DPAOs, and DGAOs (Wang et al., 2016b). Denitrification by DOHOs requires an external carbon source as an electron donor, whereas denitrification by DPAOs and DGAOs uses intercellular PHA as the carbon source. Phosphorus can be removed in anoxic zones by DPAOs with glycogen replenishment. In aerobic zones, nitrification and phosphorus uptake occur simultaneously.

Traditional nitrification is a two-step process comprised of AOB nitritation and NOB nitratation. AOB nitritation converts ammonia to nitrite, and NOB nitratation oxidizes nitrite to nitrate with oxygen (Metcalf et al., 2014). Furthermore, PAOs contribute to phosphorus uptake with glycogen replenishment (Metcalf et al., 2014). Based on these processes, activity tests can be conducted by creating targeted environments to study specific nitrogen removal pathways.

A clear understanding of microorganisms that are responsible for nitrification can connect the performance of ammonia oxidation and nitrite oxidation to microorganism community analysis. In the first step of nitrification (e.g., nitritation), β-*proteobacteria* including *Nitrosomonas* and *Nitrosospira* who are considered as AOB are responsible (Mobarry et al., 1996). In the second step of nitrification (e.g., nitratation), NOB that are mainly α-*proteobacteria* including *Nitrospira* and *Nitrobacter* are the main contributors (Mobarry et al., 1996). By identifying the nitrifiers, nitrification in the SNDPR process can be understood.

The identification of the dominant PAOs can help understand the status of biological phosphorus removal. Many studies have identified the dominant groups of PAOs are *Ca.* Accumulibacter and *Tetrasphaera* (Close et al., 2021; Marques et al., 2018). PAO-rich systems have been observed both in lab-scale and full-scale studies (Oehmen et al., 2005c; Saunders et al., 2016). Many studies have found that most PAOs are classified under *Proteobacteria* (Fernández et al., 2008; Mao et al., 2013). In addition, *Proteobacteria* and *Bacteroidetes* are found to be dominant in cold-region WWTPs due to their characteristics as psychrophilic bacteria (Cui et al., 2012; Li et al., 2019; Ou et al., 2018; Wen et al., 2015). Many studies have shown that *Tetrasphaera* is capable of fermentation and phosphorus uptake under aerobic conditions (Close et al., 2021). In addition, several members of the genus *Tetrasphaera* are highly competitive at low temperatures (Welles et al., 2015). Therefore, *Ca.* Accumulibacter and *Tetrasphaera* could be the dominant microbes at low temperatures in this study.

DPAOs can perform both denitrification and biological phosphorus uptake under anoxic conditions, which is another important component for SNDPR. Many studies have found that *Accumulibacter* can be distinguished as either Type I or II, which are correlated to nitrate-reducing and non-nitrate-reducing PAOs (Carvalho et al., 2007; Oehmen et al., 2010a). The nitrate-reducing PAOs (*Accumulibacter* Type I) can perform both denitrification via nitrate and nitrite and phosphorus uptake under anoxic conditions, which are considered as DPAOs. The non-nitrate-reducing PAOs (*Accumulibacter* Type II) can only perform denitrification via nitrite and phosphorus uptake under anoxic conditions, which are considered as PAOs. Genera *Dechloromonas*, *Zoogloea*, and *Paracoccus* which have the ability of denitrification via nitrate and phosphorus uptake under anoxic conditions are considered as DPAOs (Wang et al., 2015). Comparing the phosphorus uptake rate by DPAOs and PAOs under anoxic and aerobic conditions, it has found the phosphorus uptake rate by DPAOs is significantly lower than that by PAOs, which are 20 and 70 mg P/(g VSS·h), respectively (Carvalho et al., 2007; Filipe & Daigger, 1999). Therefore, conducting microbial community analysis to identify genus related to DPAOs can help determine whether the nitrogen removal at low DO concentrations involves DPAO denitrification.

The proliferation of GAOs can impact on the success of EBPR since excessive GAOs may lead to the failure of biological phosphorus removal. Under anaerobic conditions, GAOs and PAOs compete for VFAs, while GAOs do not contribute to phosphorus removal (Metcalf et al., 2014). Studies have shown that pH of 7-7.5 and temperatures lower than 20℃ are less favorable for GAO growth (Lopez-Vazquez et al., 2009b). The main genus that is considered as a GAO is *Defluvicoccus* (Metcalf et al., 2014). *Defluvicoccus* can be divided into *Defluviicoccus* Cluster I and *Defluviicoccus* Cluster II, which are able to reduce nitrate but not nitrite and unable to denitrify, respectively (Burow et al., 2007; Wang et al., 2008). Overall, identifying the genus related to GAOs can help understand the status of EBPR.

DGAOs can contribute to the performance of SNDPR systems. The difference between GAOs and DGAOs is that DGAOs can perform denitrification via nitrate and nitrite under anoxic conditions (Zeng et al., 2003c). Therefore, DGAOs contribute to SNDPR by reducing nitrogen under low DO conditions. Under anoxic

conditions, DGAOs can reduce nitrate to nitrite, then *Accumulibacter* Type II can use the produced nitrite for denitrification and phosphorus uptake (Rubio-Rincón et al., 2017). *Ca.* Competibacter is considered as the main DGAO, which has been widely observed in phosphorus removal systems (Zeng et al., 2003c). Overall, DGAOs are worth investigating in the SNDPR systems to gain better understanding of nitrogen and phosphorus removal at low DO concentrations.

In summary, microbial community analysis should be conducted to fully understand the microbial ecology in the SNDPR system. A clear presentation of microbial ecology can help with understanding the performance of SNDPR. In addition, by improving the desire microorganism living conditions, it may be possible to improve SNDPR performance and design novel reactors/processes for SNDPR.

2.2. Impact of operational conditions on the responses of SNDPR

SNDPR, as previously discussed, is a complicated process that will be impacted by external factors. These factors include: temperature, oxygen concentration, carbon composition, pH, atmosphere pressure, etc (Chen et al., 2020; Lopez-Vazquez et al., 2009a; Oehmen et al., 2010b; Oehmen et al., 2005a; Oehmen et al., 2005b). The effects of temperature and oxygen concentration on SNDPR in terms of functional bacteria and biological reactions are discussed below due to their universality and importance.

2.2.1. The impacts of temperature on the SNDPR system response

Temperature plays a vital role in the SNDPR process. It has a significant impact on bacteria biochemical reactions (i.e., bacteria growth, substrate utilization, and bacteria decay) (Huang et al., 2015). In this study, low temperatures (around 10°C) are expected to pose a challenge for nutrient removal. Low microbial activity is associated with low temperatures; approximately a 50% reduction in microbial activity occurs

for every 10℃ decline (Rajeshwari et al., 2000). Even though many studies have been conducted to study SNDPR, there are limited studies to investigate SNDPR at 10℃, which is the temperature in the winter session of Canada.

The effects of temperature on different types of bacteria and related processes differ. Nitrifiers (AOB and NOB) and denitrifiers (DOHOs, DPAOs, and DGAOs) have been shown to be significantly impacted by low temperatures (Guo et al., 2013; Hellinga et al., 1998). Reducing the temperature can facilitate NOB to outcompete AOB to mitigate nitrite accumulation (Bougard et al., 2006). A temperature of 15℃ was reported to be a critical temperature for AOB and NOB growth as shown in Figure 2-3. At temperatures lower than 15℃, the specific growth rate of NOB is higher than that of AOB, whereas at temperatures higher than 15℃, the reverse is true (Hellinga et al., 1998). In addition, many studies have illustrated that low temperatures can cause low nitrification rates (Choi et al., 1998; Guo et al., 2013). Overall, the literature shows that both nitrification and denitrification are reduced with a reduction of temperature. However, there is a need to investigate the status of nitrification and whether there is nitrite accumulation at the studied low temperature (10℃).

Various studies have examined the effects of temperature on phosphorus removal. DPAOs have been reported to be more affected by low temperatures than aerobic PAOs, which results in a greater reduction of phosphorus uptake in the anoxic stage than in the aerobic stage at low temperatures (Ferrentino et al., 2017; Haiming et al., 2014). PAOs are known to be psychrophilic, therefore, low temperatures favor PAOs over GAOs (Erdal, 2003; Lopez-Vazquez et al., 2009a; Tian et al., 2017b). In contrast, GAOs can outcompete PAOs under higher temperatures (>20℃) (Brdjanovic et al., 1998; Lopez-Vazquez et al., 2009a). Furthermore, low temperatures also favor the competition of PAOs over nitrifiers for oxygen since nitrification is inhibited at low temperatures, which favors the growth and enrichment of PAOs (Baetens et al., 1999). Overall, low temperatures favor the growth of PAOs instead of DPAOs, GAOs, and nitrifiers, which was considered when interpreting the results of activity tests and microbial community analysis in the current study.

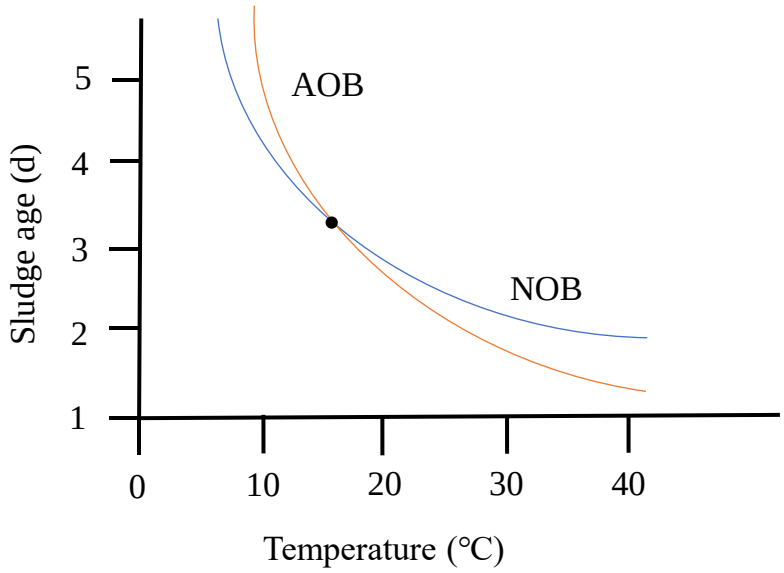

Figure 2-3. The effect of temperature on sludge age for AOB and NOB; Modified from (Hellinga et al., 1998)

Recent studies of the effects of temperature on SNDPR in SBR are summarized in Table 2-2. Temperatures around 20℃ have been found to result in nitrogen and phosphorus removal efficiencies around 95% (Münch et al., 1996; Zeng et al., 2003a). However, the reduction in temperature has been observed to significantly reduce nitrogen removal efficiency with little impact on phosphorus removal efficiency. Jia et al. (2016) found that a reduction of temperature (from 25 to 10℃) caused total nitrogen (TN) removal efficiency to be reduced from 77.7% to 66.5% although total phosphorus (TP) removal efficiency remained stable around 95%. Similar findings were reported by Guo et al. (2013), where a reduction of temperature from 20 to 10 to 5℃ resulted in reduced nitrogen removal efficiencies of 70.9%, 62%, and 34%, respectively. However, nitrogen and phosphorus removal efficiencies were not influenced at 10℃, which was reported by Pan et al. (2017). This result was attributed to the use of intermittent aeration and a high oxygen concentration of 2 mg/L. The common SBR operational ranges summarized in Table 2-2 were considered in the design of SBR in this study.

In summary, operational temperature can significantly influence SNDPR by having a significant impact on biological reactions. Under low temperatures: 1) nitrification and denitrification rates are reduced; 2) NOB can outcompete AOB; 3) PAOs can outcompete GAOs and nitrifiers for oxygen; 4) nitrogen removal efficiency is reduced, but phosphorus removal efficiency is less impacted. However, limited work has been conducted to study SNDPR at low temperatures in terms of removal pathways of nitrogen. Therefore, there is a need to design activity tests to understand the nitrogen removal pathways in SNDPR at low temperatures.

Table 2-2. Prior studies of simultaneous nitrification, denitrification and phosphorus removal in SBRs

Note: A-O-A-O-A-O-A-O-S-D: anaerobic-oxic-anaerobic-oxic-anaerobic-oxic-anaerobic-oxic-settle-decant A-O-S-D: anaerobic-oxic-settle-decant;

Process types	Wastewater type	T (℃)	SRT (day)	HRT (hour)	DO (mg/L)	pH	Cycle time (hour)	Stage type	SBR each stage time (min)	COD /TN	COD/ TP	Stirring rate (rpm)	TN removal eff	TP removal eff	References
SBR	Slaughterhouse wastewater	11	16	6.7	2	7.8	12	A-O-A-O-A-O-A-O-S-D	60-100-60-100-60-100-60-100-70-10	10	109	-	97.7%	97.9%	Pan et al. (2017)
SBR	Synthetic	25	16	12	0.35-0.65	7.0-7.5	6	A-O-S-D	90-210-45-15	10	27	-	77.7	95.6	Jia et al. (2016)
SBR	Synthetic	10	16	12	0.35-0.65	7.0-7.5	6	A-O-S-D	90-210-45-15	10	27	-	66.5	93.8	Jia et al. (2016)
SBR	Domestic	18-22	15	18	1.2	-	6	A-O-S-D	150-180-20-10	9.4	57	160	87.2	-	Münch et al. (1996)
SBR	Abattoir wastewater	18-22	15	36	0.2-0.6	7.0-8.0	6	A-O-S-D	150-180-20-10	9.3	61	-	95	-	Pochana & Keller (1999)
SBR	Synthetic	18	15	9.6	0.45-0.55	7.0-7.5	4.8	A-O-S-D	60-180-43-5	10	27	250	>95	>90	Zeng et al. (2003a)
SBR	Synthetic	5	20	10	1.0-2.5	7.0-8.0	8.5	O-S-D	480-30-5	8	-	100	34	-	Guo et al. (2013)
SBR	Synthetic	10	15	10	1.0-2.0	7.0-8.0	7.5	O-S-D	420-30-5	8	-	100	62	-	Guo et al. (2013)
SBR	Synthetic	20	10	10	1.0-2.0	7.0-8.0	7.5	O-S-D	420-30-5	10	-	100	70.9	-	Guo et al. (2013)

O-S-D: oxic-settle-decant

2.2.2. Impact of oxygen concentration on SNDPR system behavior

This section presents an overview of the impact of oxygen concentration on SNDPR. The effects of oxygen concentration on SNDPR have been separated into the impacts on both bacteria and each biological reaction process. The oxygen concentration is an important component for nitrification and phosphorus removal since AOB, NOB, and PAOs require oxygen for respiration. Therefore, literature in this regard was reviewed to better understand the dependencies of microbial rates on oxygen concentration.

Oxygen concentration has different effects on AOB and NOB. It is known that both AOB and NOB growth need oxygen as the electron acceptor, but the half-saturation coefficients for AOB (0.2-0.4 mgO_2/L) and NOB (1.2-1.5 mgO_2/L) are quite different (Henze et al., 2008). Therefore, oxygen concentration highly affects the degree of nitrification (Ruiz et al., 2003). Table 2-3 summarizes the effects of DO concentration on nitrification. As it is shown, oxygen concentrations higher than 1.7 mg/L yielded full nitrification, indicating that both AOB and NOB had a high growth rate without limitation (Rubilar et al., 2005; Ruiz et al., 2003). With the reduction of oxygen concentration from 1.7 mg/L to 0.7 mg/L, the ammonia oxidation rate is reduced gradually, and NOB inhibition has been inferred in the basis of nitrite accumulation in the process (Rubilar et al., 2005; Ruiz et al., 2003). Further reducing oxygen concentration to less than 0.5 mg/L was observed to lead to nitrite and ammonia accumulation (Ruiz et al., 2003). Overall, the oxygen concentration plays an important role for AOB and NOB growth. It is expected that reducing oxygen concentration can inhibit NOB and AOB growth successively.

Table 2-3. Effect of oxygen concentration on nitrification in activated sludge

DO (mg/L)	Effect	Reference
<0.5	Nitrite and ammonia accumulation	Ruiz et al. (2003)
0.7	Nitrite accumulation up to 65 % of the applied NH_4^+	Ruiz et al. (2003)
1.0	80 % oxidation of NH_4^+, 80 % as NO_2^-	Rubilar et al. (2005)
1.4	99 % oxidation of NH_4^+, 70 % as NO_2^-	Rubilar et al. (2005)
>1.7	Full nitrification	Ruiz et al. (2003)
2.4	99 % oxidation of the applied NH_4^+, less than 10 % as NO_2^-	Rubilar et al. (2005)

The control of oxygen concentration is also essential for denitrification. Denitrification can be best achieved with a zero-oxygen concentration and the provision of sufficient carbon source. Denitrification has been found to be reduced with oxygen concentrations above 0.2 mg/L (Bliss & Barnes, 1986). At the same time, Münch et al. (1996) also found that DO of 0.5 mg/L could lead to complete SND. Jimenez et al. (2010) found the optimal DO concentration range in the bulk to achieve SND is from 0.3 to 0.7 mg/L. In summary, denitrification is reduced with the increase of oxygen concentration, and oxygen concentration in the range of 0.3 to 0.7 mg/L should be tested in this study in order to achieve SND.

The effects of oxygen concentration on phosphorus removal are not obvious. Both PAOs and DPAOs can take up phosphorus under either aerobic or anoxic conditions. With the reduction of oxygen, opposing findings have been observed in different studies. Zhang et al. (2014) pointed out that DPAO percentage were reduced with the reduction of aeration rate, whereas Wang et al. (2016a) found that the DPAO percentage increased with a decrease of DO from 2 to 0.5 mg/L. This contrasting finding might be attributed to differences in the extent of phosphorus uptake and secondary phosphorus release that can happen at low oxygen concentrations. Overall, there is a need to determine the minimal DO concentration that does not impact biological phosphorus removal.

2.3. SNDPR simulation

Modeling is increasingly being employed to understand active mechanisms, optimize systems, and simulate alternative scenarios in support of process design (Rieger et al., 2012). As an example, the ASMs created by IWA have been widely acknowledged and used to describe carbon, nitrogen, and phosphorus transformation in flocculent sludge and biofilm systems (Eberl et al., 2006; Melcer, 2004). Modeling has been proved to be a convenient and economically attractive method to understand complex systems.

Even though ASMs are widely used, simulation of SNDPR with low DO has proved difficult due to challenges with obtaining accurate half-saturation coefficients (K_s) for various nutrients (Hauduc et al., 2011). Measured K_s values reflect the effects of advection and diffusion limitations, and hence can be considered as "extant" values (Arnaldos et al., 2015). In SNDPR systems employing flocculant sludge, several factors can impact extant K_s values, including mixing conditions and hydraulics that impact advective transport (Liu et al., 2010; Münch et al., 1996), and floc size, density, and porosity which impact diffusion (Manser et al., 2005; Pochana et al., 1999; Wang et al., 2007). Half-saturation coefficients of oxygen (K_o) are particularly important in SNDPR systems due to the low DO values employed and the importance of this value in determining several key biological reaction rates (Daigger et al., 2007). Therefore, it can be challenging to simulate SNDPR performance with extant K_s values due to the wide range of values reported in the literature (Hauduc et al., 2011), and there is a need to find innovative solutions to solve this challenge.

Employing intrinsic K_s parameters in a model that includes mass transfer processes is a strategy that can solve this challenge since this strategy can better reflect the impacts of system conditions on extant K_s values. The term "intrinsic" refers to the actual K_s of a specific biomass species in the absence of substrate diffusion limitations. This approach has been employed to simulate the transformation of carbon, nitrogen, and phosphorus in activated sludge (AS) systems as shown in Table 2-4 (Eberl et al., 2006; Pérez et al.,

2005; Pochana et al., 1999; Shaw et al., 2013; Wang et al., 2007). The intrinsic K_s parameters have also been used to simulate aerobic and anaerobic granular sludges (Baeten et al., 2019). Therefore, the application of intrinsic K_s parameters and explicit mass transfer term has been demonstrated to work, however, the intrinsic K_s values of PAOs and GAOs have not been fully explored.

Table 2-4. COD, nitrogen and phosphorus removal simulation studies using floc models

Model	Sludge type	Unknown parameters	Simulation platform	Nutrient removal	Reference
Floc model + ASM1	Activated sludge floc	Diffusivity	--	COD and N	Pochana et al. (1999)
Floc model+ASM	Aerobic granular	Detachment rate, several yield coefficients and several substrate half-saturation coefficients	AQUASIM	COD	Ni et al. (2010)
Floc model+ASM1	Activated sludge floc	Diffusivity and oxygen half-saturation coefficients	--	COD and N	Wang et al. (2007)
Floc model+ASM1	Activated sludge floc	Effectiveness factors	--	COD and N	Tyagi et al. (1996)
Floc model+ASM	Granular	Maximum growth rates, decay rates, and substrate half-saturation coefficients	AQUASIM	COD and N	Soler-Jofra et al. (2019)
Floc model+ASM	Granular	Substrate half-saturation coefficients	AQUASIM	COD, N, and P	De Kreuk et al. (2007)

Several floc models have been used to simulate diffusion-limiting systems (Pochana et al., 1999; Wang et al., 2007). These floc models were used to simulate carbon and nitrogen compounds in the floc under low DO concentrations. The common assumptions of these floc models were negligible boundary layer, uniform distribution of microbes, and limited movement of solids within a floc. These assumptions were made to simplify the simulation process. However, these aspects are also important for simulating SNDPR systems.

A comprehensive floc model should include boundary layer, reduction factor for diffusivity, particle components movement within a floc, and biological phosphorus removal related processes to simulate SNDPR. The inclusion of the boundary layer allows mixing intensity to be considered in the model, since low mixing intensity that happens in SNDPR systems might have a significant impact on SNDPR performance (Nogueira et al., 2015). The incorporation of particulate movement within a floc can be used to prevent inert component accumulation in the inner portion of a floc and facilitate a dynamic microbial

population distribution (Baeten et al., 2019). In addition, PAOs and GAOs need to be included in the model to simulate SNDPR, in which phosphorus and nitrogen removal under low DO conditions could occur (Rubio-Rincón et al., 2017). Therefore, the benefits of incorporating these aspects in a new floc model to comprehensively study the SNDPR system should be investigated.

In summary, prior studies using ASMs can be used to simulate AS system, however, the models can not simulate SNDPR accurately due to variable extant K_s values. The use of intrinsic K_S values and explicit mass transfer term has been demonstrated to be one of the solutions. However, due to the simplification assumptions of prior floc models, there is a need to develop a comprehensive floc model to simulate SNDPR which should also incorporate boundary layer, reduction factor of diffusivity, attachment and detachment, intra-floc particle components transport, and phosphorus-related processes.

2.4. SNDPR to treat municipal wastewater

At low temperatures, successful SNDPR has been reported in studies that have used synthetic wastewaters (Li et al., 2019; Salehi et al., 2019); however, few reports have been published using real municipal wastewaters. Typically, synthetic and municipal wastewaters differ in the complexity of the mixture of organics that are present (He et al., 2016; Zaman et al., 2021). Most of the carbon sources employed in studies using synthetic wastewaters have consisted of simple VFAs. In comparison, VFAs represent only 5% - 18% of the total COD in real municipal wastewaters, and additional VFAs need to be generated through fermentation of rbCOD that typically accounts for 47% - 53% of the total COD (Henze & Comeau, 2008). Additionally, slowly biodegradable COD needs to be hydrolyzed before utilization for nitrogen and phosphorus removal. In addition, real municipal wastewaters contain organic nitrogen that releases ammonia through hydrolysis. The additional ammonia generated from hydrolysis increases the required nitrification capacity and biodegradable COD required for subsequent denitrification (Zhu et al., 2021). The

increased complexity of real wastewaters creates some uncertainty about whether SNDPR operational strategies that were developed with synthetic wastewaters can be directly transferred to real wastewater applications. Therefore, it is necessary to investigate whether real wastewaters can be treated with the same SNDPR operational strategies that were found to work for synthetic wastewaters.

SNDPR has been successfully employed to treat a variety of wastewaters including those from abattoirs (Yilmaz et al., 2008), food-processing (Cheng et al., 2021), and aniline production (Yang et al., 2021)). In addition, performance under a range of operating conditions including low C/N ratio (Wang et al., 2016c), low organic loadings due to wet weather (Li et al., 2021), and low atmosphere pressure (Chen et al., 2020) have been reported. However, limited studies have been conducted to study the performance of SNDPR in municipal wastewater context at low temperatures. At low temperatures, the activities of biological processes including hydrolysis of biodegradable particulate matter, fermentation, nitrification, denitrification, and phosphorus release and uptake are significantly reduced or inhibited (Henze et al., 2000). Of particular, significance to SNDPR processes are the low reaction rates for hydrolysis and fermentation at low temperatures that can limit the availability of readily biodegradable organics to support nitrogen and phosphorus removal (Yuan et al., 2011). Therefore, there is a need to achieve SNDPR when treating municipal wastewater at low temperatures.

SNDPR has been reported to treat municipal wastewaters in both anaerobic/aerobic (AO) and anaerobic/aerobic/anoxic (AOA) process configurations at room temperatures. In the AO mode, intracellular carbon storage (PHA and glycogen) is enhanced by extending the anaerobic phase, and SND is conducted by both DPAOs and OHOs in the aerobic zone that is operated with low DO concentrations (lower than 0.5 mg/L) (Wang et al., 2015; Zaman et al., 2021). In the AOA mode, SND can occur during the aerobic phase when operated with low DO concentrations, and further nitrogen removal is achieved by denitrification in the post anoxic phase using hydrolyzed carbon or stored carbon (Wang et al., 2016c; Winkler et al., 2011; Zhao et al., 2018). In addition, the reduction of nitrate and oxygen in the post anoxic zone further enhances the uptake of influent rbCOD by PAOs to maintain stable EBPR. Typically, the AOA

mode can achieve higher total inorganic nitrogen (TIN) and phosphorus removal efficiencies (above 80% and 90%) than the AO mode (around 70% and 90%) (Wang et al., 2015; Wang et al., 2016c; Winkler et al., 2011; Zaman et al., 2021; Zhao et al., 2018). While AO and AOA operations have received considerable study at room temperatures, limited research has been conducted to study the impact of different process configurations (AO and AOA) on SNDPR when treating municipal wastewaters at low temperatures. Hence, there is a need to understand the performance of the two configurations when treating real municipal wastewaters at low temperatures.

In summary, most prior studies have demonstrated SNDPR when using synthetic wastewaters, however, it is not clear whether the same operational strategies developed to treat synthetic wastewater can also work to treat municipal wastewater, especially at low temperatures. At low temperatures, biological reaction rates are reduced, especially hydrolysis and fermentation rates, which could be a potential challenge for nitrogen and phosphorus removal due to insufficient rbCOD and VFAs. Reduced availability of rbCOD and VFAs might be solved by reducing the nitrate concentration that is present at the beginning of the anaerobic phase of the AOA configuration. However, direct comparisons of AO and AOA configurations treating real municipal wastewaters have not been reported. Therefore, there is a need to compare the impact of the two configurations (AO and AOA) on SNDPR when treating real municipal wastewaters at low temperatures.

2.5. Summary of literature review

Overall, SNDPR has become an attractive treatment method due to its potential for energy saving. The mechanisms of SNDPR are that nitrogen removal is through partial nitrification and denitrification in the aerobic stage when low oxygen concentrations are maintained. Phosphorus removal is achieved through alternating the anaerobic and aerobic zones with anaerobic phosphorus release and aerobic phosphorus uptake. A total of seven types of bacteria (OHOs, AOB, NOB, PAOs, DPAOs, GAOs, and DGAOs) are involved in the SNDPR process. Furthermore, the change of operational conditions (temperature and

oxygen concentration) impacts bacteria and related biological reactions. Reducing temperature can result in poor nitrogen removal but not impact on phosphorus removal. Reducing oxygen concentration can lead to poor nitrification and improved denitrification. However, no agreement has stated in terms of phosphorus removal with reduced oxygen concentration. Simulating SNDPR using ASMs with extant Ks values poses challenges due to variable Ks values, however, floc models with intrinsic Ks and explicit mass transfer terms have been demonstrated success to simulate SNDPR at low DO. As for treating municipal wastewater using SNDPR, two process configurations (AO and AOA) have been demonstrated success at room temperatures. However, at low temperatures, hydrolysis and fermentation rates are low, which might be a challenge to achieve SNDPR.

2.6. Gaps in the research

Although there have been a number of studies of SNDPR the following gaps have been identified:

1. The nitrogen removal pathways in the SNDPR system at low temperatures are not well understood.
2. The composition of the microbial community in SNDPR systems operating at low temperatures has not been examined in parallel with metrics of SNDPR performance.
3. A comprehensive floc model has not been developed to address all of the characteristics of SNDPR systems. Such a model should include intrinsic K_s values, boundary layer, intra-floc particulate transport, and phosphorus-related processes.
4. Few studies have examined the performance of SNDPR systems when treating real municipal wastewater at low temperatures.
5. Studies of SNDPR have not compared AO and AOA configurations when treating real municipal wastewaters at low temperatures.

6. The appropriateness of operational strategies developed to treat synthetic wastewater for treating real municipal wastewater, at low temperatures, has not be examined.
7. The microbial community observed when treating complex synthetic wastewater has not been compared with that developed when real municipal wastewater is treated at low temperatures.

Chapter 3 Nitrogen removal pathways during simultaneous nitrification, denitrification, and phosphorus removal under low temperature and dissolved oxygen conditions

Abstract

Nitrogen removal pathways of simultaneous nitrification, denitrification, and phosphorus removal (SNDPR) at low dissolved oxygen (0.3 mg/L) and temperature (10°C) were explored to understand nitrogen removal mechanisms. Biological nitrogen and phosphorus removal were sustained with total inorganic nitrogen removal, phosphorus removal, and simultaneous nitrification and denitrification (SND) efficiencies of 62.6%, 97%, and 31%, respectively. The SND was observed in the first 2 h of the aerobic phase and was attributed to denitrifying ordinary heterotrophic organisms using readily biodegradable chemical oxygen demand and denitrifying phosphorus accumulating organisms (DPAOs), which removed 15% and 12% of influent nitrogen, respectively. A phosphorus accumulating organism (PAO)-rich community was indicated by stoichiometric ratios and supported by 16S rRNA gene analysis, with *Dechloromonas*, *Zoogloea*, and *Paracoccus* as DPAOs, and *Ca.* Accumulibacter and *Tetrasphaera* as PAOs. Even though *Ca.* Competibacter (10.4%) was detected, limited denitrifying glycogen accumulating organism denitrification was observed, which might be due to low temperatures. This research was the few researches that investigated the SNDPR process at 10°C by using a complex synthetic wastewater, investigated the nitrogen removal pathways in the aerobic phase using an experimental method, and integrated microbial community analysis with experimental findings.

Keywords: Functional annotation of prokaryotic taxa; Low temperature; Phosphorus accumulating organism; Glycogen accumulating organism; Simultaneous nitrification, denitrification, and phosphorus removal

3.1. Introduction

Modern municipal wastewater treatment plants (WWTPs) are required to reduce organic carbon, nitrogen, and phosphorus to minimize impacts on receiving waters. Traditionally, nitrogen is removed through nitrification and denitrification, and phosphorus is removed through either biological or chemical treatment. The drawbacks of these traditional approaches include high energy consumption, chemical requirements for phosphorus removal, carbon requirements for nitrogen removal, and treatment configuration complexity (Kärrman, 2001). Therefore, it is desirable to develop alternative processes that can remove nutrients in a more sustainable manner than these traditional technologies.

Simultaneous nitrification, denitrification, and phosphorus removal (SNDPR) has been proposed as an alternative to conventional biological nitrogen and phosphorus removal (Ji et al., 2020; Yuan et al., 2020). For nitrogen removal, simultaneous nitrification and denitrification (SND) can be achieved by operating at low dissolved oxygen (DO) concentrations. Depending on oxygen diffusion within a sludge floc, two different zones can develop. The oxic zone, at the outer layer of the floc, supports nitrification by ammonia-oxidizing bacteria (AOB) and nitrite-oxidizing bacteria (NOB), whereas the anoxic zone, within the floc, permits denitrification by ordinary heterotrophic organisms (OHOs), denitrifying phosphorus accumulating organisms (DPAOs), and denitrifying glycogen accumulating organisms (DGAOs) using diffused carbon and intracellular carbon sources (Wang et al., 2016b). In addition, short-cut nitritation (ammonia to nitrite) and denitritation have been demonstrated to occur at low DO concentrations because AOB are known to have a higher affinity for oxygen than NOB (Kunapongkiti et al., 2020). By applying short-cut nitritation and denitritation, up to 25% of energy for aeration and 40% of carbon for denitrification can be conserved (Kunapongkiti et al., 2020).

Potential denitrification pathways in SNDPR systems include OHOs using readily biodegradable COD (rbCOD), DPAOs and DGAOs using intracellular polyhydroxyalkanoates (PHA), and denitrifying OHOs using hydrolyzed carbon (Ji et al., 2020; Yuan et al., 2020). The DPAOs (e.g., *Pseudomonas* and *Dechloromonas*) and DGAOs (*Ca.* Competibacter) have been reported to simultaneously remove nitrate/nitrite under anoxic conditions (Yuan et al., 2020). At the same time, phosphorus can be taken up by DPAOs (Wang et al., 2016b). Hence, potential nitrogen removal pathways in the SNDPR system are complicated, and few studies have fully differentiated these processes. Even though several studies have reported nitrogen removal pathways based on the stoichiometric parameters of each microorganism (Wang et al., 2016b), there is limited research using experimental methods to quantitatively characterize the biological nitrogen removal pathways.

Low operating temperatures can challenge the performance of a SNDPR system because the growth of nitrifiers (AOB and NOB), denitrifiers (DPAOs, DGAOs, and OHOs), and BioP-related bacteria (PAOs and GAOs) has been shown to be significantly and differentially reduced (Hellinga et al., 1998). Although the specific growth rates of NOB may be higher than those of AOB at temperatures lower than 15℃, the opposite is true for temperatures higher than 15℃ (Hellinga et al., 1998). Therefore, short-cut nitritation and denitritation may be less feasible at low temperatures. Moreover, less soluble biodegradable organic material is produced through hydrolysis and fermentation at low temperatures, reducing the rate of denitrification and deteriorating biological phosphorus removal (Yuan et al., 2011). Because PAOs are known to be psychrophilic, low temperatures favor PAOs over GAOs (Tian et al., 2017). Indeed, reducing the temperature from 25℃ to 10℃ had little impact on phosphorus removal efficiency (95%) when tested with a synthetic wastewater with a simple carbon source (Wang et al., 2016a). Others have reported that hydrolysis and fermentation are rate-limiting processes for biological phosphorus removal when using real wastewater, especially at low temperatures (Yuan et al., 2011). Hence, although SND and BioP have been studied at low temperatures, the pathways contributing to biological nitrogen and phosphorus removal using complex carbon sources at a constant low DO and low temperature have not been quantified in detail.

Microbial community analysis can be employed to understand microorganisms in SNDPR systems and, by extension, their contributions to biomass activity. Key AOB (e.g., *Nitrosomonas* and *Nitrosomonadaceae*), NOB (e.g., *Nitrospira*), PAOs (e.g., *Ca.* Accumulibacter), GAOs (e.g., *Deflviicoccus*), DPAOs (e.g., *Dechloromonas* and *Pseudomonas*), and DGAOs (e.g., *Ca.* Competibacter) have been reported in SNDPR systems (Liu et al., 2019; Yuan et al., 2020). However, microbial community characterization has typically been reported separately from measures of community activity. Few studies have attempted to link the results from microbial community structure analysis to biological activity. Therefore, there is a need to integrate microbial analysis with activity-based testing to verify the activity of the observed microorganisms in the bioreactors.

Here nitrogen removal pathways of SNDPR were studied when operated with a complex wastewater under low temperature and dissolved oxygen conditions. A bench-scale sequencing batch reactor (SBR) was operated at 10℃ under the anaerobic/aerobic configuration with the DO in the aerobic phase of 0.3 mg/L to study the performance of the SNDPR system. The startup period was evaluated to quantify biological nitrogen and phosphorus removal and confirm steady-state conditions. Dynamic tests were conducted in the SBR to characterize the rate of change of each substrate and assess active biological processes. Activity tests were conducted to quantitatively verify nitrogen removal pathways in the aerobic phase. Microbial community composition was analyzed to explore microorganisms that contribute to SNDPR in the SBR.

3.2. Materials and methods

3.2.1. Reactor setup and operation

A bench-scale SBR with a working volume of 18 L was operated with a total cycle duration of 8 h to study SNDPR processes at 10℃ (Figure 3-1). Each cycle consisted of an “anaerobic phase” of 1 h (including 15 min of feeding time), an “aerobic phase” of 6 h (including 5 min of wasting time at the end), a “settling

phase" of 45 min, and a "decant phase" of 15 min. During the feeding, 9 L of wastewater was added to the SBR, resulting in a hydraulic retention time of 16 h. A volume of 200 mL of mixed liquor was wasted each cycle, yielding a total sludge retention time (SRT) of 30 days.

The SBR was equipped with a vertical flat blade turbine for mixing, a luminescent DO probe with temperature sensing (Hach LDO probe, Product #5790000, Hach Company, Loveland, CO, USA), and a Bubble Mist – Bendable Air Wall air diffuser (Big Al's Canada, Woodbridge, ON, Canada). Four stainless steel tubes entered through the lid to allow for feeding, aeration, waste, and decanting activities. Three peristaltic pumps (MASTERFLEX Console Pump Drives, Model #77521-40 and Model #77521-50, Cole-Parmer Instrument Company, Vernon Hills, IL, USA) were used to feed the wastewater, pump out wasted mixed liquor suspended solids (MLSS), and decant treated wastewater.

The SBR was controlled automatically using an algorithm encoded in LabVIEW (National Instruments, Austin, TX, USA). DO values from the DO probe were input into a LabVIEW program to inform the control of the air supply pump that was operated in the on/off mode. In order to maintain the accuracy of the DO probe, regular maintenance was performed once every two weeks, including probe calibration, cap cleaning, etc. During the aerobic phase, the DO concentration in the liquid was maintained at 0.3 ± 0.1 mg/L. The DO probe was maintained and calibrated every two weeks to ensure the accuracy of data. The feed, decant, and waste MLSS pumps, and the mechanical mixer, were controlled by the LabVIEW program to provide the targeted SBR operation. The temperature was maintained at 10°C by means of an external water jacket (Wang et al., 2020). The mixer rotation speed was held at 130 rpm with a G value of 123 s^{-1} to provide complete mixing for anaerobic and aerobic phases.

The SBR was inoculated with mixed liquor from the Elmira municipal wastewater treatment plant (Elmira, Ontario, CA) that was operated for biological nitrogen and phosphorus removal around August 2020. 9 L of mixed liquor was collected from the aerobic zone in the Elmira plant and placed into the SBR in the lab within 1h. The mixed liquor was washed three times with deionized water and then synthetic wastewater

was fed into the SBR for regular operation. The performance of the SBR was assessed three times per week with respect to soluble COD (sCOD), NH_4-N, NO_2-N, NO_3-N, PO_4-P, MLSS, and mixed liquor volatile suspended solids (MLVSS) at the end of the aerobic phase. The SBR was assumed to be at a steady state when all responses varied less than 4% over a two-week period.

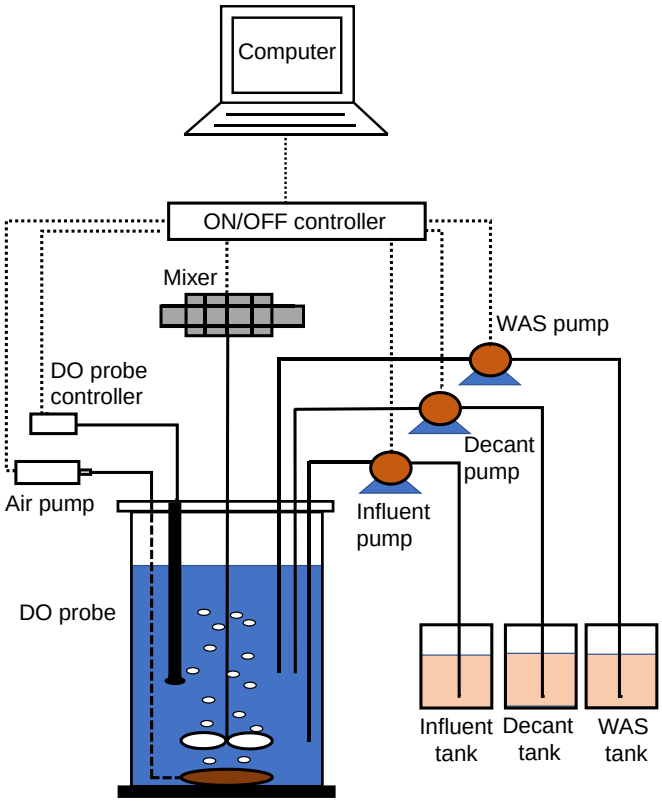

Figure 3-1. Experimental devices to conduct SNDPR.

3.2.2. Wastewater

The wastewater used for this study included acetate and propionate at a mass ratio of 3:1 that contributed 54% of the COD, and the remaining COD was contributed by yeast extract, which represented a source of complex organic matter (Lopez-Vazquez et al., 2009b). The composition of the wastewater contained (per liter): 183.5 mg sodium acetate and 61 mg sodium propionate (acetate and propionate at a mass ratio of 75:25%) (191.5 mg COD/L), 150 mg yeast extract (162.5 mg COD/L), 114 mg NH_4Cl (30.0 mg/L of NH_4-

N), 30.7 mg KH_2PO_4 (6.5 mg/L of PO_4-P), 15 mg $MgSO_4$, 300 mg $NaHCO_3$, 10 mg $CaCl_2$, and trace elements I and II with 1mL/L. Trace elements I and II were the same as Van de Graaf et al. (1996). Trace element I included EDTA (5.0 g/L) and $FeSO_4 \cdot 7H_2O$ (9.15 g/L). Trace element II included EDTA (15.0 g/L), $ZnSO_4 \cdot 7H_2O$ (0.430 g/L), $C_O(NO_3) \cdot 6H_2O$ (0.294 g/L), $MnCl_4 \cdot 4H_2O$ (0.990 g/L), $CuSO_4 \cdot 5H_2O$ (0.250 g/L), $(NH_4)_6MO_7O_{24}$ (0.177 g/L), $NiCl_2 \cdot 6H_2O$ (0.190 g/L), Na_2SeO_3 (0.105 g/L), and H_3BO_3 (0.0111 g/L). On average, the wastewater contained a COD of 354 ± 15 mg COD/L, NH_4-N of 30 ± 1.4 mg/L, PO_4-P of 6.5 ± 0.3 mg/L, and soluble biodegradable organic nitrogen of 19 ± 0.4 mg N/L. After preparation, the wastewater was maintained at 10℃ for up to two days before use.

3.2.3. Dynamic tests

After the SBR system reached steady state, dynamic tests were conducted over a full SBR cycle on three separate days (i.e., days 128, 131, and 133) to investigate transformation rates of nitrogen species, phosphorus, sCOD, PHA, and glycogen. Temperature and DO were recorded continuously during the dynamic tests using the DO sensor, and pH was monitored regularly using a symPhony BENCHTOP pH probe (VWR, USA). At the end of the aerobic phase, the mixed liquor was collected to measure MLSS and MLVSS. Influent wastewater and collected mixed liquor samples were sampled in each cycle to measure sCOD, NH_4-N, NO_2-N, NO_3-N, PO_4-P, and soluble total Kjeldahl nitrogen (sTKN). Mixed liquor samples of 10 mL were collected at intervals of 10 min for the first two hours and then every 30 min for the remainder of the cycle. Mixed liquor samples were filtered with a 0.45-µm filter (VWR, USA) prior to analysis. In addition, solids were collected and stored at -70℃ prior to analysis of PHA and glycogen. Coefficients of variation (CV) were calculated for all values and then averaged over the time frame of the tests to quantify the variability among triplicate tests.

3.2.4. Activity tests

Activity tests (Table 3-1; Tests 1-6) were conducted at 10°C to test for the presence of denitrifying OHOs, DGAOs, and DPAOs (Tests 1-3) and then to quantify active denitrification pathways and corresponding nitrogen removal activities under low DO conditions of the SBR aerobic phase (DO of 0.3 mg/L; Tests 4-6). Potential denitrification pathways that were investigated included OHOs using either residual rbCOD from the anaerobic phase or hydrolyzed carbon, DPAOs using intracellular PHA, and DGAOs using intracellular PHA species. All tests were conducted in triplicate from days 135 to 150. CVs were calculated to quantify the variability among triplicate tests. Tests 1 to 3 were conducted to evaluate the presence of denitrifying OHOs, DGAOs, and DPAOs in the system because they have been reported to conduct denitrification during the aerobic phase at low DO concentrations (Wang et al., 2016a).

Test 1 was conducted at the end of the regular aerobic phase and involved extending the SBR cycle by two hours, but without aeration, to verify the presence of denitrifying OHOs using hydrolyzed carbon. Based on the data from dynamic tests, we established that there were negligible concentrations of sCOD, NO_2-N, and PHA at the end of the aerobic phase of each cycle, and the average NO_3-N concentration was 11.4 ± 0.5 mg/L. As a result, denitrification in the additional two hours was attributed to denitrifying OHOs using hydrolyzed carbon. Mixed liquor samples were taken every 15 or 30 min for NH_4-N, NO_2-N, NO_3-N, and PO_4-P measurements, and both MLSS and MLVSS were measured at the end of the test. The specific nitrate removal rate (SNRR) was calculated as per Eq. (3-4) to quantify the specific denitrification rate.

Test 2 was conducted to study whether DGAOs were present in the SBR. For this test, 200 mL of mixed liquor was collected at the end of the anaerobic phase and washed six times to eliminate residual soluble substrates. Washed biomass was transferred to 250-mL beakers, and concentrations of suspended solids were adjusted to match those of the parent SBR by adding deionized water. Both NH_4Cl and KH_2PO_4 were added to establish initial concentrations of 1 mg N/L and 1 mg P/L to support cell synthesis. Sodium nitrate was added to achieve 14.5 mg N/L of NO_3-N in beakers to facilitate the assessment of denitrification. The

initial pH was adjusted to 7.0 by adding either 1 M HCl or 1 M NaOH. Sodium bicarbonate was added to achieve 300 mg/L as a pH buffer. A magnetic stirrer was operated at 250 rpm to keep the sludge fully mixed in beakers. Plastic foam was used to cover the surface of the liquid to minimize oxygen transfer and maintain anoxic conditions. Sampling and analysis were conducted in the same manner as employed in Test 1. The anoxic conditions established in Test 2 were assumed to support denitrification by DGAOs using stored PHA and by denitrifying OHOs using hydrolyzed carbon, because there was negligible phosphorus present to support DPAO activity. The DGAOs were deemed present if the SNRR observed in Test 2 was higher than that of Test 1.

Test 3 was conducted to determine whether DPAOs were present in the SBR. Sludge collection, preparation, sampling, and analysis steps were the same as those employed in Test 2 with the exception that 30 mg P/L as PO_4 was established at the beginning of the test in beakers. It was assumed that denitrification could be attributed to denitrifying OHOs using hydrolyzed carbon and both DGAOs and DPAOs using PHA. Hence, DPAOs were assumed to be active if the SNRR of Test 3 was higher than that of Test 2.

Tests 1 to 3 provided insights into the presence of denitrifying OHOs, DGAOs, and DPAOs in the SBR by assessing their activities under anoxic conditions. Tests 4 to 6 were then performed to quantify the contributions of denitrifying OHOs, DGAOs, and DPAOs to denitrification in the SBR under low DO conditions (i.e., 0.3 mg/L).

Test 4 was conducted in the SBR to quantify denitrification by denitrifying OHOs using hydrolyzed carbon under low DO conditions (i.e., 0.3 mg/L) by extending the SBR aerobic phase for two hours. With the exception of the presence of low DO concentration, Test 4 had similar assumptions and conditions as described in Test 1. Upon completion of Test 4 an SNRR value was calculated to reflect the specific rate of denitrification by denitrifying OHOs using hydrolyzed carbon. The amount of nitrogen removed by this process was calculated based on Eq. (3-8).

Test 5 was conducted in the SBR to quantify denitrification by DPAOs and DGAOs in the low DO aerobic phase (i.e., 0.3 mg/L). For one SBR cycle, the influent to the SBR was simplified to achieve complete rbCOD uptake in the anaerobic phase while also establishing a very low concentration of NH_4-N in the anaerobic phase effluent. These conditions were employed to eliminate rbCOD-supported denitrification and minimize NO_x generation from NH_4 in the subsequent aerobic phase. The simplified SBR feed for this cycle contained 200 mg COD/L (only acetate) and 6.5 mg P/L. After the anaerobic phase, sCOD and NH_4-N were tested and found to be 3.5 ± 0.5 mg COD/L and 1.61 ± 0.1mg N/L, respectively, and sodium nitrate was added to the SBR to achieve 14 mg N/L at the beginning of the aerobic phase. PHA was determined to be present in the mixed liquor throughout the two-hour test while phosphorus was depleted in the first hour. Therefore, the conditions established in the SBR at the beginning of the low DO aerobic phase (the first hour) were expected to support denitrification by DPAOs, DGAOs, and denitrifying OHOs using hydrolyzed carbon. Once phosphorus uptake by PAOs was complete, denitrification was attributed to DGAOs and denitrifying OHOs using hydrolyzed carbon (the second hour). Therefore, the specific total inorganic nitrogen removal rate (STINRR) for denitrification by DPAOs was estimated by subtracting that of the second hour from that of the first hour. The STINRR for denitrification by DGAOs was calculated by subtracting SNRR of Test 4 from STINRR of the second hour of Test 5. The amount of nitrogen removed by each process was calculated based on Eq. (3-8).

Test 6 was conducted to quantify nitrogen removal by denitrifying OHOs using residual rbCOD from the anaerobic phase. The influent of this test was similar to that employed in the dynamic tests, with the exception that NH_4 was excluded from the feed to minimize NO_3 generation in the aerobic phase. Hence, residual rbCOD was expected to be available after the anaerobic phase for denitrification by denitrifying OHOs based on the results of dynamic tests. To confirm these assumptions, sCOD and NH_4-N concentrations at the end of the anaerobic phase were measured and found to be 44 ± 2.4 mg COD/L and 3.3 ± 0.14 mg N/L, respectively. At the start of the aerobic phase, 14 mg N/L nitrate was achieved by adding sodium nitrate for denitrification. Test 6 was conducted for one hour while PHA, sCOD, and phosphorus

were present in the reactor. Overall, the potential denitrification pathways of Test 6 at the beginning of the low DO aerobic phase were considered to include denitrifying OHOs using rbCOD and hydrolyzed carbon, and DPAOs and DGAOs using PHA. Hence, the difference between the STINRR values of Test 6 and those in the first hour of Test 5 were attributed to denitrifying OHOs using residual rbCOD. The amount of nitrogen removed by this process was calculated based on Eq. (3-8).

Table 3-1. Experimental conditions for six activity tests.

Test number	Reactor	The time to initiate the test in a cycle	Initial achieved substrate concentration in the reactor (mg/L)		Operating DO (mg/L)	Operational mode	Experimental purpose
			PO_4-P	NO_3-N			
1	SBR	7th hour	NA	NA	0	2h anoxic stir	N removal by denitrifying OHOs using hydrolyzed carbon and the SNRR
2	Beaker	1st hour	1.0	14.5	0	1h anoxic stir	N removal by DGAOs and the SNRR
3	Beaker	1st hour	30.0	14.5	0	1h anoxic stir	N removal by DPAOs and the specific N and P removal rates
4	SBR	7th hour	NA	NA	0.3	2h aerobic stir	N removal by denitrifying OHO denitrification using hydrolyzed carbon during the aerobic phase
5	SBR	1st hour	NA	14.0	0.3	2h aerobic stir	N removal by DPAOs and DGAOs during the aerobic phase, respectively
6	SBR	1st hour	NA	14.0	0.3	1h aerobic stir	N removal by denitrifying OHOs using residual rbCOD during the aerobic phase

Note: Ammonia and phosphorus were added into the beakers to achieve 1 mg N/L and 1 mg P/L, which were used for bacteria growth.

3.2.5. Analytical methods

Both DO and temperature were recorded in LabVIEW by a sensor (Hach LDO probe, Hach Company, Loveland, CO, USA). The pH was measured using a symPhony BENCHTOP pH meter (VWR, USA). When necessary, samples were filtered initially through a 1.2-µm filter (Whatman filter paper) and then a 0.45-µm cellulose filter prior to analysis of sCOD, NH_4-N, NO_2-N, NO_3-N, PO_4-P, and sTKN. COD, suspended solids, and volatile suspended solids were analyzed according to Standard Methods (APHA, 2005). Both NH_4-N and TKN were tested by HACH kits. For measurements of NO_2-N, NO_3-N, and PO_4-P, ion chromatography (Lachat Quik-Chem8000, Lachat Instrument, USA) was used. Mixed liquor solids were collected on 1.2-µm filters and stored at -70°C. Frozen samples were dried using a vacuum freeze dryer (LABCONCO Freeze Dryer System, Model 76700 Series, USA) for PHA and glycogen measurements. Concentrations of PHA were quantified in terms of poly-β-hydroxybutyrate (PHB), poly-β-hydroxyvalerate (PHV), and poly-β-hydroxy-2-methylvalerate (PH2MV) as suggested previously (Oehmen et al., 2005). Glycogen was measured based on the phenol method (Reddy et al., 2007).

3.2.6. Equations

The fate of organic carbon in the anaerobic phase of SBR operation was characterized with respect to its utilization for N and P removal. In this analysis, it was assumed that organic carbon was rapidly consumed to denitrify residual nitrite and nitrate remaining at the end of the prior aerobic cycle. Organic carbon remaining after denitrification was assumed to be available to be taken up in the anaerobic phase by PAOs and GAOs, stored as PHA and glycogen, and subsequently employed under oxic conditions for denitrification. Intracellular storage efficiency was defined as the proportion of COD stored as intracellular products (PHA and glycogen) over total COD consumed in the anaerobic phase. Eq. (3-1) – Eq. (3-3) were employed to calculate organic carbon fate in the anaerobic phase when expressed as COD (Wang et al., 2016a; Wang et al., 2016b).

$$COD_{consum} = COD_{dn} + COD_{intra} = COD_i - COD_{ana,end} \quad \text{Eq. (3-1)}$$

$$COD_{dn} = 2.86/(1\text{-}Y_{OHO,VFA,anox}) \times NO_3\text{-}N_{ana} + 1.71/(1\text{-}Y_{OHO,VFA,anox}) \times NO_2\text{-}N_{ana} \quad \text{Eq. (3-2)}$$

$$COD_{intra}\ \text{efficiency} = COD_{intra}/COD_{consum} \times 100\% \quad \text{Eq. (3-3)}$$

Where COD_{consum} is the amount of COD consumed in the anaerobic phase, mg/L; COD_{intra} is the COD stored by PAOs and GAOs as PHA and glycogen, mg/L; COD_{dn} is the COD used for denitrification in the anaerobic phase, mg/L; 2.86 is the oxygen equivalent of nitrate, mg COD/mg N; 1.71 is the oxygen equivalent of nitrite, mg COD/mg N; COD_i, $NO_3\text{-}N_{ana}$, and $NO_2\text{-}N_{ana}$ are the initial concentration of sCOD, nitrate, and nitrite at the beginning of the anaerobic phase. $COD_{ana,end}$ is the sCOD concentration at the end of the anaerobic phase. $Y_{OHO,VFA,anox}$ is the OHO yield using VFAs for denitrification, which was assumed to be 0.45 mg COD_{OHO}/mg COD_{VFA} (Metcalf et al., 2014).

The specific nitrate removal rates (SNRRs) were calculated to assess denitrification in Tests 1, 4, 5, and 6, as shown in Eq. (3-4), whereas STINRRs rather than SNRRs were calculated to evaluate denitrification performance for Tests 2 and 3 (Eq. (3-5)) because a small amount of ammonia remaining after the anaerobic phase was included in the analysis. Specific phosphorus removal/release rate (SPRR) (Eq. (3-6)) was investigated to assess the phosphorus removal/release by PAOs. Specific sCOD reduction rate (SCRR) was calculated by using sCOD reduction rate divided by MLVSS (Eq. (3-7))

$$\text{SNRR} = \frac{NO_3\text{-N removal rate}}{\text{MLVSS}} \quad \text{Eq. (3-4)}$$

$$\text{STINRR} = \frac{\text{TIN removal rate}}{\text{MLVSS}} \quad \text{Eq. (3-5)}$$

$$\text{SPRR} = \frac{PO_4\text{-P removal/release rate}}{\text{MLVSS}} \quad \text{Eq. (3-6)}$$

$$\text{SCRR} = \frac{\text{sCOD removal rate}}{\text{MLVSS}} \quad \text{Eq. (3-7)}$$

Where SNRR is the specific nitrate removal rate, mg N/(g VSS·h); STINRR is the specific total inorganic nitrogen removal rate, mg N/(g VSS·h); SPRR is the specific phosphorus removal/release rate, mg P/(g VSS·h); MLVSS is mixed liquor volatile suspended solids in the SBR, g VSS/L; TIN is total inorganic nitrogen in the SBR including NH_4-N, NO_2-N, and NO_3-N, mg N/L; NO_3-N, TIN, PO_4-P, and sCOD removal rates were the rates of NO_3-N, TIN, PO_4-P, and sCOD removal as estimated by linear regression of the measured NO_3-N, TIN, PO_4-P, and sCOD concentrations in the reactor vessel versus time.

The mass of nitrogen removed by each denitrification metabolism in the aerobic phase of SBR operation cycle was estimated to quantitively study the nitrogen removal pathways as shown in Eq. (3-8).

$$\text{Mass of Nitrogen Removed} = (\text{SNRR or STINRR}) \times \text{MLVSS} \times \text{V} \times \text{dt} \quad \text{Eq. (3-8)}$$

Where mass of nitrogen removed is the mass of nitrogen removed by a specific denitrification metabolism in the aerobic phase in a typical cycle, mg N; V is reactor volume, 18 L; dt is the time period over which a specific denitrification metabolism was assumed to be active in the aerobic phase, h.

TIN removal efficiency was calculated to assess the nitrogen removal performance of the SBR system as per Eq. (3-9).

$$\text{TIN removal efficiency} = 1 - \frac{\text{TIN in the effluent}}{\text{TIN in the influent}} \quad \text{Eq. (3-9)}$$

The SND efficiency (Eq. (3-10)) was calculated as the loss of nitrogen during the aerobic phase (Wang et al., 2015).

$$\text{SND} = \left(1 - \frac{NH_{4,e}^{+} + NO_{2,e}^{-} + NO_{3,e}^{-}}{NH_{4,i}^{+} - NH_{4,e}^{+}}\right) \times 100\% \quad \text{Eq. (3-10)}$$

Where $NH_{4,i}^{+}$ is the NH_4-N concentration at the beginning of the aerobic phase, mg/L; $NH_{4,e}^{+}$, $NO_{2,e}^{-}$, and $NO_{3,e}^{-}$ are the NH_4-N, NO_2-N, and NO_3-N concentrations at the end of the aerobic phase, mg/L.

3.2.7. Microbial community analysis

Microbial community composition was analyzed to help predict microorganisms responsible for the phosphorus and nitrogen removal observed in the SBR. For the sample campaign, 50 mL of mixed liquor was collected for 15 consecutive days (from day 123 to day 137; days 128, 131, and 133 were for dynamic tests) from the reactor and then stored at -70℃ until further processing. The analysis of samples from these 15 consecutive days was used to assess whether the system was operating at a steady state.

3.2.7.1. DNA extraction

Total DNA was extracted from 2 mL of MLSS using the DNeasy PowerSoil Pro Kit (Qiagen), with several modifications to the preliminary steps of the manufacturer's protocol. Specifically, the 2 mL sample was centrifuged for 5 min at 10,000 × g prior to extraction. The resulting supernatant was discarded, and the pellet was resuspended in 800 μL of solution CD1 from the DNeasy PowerSoil Pro Kit (Qiagen) before transferring into the PowerBead Pro tube. After vortexing briefly, the PowerBead Pro tube was incubated for 10 min at 65℃ with subsequent homogenization using the FastPrep-24 beadbeater (MP Biomedical, Santa Ana, CA) for 45 s at 5.5 m/s. The remainder of the extraction protocol was conducted as described in the manufacturer's protocol. Extracted DNA samples were quantified using Qubit dsDNA HS Assay Kit (ThermoFisher Scientific) and measured using the NanoDrop 2000 (ThermoFisher Scientific) to assess sample purity. Sample aliquots were stored at -20℃.

3.2.7.2. 16S rRNA gene sequencing

To determine overall microbial community composition, 16S rRNA gene amplification was performed using primers 515F-Y and 926R to target the V4-V5 region of the 16S rRNA gene (Quince et al., 2011). Triplicate PCR amplifications were run in 25-μL reaction volumes for each sample containing 1X ThermoPol buffer, 15 μg of bovine serum albumin, 200 μM of dNTPs, 0.2 μM of both forward and reverse

primers, 0.625 U of Hot Start *Taq* DNA Polymerase (New England Biolabs, MA, USA), and 1-20 ng of template DNA. Sample multiplexing was performed using uniquely barcoded adapters on both the forward and reverse primers of each sample to allow sequencing of a pooled sample library. Amplifications involved an initial denaturation at 95℃ for 3 min, followed by 35 cycles of denaturation at 95℃ for 30 s, annealing at 50℃ for 30 s, and extension at 68℃ for 1 min, with a final extension time of 7 min at 68℃. A positive control containing 1:1 *Aliivibrio fischeri* and *Thermus thermophilus* DNA and a no-template control were also included during amplification and sequencing. Triplicate PCR products were pooled for each sample and quantified using a 1% agarose gel stained with GelRed (Biotium, CA, USA). All samples were then combined at equimolar concentrations to create an amplicon library, which was then sequenced using a MiSeq (Illumina) following the manufacturer's protocol (2 X 250 base paired-end reads).

After sequencing and demultiplexing of paired-end sequences using MiSeq Reporter software version 2.5.0.5 (Illumina), analysis was done using QIIME2 version 2020.6 implemented through the AXIOME3 pipeline (Min et al., 2021). Within the pipeline, DADA2 was used to perform quality trimming, primer sequence removal, denoising, paired-end sequence merging, chimera removal, and final generation of an amplicon sequence variant (ASV) table. Taxonomic classification of amplicon sequences was performed via AXIOME3 using the SILVA database release 132. Assignment of predicted functionality for ASVs was done using Functional annotation of prokaryotic taxa (FAPROTAX) (1.2.4) run through QIIME2 version 2020.6.

3.2.8. Statistical analysis

The normality of data was initially assessed using Excel software 2016 (Microsoft) to validate the subsequent use t-tests for data comparisons. T-tests were conducted with Excel to distinguish differences between two sets of data with the confident interval of 95%. Average, standard deviation, and CV were also performed in Excel software 2016 (Microsoft).

3.3. Results and discussion

3.3.1. SNDPR treatment performance

The establishment of steady-state conditions was assessed prior to analyzing process performance and to ensure that the cycle and activity tests were reflective of steady operation (Figure 3-2). Based on a steady-state definition (i.e., <4% change in substrate concentrations over a two-week period), the SBR system was at a steady state after 60 days of operation. In addition, the microbial community composition for 15 consecutive days starting at day 123 showed consistent profiles (Figure A-1). The dominant organisms included several unique strains of *Dechloromonas*, *Ca.* Competibacter, *Ca.* Accumulibacter, and *Zoogloea* spp. that were consistently present within the SBR system across the sampling period, further indicating that steady state was achieved (Figure A-1). At steady state, effluent concentrations of NH_4-N and NO_2-N were below the method detection limit (MDL; 0.1 mg N/L), effluent concentrations of NO_3-N and PO_4-P were 11 ± 0.6 mg N/L and 0.2 ± 0.11 mg P/L, and MLSS, and MLVSS were 5238 ± 99 mg/L, and 4188 ± 99 mg/L. Overall, the SBR was deemed to have achieved steady state after 60 days of operation.

Steady state performance of the SBR, with respect to nitrogen species, was evaluated to assess the status of nitrification, denitrification, and TIN removal efficiency throughout the experiment (Figure 3-2A). Effluent ammonia was maintained below MDL, indicating the presence of significant AOB activity over the entire period. Nitrate was the main nitrification product with the ratio of effluent NO_3-N/TIN of 98% ± 0.9%, indicating substantial NOB activity in the system. Although prior studies have demonstrated that NOB were washed out in a system with a DO of 0.5 mg/L (Xu et al., 2015), other studies have found that *Nitrospira* lineage I could adapt to oxygen-limiting conditions, resulting in the retention of NOB activity (Zaman et al., 2021). In addition, low temperatures may support NOB activity because the growth rates of NOB are favored (Hellinga et al., 1998). The TIN removal efficiency (as calculated by Eq. (3-9)) was stable with an average value of 62.6% ± 1.7% over the duration of the experiment. Viewed collectively, it is apparent that

substantial biological nitrogen removal was achieved at a low DO concentration (0.3 mg/L) and a low temperature (10℃).

The extent of biological phosphorus removal was assessed to study whether this activity could be sustained under the targeted operating conditions (Figure 3-2B). Effluent phosphorus concentrations were maintained around 0.2 ± 0.1 mg P/L over the whole period. The results are consistent with earlier studies that demonstrated active PAO activity at low temperatures (Lopez-Vazquez et al., 2009b; Wang et al., 2016a). Such PAO performance in the prior studies can be partially attributed to the use of simple carbon sources (e.g., sodium acetate and sodium propionate) that reduced the need for hydrolysis and fermentation, which are typically needed when more complex wastewaters are treated. In the current study, a mix of simple (VFAs) and complex (yeast extract) carbon sources was employed, and the phosphorus removal efficiency of 97% was achieved at 10℃. As will be subsequently demonstrated (Section 3.3.2.), the establishment of SND in the aerobic phase reduced NO_3-N concentrations at the start of the anaerobic phase, leading to low VFA consumption for denitrification in the anaerobic phase. On average, denitrification was estimated to consume 57.7 ± 3.0 mg COD/L of VFAs (as calculated by Eq. (3-2)), leaving an average VFA concentration (not including VFAs generated from yeast extract fermentation) of 132.3 ± 3.0 mg COD/L for uptake by PAOs and GAOs. Hence, the average VFA:P ratio after denitrification was 20.4 ± 0.5, which was higher than the recommended ratio of 8 required for active biological phosphorus removal (Metcalf et al., 2014). Overall, biological phosphorus removal was sustained at 10℃ due to the presence of sufficient VFAs in the influent.

In this study, filamentous bacteria which can cause bulking sludge under low DO were considered. Even though previous studies have illustrated that long SRTs and low DO in the aerobic tank may contribute to serious bulking sludge problems (Kunst and Reins, 1994; Gabb et al., 1991), bulking sludge in this study was not observed. This was consistent with reports that reducing rbCOD loading to the aerobic phase can avoid filamentous bacteria (Jenkins et al., 1993). Around 40 mg/L of rbCOD were consumed in the initial 30 min of the aerobic phase in the current study (Section 3.3.2) and the results suggest that this was

insufficient for the establishment of a filamentous bacteria population. Overall, bulking sludge was not an issue in this study and this was attributed to the low loading of rbCOD to the aerobic phase.

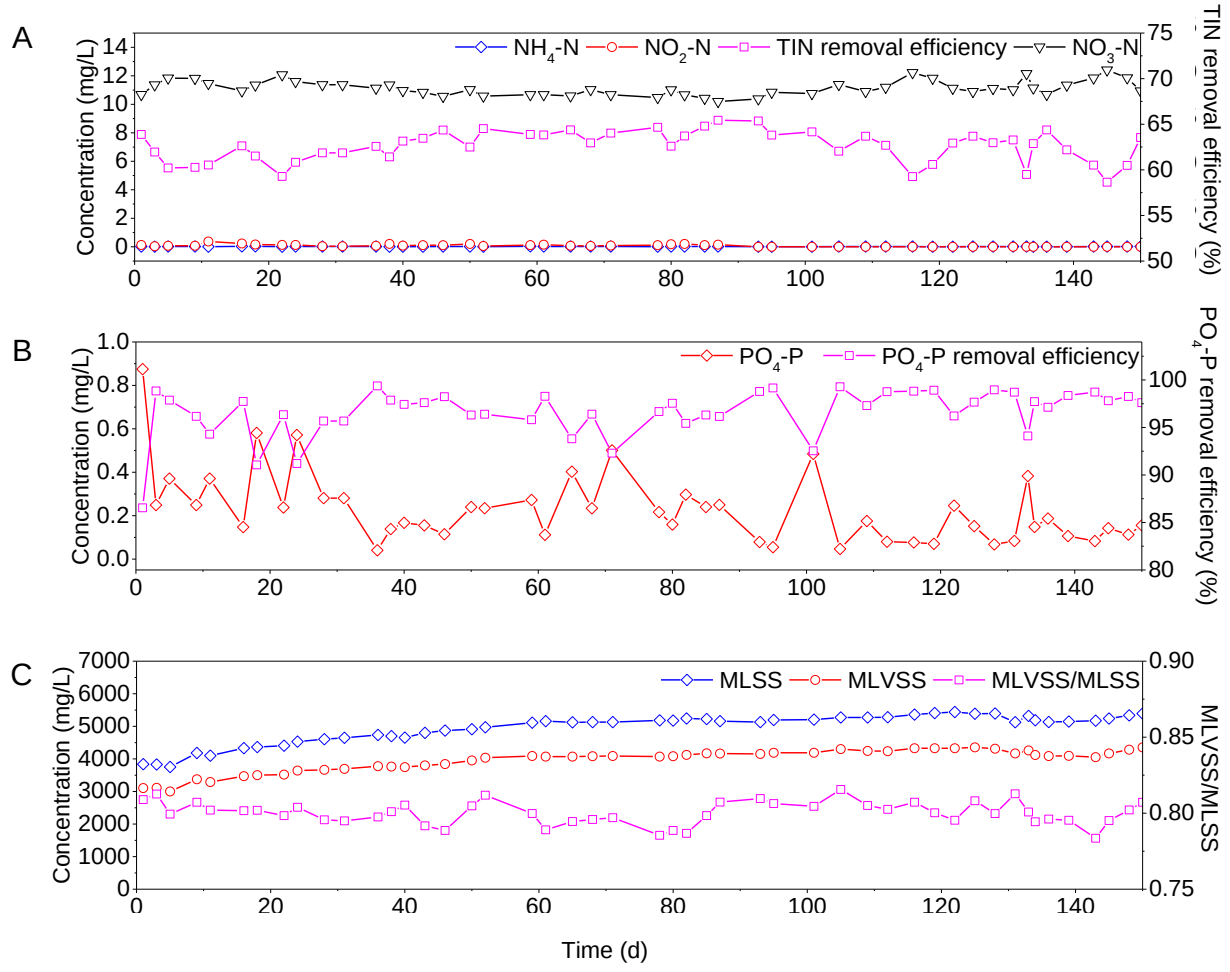

Figure 3-2. Performance of the SNDPR system with the DO in the aerobic phase of 0.3 mg/L and at 10°C.

3.3.2. Dynamic nutrient responses

Although steady-state data provided evidence of overall performance, it provided limited insights into the active metabolisms. Hence, further insights into the biological processes were obtained by conducting dynamic tests under steady-state conditions where the transient responses of nitrogen species, phosphorus,

sCOD, PHA, and glycogen in the SBR were characterized through intensive sampling and analysis (Figure 3-3). Low average CVs ranged from 2% to 25%, indicating a high degree of reproducibility and consistency within the SBR over the period of the triplicate testing.

In the anaerobic phase, ammonification was assessed by evaluating the increase of ammonia concentrations that were reduced due to nitrification in the following aerobic phase (Figure 3-3A). Average ammonia concentrations increased from 14.6 ± 0.1 to 16.6 ± 0.1 mg N/L after the addition of influent, which was attributed to ammonification of organic nitrogen from the yeast extract. Compared with a prior study that employed a simple carbon source (Wang et al., 2016a), the use of a complex carbon source in the system generated more ammonia via ammonification that needed to be removed in the subsequent aerobic phase.

In the anaerobic phase, polyphosphate hydrolysis to release phosphorus was assessed within the context of PAO activity (Figure 3-3B). Phosphorus concentrations increased from minimal to 34.6 ± 1.3 mg P/L in the anaerobic phase. Specific phosphorus release rates were calculated through Eq. (3-6) and found to be 12.5 mg P/(g VSS·h) in the first 40 minutes and 0.9 mg P/(g VSS·h) for the next 20 minutes. In the first stage (first 40 min), phosphorus release was attributed to the storage of influent VFAs by PAOs, whereas in the second stage (40 min to 60 min) phosphorus release was attributed to VFAs that were fermented from yeast extract. The release of phosphorus due to hydrolysis of organic phosphorus from the yeast extract was negligible because the yeast extract solution was found to have minimal soluble organic phosphorus. Overall, two-stage phosphorus release was observed due to the presence of the complex carbon source in the influent.

In the anaerobic phase, sCOD was assessed to confirm the hypotheses regarding phosphorus release (Figure 3-3B). The sCOD was reduced linearly to 64.2 ± 3.1 mg COD/L in the first 40 min. Specific sCOD reduction rates were calculated through Eq. (3-7) with values of 13.4 and 7.1 mg COD/(g VSS·h) for the first 40 and subsequent 20 minutes, respectively. The reduction of sCOD in the first stage (first 40 min) was attributed to uptake of influent VFAs by PAOs and GAOs, and the second stage (40 min to 60min)

response was attributed to uptake of VFAs that were produced by yeast extract fermentation. The two-stage sCOD reduction showed interrelationship with the two-stage phosphorus release. Most of sCOD reduction was estimated to be stored as intracellular carbon with the COD_{intra} efficiency of 77% using Eq. (3-3). Hence, the use of complex carbon sources resulted in two stages of sCOD reduction and phosphorus release in the anaerobic phase.

Using the 16S rRNA gene microbial community data, FAPROTAX analysis was performed to better predict taxa responsible for yeast extract fermentation to VFAs. The definition of FAPROTAX categories and terminology is presented in Appendix A-3. The values presented are based on the results obtained on the days when the dynamic tests were conducted (days 128, 131, and 133; Figure 3-4). The results suggest that 3.6% ± 0.4% of microbial community with confident functional assignments were associated with fermentation. Fermentation was predicted specifically for the genera *Lactococcus* and *Tetrasphaera* that had relative abundances of 1% ± 0.1% and 1.2% ± 0.6% within the total community, respectively. Previous study has shown that these genera can ferment carbohydrates to lactic acid, acetic acid, and formic acid (Liu et al., 2019). These bacteria likely contributed to the fermentation that occurred in the anaerobic phase.

The ratio of P released to sCOD uptake was evaluated as an indicator of PAOs and GAOs in the SBR. The average value of this ratio was 0.28 ± 0.01 mg P/mg COD (0.25 ± 0.01 mol P/mol C), which was consistent with reported values of 0.3-0.43 mg P/ mg COD in PAO-rich systems (Kuba et al., 1997; Zaman et al., 2021). The ability of PAOs to outcompete GAOs under low DO conditions has been attributed to the higher oxygen affinity of PAOs as compared to GAOs (Zaman et al., 2021). Low temperatures (10°C) have also been reported to favor the growth of PAOs over GAOs (Tian et al., 2017) because PAOs have lower anaerobic maintenance requirements, and GAOs have lower growth rates at low temperatures (10-20°C) (Lopez-Vazquez et al., 2008). Based on the observed ratio of P released to sCOD uptake, it was anticipated that PAOs were the dominant bacteria responsible for sCOD uptake in the anaerobic phase. This was further

evaluated in the activity tests where the roles of DGAOs and DPAOs in subsequent denitrification were assessed.

The responses of PHA and glycogen in the anaerobic phase were assessed along with other substrates to further evaluate the prevalence of PAOs in the system (Figure 3-3C). In this analysis, PHA concentrations consisted of the sum of PHB, PHV, and PH2MV. The PHA concentration increased from 2.4 ± 0.23 to 5.6 ± 0.11 mmolC/L and glycogen decreased from 1.77 ± 0.12 to 0.56 ± 0.11 mmolC/L in the anaerobic phase. The increase of PHA concentrations has been associated with VFA uptake and glycogen consumption (Metcalf et al., 2014). The ratios of P release to PHA generation (0.36 ± 0.03 molP/molC), PHA generation to glycogen consumption (2.69 ± 0.45 molC/molC), and PHA generation to COD storage (1.68 ± 0.28 molC/molC) were estimated to characterize the stoichiometry of the storage process. The estimated values were found to be consistent with those reported for a PAO-rich system (0.38 molP/molC, 2.66 molC/molC, and 1.33 molC/molC) (Smolders et al., 1994). In summary, PHA and glycogen data provided further evidence to indicate that the SBR was a PAO-rich system.

In the aerobic phase, the responses of NH_4-N, NO_2-N, and NO_3-N with time were assessed to investigate AOB nitritation and NOB nitratation activities (Figure 3-3A). The NH_4-N concentration decreased from 16.6 ± 0.1 to 0.6 ± 0.2 mg N/L within 4 h. In contrast, NO_2-N concentrations reached a maximum at 5 h, with an average value of 0.3 ± 0.1 mg N/L. The NO_3-N concentration reached a maximum of 11.6 ± 0.3 mg N/L at 5.5 h, indicating active NOB nitratation. Although prior studies have suggested that low DO concentrations could be used to washout NOB with nitrite accumulation (Zaman et al., 2021), NOB were active in the current system, indicating that NOB adapt to low DO and were retained at the SRT of 30 days. Viewed collectively, AOB nitritation and NOB nitratation were active in the system operated at a DO of 0.3 mg/L and 10°C; nitrate was the main product.

The FAPROTAX analysis revealed predicted metabolic functionality of the microbial community associated with nitrification in the SBR (Figure 3-4). Aerobic ammonia oxidation and aerobic nitrite

oxidation functions were predicted to represent 0.5% ± 0.1% and 0.4% ± 0.1% of the total community. Specifically, the results indicate that ammonia oxidation (nitritation) within the SBR was likely performed by AOB associated with the family *Nitrosomonadaceae* (0.61% ± 0.2%); members of this family are well characterized AOB (Metcalf et al., 2014). Although the relative abundance of predicted aerobic ammonia oxidation metabolism comprised a small proportion of the total community, full nitrification of ammonia in the dynamic tests was established. The genera *Nitrospira* and *Nitrotoga*, representing 0.5% ± 0.1% and 0.3% ± 0.03% of the total microbial community respectively, were the dominant bacteria associated with aerobic nitrite oxidation, and both are well-known NOB (Metcalf et al., 2014). The dominant presence of *Nitrospira* and *Nitrotoga* under low DO conditions may be a result of their high affinity for oxygen (Metcalf et al., 2014). *Nitrospira* uses carbon (CO_2) fixation pathways that contain enzymes which are sensitive to the presence of oxygen, so *Nitrospira* often favors lower oxygen concentration environments compared with organisms that do not have oxygen sensitive carbon fixation pathways (Lücker et al., 2010). The *Nitrospira* have also been observed to increase in winter seasons, implying adaptation at low temperatures (Liu et al., 2019). Nitrification in the SBR appeared to be primarily due to genera *Nitrosomonas*, *Nitrotoga*, and *Nitrospira*.

The nitrogen species responses in the aerobic phase were further analyzed to investigate the extent to which SND was active (Figure 3-3A). The ratios of the accumulated NO_x-N/oxidized NH_4-N were calculated for each hour in the aerobic phase as an indicator of SND activity. For the first and second hour of the aerobic phase, the ratios were 12% ± 1% and 68% ± 4%, respectively, whereas the ratios were near 100% for subsequent hours. Hence, a majority of SND appeared to occur in the initial portion of the aerobic phase. In addition, the overall SND efficiency of the aerobic phase was calculated by Eq. (3-10) to evaluate SND activity and determined to be 31%. The denitrification observed in the early portion of the aerobic phase may have been conducted by denitrifying OHOs using residual rbCOD from the anaerobic phase and/or DPAO and DGAO denitrification, because rbCOD, phosphorus, and PHA were available during this period. Denitrification by DPAOs and DGAOs has been previously reported to occur under low DO conditions (Ji

et al., 2020; Wang et al., 2016b). Separate tests, that are subsequently described (see Section 3.3.4.), were conducted to delineate the contribution of bacterial populations to denitrification in the aerobic phase.

Phosphorus uptake in the aerobic phase was examined to gain insights into the activity of PAOs in the SBR (Figure 3-3B). Phosphorus concentrations were reduced from 35.7 ± 1.3 to 0.5 ± 0.1 mg P/L in the first hour (1 h-2 h), and this might be a result of aerobic and anoxic PAO uptake. Phosphorus concentrations remained low for the remainder of the phase, suggesting minimal subsequent PAO activity. Biological phosphorus removal was consistent with the high sCOD/TP ratio of 43 ± 1.2 mgCOD/mgP after denitrification in the anaerobic phase and the high value of COD_{intra} efficiency of 77% ± 1% that were previously discussed. The presence of biological phosphorus removal indicates that biological phosphorus removal can be sustained at a low DO of 0.3 mg/L and low temperature of 10°C if substrate and operating conditions (i.e., SRT) are appropriate.

For the aerobic phase, PHA and glycogen concentrations (Figure 3-3C) were assessed in combination with the phosphorus response to further characterize the status of PAOs in the SBR. The ratios of phosphorus uptake to PHA oxidized (0.36 ± 0.03 molP/molC) and glycogen replenishment to PHA consumption (0.38 molC/molC) were estimated and found to be similar to ratios reported for a PAO-rich system (0.406 molP/molC and 0.42 molC/molC, respectively) (Smolders et al., 1994). These results provide further evidence that the community established under low DO and temperature conditions was rich in PAOs.

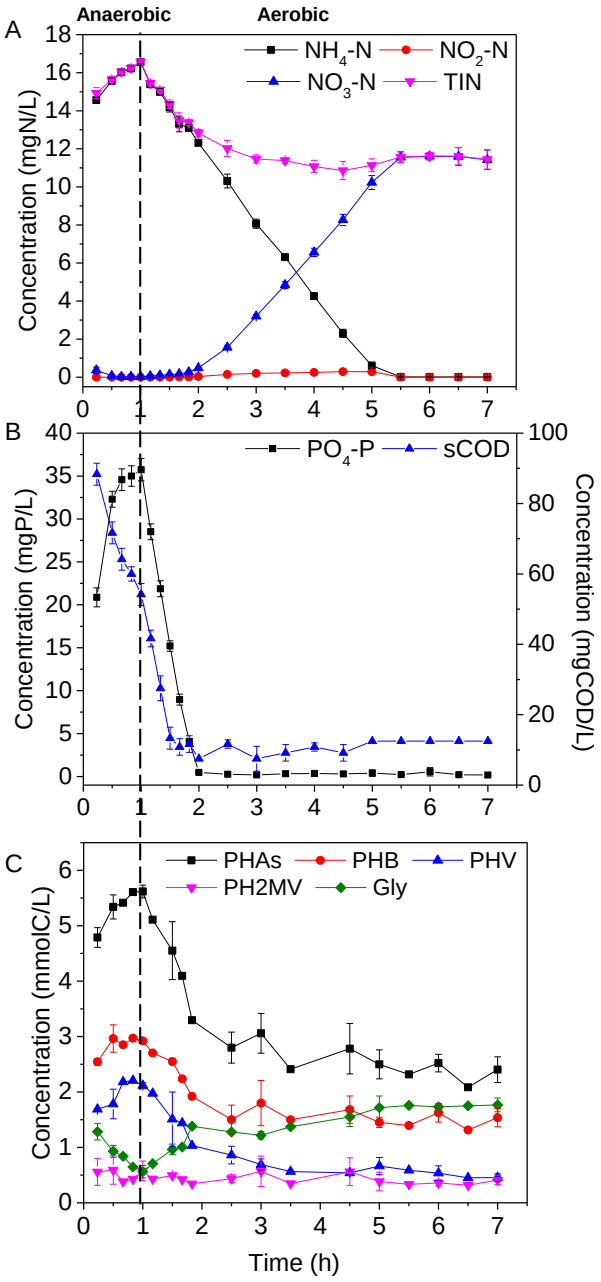

Figure 3-3. Transient responses observed in triplicate SBR cycles with the DO in the aerobic phase of 0.3 mg/L and at 10°C. A: nitrogen species profiles; B: phosphorus and soluble COD profiles; C: PHB, PHV, PH2MV, PHAs, and glycogen profiles. Markers represent average values of triplicate tests, and error bars represent associated standard deviations.

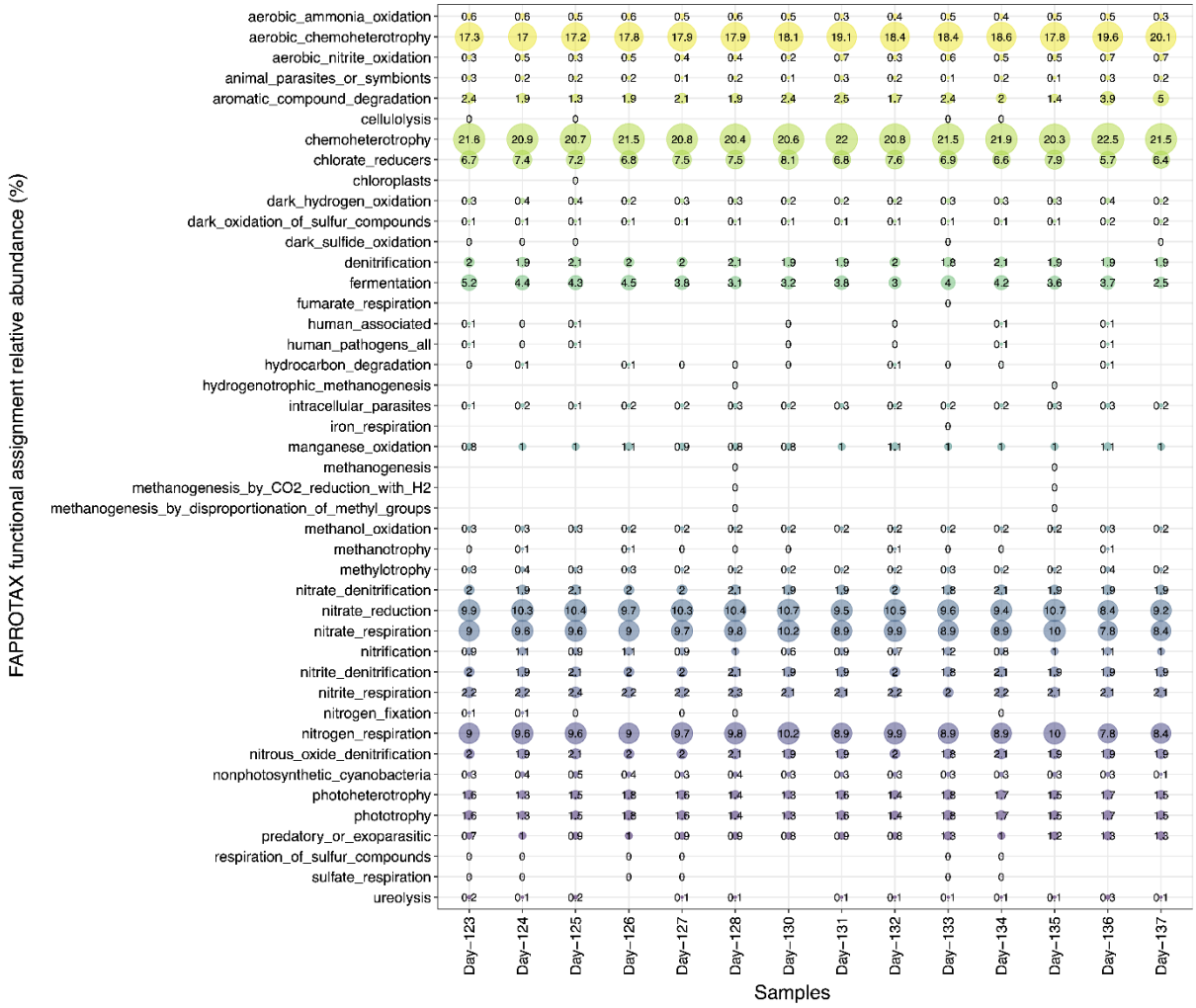

Figure 3-4. Metabolic functions of bacteria based on FAPROTAX results for 15 consecutive days (the numbers inside circles represent relative abundances in percent). Days 128, 131, and 133 were the days of dynamic tests.

3.3.3. Evaluation of denitrification under anoxic conditions

Tests 1-3 were conducted under anoxic conditions at 10℃ to investigate denitrifying OHO, DGAO, and DPAO activities through observation of denitrification responses under different environments (Figure 3-5). Triplicate tests were conducted for each test to confirm the reproducibility and analyze the uncertainty in these tests. The average CV values of each species in Tests 1-3 were in the range of 1%-2%, indicating consistent results with high reproducibility.

Test 1 studied the metabolism of denitrifying OHOs using hydrolyzed carbon under anoxic conditions to assess the existence of denitrifying OHOs in the SBR (Figure 3-5A). Nitrate was reduced linearly from 11.6 ± 0.5 to 8.1 ± 0.1 mg N/L over two hours, yielding an SNRR value of 0.44 ± 0.08 mg N/(g VSS·h). Because there was limited sCOD, NO_2-N, PO_4-P, and PHA in the system at the beginning of these tests, the reduction of nitrate was attributed to denitrifying OHOs using hydrolyzed carbon. Cell decay can provide a source of particulate biodegradable material, which can be converted to rbCOD through hydrolysis. The linear nitrate response indicates that cell decay and hydrolysis were occurring at constant rates to provide rbCOD for denitrifying OHO denitrification. In summary, denitrifying OHOs were demonstrated to exist with an SNRR value of 0.44 mg N/(g VSS·h) when hydrolyzed carbon was used as a carbon source under anoxic conditions at 10℃.

Test 2 was designed to identify nitrate reduction by the combination of denitrifying OHOs using hydrolyzed carbon and DGAOs using stored polymers under anoxic conditions. The presence of DGAO activity was assessed by comparing Test 2 SNRR values that were calculated based on Eq. (3-4) with those of Test 1. Nitrate was reduced linearly from 14.7 ± 0.2 to 12.9 ± 0.1 mg N/L with the SNRR values estimated to be 0.47 ± 0.06 mg N/(g VSS·h) (Figure 3-5B), which was not significantly different from that of Test 1 (p>0.05), indicating limited DGAO activity in the system.

The microbial profile data were investigated to determine whether known DGAOs were detected in the system. Prior studies have shown that *Ca.* Competibacter has the ability to reduce nitrate to nitrite under

anoxic conditions and function as a DGAO (Lemaire et al., 2006; Rubio-Rincón et al., 2017). Hence, its presence in the community was specifically examined. Although ASVs associated with *Ca*. Competibacter were detected in the reactor (10.4% ± 0.6%), reduction of nitrate was not observed in Test 2, indicating lack of activity of *Ca*. Competibacter at 10°C. Prior studies have indicated that anaerobic carbon storage by *Ca.* Competibacter was inactive at 10°C (Lopez-Vazquez et al., 2009a), which supports limited DGAO activity observed under anoxic conditions in Test 2 because DGAOs need stored carbon for denitrification (Wang et al., 2016a). Overall, *Ca.* Competibacter existed in the system as a potential DGAO but it did not appear to be active due to the low temperature (10°C).

Test 3 evaluated denitrification by the combination of denitrifying OHOs using hydrolyzed carbon and DGAOs and DPAOs using PHA under anoxic conditions (Figure 3-5C). Hence, the activity of DPAOs was assessed by comparing SNRR values that were calculated by Eq. (3-4) to those from Test 2. We observed linear reduction in nitrate that yielded an SNRR value of 2.98 ± 0.07 mg N/(g VSS·h). The difference in SNRR values between Tests 3 and 2 was attributed to the addition of phosphorus in Test 3 that supported DPAO activity in addition to the previously described mechanisms. Compared with SNRRs of Test 2, SNRRs of Test 3 increased by 2.53 ± 0.1 mg N/(g VSS·h), which was attributed to the substantial role of DPAO denitrification (i.e., 559% increase from the average of Tests 3 and 2). Therefore, DPAO denitrification was demonstrated as a dominant process for nitrogen removal under anoxic conditions in the absence of rbCOD.

The members of the SBR microbial community that may have been associated with DPAO denitrification were investigated using FAPROTAX analysis, which revealed that 9.8% of the predicted metabolic function within the community was associated with nitrate reduction, a preliminary step in the denitrification pathway (Figure 3-4). The genera *Aeromonas* (0.2%), *Ideonella* (0.6%), *Thauera* (0.3%), *Paracoccus* (0.3% ± 0.01%), *Dechloromonas* (9.5% ± 0.9%), and *Zoogloea* (2.3% ± 0.3%) have a predicted nitrate reduction metabolism based on FAPROTAX analysis. Among these genera, *Dechloromonas* (9.5% ± 0.9%), *Zoogloea* (2.3% ± 0.3%), and *Paracoccus* (0.3% ± 0.01%) have predicted metabolic functions for

both nitrate reduction and phosphorus uptake, making them likely candidates as DPAOs in the SBR (Wang et al., 2015). The high abundance of these genera likely resulted in the elevated SNRR observed under anoxic conditions in Test 3. Many studies have also shown that *Dechloromonas* is the dominant DPAO at low temperatures (He et al., 2020b; Wang et al., 2020). Therefore, reductions of nitrate and phosphorus in Test 3 were likely mainly due to the activity of *Dechloromonas* as a DPAO.

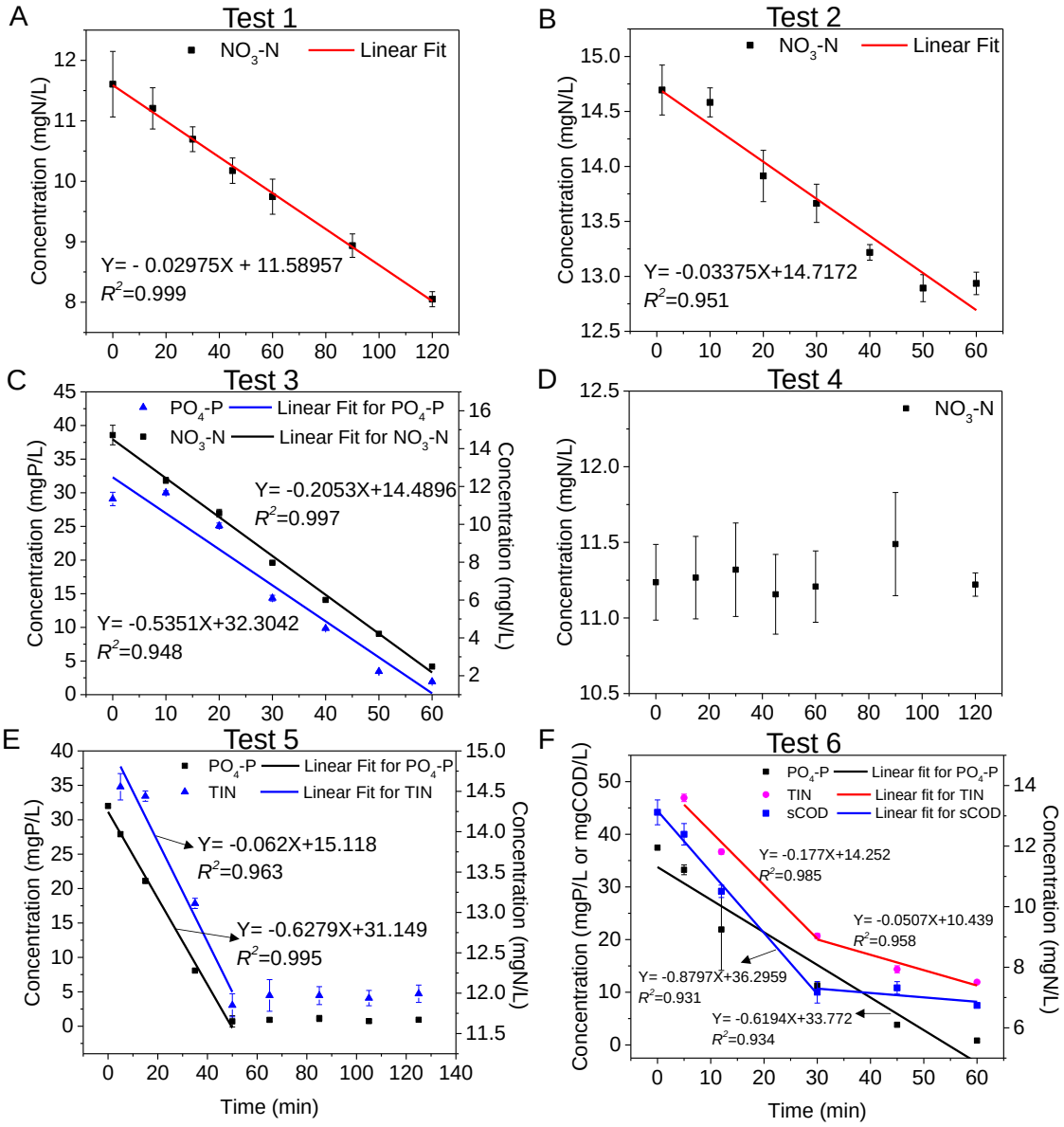

Figure 3-5. The status of denitrification by denitrifying OHOs using hydrolyzed carbon (A), DGAOs (B), and DPAOs (C) in the SNDPR system under anoxic conditions at 10°C (Tests 1-3) and denitrification by denitrifying OHOs using hydrolyzed carbon (D), DGAOs and DPAOs (E), and denitrifying OHOs using residual rbCOD from the anaerobic phase (F) under oxic conditions at a DO of 0.3 mg/L and 10°C (Tests 4-6). Markers represent average values of triplicate tests, and error bars represent associated standard deviations.

3.3.4. Evaluation of denitrification under low dissolved oxygen conditions

Tests 4-6 were conducted to study the active denitrification pathways and the corresponding nitrogen removal amounts during the aerobic phase which was operated at a low dissolved oxygen concentration (i.e., 0.3 mg/L) and temperature (i.e., 10°C). As with Tests 1-3, the potential denitrification pathways that were investigated included denitrifying OHOs using hydrolyzed carbon (Test 4), DPAOs using intracellular PHA (Test 5), DGAOs using intracellular PHA (Test 5), and denitrifying OHOs using residual rbCOD from the anaerobic phase (Test 6). The uncertainty of each substrate was assessed based on average CV of each substrate. The average CV values were in the range of 1% to 21%, which revealed consistent results and high reproducibility.

Test 4 was designed to study nitrogen removal by denitrifying OHOs using hydrolyzed carbon at a DO of 0.3 mg/L under conditions that were representative of the aerobic phase of the SBR (Figure 3-5D). Observed nitrate concentrations remained constant at 11.3 ± 0.3 mg N/L. Compared to Test 1, which showed denitrification by denitrifying OHOs using hydrolyzed carbon under anoxic conditions, the results of Test 4 indicate that denitrification by denitrifying OHOs using hydrolyzed carbon did not occur at a significant rate when the DO was 0.3 mg/L, which was consistent with the results of the dynamic SBR tests (5.5 h to 7 h). Hence, this pathway likely did not contribute substantially to nitrogen removal in the SBR in the aerobic phase.

Test 5 was divided into two periods based on the trends of TIN and phosphorus concentrations (Figure 3-5E), which allowed for separate investigation of denitrification by DPAOs and DGAOs using intracellular PHA at a DO of 0.3 mg/L. Most of the TIN was present as NO_3-N, with only 8% present as NH_4-N at the beginning of the test due to ammonification in the anaerobic phase. The STINRR and SPRR values were calculated based on Eq. A5 and Eq. (3-6). During the period from 0 min to 50 min, TIN and phosphorus were reduced linearly, yielding STINRR and SPRR values of 0.89 ± 0.02 mg N/(g VSS·h) and 9.01 ± 0.24 mg P/(g VSS·h), respectively. During the period from 50 min to 130 min, TIN and phosphorus

concentrations remained constant around 12.0 ± 0.1 mg N/L and less than 1 mg P/L, respectively. The results demonstrate that limited denitrification happened in the second period where phosphorus was absent. Therefore, it is concluded that denitrification by DGAOs and denitrifying OHOs did not occur at a DO of 0.3 mg/L, which was consistent with the conclusions of the dynamic tests (3 h to 7 h) and Test 2.

The difference between the first (from 0 min to 50 min) and second (from 50 min to 130 min) periods in Test 5 was employed to quantify denitrification by DPAOs at a DO of 0.3 mg/L. Because low concentrations of sCOD were present (10.1 ± 2.4 mg/L) at the start of the first period, we conclude that denitrifying OHOs using residual rbCOD did not contribute substantially to denitrification in this period. Hence, the observed TIN reduction in the first period was attributed to DPAO denitrification because both the reductions of TIN and phosphorus were observed and DGAO denitrification was found to be inactive. In summary, with a DO of 0.3 mg/L, a temperature of 10℃, and limited rbCOD availability, nitrogen removal in the initial period of the aerobic phase was attributed to DPAO denitrification with an STINRR of 0.89 ± 0.02 mg N/(g VSS·h).

The ASV table was assessed to investigate whether the PO_4-P uptake in the first period (from 0 min to 50 min) of Test 5 was due to both aerobic growth by PAOs and anoxic growth by DPAOs. As shown earlier, PO_4-P uptake by DPAOs was demonstrated by the reductions of PO_4-P and NO_3-N in the first period of Test 5 and by the presence of recognized DPAOs in the community. In addition, the ASV table indicates that *Ca.* Accumulibacter, a known aerobic PAO (Yuan et al., 2020), was detected in the system with a relative abundance of 3.5% ± 0.3%. Further, *Tetrasphaera*, which has been identified to be capable of fermentation, has also been acknowledged to act as an aerobic PAO (Close et al., 2021). Therefore, it was concluded that the observed phosphorus reduction in the first period of Test 5 was due to both PAOs and DPAOs.

Test 6 was used to quantify nitrate removal by denitrifying OHOs using residual rbCOD from the anaerobic phase (Figure 3-5F). The STINRR and SPRR values were calculated based on Eq. (3-5) and Eq. (3-6) to

facilitate interpretation of active processes in the test. The results show that in the first period (0 min to 30 min) sCOD, PO_4-P, and TIN were reduced linearly with specific reduction rates of 16.9 ± 0.4 mg COD/(g VSS·h), 9.05 ± 0.5 mg P/(g VSS·h), and 2.59 ± 0.1 mg N/(g VSS·h), respectively. In the second period (30 min to 60 min), phosphorus uptake continued at the same SPRR, the STINRR was reduced to 0.74 ± 0.05 mg N/(g VSS·h), and sCOD concentrations (9.4 ± 1.1 mg/L) did not change. The reduction in STINRR values between the first and second periods of the test appeared to correspond to depletion of rbCOD in the second period. Hence, enhanced denitrification in the first period was attributed to denitrifying OHOs using residual rbCOD from the anaerobic phase. The SPRR value of 9.05 ± 0.5 mg P/(g VSS·h) was similar to that of Test 5 (9.01 ± 0.24 mg P/(g VSS·h)), suggesting a similar mechanism of P uptake despite the increased rbCOD available in Test 6. The STINRR value of 0.74 ± 0.05 mg N/(g VSS·h) in the second period of Test 6 was similar to that observed in Test 5 (0.89 ± 0.02 mg N/(g VSS·h)), which had been attributed to DPAO activity. The STINRR value associated with denitrifying OHO denitrification using residual rbCOD was estimated as the difference between those from periods 1 and 2 of Test 6 and determined to be 1.84 ± 0.16 mg N/(g VSS·h). Overall, the reduction of nitrogen is dependent on both denitrification by denitrifying OHOs using residual rbCOD and DPAOs with the denitrification by denitrifying OHOs as the dominant process.

Nitrogen mass balance was performed to study the nitrogen removal pathways in the SNDPR system (Table 3-2). In the analysis, nitrogen entered from the influent, and left through four ways: 1) decanting; 2) biomass synthesis; 3) denitrification by denitrifying OHOs in the anaerobic phase; and 4) denitrification by denitrifying OHOs using residual rbCOD and DPAOs in the aerobic phase. The detailed calculations to obtain the values in Table 3-2 are shown in Appendix A. The relative error in the mass balance closure using this approach was 7% ± 1.6%, which was deemed to be acceptable as it was within the range of measurement errors. The mass balance closure provided a high level of confidence in the estimated nitrogen fate mechanisms.

The fate of nitrogen through the SBR in each cycle was estimated on the basis of observed influent and effluent mass flows, and estimates of the contributions of each denitrification process to nitrogen removal that were derived from the activity tests (Table 3-2). The results show that 27% ± 1% of influent nitrogen was removed through SND in the aerobic phase by denitrifying OHO denitrification using residual rbCOD (15% ± 1%) and DPAO denitrification (12% ± 1%). It was predicted that more nitrogen might be removed in the aerobic phase if the DO was maintained at a value lower than 0.3 mg/L to trigger denitrification by denitrifying OHOs using hydrolyzed carbon. However, the nitrification rate would be reduced at a lower DO level, resulting in the need for a longer hydraulic retention time. Nitrogen removal through cell synthesis accounted for 18% ± 1% of the total influent nitrogen, which is similar to 24% if the bacteria formula was assumed to be $C_5H_7O_2N$ (Metcalf et al., 2014). Due to the presence of sufficient rbCOD from the influent, all the residual nitrate from the prior cycle was denitrified in the anaerobic phase, which represented 22% ± 1% of the influent nitrogen mass. The nitrogen removal mass in the anaerobic phase was less than that in the aerobic phase due to denitrification and cell growth, which indicated that SND in the aerobic phase removed a substantial nitrogen in the system, leading to an improvement of nitrogen removal efficiency. During the decant stage, 50% of liquid volume was decanted, in which nitrate and soluble organic nitrogen were the main nitrogen components, resulting in 33% ± 1% of the influent nitrogen removal. Overall, 45% of the influent nitrogen was removed through cell synthesis and SND in the aerobic phase, indicating the level of success of the SNDPR process.

The potential for nitrous oxide (N_2O) emissions were considered when determining whether nitrogen removed through N_2O emission should be included in the nitrogen mass balance. Even though many studies have found that N_2O could be generated when operating under low DO conditions, most reports have indicated that nitrogen removed through N_2O emission is less than 3% of the nitrogen load (Kampschreur et al., 2009). Liu et al. (2021) demonstrated nitrogen removed through N_2O emission was 0.11% when a system was operated at a DO of 0.41mg/L for an extended period of time. Therefore, nitrogen removal through N_2O emission was deemed to be too low to be considered in the nitrogen mass balance.

Table 3-2. Nitrogen mass balance for a typical cycle with the DO in the aerobic phase of 0.3 mg/L and at 10℃.

N mass component	Mass[1] (mg N)	Proportion (%)
N mass in from influent	441 ± 22	
N mass used for cell synthesis	87 ± 4	18 ± 1
N mass decant from the system	157 ± 12	33 ± 1
N mass denitrified in the anaerobic phase	103 ± 5	22 ± 1
N mass removed through denitrifying OHOs using residual carbon in the aerobic phase	70 ± 6	15 ± 1
N mass removed through DPAOs using PHA in the aerobic phase	56 ± 4	12 ± 1
Calculated N mass in from influent	472 ± 18	

Note: The calculation of values is shown in Appendix A. Relative error is 7% ± 2%.

[1] Volume of the SBR was 18 L, and the volume of feed and decant was 9 L.

3.4. Conclusions

The results of this study demonstrate that SNDPR was achieved at 10℃ with TIN and PO_4-P removal efficiencies of 62.6% and 97%, respectively. Fermentation was not the rate-limiting process for SNDPR at low temperatures in this study. SND in the aerobic phase was due to denitrifying OHOs using residual rbCOD and DPAOs. A PAO-rich system was supported by both stoichiometric ratios and 16S rRNA gene analysis, with *Dechloromonas*, *Zoogloea*, and *Paracoccus* predicted as DPAOs, and *Ca.* Accumulibacter and *Tetrasphaera* as PAOs. This demonstrated that PAOs are favor to grow at low temperatures. *Ca.* Competibacter (10.4%) was detected, whereas limited DGAO denitrification was observed, which might be due to low temperatures. This research was the few researches that investigated the SNDPR process at 10℃ by using a complex synthetic wastewater, investigated the nitrogen removal pathways in the aerobic phase using an experimental method, and integrated microbial community analysis with experimental findings.

Chapter 4 Simultaneous nitrification, denitrification, and phosphorus removal to treat real municipal wastewater in an activate sludge system at a low temperature

Abstract

The feasibility of simultaneous nitrification, denitrification, and phosphorus removal (SNDPR) at a low temperature (10℃) when treating real municipal wastewater was explored by implementing two process configurations (anaerobic/aerobic and anaerobic/aerobic/anoxic). It was found that SNDPR in the anaerobic/aerobic configuration failed, however, SNDPR in the anaerobic/aerobic/anoxic configuration was achieved with total nitrogen removal, phosphorus removal, and simultaneous nitrification and denitrification (SND) efficiencies of 91.1%, 92.4%, and 28.5%, respectively. The main nitrogen removal pathways were denitrification by denitrifying phosphorus accumulating organisms (DPAOs) in the aerobic phase and denitrifying ordinary heterotrophic organisms using hydrolyzed carbon in the anoxic phase, which accounted for 16% and 56% of influent nitrogen, respectively. A phosphorus accumulating organism (PAO)-rich system was indicated by stoichiometric ratios and supported by 16S rRNA gene analysis, with *Dechloromonas* and *Ca.* Accumulibacter as dominant DPAOs and PAOs. *Ca.* Competibacter was detected, whereas limited denitrifying glycogen accumulating organism denitrification was observed, which might be due to low temperatures. This research was the first to 1) investigate the performance of SNDPR when real municipal wastewater was treated under low temperature conditions (10℃); 2) investigate whether operational conditions that have been successfully employed to treat synthetic wastewaters can also be applied to real municipal wastewaters; 3) compare the performance of SNDPR when operated in different process configurations (AO and AOA).

Keywords: Low temperature; Simultaneous nitrification, denitrification, and phosphorus removal; Anaerobic/aerobic/anoxic; Municipal wastewater; Functional annotation of prokaryotic taxa

4.1. Introduction

Simultaneous nitrification, denitrification, and phosphorus removal (SNDPR) has been demonstrated to be a successful advanced nutrient removal technology (Ji et al., 2020; Yuan et al., 2020). The advantages of SNDPR include low energy consumption, reduced chemical requirements, and reduced footprint (Ju et al., 2007). SNDPR has been successfully employed to treat a variety of wastewaters including those from abattoirs (Yilmaz et al., 2008), food-processing (Cheng et al., 2021), and aniline production (Yang et al., 2021)). In addition, performance under a range of operating conditions including low C/N ratio (Wang et al., 2016c), low organic loadings due to wet weather (Li et al., 2021), and low atmosphere pressure (Chen et al., 2020) has been reported. Viewed collectively, it is apparent that SNDPR is a promising technology for removing carbon, nitrogen, and phosphorus in a broad range of applications.

Even though SNDPR has been demonstrated in room temperatures, low-temperature operation (lower than 15℃) is still not fully understood. At low temperatures, the activities of biological processes including hydrolysis of biodegradable particulate matter, fermentation, nitrification, denitrification, and phosphorus release and uptake are significantly reduced or inhibited (Henze et al., 2000). Of particular significance to SNDPR processes is the low reaction rates for hydrolysis and fermentation at low temperatures that can limit the availability of readily biodegradable organics to support nitrogen and phosphorus removal (Yuan et al., 2011). Hence a detailed understanding of carbon transformations in low temperature conditions is critical for optimizing SNDPR processes for winter operations.

At low temperatures, successful SNDPR has been reported in studies that have used synthetic wastewaters (Li et al., 2019; Bai et al., 2022); however, few reports describing use of real municipal wastewaters have

been published. Typically, synthetic and municipal wastewaters differ in the complexity of the organic matter (He et al., 2016; Zaman et al., 2021). Most of the carbon sources employed in studies using synthetic wastewaters have been composed of simple volatile fatty acid mixtures (VFAs) (Li et al., 2019). In comparison, VFAs represent only 5%-18% of the total chemical oxygen demand (COD) in real municipal wastewaters, and additional VFAs need to be generated through fermentation of readily biodegradable COD (rbCOD), that typically accounts for 47%-53% of total COD (Henze & Comeau, 2008). Additionally, slowly biodegradable COD needs to be hydrolyzed before utilization for nitrogen and phosphorus removal. Besides carbon substrates, real municipal wastewaters contain organic nitrogen that releases ammonia through hydrolysis. The additional ammonia generated from hydrolysis increases the required nitrification capacity and biodegradable COD needed for denitrification in the SNDRP process (Zhu et al., 2021). The increased complexity of real municipal wastewaters creates some uncertainty about whether SNDPR operational strategies that were developed with synthetic wastewaters can be directly transferred to real municipal wastewater applications. Therefore, it is necessary to investigate whether real municipal wastewaters can be treated with the same SNDPR operational strategies that were found to work for synthetic wastewaters.

Besides operational temperature and influent characteristics, the process configuration and redox cycling should be considered in the adoption of SNDPR for real municipal wastewater treatment. SNDPR has been reported during treatment of municipal wastewaters in both anaerobic/aerobic (AO) and anaerobic/aerobic/anoxic (AOA) process configurations. In the AO configuration, intracellular carbon storage (polyhydroxyalkanoates (PHA) and glycogen) is enhanced by extending the anaerobic phase, and SND is conducted by both denitrifying phosphorus accumulating organisms (DPAOs) and denitrifying ordinary heterotrophic organisms (OHOs) in the aerobic phase that is operated with low dissolved oxygen (DO) concentrations (lower than 0.5 mg/L) (Wang et al., 2015; Zaman et al., 2021). In the AOA configuration, SND can occur in the aerobic phase when operated with low DO concentrations, and further nitrogen removal is achieved by denitrification in the post anoxic phase using hydrolyzed carbon or stored

carbon (Wang et al., 2016c; Winkler et al., 2011; Zhao et al., 2018). The reduction of nitrate and oxygen in the post anoxic phase further enhances the uptake of influent rbCOD by PAOs in the anaerobic phase to maintain stable enhanced biological phosphorus removal (EBPR). Typically, the AOA configuration can achieve higher total inorganic nitrogen (TIN) and phosphorus removal efficiencies (above 80% and 90%) than the AO configuration (around 70% and 90%) (Wang et al., 2015; Wang et al., 2016c; Winkler et al., 2011; Zaman et al., 2021; Zhao et al., 2018). While AO and AOA operations have received considerable attention at room temperatures, limited research has been conducted to treat real municipal wastewaters at low temperatures. Hence, there is a need to understand the performance of the two configurations when treating real municipal wastewaters at low temperatures.

Quantifying the nitrogen removal pathways in the aerobic phase can lead to an improved understanding of nitrogen removal mechanisms that could be employed to improve nutrient removal performance in SNDPR. In the aerobic phase with low DO concentrations, denitrification can be performed by denitrifying OHOs using rbCOD, DPAOs, and denitrifying glycogen accumulating organisms (DGAOs) (Ji et al., 2020; Wang et al., 2021; Yuan et al., 2020). Several studies have used a modeling method to investigate the nitrogen removal pathways. However, the model parameters have been found to differ between studies (Kuba et al., 1996; Wang et al., 2016b), and hence a comprehensive experimental methodology has been developed to investigate the nitrogen removal pathways in SNDPR to treat synthetic wastewater (Bai et al., 2022). These methods have not yet been employed to investigate nitrogen removal pathways in SNDPR treating real municipal wastewaters although it could be anticipated that there will be differences in the contributions of the various pathways due to the differences in wastewater composition.

Microbial community analysis can be employed to investigate the corresponding functional microorganisms that are responsible for SNDPR. Several studies have identified key microorganisms in SNDPR, including ammonia-oxidizing bacteria (AOB) (e.g., *Nitrosomonas* and *Nitrosomonadaceae*), nitrite-oxidizing bacteria (NOB) (e.g., *Nitrospira*), PAOs (e.g., *Ca.* Accumulibacter), GAOs (e.g., *Deflviicoccus*), DPAOs (e.g., *Dechloromonas* and *Pseudomonas*), and DGAOs (e.g., *Ca.* Competibacter)

(Chen et al., 2020; Liu et al., 2019; Yuan et al., 2020). Bai et al. (2022) investigated the microorganisms responsible for SNDPR when a complex synthetic wastewater was treated at 10℃. However, limited research has been conducted to study the microbial community structure in the SNDPR system when treating real municipal wastewater at low temperatures. It can be anticipated that the microbial structure of SNDPR will differ when treating real municipal wastewaters due to the differences in wastewater composition and the continual seeding of organisms from the raw wastewater. Hence, concurrent investigation of nitrogen removal pathways and microbial community composition can provide enhanced insight into these complex systems.

The objectives of this study are to 1) investigate the performance of SNDPR when real municipal wastewater was treated under low temperature conditions (10℃); 2) investigate whether operational conditions that have been successfully employed to treat synthetic wastewaters can also be applied to real municipal wastewaters; 3) compare the performance of SNDPR when operated in different process configurations (AO and AOA). To achieve these objectives, a bench-scale sequencing batch reactor (SBR) was operated in continuous and batch modes under low temperature conditions (10℃). Period 1 involved operation in the AO configuration under similar operational conditions as a prior study where a complex synthetic wastewater was treated (Bai et al., 2022). The SNDPR performance in Period 1 was compared with the results of the prior study (Bai et al., 2022) to assess whether the conditions that provided successful treatment of synthetic wastewaters could be applied to real municipal wastewaters. In Period 2 the AOA configuration was used to determine whether the SNDPR performance in this configuration could improve upon the AO configuration. Activity tests were conducted to investigate the nitrogen removal pathways in the aerobic phase of the AOA configuration. Microbial community composition was analyzed in parallel with the activity tests to explore the microorganisms that were contributing to N removal in the AOA configuration when treating real municipal wastewaters.

4.2. Materials and methods

4.2.1. Reactor setup and operation

A bench-scale SBR with a working volume of 18 L was used to study the performance of SNDPR to treat real municipal wastewater at 10℃. A detailed description of the SBR was reported by Bai et al. (2022). The SBR system was equipped with a mechanical mixer, an air pump, a luminescent DO probe with temperature sensing (Hach LDO probe, Product #5790000, Hach Company, Loveland, CO, USA), and a Bubble Mist – Bendable Air Wall air diffuser (Big Al's Canada, Woodbridge, ON, Canada). Three peristaltic pumps (MASTERFLEX Console Pump Drives, Model #77521-40 and Model #77521-50, Cole-Parmer Instrument Company, Vernon Hills, IL, USA) were used to feed the wastewater, pump out wasted MLSS, and decant treated wastewater. LabVIEW (National Instruments, Austin, TX, USA) was used to control the operation of these devices. During the whole operation, the temperature in the SBR was controlled at 10 ± 1℃ through an external water jacket (Li et al., 2011). The DO in the aerobic phase was controlled at 0.3 ± 0.1 mg/L. The volume exchange ratio was 50%.

The operation of the SBR was divided into 2 periods based on different process configurations. Period 1 (Day 1 to 67) was operated in the AO configuration with the same operational parameters as described by Bai et al. (2022). The comparison of SNDPR performance observed in Period 1 and a prior study that employed a complex synthetic wastewater (Bai et al. 2022) was used to assess whether the same operational parameters developed to treat synthetic wastewaters could also be used for real municipal wastewaters. The total cycle time was 8 hours, including 1 h of anaerobic operation (including 12 min of feeding time), 6 h of aerobic operation (including 5 min of wasting time at the end of the phase), and 1 h of settling and decanting. The sludge retention time (SRT) and hydraulic retention time (HRT) were controlled at 30 days and 16 hours by wasting 200 mL of mixed liquor and feeding 9 L of real municipal wastewater per cycle, respectively.

In Period 2 (Day 67 to 158) the SBR was operated in the AOA configuration. The results obtained in Period 2 were compared to those from Period 1 to assess the impact of operational configuration on SNDPR performance. The total cycle time was 16 hours with 1 h of anaerobic operation (including 12 min of feeding time), 6 h of aerobic operation, 8 h of anoxic operation (including 5 min of wasting time at the end of the phase), and 1 h of settling and decanting. The SRT and HRT were controlled at 60 days and 32 hours by wasting 200 mL of mixed liquor and feeding 9 L of real municipal wastewater per cycle, respectively.

The municipal wastewater that was fed into the SBR was collected from the City of Waterloo sewer system and filtered through a 2 mm mesh to eliminate large particles. It was then stored in a 90 L feed tank at 10°C for up to two days before being fed to the SBR. Total suspended solids (TSS), volatile suspended solids (VSS), Total COD, NH_4-N, NO_2-N, NO_3-N, and PO_4-P were measured in the influent, and soluble COD (sCOD), NH_4-N, NO_2-N, NO_3-N, and PO_4-P were measured in the effluent three times per week to monitor the SBR performance. Mixed liquor suspended solids (MLSS) and mixed liquor volatile suspended solids (MLVSS) were measured at the end of the reaction phase at the same frequency to monitor any changes in the sludge concentration.

4.2.2. Dynamic tests

Dynamic tests were conducted over three consecutive cycles of the SBR, during steady state operation, to observe the responses of nitrogen species, phosphorus, sCOD, PHA, and glycogen with time. The dynamic tests involved collecting mixed liquor samples at discrete time intervals of 10 min for the first 2 hours and then 30 min for the remainder of the reaction period. Collected samples were filtered through a 0.45-µm filter (VWR, USA) to separate solids and liquid. Solids were collected and stored at -70°C prior to analysis of poly-β-hydroxybutyrate (PHB), poly-β-hydroxyvalerate (PHV), poly-β-hydroxy-2-methylvalerate (PH2MV), and glycogen. Filtered liquid was used to measure soluble parameters. sCOD, PHB, PHV, PH2MV, and glycogen were measured to study the carbon conversion pathways. PO_4-P concentrations

were measured to establish the extent of phosphorus release in the anaerobic phase and phosphorus uptake in the aerobic/anoxic phase. NH_4-N, NO_2-N, and NO_3-N were tested to study the performance of SND in the aerobic/anoxic phase. MLSS and MLVSS concentrations were measured at the end of reaction to facilitate calculations of specific uptake/release rates of selected species (sCOD, NH_4-N, NO_3-N, and PO_4-P). Total nitrogen (TN) and total phosphorus (TP) concentrations in the influent and effluent were measured to calculate TN and TP removal efficiencies. Coefficients of variation (CV) were calculated for all values and then averaged over the time frame of the tests to quantify the variability among triplicate tests. The DO, pH, and temperature were recorded continuously during the dynamic tests. Mixed liquor samples were taken from the SBR during the dynamic tests conducted in Period 2 (Days 139 and 140) for microbial community analysis. The microbial community analysis was used to investigate the microorganisms that were predicted to have corresponding functionality for SNDPR, and link the microorganisms with the nutrient transformations in the dynamic tests and the following activity tests.

4.2.3. Activity tests

Three activity tests were conducted in the SBR. Test 1 was conducted to determine the duration of the post anoxic phase that was required to achieve negligible nitrate (NO_3-N<0.2 mg N/L). Tests 2 and 3 were conducted to gain insight into the nitrogen removal pathways that were active in the aerobic phase of operation. All activity tests were conducted in triplicate to assess reproducibility and analyze uncertainty. CVs were calculated to quantify the variability among triplicate tests.

Activity Test 1: Test 1 was conducted upon completion of the dynamic tests in Period 1. During the test, the SBR cycle was extended by four hours without any aeration to promote denitrification by denitrifying OHOs using hydrolyzed carbon. The dynamic tests conducted in Period 1 revealed negligible quantities of sCOD and PHA after 7 hours of aerobic operation, and hence any denitrification was attributed to denitrifying OHOs using hydrolyzed carbon. Mixed liquor samples were collected every 30 min for NH_4-

N, NO_2-N, NO_3-N, and PO_4-P measurements. The NO_3-N removal rate was estimated through linear regression of nitrate concentrations with time.

Activity Test 2: Test 2 was conducted upon completion of the dynamic tests in Period 2 to measure the rate of denitrification by denitrifying OHOs using hydrolyzed carbon from the aerobic phase (DO of 0.3 mg/L). The test extended the aerobic cycle of the SBR for an additional two hours while maintaining a consistent DO concentration (i.e., 0.3 mg/L). Test 2 had similar assumptions and conditions as described in Test 1, except that Test 2 was conducted under aerobic conditions with a DO of 0.3 mg/L while Test 1 was under anoxic conditions. Any nitrogen removal observed in this test was attributed to denitrification by denitrifying OHOs using hydrolyzed carbon at a DO of 0.3 mg/L. Samples of the mixed liquor were collected at a 15-min interval for NH_4-N, NO_2-N, NO_3-N, and PO_4-P measurements. The specific NO_3-N removal rate was calculated based on Eq. (4-4).

Activity Test 3: Test 3 was conducted in the SBR to determine the rate of denitrification by DGAOs and DPAOs in the aerobic phase of the AOA configuration. Test 3 was conducted triplicate with a synthetic wastewater (see Appendix B) containing a mixture of VFAs with a total concentration of 100 mg COD/L and NH_4-N and PO_4-P concentrations of 1 mg N/L and 2 mg P/L, respectively. The synthetic wastewater was fed for three cycles, and then real municipal wastewater was fed to the SBR again. The synthetic wastewater was employed to establish conditions where the quantity of stored PHAs were sufficient for denitrification by DPAOs and DGAOs in the aerobic phase while there were minimal quantities of VFAs remaining after the anaerobic phase. Before the start of the test cycle, the settled sludge was washed three times with deionized water to minimize NH_4-N concentration at the beginning of the test cycle in order to minimize NO_3-N generation in the aerobic phase. The anaerobic phase was extended to 1.5 h to maximize VFA uptake, thereby eliminating denitrification by denitrifying OHOs using residual VFAs. $NaNO_3$ and KH_2PO_4 were added to the SBR at the beginning of the aerobic phase to achieve NO_3-N and PO_4-P initial concentrations of 10 mg N/L and 20 mg P/L, respectively in the SBR. In the aerobic phase (DO of 0.3 mg/L), mixed liquor samples were taken every 15 min for 2.5 hours to measure PO_4-P and NO_3-N. The

profiles of PO_4-P and NO_3-N with time were used to assess denitrification by DGAOs and DPAOs. Reduction of NO_3-N without PO_4-P uptake was attributed to denitrification by DGAOs. Simultaneous reductions of NO_3-N and PO_4-P were attributed to denitrification by DPAOs and DGAOs. The specific NO_3-N removal rate was calculated based on Eq. (4-4).

4.2.4. Analytical methods

In the SBR, DO and temperature were monitored using a Hach LDO® probe (Hach Company, Loveland, CO, USA). The pH was measured using a symPhony BENCHTOP pH meter (VWR, USA). The COD, MLVSS, MLSS, TSS, and VSS analyses were conducted as per Standard Methods (Eaton et al., 2005). Filtered COD was determined on samples after filtration through 1.2-µm filters (Whatman filter paper), while flocculant filtered COD was determined on samples that were initially flocculated by adding 1 mL of 100 g/L zinc sulfate solution, adjusted pH to 10.5 using 6 M sodium hydroxide solution, and then filtered through 0.45-µm cellulose filter (VWR) (Melcer, 2004). The NO_2-N, NO_3-N, and PO_4-P were analyzed by ion chromatography (Lachat Quik-Chem8000, Lachat Instrument, USA) after filtration through 0.45-µm cellulose filters. The NH_4-N, TP and TN were measured using HACH kits, which were accepted by USEPA and equivalent to Standard Methods. Mixed liquor solids were collected on 1.2-µm filters and stored at -70°C. Frozen samples were dried using a vacuum freeze dryer (LABCONCO Freeze Dryer System, Model 76700 Series, USA) for PHA and glycogen measurements. PHA is the combination of PHB, PHV, and PH2MV, which were measured using gas chromatography as described in Wang et al. (2009). For glycogen, the phenol method as described in Reddy et al. (2007) was used.

4.2.5. Microbial community analysis

The microbial community in the SNDPR process wastewater was investigated to gain insight into the organisms responsible for nutrient transformations in the SBR. Mixed liquor samples were taken during the

dynamic tests of Period 2 (Days 139 and 140) for microbial community analysis. DNeasy PowerSoil Pro Kit (Qiagen) was used for total DNA extraction. Then 16S rRNA gene sequencing was conducted to determine the overall microbial community composition. The detailed procedures are shown in Bai et al. (2022). An amplicon sequence variant (ASV) table was generated from 16S rRNA gene sequencing. Functional annotation of prokaryotic taxa (FAPROTAX) (1.2.4) was generated to predict functionality of ASVs by running through QIIME2 version 2020.6.

4.2.6. Equations

TN, TP, and TIN removal efficiencies through the SBR were calculated to assess the nitrogen and phosphorus removal performance as per Eq. (4-1) – Eq. (4-3).

$$\text{TN removal efficiency} = 1 - \frac{\text{TN in the effluent}}{\text{TN in the influent}} \quad \text{Eq. (4-1)}$$

$$\text{TP removal efficiency} = 1 - \frac{\text{TP in the effluent}}{\text{TP in the influent}} \quad \text{Eq. (4-2)}$$

$$\text{TIN removal efficiency} = 1 - \frac{\text{TIN in the effluent}}{\text{TIN in the influent}} \quad \text{Eq. (4-3)}$$

Where TN is total nitrogen, mg N/L; TP is total phosphorus, mg P/L; TIN is total inorganic nitrogen, which included NH_4-N, NO_2-N, and NO_3-N, mg N/L.

The rate of increase or reduction of each substrate (sCOD, NH_4-N, NO_3-N, and PO_4-P) in dynamic tests and activity tests was estimated based on linear regression of measured substrate concentrations with time. The specific increase or reduction rate of each substrate was calculated by the increase or reduction rate of each substrate divided by MLVSS (Eq. (4-4)).

$$\text{The specific increase or reduction rate} = \frac{\text{The increase or reduction rate}}{\text{MLVSS}} \quad \text{Eq. (4-4)}$$

Where MLVSS is the mixed liquor volatile suspended solids, mg/L.

The SND efficiency (Eq. (4-5)) in the SBR at steady state was defined as the percentage of TIN loss in the aerobic phase either due to denitrification or cell synthesis (Wang et al., 2015).

$$\mathrm{SND} = \left(1 - \frac{\mathrm{NH_{4,e}^{+}} + \mathrm{NO_{2,e}^{-}} + \mathrm{NO_{3,e}^{-}}}{\mathrm{NH_{4,i}^{+}} - \mathrm{NH_{4,e}^{+}}}\right) \times 100\% \qquad \text{Eq. (4-5)}$$

Where, $\mathrm{NH_{4,i}^{+}}$ is the NH_4-N concentration at the beginning of the aerobic phase, mg/L; $\mathrm{NH_{4,e}^{+}}$ is the NH_4-N concentration at the end of the aerobic phase, mg/L; $\mathrm{NO_{2,e}^{-}}$ is the NO_2-N concentration at the end of the aerobic phase, mg/L; $\mathrm{NO_{3,e}^{-}}$ is the NO_3-N concentration at the end of the aerobic phase, mg/L.

Eq. (4-6) to Eq. (4-8) were used to quantify the fate of carbon in the anaerobic phase (Wang et al., 2016b). It was assumed that organic carbon was consumed for denitrification of residual NO_x from prior cycle first and then used for PAO and GAO storage as PHA (Eq. (4-6)). Eq. (4-7) represents the COD used for denitrification. Intracellular storage efficiency (COD_{intra} efficiency) was defined as the percentage of COD stored as intracellular products over total COD consumed in the anaerobic phase.

$$COD_{consum} = COD_{dn} + COD_{intra} = COD_{i} - COD_{ana,end} \qquad \text{Eq. (4-6)}$$

$$COD_{dn} = 2.86/(1\text{-}Y_{OHO,VFA,anox}) \times NO_3\text{-}N_{ana} + 1.71/(1\text{-}Y_{OHO,VFA,anox}) \times NO_2\text{-}N_{ana} \qquad \text{Eq. (4-7)}$$

$$COD_{intra}\ \text{efficiency} = COD_{intra}/COD_{consum} \times 100\% \qquad \text{Eq. (4-8)}$$

Where, COD_{consum} is the amount of soluble COD consumed in the anaerobic phase, mg/L; COD_{intra} is COD stored by PAOs and GAOs as PHA and glycogen, mg/L; COD_{dn} is COD used for OHO denitrification, mg/L; 2.86 is the oxygen equivalent of nitrate, mg COD/mg N; 1.71 is the oxygen equivalent of nitrite, mg COD/mg N; COD_i, $NO_3\text{-}N_{ana}$, and $NO_2\text{-}N_{ana}$ are the initial concentration of sCOD, nitrate, and nitrite at the beginning of the anaerobic phase. $COD_{ana,end}$ is the sCOD concentration at the end of the anaerobic phase. $Y_{OHO,VFA,anox}$ is the OHO yield using VFAs for denitrification, which was assumed to be 0.45 mg COD_{OHO}/mg COD_{VFA} (Metcalf et al., 2014).

The mass of nitrogen removed through DPAO denitrification in the aerobic phase of Period 2 was calculated as the product of the specific NO_3-N reduction rate, MLVSS, liquid volume, and reaction time as shown in Eq. (4-9).

$$\text{Mass of Nitrogen Removed} = \text{SNRR} \times \text{MLVSS} \times \text{V} \times \text{dt} \quad \text{Eq. (4-9)}$$

Where mass of nitrogen removed is the mass of nitrogen removed through DPAOs using PHA in the aerobic phase of a typical cycle, mg N; SNRR is the specific NO_3-N removal rate of DPAO denitrification in the aerobic phase as determined by Eq. (4-4), mg N/(g VSS·h); MLVSS is the MLVSS in the SBR, g VSS/L; V is liquid volume, 18 L; dt is the time of DPAO denitrification in the aerobic phase, which was 1.5 h in this study based on the results of dynamic tests in Period 2, h.

4.2.7. Statistical analysis

Normality of data was initially assessed with Excel software 2016 (Microsoft) to validate subsequent use of t-tests. T-tests were conducted with Excel to distinguish differences between two sets of data with a confidence interval of 95%. Average, standard deviation, and CV calculations were performed in Excel software 2016 (Microsoft).

4.3. Results and discussion

4.3.1. Long term reactor performance

In Period 1, C, N, and P species (Figure B-1) were evaluated to assess the performance of SNDPR in the AO configuration, and compare with a prior study (Bai et al., 2022) to determine whether the operational conditions that were employed to treat synthetic wastewaters could be applied to a real municipal

wastewater. The effluent sCOD was lower than 30 mg COD/L consistently (not shown in Figure B-1), indicating at least 90% COD removal throughout the experiment. At steady state, the effluent NH_4-N concentrations, and the TIN removal, SND, and PO_4-P removal efficiencies were 0.4 ± 1.0 mg N/L, 51.9% ± 7.9%, 3.8% ± 15.8%, and 36.1% ± 24%, respectively (Figure 4-1). The results showed full ammonia oxidation but unstable N and P removal which was inconsistent with the prior study that treated a synthetic wastewater.

The composition of the wastewaters was compared to identify the cause of the different performances. It was determined that only 22% ± 6.7% of the TCOD of the real municipal wastewater could be considered as rbCOD. Approximately 84% ± 34% of this rbCOD (as calculated by Eq. (4-7)) was used for denitrification by OHOs in the anaerobic phase. Hence, it was estimated that only a small fraction of the rbCOD (16% ± 34%) was available for storage as PHA in PAOs. Without sufficient PHA accumulation, EBPR and SND were limited in the AO configuration. The results of this analysis suggest that prior studies which indicated successful SNDPR performance using an AO configuration at low temperatures with simple synthetic wastewaters may need to be re-examined.

In Period 2, C, N, and P species (Figure B-1) were evaluated to compare the performance of SNDPR in the AOA configuration with that in the AO configuration. The effluent sCOD was lower than 30 mg COD/L consistently, which was consistent with Period 1 (not shown in Figure B-1). At steady state, effluent NH_4-N concentrations in Period 2 were always below 0.5 mg N/L. The effluent NO_3-N concentrations in Period 2 were 77.4% ± 19.2% less than those with the AO configuration in Period 1. The TIN removal efficiency increased from 51.9% ± 7.9% in Period 1 to 86.8% ± 4.8% in Period 2. PO_4-P concentrations in the effluent were less than 0.4 mg P/L with the PO_4-P removal efficiency of 92.8% ± 7.7%, demonstrating effective EBPR. Viewed collectively, the AOA configuration showed similar COD removal efficiency (p>0.05), enhanced EBPR (p<0.05), and enhanced TIN removal efficiency (p<0.05) when compared with the AO configuration.

The significant improvement in SNDPR performance was attributed to the 8-hour post anoxic phase, which reduced the effluent nitrate concentration and the associated consumption of influent rbCOD for denitrification. Several studies have also shown successful EBPR with P removal efficiencies above 90% in the AOA configuration when operated at room temperature (Wang et al., 2016c; Winkler et al., 2011; Zhao et al., 2018). The results of the current study indicate that this performance can be achieved at lower temperatures when the operating parameters are properly established. The nutrient removal pathways that were active in the AOA configuration were investigated in detail using data gathered in the activity tests and are subsequently discussed.

In this study, the potential for bulking sludge was considered due to the long SRT and low DO conditions. Previous studies have shown that low DO and long SRTs could lead to serious sludge bulking due to filamentous bacteria growth (Kunst and Reins, 1994; Gabb et al., 1991), however this sludge was not observed in the current study. This was attributed to the limited loading of rbCOD to the aerobic phase (Figure 4-2) (Jenkins et al., 1993). The results suggest that rbCOD consumption in the anaerobic phase eliminated any bulking sludge development.

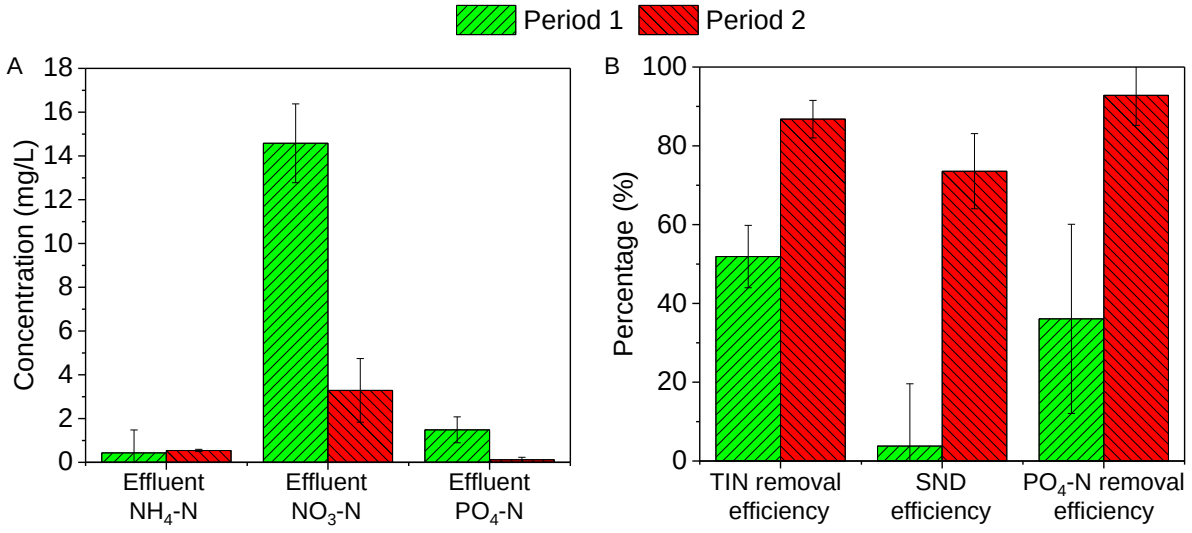

Figure 4-1. Steady state performance of SBR in Periods 1 and 2 (A: Effluent NH_4-N, effluent NO_3-N, effluent PO_4-P; B: TIN removal efficiency, SND efficiency, PO_4-P removal efficiency).

4.3.2. Dynamic nutrient responses in Period 1

Dynamic tests were conducted while the system was operated in AO to obtain insight into the causes of poor SNDPR performance with the goal of using this information to inform the design of an improved operation. The dynamic tests sought to obtain increased insight into the pathways contributing to carbon, nitrogen, and phosphorus transformation in the SBR. The profiles of NH_4-N, NO_2-N, NO_3-N, TIN, PO_4-P, sCOD, PHA, PHB, PHV, PH2MV, and glycogen that were observed in the dynamic tests are shown in Figures 4-2A, 4-2B, and 4-2C. Triplicate dynamic tests were performed to account for uncertainty and show the reproducibility of the tests. Average CVs of each substrate were calculated in the range of 5%-16%, indicating the high reproducibility of results.

In the anaerobic phase, sCOD, PO_4-P, PHA, and glycogen (Figures 4-2B and 4-2C) were analyzed together to quantify carbon utilization pathways and show the status of phosphorus release in this phase. sCOD was reduced linearly from 38.3 ± 4.7 to 18.3 ± 4.3 mg COD/L with a specific removal rate of 8.0 ± 2.1 mg COD/g VSS/h (Eq. (4-4)). During this period, most of the sCOD was used to denitrify NO_3-N that remained from the prior cycle with low COD_{intra} efficiency of 4% ± 2% based on Eq. (4-8). PHA and glycogen concentrations were around 1.6 ± 0.3 mmolC/L and 0.3 ± 0.02 mmolC/L, which indicated limited carbon storage by PAOs and GAOs. This result also aligned with the low COD_{intra} efficiency. In addition, PO_4-P was not released in the anaerobic phase, indicating limited EBPR. The low COD_{intra} efficiency and limited PHA accumulation in the anaerobic phase forecasted the failure of phosphorus release. Overall, most of the influent biodegradable COD was used for denitrification to remove nitrate from prior cycle, leading to the deterioration of EBPR.

In the aerobic phase, PO_4-P, PHA, and glycogen responses were analyzed together to assess the status of EBPR. Figure 4-2B and Figure. 4-2C show PO_4-P, PHA, and glycogen were consistently around 2-3 mg P/L, 1.6 ± 0.3 mmolC/L, and 0.3 ± 0.03 mmolC/L, respectively. This strongly suggested limited PHA

utilization and PO_4-P uptake. Overall, limited PHA accumulation in the anaerobic phase was responsible for the limited phosphorus uptake in the aerobic phase.

In the aerobic phase, nitrogen species (NH_4-N, NO_2-N, and NO_3-N) (Figure 4-2A) were assessed to establish the status of nitrification in the SBR. NH_4-N was reduced from 12.0 ± 0.3 to 0.2 ± 0.1 mg N/L within 4.5 h with a specific NH_4-N removal rate of 0.8 ± 0.01 mg N/g VSS/h (Eq. (4-4)). With the reduction of NH_4-N, a small amount of NO_2-N (less than 0.5 mg N/L) was generated, and NO_3-N was the main product of nitrification with the specific increase rate of 0.7 ± 0.01 mg N/g VSS/h (based on Eq. (4-4)). Full nitrification was also observed when the system was operated under the same conditions to treat synthetic wastewater (Bai et al., 2022). Overall, nitrification in the AO process was consistent when treating synthetic and municipal wastewaters.

In the aerobic phase, the SND efficiency and the ratios of the accumulated NO_x-N/oxidized NH_4-N of each hour were calculated to assess whether SND was occurring in the SBR. The SND efficiency was calculated to be 0.3% ± 3.8% (based on Eq. (4-5)), revealing negligible SND in the aerobic phase. Bai et al. (2022) stated that main pathways for SND in the aerobic phase were through denitrification by denitrifying OHOs using residual carbon from the anaerobic phase and DPAOs at a DO of 0.3 mg/L. In this study, these two denitrification pathways were not active due to limited sCOD reduction and phosphorus uptake in the aerobic phase, which were required for OHO and DPAO denitrification, respectively. Therefore, limited storage of carbon in PAOs and a lack of residual rbCOD from the anaerobic phase were likely responsible for the lack of SND.

The results of Period 1 were compared with the results of a prior study to obtain insight into why the operational conditions that were successfully employed to treat a synthetic wastewater were not effective for the real wastewater. Employing the same operational strategy for the AO configuration, Bai et al. (2022) achieved successful SNDPR as indicated by TIN removal, phosphorus removal, and SND efficiencies of 62.6%, 97%, and 31%, respectively, when treating a complex synthetic wastewater. However, SNDPR was

not achieved in the current study as illustrated by TN and TP removal efficiencies of 56.7% ± 1% and 12.8% ± 1.7%, respectively. Denitrification of NO_3-N that remained from the prior cycle consumed most of the influent rbCOD (96% ± 2%) and hence a limited amount of rbCOD was stored by PAOs and GAOs, resulting in limited EBPR. The lack of phosphorus uptake and limited rbCOD from the anaerobic phase resulted in limited SND in the aeration phase. In order to promote SNDPR, it was deemed necessary to reduce the nitrate concentration in the effluent, such that more rbCOD could be stored by PAOs and GAOs thereby promoting EBPR and SND.

Test 1 (Figure 4-3A) was conducted upon completion of the dynamic tests of Period 1 to investigate the time needed for denitrification by OHOs using hydrolyzed carbon to reduce NO_3-N concentrations to negligible levels (NO_3-N<0.2 mg N/L) and thereby promote SNDPR. From Fig 3A it can be seen that NO_3-N concentrations were reduced linearly at a specific rate of 1.85 mg N/L/h (based on Eq. (4-4)). sCOD and PO_4-P concentrations remained at low values (20.2 ± 5 mg COD/L and 0.9 ± 0.5 mg P/L, respectively), indicating limited denitrification by either OHOs or DPAOs. In addition, the dynamic tests conducted in Period 1 showed limited PHA storage (1.6 ± 0.3 mmolC/L), eliminating the likelihood of denitrification by DGAOs. Therefore, the reduction of NO_3-N was attributed to OHO denitrification using hydrolyzed carbon. The generation of hydrolyzed carbon that comes from the hydrolysis of cell decay products was deemed to be the rate-limiting process (Drewnowski & Makinia, 2013). Based on the specific NO_3-N removal rate of 1.9 mg N/L/h and initial NO_3-N of 14.8 mg N/L, it was concluded that 8 hours would be required to reduce NO_3-N to negligible.

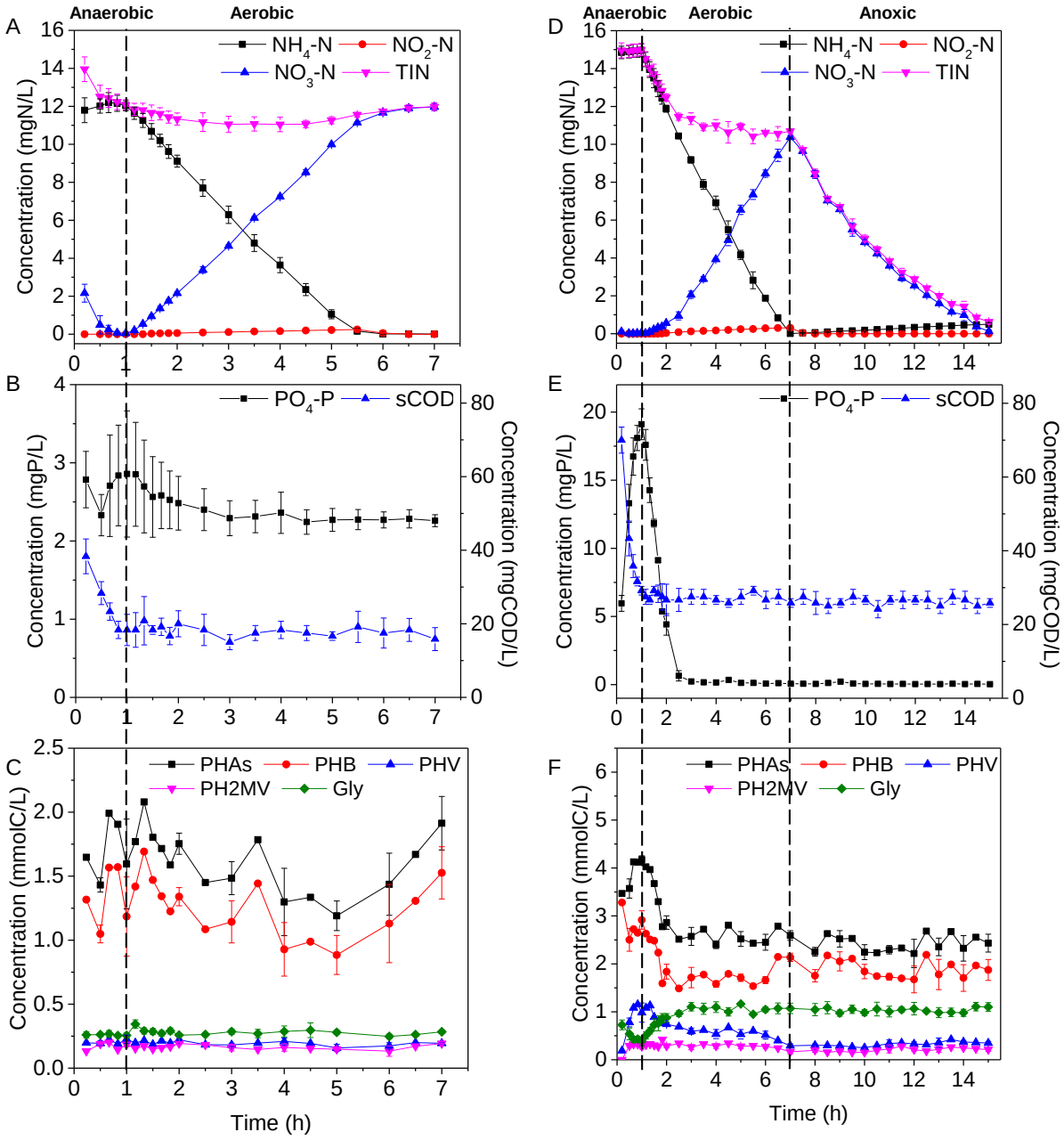

Figure 4-2. Transient responses observed in triplicate SBR cycles. A: nitrogen species profiles in Period 1; B: phosphorus and soluble COD profiles in Period 1; C: PHB, PHV, PH2MV, PHAs, and glycogen profiles in Period 1; D: nitrogen species profiles in Period 2; E: phosphorus and soluble COD profiles in Period 2; F: PHB, PHV, PH2MV, PHAs, and glycogen profiles in Period 2. Markers represent average values from triplicate tests and error bars represent associated standard deviations.

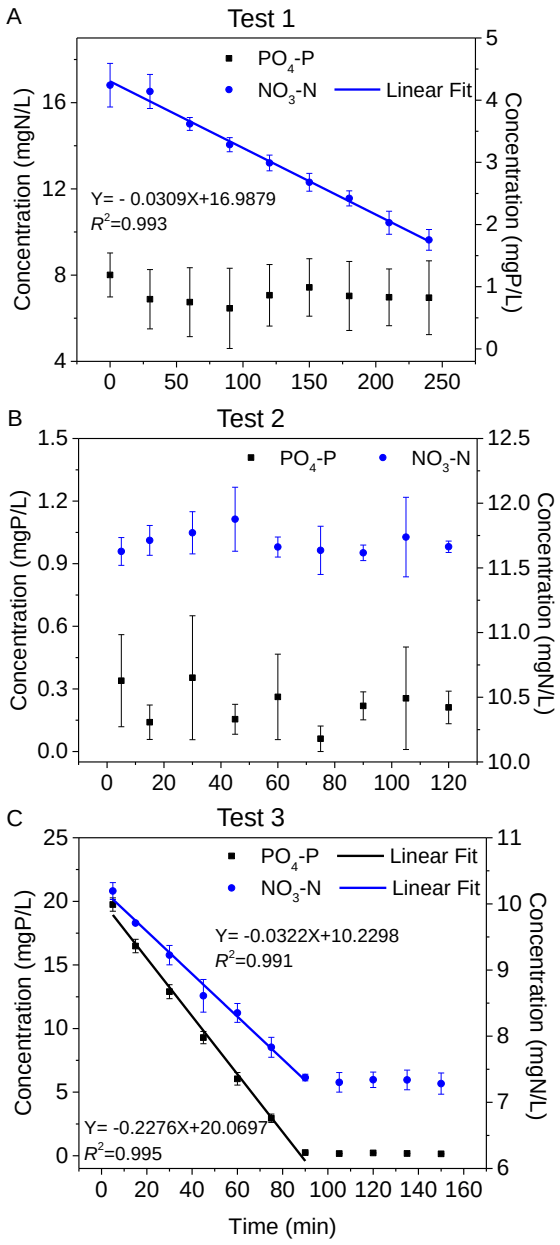

Figure 4-3. The status of denitrification by denitrifying OHOs using hydrolyzed carbon (A) under anoxic conditions at 10°C in Period 1, denitrifying OHOs using hydrolyzed carbon (B), and DGAOs and DPAOs (C) under oxic conditions at a DO of 0.3 mg/L and 10°C in Period 2 (Tests 1-3). Markers represent average values of triplicate tests, and error bars represent associated standard deviations.

4.3.3. Dynamic nutrient responses in Period 2

The biological processes responsible the successful SNDPR in Period 2 were investigated through dynamic tests. In addition, the microbial community composition was assessed to gain insight into the key organisms contributing to SNDPR. Figures 4-2D, 4-2E, and 4-2F shows the profiles of NH_4-N, NO_2-N, NO_3-N, TIN, PO_4-P, sCOD, PHA, PHB, PHV, PH2MV, and glycogen that were observed over the SBR cycle. Triplicate dynamic tests were performed to analyze reproducibility and uncertainty. Average CVs of each substrate over the reaction period were calculated and found in the range of 3% to 23%, implying the high reproducibility of results.

In the anaerobic phase, sCOD (Figure 4-2E) was measured to quantitatively study the consumption pathways. From the Figure it can be seen that the reduction of sCOD could be distinguished into two stages. During the first stage (first 40 min), sCOD was reduced from 70.3 ± 3.5 to 35.8 ± 3.1 mg COD/L with a specific removal rate of 23.7 ± 0.5 mg COD/g VSS/h as calculated by Eq. (4-4). During the second stage (later 20 min), sCOD was reduced from 35.8 ± 3.1 to 29.2 ± 1.2 mg COD/L with a reduced specific removal rate of 8.3 ± 1.1 mg COD/g VSS/h as calculated by Eq. (4-4). The reduction in the specific removal rate was attributed to exhaustion of rbCOD and the relatively slow hydrolysis of the remaining COD (Drewnowski & Makinia, 2013).

The sCOD that was removed in the anaerobic phase was investigated. Based on Eq. (4-7), the sCOD that was used for denitrification was estimated to be 0.7 ± 0.3 mg COD/L, which accounted for only 2% ± 1% of the COD consumed in the anaerobic phase. The COD_{intra} efficiency was calculated to be 98% ± 1% as calculated by Eq. (4-8), which was significantly higher than that in Period 1 (4% ± 2%). The increased storage of COD in Period 2 would support the improved EBPR performance when compared to Period 1.

A FAPROTAX analysis was conducted to investigate microorganisms that could be predicted to contribute to fermentation in the anaerobic phase. The FAPROTAX results show that 10.1% ± 0.8% of the microbial community (Figure 4-4) was predicted to perform fermentation, with the main genera including *Rhodoferax*

(5.2% ± 0.7%), *Trichococcus* (1.5% ± 1.1%), *Lautropia* (1.2% ± 0.2%), and *Romboutsia* (1.1% ± 0.1%) (Figure B-2). The prominence of fermentation-related microorganisms in this study were higher than that (3.6% ± 0.4%) reported by Bai et al. (2022) when a complex synthetic wastewater was treated. The increased fraction of fermentation bacteria when treating real municipal wastewater may have been due to the introduction of fermentation bacteria from the municipal wastewater. It is believed that the high proportion of fermentative bacteria in the system promoted the conversion of rbCOD to VFAs, leading to the success of EBPR. Overall, fermentation-related bacteria accounted for a large proportion of the community when treating real municipal wastewater, which was benefit for the generation of fermented VFAs and EBPR.

In the anaerobic phase, the response of PO_4-P (Figure 4-2E) was investigated to quantify the phosphorus release as an indicator of the activity of PAOs in this phase. The increase of PO_4-P was observed to occur in two stages, which corresponded to the two-stage sCOD removal. During the first stage (first 40 min), PO_4-P increased from a negligible concentration to 16.7 ± 1.4 mg P/L with a specific increase rate of 7.3 ± 0.7 mg P/g VSS/h as calculated by Eq. (4-4). The increase of PO_4-P was attributed to the uptake of influent VFAs and fermented rbCOD. During the second stage (later 20 min), the PO_4-P concentration increased from 16.7 ± 1.4 mg P/L to 19.1 ± 1.1 mg P/L with a lower specific increase rate of 2.2 ± 0.3 mg P/g VSS/h as calculated by Eq. (4-4). The reduction in the rate of increase in the second stage was attributed to relatively slow hydrolysis of slowly biodegradable COD. Compared to Period 1, Period 2 showed obvious phosphorus release, which was due to the high COD_{intra} efficiency. Overall, the AOA configuration was found to promote phosphorus release in the anaerobic phase, which likely contributed to SND in the subsequent aerobic phase due to the storage of carbon.

Several stoichiometric ratios (involving sCOD, PO_4-P, PHA, and glycogen) in the anaerobic phase were calculated to evaluate whether PAOs or GAOs were the dominant bacteria contributing to sCOD removal. The ratios of PO_4-P release to sCOD uptake in the two stages were 0.3 ± 0.03 and 0.3 ± 0.02 mg P/mg COD, which were consistent with reported values in PAO-rich systems (0.3-0.43 mg P/mg COD (Kuba et al.,

1997; Zaman et al., 2021)). The ratios of P release to PHA generation (0.4 ± 0.05 mol P/mol C), PHA generation to glycogen consumption (2.4 ± 0.3 mol C/mol C), and PHA generation to COD storage (1.7 ± 0.2 mol C/mol C) were found to be consistent with those (0.38 mol P/mol C, 2.66 mol C/mol C, and 1.33 mol C/mol C) reported in a PAO-rich system (Smolders et al., 1994). The dominance of PAOs over GAOs in systems with low DO and temperature has been reported to be associated with the higher oxygen affinity of PAOs when compared to GAOs (Zaman et al., 2021). In addition, GAOs have been reported to have lower growth rates at low temperatures (10-20°C) (Tian et al., 2017b; Bai et al., 2022). In summary, these stoichiometric ratios suggested that an active PAO-community was present in the SBR in the AOA configuration. This was further investigated by assessing 16S rRNA gene microbial community data as subsequently discussed.

In the aerobic phase, the responses of key nitrogen species (NH_4-N, NO_2-N, and NO_3-N) (Figure 4-2D) were examined to assess the existence of SND in the SBR. NH_4-N concentrations were reduced from 15.0 ± 0.4 to 0.01 ± 0.02 mg N/L within 7 hours with a specific removal rate of 0.8 ± 0.03 mg N/g VSS/h (based on Eq. (4-4)). With the reduction of NH_4-N, limited NO_x was generated from 1 h to 2.5 h, indicating the existence of SND. Then NO_3-N was generated as the main product with a specific increase rate of 0.7 ± 0.01 mg N/g VSS/h (based on Eq. (4-4)). The similar specific NH_4-N removal rate and the NO_3-N increase rate indicated limited SND after 2.5 h in the aerobic phase. Overall, SND was demonstrated in the aerobic phase.

The FAPROTAX analysis was used to investigate the predicted nitrification metabolic functionality and the associated microorganisms in the SBR (Figure 4-4). The predicted nitrification function (3.5% ± 0.8%) included aerobic ammonia oxidation (3.0% ± 0.1%) and aerobic nitrite oxidation (0.8% ± 0.7%). The dominant microorganisms associated with aerobic ammonia oxidation and aerobic nitrite oxidation were associated with the genus *Nitrosomonas* (3.2% ± 0.2%), and genera *Nitrospira* (0.1% ± 0.1%) and *Nitrotoga* (0.4% ± 0.6%), respectively. These microorganisms are acknowledged to be AOB and NOB, respectively (Metcalf et al., 2014). The dominant presence of these microorganisms was also observed in similar studies

at a DO of 0.3 mg/L and 10℃ when treating synthetic wastewater (Bai et al., 2022), indicating the minor impact of wastewater composition on nitrifier community. Overall, nitrification in the system was appeared to be primarily due to the activity of *Nitrosomonas*, *Nitrospira*, and *Nitrotoga*.

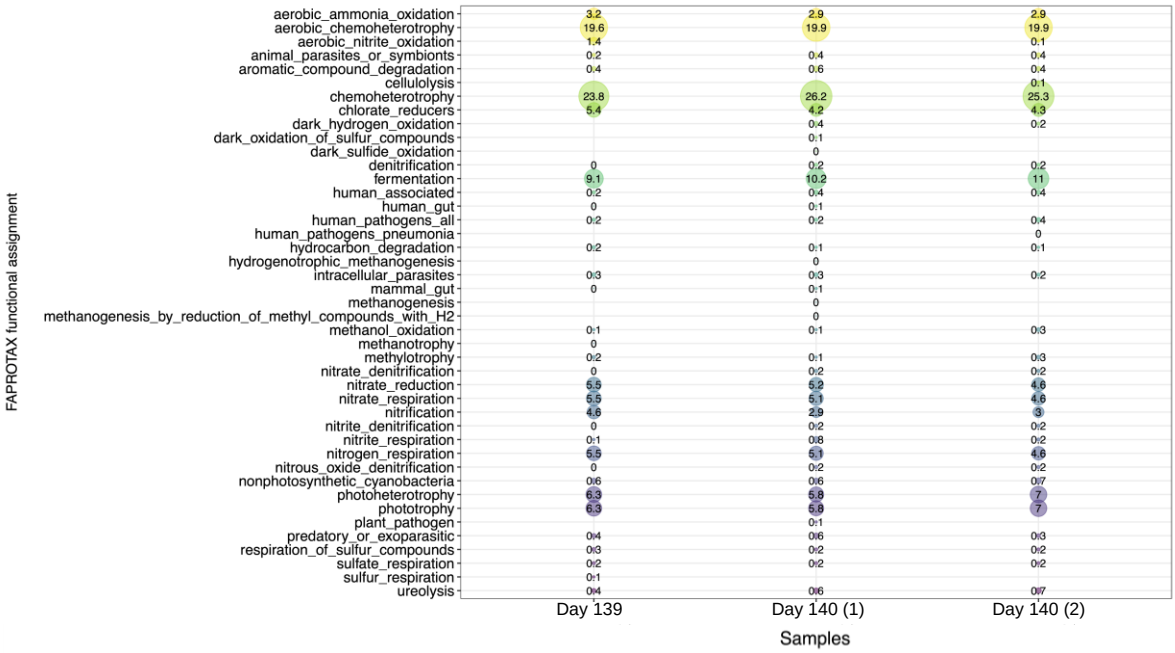

Figure 4-4. Metabolic functions of bacteria based on FAPROTAX results for three dynamic tests in Period 2 (the numbers inside circles represent relative abundances in percent).

In the aerobic phase, the SND efficiency and the ratios of the accumulated NO_x-N/oxidized NH_4-N of each hour were quantified to evaluate whether SND existed in Period 2. The SND efficiency was determined to be 28.5% ± 1% (based on Eq. (4-5)), indicating substantial SND activity in the aerobic phase. The ratios of the accumulated NO_x-N/oxidized NH_4-N in each hour of the aerobic phase were used to assess when SND occurred in the aerobic phase, and were calculated to be 0.2 ± 0.01 and 0.6 ± 0.06 for the first two hours and approximately one for the rest of time. On the basis of these ratios, it appeared that SND occurred in the first two hours of the aerobic phase, which corresponded to the reduction of TIN at the first 1.5 hours. The SND in the aerobic phase might result from denitrification by OHOs and DPAOs as indicated by Bai

et al. (2022). Overall, the AOA configuration can promote SND at a DO of 0.3 mg/L and 10°C when treating real municipal wastewater.

In the aerobic phase, the response of PO_4-P (Figure 4-2E) was assessed to gain insight into the progress of phosphorus uptake by PAOs with reaction time. Phosphorus was reduced from 19.1 ± 1.1 to 0.6 ± 0.4 mg P/L in the first 1.5 hours and then remained at minimal concentrations for the remainder of the aerobic phase. The specific removal rate was 4.2 ± 0.2 mg P/g VSS/h (based on Eq. (4-4)). When compared with Period 1, Period 2 demonstrated successful phosphorus uptake, which was due to the high COD_{intra} efficiency (98% ± 1%) in the anaerobic phase. Hence, the success of EBPR demonstrated the necessary of the implementation of the AOA configuration when treating real municipal wastewater at 10°C.

In the aerobic phase, PHA and glycogen (Figure 4-2F) were analyzed together with phosphorus to assess the dominant microbial group contributing to EBPR. PHA was reduced from 4.2 ± 0.08 to 2.5 ± 0.09 mmolC/L while glycogen increased from 0.4 ± 0.09 to 1.0 ± 0.06 mmolC/L in the first 1.5 h of the aerobic phase. Subsequently, PHA and glycogen remained at 2.5 ± 0.2 mmolC/L and 1.1 ± 0.1 mmolC/L, respectively. The timing of the changes in PHA and glycogen concentrations were aligned with the P uptake, indicating active PAO activity. In addition, the ratios of phosphorus uptake to PHA consumption (0.4 ± 0.05 mol P/mol C) and glycogen replenishment to PHA consumption (0.4 ± 0.05 mol C/mol C) were found to be similar to ratios reported for a system with active PAOs (0.41 mol P/mol C and 0.42 mol C/mol C) (Smolders et al., 1994). Overall, these ratios indicated again the system under low DO and temperature conditions was rich in PAOs.

In the post anoxic phase, PHA, glycogen, and PO_4-P concentrations (Figures 4-2E and 4-2F) were examined to assess whether stored carbons (PHA and glycogen) might contribute to N removal and to evaluate whether the anoxic conditions had a detrimental effect upon EBPR performance. PHA and glycogen concentrations were found to remain stable around 2.4 ± 0.2 mmolC/L and 1.0 ± 0.1 mmolC/L, respectively, and therefore it was concluded that PAOs and GAOs were not contributing to denitrification in this phase.

PO_4-P concentrations remained below 0.3 mg P/L, indicating limited secondary phosphorus release. The results were consistent with prior studies that reported stable EBPR when operated with a post anoxic phase (Coats et al., 2011; Wang et al., 2016c). Overall, EBPR was maintained when a post anoxic phase was employed, and PAOs did not contribute to denitrification in the anoxic phase.

In the post anoxic phase, nitrogen species (Figure 4-2D) were studied to evaluate the processes leading to nitrate removal. Overall, NO_3-N was reduced from 10.4 ± 0.09 to 0.1 ± 0.06 mg N/L, and NH_4-N increased from 0.01 ± 0.02 to 0.5 ± 0.07 mg N/L. Since stable PHA, glycogen, and PO_4-P concentrations were maintained in the post anoxic phase, the reduction of NO_3-N was attributed to OHO denitrification using hydrolyzed carbon.

In summary, the AOA configuration achieved improved SNDPR as compared to the AO configuration when the aerobic phase was operated at a DO of 0.3 mg/L and 10℃ to treat real municipal wastewater. TN and TP removal efficiencies were calculated to be 91.1% ± 1.3% and 92.4% ± 0.7%, respectively. The addition of the post anoxic phase resulted in the reduction of NO_3-N to a low value at the end of the reaction, resulting in less rbCOD from the influent being used for denitrification and more rbCOD from the influent stored by PAOs and GAOs. The storage of rbCOD promoted EBPR and SND in the SBR.

Additional activity tests (Tests 2 and 3) were conducted to investigate whether denitrification in the aerobic phase was performed by OHOs, DGAOs, and DPAOs. Triplicate tests were performed to allow for the assessment of reproducibility. The values and error bars in Figsure. 4-3B and 4-3C represent average values and standard deviations. The average CVs of each component were in the range of 1%-8% with an exception of 66% of PO_4-P in Test 2. The high CV of PO_4-P in Test 2 was due to low values of PO_4-P, which had limited impact on analysis. Overall, triplicate tests revealed high reproducibility.

The results of the previously described dynamic tests revealed that sCOD concentrations underwent minimal change in the aerobic phase (Figure 4-2E), and hence it was concluded that denitrification by denitrifying OHOs using residual rbCOD from the anaerobic phase was negligible. Therefore, Test 2 was

conducted to assess whether denitrification by denitrifying OHOs using hydrolyzed carbon was active in the aerobic phase. Figure 4-3B shows stable NO_3-N and PO_4-P concentrations around 11.7 ± 0.2 mg N/L and 0.2 ± 0.2 mg P/L. At the beginning of the test, sCOD and PO_4-P were 17.5 ± 2.5 mg COD/L and 0.3 ± 0.2 mg P/L, eliminating denitrification by denitrifying OHOs using residual rbCOD and DPAOs. PHA concentrations were maintained stable at the end of the aerobic phase in the dynamic tests (Figure 4-2F), which indicated denitrification by DGAOs was not possible. The stable NO_3-N and PO_4-P indicated limited denitrification by denitrifying OHOs using hydrolyzed carbon at a DO of 0.3 mg/L, which also has been demonstrated in Bai et al. (2022). Hence, denitrification by denitrifying OHOs using hydrolyzed carbon was not considered to be a significant pathway of nitrogen removal in the aerobic phase.

Test 3 assessed the contribution of DPAOs and DGAOs to nitrogen removal in the aerobic phase. The test responses (Figure 4-3C) were divided into two stages with the first stage from 0 h to 1.5 h (with the presence of both NO_3-N and PO_4-P) and the second stage from 1.5 h to 2.5 h (with the presence of NO_3-N but with minimal PO_4-P). In the test, sCOD concentrations were low (15.5 ± 2.5 mg COD/L), indicating that denitrifying OHOs using residual rbCOD from the anaerobic phase did not contribute to denitrification. In the first stage, both NO_3-N and PO_4-P were linearly reduced with SNRR and specific PO_4-P removal rates of 0.6 ± 0.03 mg N/g VSS/h and 4.4 ± 0.1 mg P/g VSS/h, respectively (based on Eq. (4-4)). At the end of the first stage, PO_4-P was reduced to minimal concentrations, eliminating the chance of denitrification by DPAOs in the second stage. During the second stage, PO_4-P had constant concentration of 0.2 ± 0.2 mg P/L, indicating limited DPAO denitrification. Therefore, denitrification by DGAOs was the only potential pathway for nitrogen removal, however, denitrification by DGAOs was demonstrated inactive by limited NO_3-N reduction (around 11.7 ± 0.2 mg N/L) in the second stage. Overall, denitrification by DPAOs was active with the SNRR of 0.6 ± 0.03 mg N/g VSS/h, while denitrification by DGAOs was not active.

Microbial community analysis was conducted to further investigate the presence of potential DGAOs in the system. The ASV table shows the relative abundance of *Ca.* Competibacter, a well-known DGAO that has the ability to reduce nitrate to nitrite under anoxic conditions, was 1.6% ± 0.2%. Even though *Ca.*

Competibacter was detected in the system, denitrification by DGAOs was not observed. The lack of activity may have been due to the low temperature of the system since anaerobic carbon storage by *Ca.* Competibacter has been reported to be inactive at 10℃ (Lopez-Vazquez et al., 2009a). Overall, the inactive denitrification by DGAOs was not due to the absense of *Ca.* Competibacter, a known DGAO, but might due to the low temperature (10℃).

Microbial community analysis and FAPROTAX analysis were conducted to study the existence of DPAOs in the system. Figure 4-4 shows that the microorganisms which were predicted to have denitrification function accounted for 5.1% ± 0.4% of total microorganisms. Within these microorganisms, the genera *Dechloromonas* (4.9% ± 0.7%), *Thauera* (0.2% ± 0.3%), *Pseudomonas* (0.1% ± 0.1%), and *Paracoccus* (0.1% ± 0.1%) were predicted to be capable of nitrate and phosphorus reduction, indicating likely candidates as DPAOs (Bai et al., 2022). The dominant genus of *Dechloromonas* (4.9% ± 0.7%) was also observed in Bai et al. (2022), indicating that the process configuration and wastewater composition did not present an important for DPAO community. Therefore, the denitrification by DPAOs under aerobic conditions was performed mainly by *Dechloromonas*.

The results of the microbial community analysis were also examined to assess whether aerobic PAOs could have been responsible for PO_4-P uptake in the aerobic phase. The ASV table shows the relative abundance of *Ca.* Accumulibacter was 0.2% ± 0.2%. *Ca.* Accumulibacter was acknowledged to take up phosphorus in the aerobic phase and accepted as an aerobic PAO (Bai et al., 2022). Compared with DPAOs, PAOs established low abundance, indicating DPAOs could be the dominant bacteria for PO_4-P uptake in the aerobic phase. Overall, *Ca.* Accumulibacter, an aerobic PAO, was detected and responsible for PO_4-P uptake in the aerobic phase.

Nitrogen mass balances (Table 4-1) were conducted in the SBR system to understand the pathways responsible for nitrogen removal. In the mass balances nitrogen was assumed to exit the SBR through 1) cell synthesis; 2) decant; 3) denitrification in the anaerobic phase; 4) DPAO denitrification in the aerobic

phase; 5) denitrifying OHO denitrification using hydrolyzed carbon in the post anoxic phase. The detailed calculations employed to create the mass balances are described in Appendix B. The relative error of the mass balance was -3% ± 2%, which demonstrated good closure. Overall, the low relative error of the mass balance provided a high level of confidence to accurately and quantitatively investigate the mass of nitrogen removed from each pathway.

The potential for nitrous oxide (N_2O) emissions was considered when identifying nitrogen removal pathways for inclusion in the mass balances. N_2O emissions can result from nitrifier nitrification, nitrifier denitrification, and heterotrophic denitrification (Kampschreur et al., 2009). Kampschreur et al. (2009) summarized that 0.05% to 25% of the nitrogen load could be removed through N_2O emission. The high variation in values was attributed to differences in testing methods. Most reports have indicated that nitrogen removed through N_2O emission was less than 3% of the nitrogen load (Kampschreur et al., 2009). Further, while several studies have shown that low DO operation leads to high N_2O emission, Liu et al. (2021) demonstrated that long-term operation at a DO of 0.41 mg/L had lower N_2O emissions (0.11%) when compared to a DO of 2 mg/L (0.24%). It was hypothesized that long term operation at low DO led to growth of ammonia-oxidizing archaea that do not produce N_2O due to the lack of canonical nitric oxide reductase genes that convert NO to N_2O. In summary, while low DO operation leads to N_2O emissions they were not considered as a major nitrogen removal pathway and hence were not included in the nitrogen mass balances.

A summary of the mass balance analysis is presented in Table 4-1. The nitrogen removed through OHO denitrification using hydrolyzed carbon in the post anoxic phase, DPAO denitrification in the aerobic phase, and denitrification in the anaerobic phase were 56%, 16%, and 0.3% of influent total nitrogen mass, respectively. Among these denitrification pathways, denitrifying OHO denitrification using hydrolyzed carbon in the post anoxic phase was the most significant contributor to remove nitrogen. Due to the substantial removal of nitrogen in the post anoxic phase, the nitrate concentration at the end of the post anoxic phase was low, leading minimal (0.3%) nitrogen removal through denitrification in the anaerobic

phase. Due to the low COD consumption for denitrification in the anaerobic phase, most of the COD was stored by PAOs and GAOs to promote SNDPR. In the aerobic phase, nitrogen mass removed through DPAO denitrification using PHA was 16% of the influent nitrogen. Approximately 20% of influent nitrogen was employed for cell synthesis. Compared with the nitrogen removal pathways in Bai et al. (2022), the nitrogen removal pathways in this study showed similar nitrogen proportion for cell synthesis, higher nitrogen proportion for denitrification in the anoxic phase, and lower nitrogen proportion for denitrification in the anaerobic and aerobic phases and decant. All differences were caused by the implementation of post anoxic, which further reduced NO_3-N in the effluent, leading to the reduction of nitrogen removed through decant and denitrification in the anaerobic phase. In order to implement SNDPR successfully at low temperatures, it is necessary to determine the post anoxic time to reduce NO_3-N to a certain level that would not consume substantial rbCOD from the influent and leave enough rbCOD for PAO storage.

Table 4-1. Nitrogen mass balance for a typical cycle of Period 2 at a DO of 0.3 mg/L and 10℃

N mass component	Mass (mg N)	Proportion (%)
N mass in from influent	324 ± 9	
N mass used for cell synthesis	66 ± 9	20 ± 3
N mass decant from the system	17 ± 7	5 ± 2
N mass denitrified in the anaerobic phase	1 ± 1	0.3 ± 0.2
N mass removed through DPAOs using PHA in the aerobic phase	51 ± 2	16 ± 1
N mass removed through denitrifying OHOs using hydrolyzed carbon in the post anoxic phase	181 ± 2	56 ± 1
Calculated N mass in from influent	316 ± 14	

Note: The calculation of values is shown in Appendix B. Relative error is -3% ± 2%.

4.4. Conclusions

The operational conditions that were successfully employed to achieve SNDPR when treating synthetic wastewaters could not achieve SNDPR when treating real municipal wastewaters due to most of the influent rbCOD being used for denitrification and thereby only a limited amount of rbCOD was stored by PAOs. When compared to the AO configuration, the AOA configuration was able to achieve SNDPR to treat real municipal wastewater at a low temperature (10°C) with TN removal, TP removal, and SND efficiencies of 91.1%, 92.4%, and 28.5%, respectively. The SND in the aerobic phase was found to be achieved through denitrification by DPAOs (*Dechloromonas*). The system was rich in PAOs as demonstrated by stoichiometric ratios and 16S rRNA gene analysis. Even though DGAOs (*Ca.* Competibacter) were detected in the system, denitrification by DGAOs was not active, which might be due to low temperatures. This research was the first to 1) investigate the performance of SNDPR when real municipal wastewater was treated under low temperature conditions (10°C); 2) investigate whether operational conditions that have been successfully employed to treat synthetic wastewaters can also be applied to real municipal wastewaters; 3) compare the performance of SNDPR when operated in different process configurations (AO and AOA).

Chapter 5 A comprehensive floc model with application to simultaneous nitrification, denitrification, and phosphorus removal at a low temperature

Abstract

A comprehensive floc model was designed to investigate simultaneous nitrification, denitrification, and phosphorus removal (SNDPR) at 10°C. The floc model was the first to incorporate phosphorus accumulating organisms (PAOs) and glycogen accumulating organisms (GAOs), intrinsic half-saturation coefficients of each microorganism, external mass transfer terms, internal diffusion, and intra-floc movement. Results show that only boundary layer thickness in the floc-related parameters established a minor impact on nitrite, and seven new incorporated parameters ($f_{P,VFA}$, $f_{PP,PHA,ox}$, and intrinsic half-saturation coefficients of oxygen of ammonia oxidizing bacteria (AOB), nitrite oxidizing bacteria (NOB), ordinary heterotrophic organisms (OHOs), PAOs, and GAOs) were deemed as sensitive parameters. The model calibration and validation were demonstrated successful based on R^2, mean square relative error, and residual analysis. After model validation, intrinsic K_O values of AOB, NOB, OHOs, PAOs, and GAOs were estimated to be 0.08, 0.18, 0.03, 0.1, and 0.07 mg/L, respectively. Based on model analysis, 87% of volatile fatty acids were stored by PAOs and GAOs, leading to successful PO_4-P uptake through PAO aerobic growth (85%) and PAO denitrification via nitrite (12%). In the aerobic phase, 93% and 5% of consumed readily biodegradable chemical oxygen demand were used for OHO aerobic growth and OHO denitrification via nitrite, respectively. Regarding to SND, nitrite was the dominant electron acceptor for denitrification by PAOs (75%) and OHOs (25%), indicating NO_2-N was easier to be used by PAOs and OHOs for denitrification than by NOB for nitrification. Microbial and dissolved oxygen profiles within the floc demonstrated that PAOs were the dominant bacteria and that SND in the aerobic phase resulted for the large DO difference between the bulk liquid and the inner layer of the floc at the beginning of the aerobic phase. This study was the first to design a comprehensive floc model that incorporated PAOs and GAOs, intrinsic half-saturation coefficients of each microorganism, external mass transfer terms, internal diffusion,

and intra-floc movement, to simulate SNDPR. A set of intrinsic half-saturation coefficients of oxygen of each microorganism was estimated for the first time.

Keywords: Floc model; Simultaneous nitrification, denitrification, and phosphorus removal; Sumo; Low temperature; Intrinsic half-saturation coefficient

5.1. Introduction

Wastewater treatment processes that employ simultaneous nitrification, denitrification, and phosphorus removal (SNDPR) have been developed to improve upon traditional biological nutrient removal methods. In these processes nitrogen is removed through simultaneous nitrification and denitrification (SND) under low dissolved oxygen (DO) conditions with nitrification and denitrification occurring within the outer layer and inner regions of flocs, respectively (Collivignarelli & Bertanza, 1999). Low DO concentrations are essential for the occurrence of SNDPR and may support short-cut nitritation and denitritation (Kunapongkiti et al., 2020). The removal of phosphorus is achieved by providing alternating anaerobic and aerobic environments, promoting the growth of phosphorus accumulating organisms (PAOs). The potential advantages of SNDPR include reductions in the consumption of energy, carbon, and oxygen (Wang et al., 2015; Zaman et al., 2021). Therefore, SNDPR is a promising alternative for nutrient removal, however the integration of the various biological processes with advanced process flowsheets is complex.

Modeling is increasingly being employed to understand active mechanisms, optimize systems, and simulate alternative scenarios in support of process design (Rieger et al., 2012). As an example, the activated sludge models (ASMs) created by International Water Association's (IWA) have been widely acknowledged and used to describe carbon, nitrogen, and phosphorus transformation in flocculent sludge and biofilm systems (Eberl et al., 2006; Melcer, 2004). Modeling has been proven to be a convenient and economically attractive method to understand complex systems.

One of the challenges of modelling SNDPR systems with ASMs is the half-saturation coefficients (K_s) in ASMs can not describe systems where diffusion limitations are present. The half-saturation coefficients in ASMs are considered as "extant" parameters, which reflect the effects of advection and diffusion (Arnaldos et al., 2015). Many factors can impact extant K_s values, including mixing conditions and hydraulics that impact advective transport (Liu et al., 2010; Münch et al., 1996), and floc size, density, and porosity which impact diffusion (Manser et al., 2005; Pochana et al., 1999; Wang et al., 2007). Half-saturation coefficients for oxygen (K_o) are particularly important in SNDPR systems due to the low DO values employed and the importance of low DO values in determining several key biological reaction rates (Daigger et al., 2007). Therefore, there is a need to develop a new model to simulate the SNDPR process with diffusion limitations.

It is expected that employing intrinsic K_s parameters in a model that includes explicit mass transfer terms would better reflect diffusion-limiting (i.e., SNDPR) systems. In this context the term "intrinsic" refers to the actual K_s of a specific biomass species in the absence of substrate diffusion limitations. An intrinsic K_s has a constant value, which avoids the variability of extant K_s in traditional simulations. The intrinsic K_s approach has been employed to simulate the transformations of carbon and nitrogen in activated sludge (AS) systems (Eberl et al., 2006; Pérez et al., 2005; Pochana et al., 1999; Shaw et al., 2013; Wang et al., 2007). The intrinsic K_s parameters have also been used to simulate aerobic and anaerobic granular systems (Baeten et al., 2019). Therefore, the application of intrinsic K_s parameters and explicit mass transfer terms has been demonstrated to be successful for modeling diffusion-limited systems, however, two microbial groups (PAOs and glycogen accumulating organisms (GAOs)) that can contribute to SNDPR have not been integrated into such models.

Several floc models have been used to simulate carbon and nitrogen compounds in diffusion-limited systems with low bulk phase DO concentrations (Pochana et al., 1999; Wang et al., 2007). Common simplifying assumptions of these floc models include negligible mass transfer limitations in the external boundary layer, uniform distribution of microbes through the floc, and limited movement of solids within a floc. However, these simplifying assumptions may not be applicable when simulating SNDPR systems.

It is hypothesized that a more comprehensive floc model should include boundary layer mass transfer, particulate component movement within the floc, and biological phosphorus removal processes to adequately simulate SNDPR. The inclusion of boundary layer mass transfer will allow mixing intensity to be considered in the model, since low mixing intensity that happens in SNDPR systems might have a significant impact on SNDPR performance (Nogueira et al., 2015). The incorporation of particulate component movement within a floc can be used to prevent inert component accumulation in the inner core of a floc and facilitate a dynamic microbial population distribution, which is important for SNDPR due to impact of differing impacts of redox conditions on the various microbial groups (Baeten et al., 2019). Finally, PAOs and GAOs should be included to simulate SNDPR, in which phosphorus and nitrogen removal occurs under low DO conditions (Rubio-Rincón et al., 2017). Therefore, these aspects were incorporated in a floc model in the current study to permit comprehensive analysis of SNDPR systems.

In this study, the previously mentioned elements were developed in the Sumo© process simulator (Dynamita, 2017). After development, a sensitivity analysis was conducted on the floc model, when configured to reflect an SNDPR process, in order to identify the parameters that have the most impact upon simulated values. The floc model was then calibrated and validated using experimental data obtained from a bench-scale sequencing batch reactor (SBR) operated for SNDPR (Bai et al., 2022). After validation, the model was employed to quantify the active pathways of carbon, nitrogen, and phosphorus transformation in the SNDPR system. The profiles of microorganisms and dissolved oxygen within the floc was studied to further understand the causes of SNDPR.

5.2. Materials and methods

5.2.1. Floc model description

A floc model was developed to study the mechanisms of SNDPR and was assembled in the Sumo© software. Figure 5-1 shows the key processes incorporated in the floc model, including diffusion, biological reactions, and intra-floc movement. The floc model was divided into biological, floc-related biofilm, and reactor sub-models based on these processes. The details of each sub-model are described in the following sections.

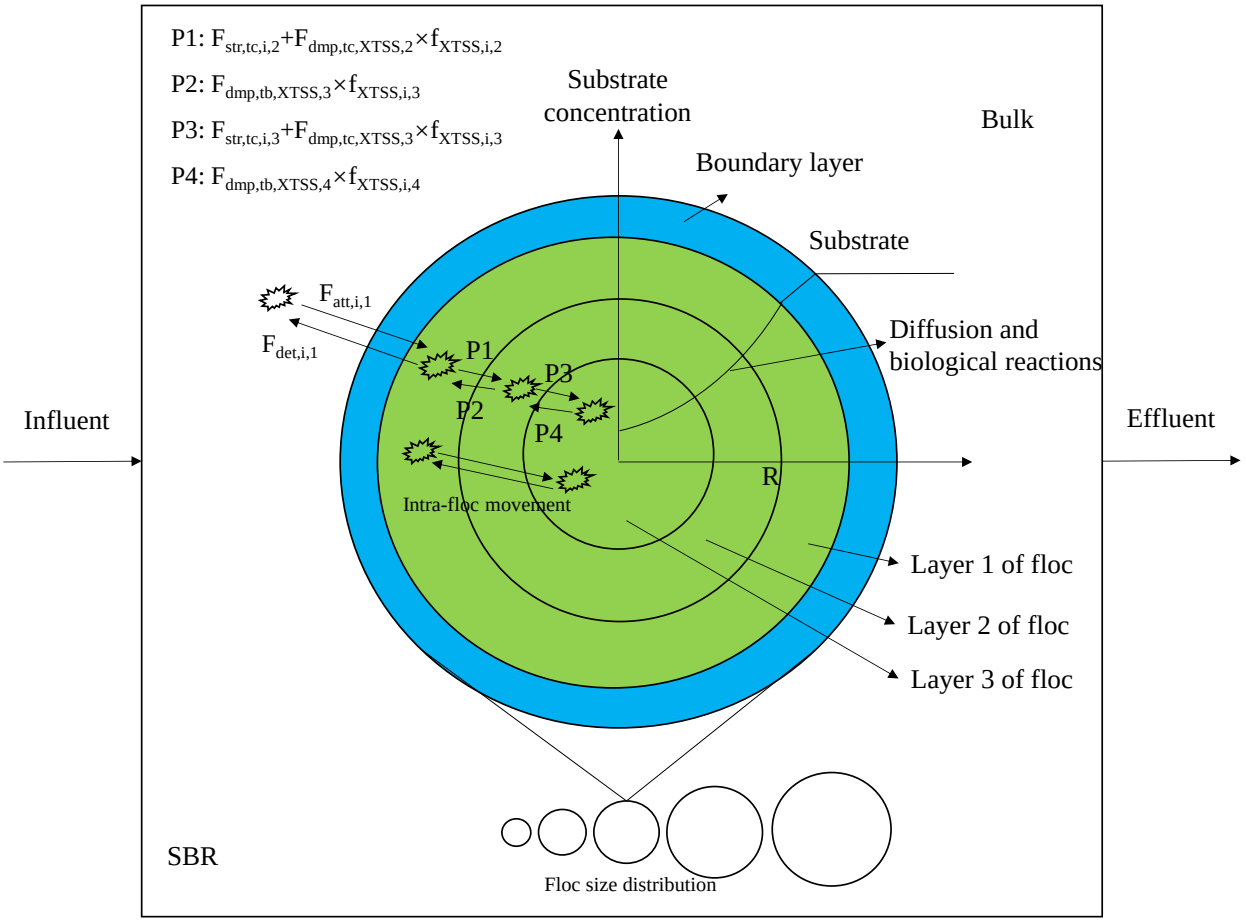

Figure 5-1. Key processes in the floc model

5.2.1.1. Biological sub-model

The biological sub-model used in this study consisted of the Sumo2 model that includes common functional microbial groups that are commonly associated with SNDPR processes including ammonia-oxidizing bacteria (AOB), nitrite-oxidizing bacteria (NOB), ordinary heterotrophic organisms (OHOs), PAOs, and GAOs (Bryant & Coats, 2021; Gazsó et al., 2017; Igos et al., 2017; Layer et al., 2020; Varga et al., 2018). The main differences between Sumo2 and ASM2d are the inclusion of GAOs, two-step nitrification by AOB and NOB, and two-step denitrification by OHOs, PAOs, and GAOs. Therefore, several more processes were included in the Sumo2 model compared to ASM2d. Under anaerobic conditions, readily biodegradable chemical oxygen demand (rbCOD) can be fermented to volatile fatty acids (VFAs) by OHOs and PAOs. VFAs can be stored by PAOs as polyhydroxyalkanoates (PHA) and by GAOs as glycogen. Under anoxic conditions, stored PHA and glycogen can be used for denitrification to reduce nitrate to nitrite and further to nitrogen gas through PAO and GAO anoxic growth and maintenance. Under aerobic conditions, PHA can be oxidized for PAO maintenance and growth to take up orthophosphate. Glycogen can be oxidized for GAO growth and maintenance. The detailed biological processes for carbon, nitrogen and phosphorus transformation are shown in Appendix C-1. The stoichiometric matrix, process rate expressions, and kinetic parameter values are presented in Tables C-3 to C-7.

5.2.1.2. Floc-related biofilm sub-model

5.2.1.2.1. External mass transfer

External mass transfer through a boundary layer was included in the biofilm sub-model (Henze et al., 2008). Mass transfer of soluble substrates from bulk to the floc surface is calculated as described in (Eq. (5-1)). The surface area of floc is calculated using Eq. (5-2) to Eq. (5-5). These equations initially estimate the total volume of biomass based upon the inventory of biomass present in the SBR. The total surface area is

then estimated based on an assumed floc radius that allows the volume of individual floc and subsequently the number of flocs in the SBR to be calculated when flocs are assumed to be sphere. In this study, the morphology of flocs was assumed to be spherical to reduce complexity. Among these parameters, diffusivity of each soluble substrate in water ($D_{W,i}$) is from Henze et al. (2008). The parameters of boundary layer thickness (Z_{BL}), floc radius (Z_F), SBR tank surface area ($A_{reactor}$), settled floc level ($h_{settled,floc}$), the water between settled floc (free water) ($V_{water,floc}$) can be set in the floc model.

$$F_i = D_{W,i} \times A_2 \times \frac{C_{b,i} - C_{f,i,2}}{Z_{BL}} \quad \text{Eq. (5-1)}$$

$$V_{flocs} = h_{settled,floc} \times A_{reactor} \times \left(1 - V_{water,floc}\right) \quad \text{Eq. (5-2)}$$

$$V_{floc,individual} = \frac{4}{3} \times \pi \times {Z_F}^3 \quad \text{Eq. (5-3)}$$

$$nflocs = \frac{V_{flocs}}{V_{floc,individual}} \quad \text{Eq. (5-4)}$$

$$A_2 = nflocs \times 4 \times \pi \times {Z_F}^2 \quad \text{Eq. (5-5)}$$

Where i is the i^{th} soluble substrate; $D_{W,i}$ is the diffusion coefficient of the i^{th} soluble substrate in the water phase (L^2/T); A_2 is the surface area of flocs (L^2); $C_{b,i}$ is the i^{th} soluble substrate concentration in the bulk (M/L^3); $C_{f,i,2}$ is the i^{th} soluble substrate concentration at the surface of the floc (M/L^3); Z_{BL} is the boundary layer thickness (L); F_i is the mass transfer rate of the i^{th} soluble substrate from bulk to floc surface (M/T); V_{flocs} is the total volume of flocs (L^3); $h_{settled,floc}$ is settled floc level (L); $A_{reactor}$ is the surface area of the SBR reactor (L^2); $V_{water,floc}$ is the water between settled floc (free water) (calculated from settled spheres with lattice packing to be 0.26 on the assumption that distances between flocs after settling are negligible); $V_{floc,individual}$ is the volume of one floc (L^3); Z_F is the floc radius (L); nflocs is the number of flocs.

5.2.1.2.2. Internal diffusion

Internal diffusion refers to diffusion activities within the floc. The driving force for diffusion in the floc is the substrate concentration difference between two adjacent layers. Eq. (5-6) describes the mass transfer of soluble substrates due to diffusion (Henze et al., 2008). The floc continuum is divided into n layer of equivalent thickness (Z_L) (Eq. (5-8)), and hence the surface area of each layer is calculated by Eq. (5-9) and Eq. (5-10). Among these parameters, the reduction factor of diffusivity (f_d) and layer number (n) can be set in the floc model. The diffusivity reduction factor was assumed to be the same for all soluble components to avoid complexity. The number of floc layers was assumed to be three in consideration of computational power requirements.

$$F_{diff,tc,i,j} = D_{W,i} \times f_d \times A_{j+1} \times \frac{C_{f,i,j} - C_{f,i,j+1}}{Z_L} \quad \text{Eq. (5-6)}$$

$$F_{diff,tb,i,j+1} = -F_{diff,tc,i,j} \quad \text{Eq. (5-7)}$$

$$Z_L = \frac{Z_F}{n-1} \quad \text{Eq. (5-8)}$$

$$A_{j+1} = nflocs \times 4 \times \pi \times (ZA_{j+1})^2 \quad \text{Eq. (5-9)}$$

$$ZA_{j+1} = (n - j + 1) \times Z_L \quad \text{Eq. (5-10)}$$

Where j is the indicator of the $(j-1)^{th}$ layer (j=1 represents bulk; j=2 represents layer 1 in the floc (e.g., outer layer); j=3 represents layer 2 in the floc; the max j is n+1); n is the assumed layer number; $F_{diff,tc,i,j}$ is the mass transfer rate of the i^{th} soluble substrate towards floc core by diffusion from the $(j-1)^{th}$ layer (M/T); $F_{diff,tb,i,j+1}$ is the mass transfer rate of the i^{th} soluble substrate towards bulk by diffusion from the j^{th} layer (M/T); f_d is the reduction factor of diffusivity; A_{j+1} is the surface area of the j^{th} layer (L^2); $C_{f,i,j}$ is the i^{th} soluble substrate concentration at the $(j-1)^{th}$ layer in the floc (M/L^3); Z_L is the floc layer thickness (L); ZA_{j+1} is the distance from the core to the surface of the j^{th} layer (L).

5.2.1.2.3. Mass balances of soluble components in the floc

The change of soluble substrate concentration in the floc is due to diffusion and biological reactions. Eq. (5-11) calculates the mass balance of soluble components in the floc. The left side of the equation ($V_j \times \frac{dC_{f,i,j}}{dtt}$) represents the mass change rate of the soluble substrate in the floc. The first two terms on the right side of the equation ($-F_{diff,tc,i,j} - F_{diff,tb,i,j}$) represent mass change rate of soluble substrates in the floc due to diffusion. The last term on the right side of the equation ($V_j \times r_{i,j}$) represents the mass change rate of the soluble substrate in the floc due to biological reactions. Eq. (5-12) - Eq. (5-14) are substituted into Eq. (5-11) to solve for soluble component concentration in a specific floc layer. Eq. (5-13) represents the volume of a specific floc layer, which is calculated by the multiplication of flocs volume and the volume fraction of that layer over the entire floc. The volume fraction of each layer over the entire floc is shown in Eq. (5-14) when the floc is assumed to be sphere with three layers.

$$V_j \times \frac{dC_{f,i,j}}{dt} = -F_{diff,tc,i,j} - F_{diff,tb,i,j} + V_j \times r_{i,j} \quad \text{Eq. (5-11)}$$

$$r_{i,j} = \sum_{k=1}^{m} v_{i,k}\beta_{j,k} \quad \text{Eq. (5-12)}$$

$$V_j = V_{flocs} \times Vf_j \quad when\ j > 1 \quad \text{Eq. (5-13)}$$

$$Vf_j = \begin{cases} \frac{\frac{4}{3}\times\pi\times({Z_F}^3 - \left(\frac{2}{3}Z_F\right)^3)}{\frac{4}{3}\times\pi\times{Z_F}^3} = 0.7037 \quad when\ j = 2 \\ \frac{\frac{4}{3}\times\pi\times(\left(\frac{2}{3}Z_F\right)^3 - \left(\frac{1}{3}Z_F\right)^3)}{\frac{4}{3}\times\pi\times{Z_F}^3} = 0.2593 \quad when\ j = 3 \\ \frac{\frac{4}{3}\times\pi\times\left(\frac{1}{3}Z_F\right)^3}{\frac{4}{3}\times\pi\times{Z_F}^3} = 0.037 \quad when\ j = 4 \end{cases} \quad \text{Eq. (5-14)}$$

Where V_j is the volume of the (j-1)th layer (L^3); $V_j \times r_{i,j}$ is the mass transfer rate of the ith soluble substrate at the (j-1)th layer (M/T); $v_{i,k}$ is the stoichiometric coefficient of the ith soluble component at the kth process; m is the total number of biological processes; $\beta_{j,k}$ is the kth process rate at the (j-1)th layer; Vf_j is the volume fraction of the (j-1)th layer in a floc.

5.2.1.2.4. Solids transfer inside the floc

Solids in the floc refer to microbial species and other particulate components (organic particulate substrates, inert particulate materials, etc.). The movement of these solids in the floc is associated with transformation and transport processes **(**Wanner, 1996**)**. The transformation processes refer to cell growth, cell decay, hydrolysis of organic particles, etc. The transport processes are associated with the transformation processes. For example, cell generation leads to the movement of cells to outer space. In addition, due to different redox zone created in the floc, different biological reactions happen at different layers, leading to dynamic distribution of the microbial populations in the floc (Li & Bishop, 2004). One assumption is made to simplify this process: the movement of solids in the floc is similar to soluble component diffusion in the floc based on Fick's first law of diffusion (Layer et al., 2020). Therefore, the solids transfer equation is represented by Eq. (5-15) based on an assumed internal solids transfer rate in the floc (D_X) (Dynamita, 2017).

$$F_{str,tc,i,j} = D_X \times A_{j+1} \times \frac{X_{f,i,j} - X_{f,i,j+1}}{Z_L} \quad \text{Eq. (5-15)}$$

$$F_{str,tb,i,j+1} = -F_{str,tc,i,j} \quad \text{Eq. (5-16)}$$

Where $F_{str,tc,i,j}$ is the mass transfer rate of the i^{th} particulate substrate towards floc core by solids transfer from the $(j-1)^{th}$ layer (M/T); $F_{str,tb,i,j+1}$ is the mass transfer rate of the i^{th} particulate substrate towards bulk by solids transfer from the j^{th} layer (M/T); D_X is internal solids transfer rate in the floc (L^2/T); $X_{f,i,j}$ is the i^{th} particulate substrate concentration at the $(j-1)^{th}$ layer in the floc (M/L^3).

5.2.1.2.5. TSS controller inside the floc

Except for the consideration of each particulate component in the floc, the relationship of TSS concentration in each layer should also be considered to avoid significant TSS differences in different layers. Since the real condition of TSS concentration in each layer is unknown and lacks mechanistic knowledge, the simplest assumption, which is similar TSS concentrations in the floc layers, is made to simplify the condition (Layer et al., 2020). Therefore, the purpose of the TSS controller is to move TSS from one layer to the other to maintain similar TSS concentration in the floc layers. Eq. (5-17) illustrates the mass transfer rate of TSS by displacement. The mass transfer rate of TSS by displacement is similar to soluble component diffusion in the floc with an assumed TSS controller displacement rate gain of solids between floc layers ($r_{dpm,max}$).

$$F_{dpm,tc,XTSS,j} = r_{dpm,max} \times A_{j+1} \times \frac{X_{f,TSS,j} - X_{f,TSS,j+1}}{Z_L} \quad \text{Eq. (5-17)}$$

$$F_{dpm,tb,XTSS,j+1} = -F_{dpm,tc,XTSS,j} \quad \text{Eq. (5-18)}$$

Where $F_{dpm,tc,XTSS,j}$ is the mass transfer rate of TSS towards floc core by displacement from the $(j-1)^{th}$ layer (M/T); $F_{dpm,tb,XTSS,j+1}$ is the mass transfer rate of TSS towards bulk by displacement from the j^{th} layer (M/T); $r_{dpm,max}$ is TSS controller displacement rate gain of solids between floc layers (L^2/T); $X_{f,TSS,j}$ is the TSS concentration at the $(j-1)^{th}$ layer in the floc (M/L^3).

5.2.1.2.6. Mass balance of particulate component in the floc

The change of particulate component concentration in the floc is due to solids transfer (F_{str}), displacement ($F_{dmp,XTSS} \times f_{XTSS,i}$), and biological reactions ($V_j \times r_{i,j}$). Figure 5-1 shows the movement of particulate components in each layer. The mass balances of particulate component in each layer are shown in Eq. (5-19) and Eq. (5-24) (Dynamita, 2017). Eq. (5-20) - Eq. (5-23) are substituted into Eq. (5-19) to solve for

particulate component concentration in layer 1. In these equations, the attachment rate (r_{attach}), detachment rate (r_{detach}), the slope of switching function around $X_{TSStarget}$ (sl), the dry matter content of flocs ($X_{TSS,F}$), and the floc density (ρ_F) can be set in the floc model.

When j=2

$$V_j \times \frac{dX_{f,i,j}}{dt} = F_{att,i,1} - F_{det,i,1} - F_{str,tc,i,j} - F_{dpm,tc,XTSS,j} \times f_{XTSS,i,j} + F_{dpm,tb,XTSS,j+1} \times f_{XTSS,i,j+1} + V_j \times r_{i,j} \quad \text{Eq. (5-19)}$$

$$F_{att,i,1} = \frac{r_{attach} \times A_2 \times X_{TSS,1}}{Z_{BL}} \times f_{XTSS,i,1} \quad \text{Eq. (5-20)}$$

$$F_{det,i,1} = \frac{f_{dpm} \times r_{detach,sl} \times A_2 \times X_{TSS,2}}{Z_{BL}} \times f_{XTSS,i,2} \quad \text{Eq. (5-21)}$$

$$r_{detach,sl} = r_{detach} \times \frac{1}{1+e^{-sl \times (X_{TSS,2} - X_{TSS,target})}} \quad \text{Eq. (5-22)}$$

$$X_{TSS,target} = X_{TSS,F} \times \rho_F \quad \text{Eq. (5-23)}$$

When j>2

$$V_j \times \frac{dX_{f,i,j}}{dt} = -F_{str,tc,i,j} - F_{dpm,tc,XTSS,j} \times f_{XTSS,i,j} - F_{str,tb,i,j} - F_{dpm,tb,XTSS,j} \times f_{XTSS,i,j} + F_{dpm,tb,XTSS,j+1} \times f_{XTSS,i,j+1} + F_{dpm,tc,XTSS,j-1} \times f_{XTSS,i,j-1} + V_j \times r_{i,j} \quad \text{Eq. (5-24)}$$

Where $f_{XTSS,i,j}$ is the fraction of the i^{th} particulate component over TSS at the $(j-1)^{th}$ layer; $F_{att,i,1}$ is the mass transfer rate of the i^{th} particulate substrate from the bulk by attachment (M/T); $F_{det,i,1}$ is the mass transfer rate of the i^{th} particulate substrate to the bulk by detachment (M/T); r_{attach} is the attachment rate (L^2/T); $f_{XTSS,i,1}$ is the fraction of the i^{th} particulate substrate over TSS in the bulk; $r_{detach,sl}$ is the corrected detachment rate (L^2/T); r_{detach} is the detachment rate (L^2/T); sl is the slope of switching function around $X_{TSStarget}$ (L^3/M);

$X_{TSS,target}$ is the target TSS concentration in the floc (M/L^3); $X_{TSS,F}$ is the dry matter content of flocs; ρ_F is the floc density (M/L^3).

5.2.1.3. Reactor sub-model

5.2.1.3.1. Mass balance of soluble components in SBR tank

The mass balance of soluble substrates in the SBR tank is represented by Eq. (5-25) (Dynamita, 2017), including the substrate mass entering through influent ($Q_{inf} \times C_{inf,i}$), substrate mass out through effluent ($Q_{eff} \times C_{eff,i}$) and wasting ($Q_{waste} \times C_{eff,i}$), substrate mass diffusing from bulk into flocs ($F_{diff,tc,i,1}$), and substrate mass change through biological reactions in the bulk ($V_1 \times r_{i,1}$).

$$V_1 \frac{dC_{b,i}}{dt} = Q_{inf} \times C_{inf,i} - Q_{eff} \times C_{eff,i} - Q_{waste} \times C_{eff,i} - F_{diff,tc,i,1} + V_1 \times r_{i,1} \quad \text{Eq. (5-25)}$$

$$V_1 = V_{reactor} - V_{flocs} \quad \text{Eq. (5-26)}$$

Where V_1 is the bulk volume (L^3); Q_{inf} is the flow rate of influent (L^3/T); Q_{eff} is the flow rate of effluent (L^3/T); Q_{waste} is the flow rate of waste (L^3/T); $C_{inf,i}$ is the i^{th} soluble substrate concentration in the influent (M/L^3); $C_{eff,i}$ is the i^{th} soluble substrate concentration in the effluent (M/L^3); $F_{diff,tc,i,1}$ is the mass transfer rate of the i^{th} soluble substrate diffusion from bulk to flocs (M/T); $r_{i,1}$ is the mass transfer rate of the i^{th} soluble substrate in the bulk (M/T); $V_{reactor}$ is the liquid volume of the SBR reactor (L^3).

5.2.1.3.2. Mass balance of particulate component in the SBR tank

Except for the mass balance of particulate component in the floc (Eqs. (5-19) and (5-24)), the mass balance of particulate component in the bulk is represented by Eq. (5-27) (Dynamita, 2017), including the particulate component mass entering through influent, particulate component mass out through effluent and wasting, particulate component mass attaching to flocs, particulate component mass detaching to bulk, and

particulate component mass change through biological reactions in the bulk. The mass change rates through attachment and detachment are represented by Eq. (5-20) to Eq. (5-21).

$$V_1 \frac{dX_{b,i}}{dt} = Q_{inf} \times X_{inf,i} - Q_{eff} \times X_{eff,i} - Q_{waste} \times X_{b,i} - F_{att,i,1} + F_{det,i,1} + V_1 \times r_{i,1} \quad \text{Eq. (5-27)}$$

Where $X_{b,i}$ is the i^{th} particulate substrate concentration in the bulk (M/L^3); $X_{inf,i}$ is the i^{th} particulate substrate concentration in the influent (M/L^3); $X_{eff,i}$ is the i^{th} particulate substrate concentration in the effluent (M/L^3).

5.2.1.3.3. Sludge retention time

In the model, with the growth of bacteria, total suspended solids (TSS) increase and come to a target mass amount, which is the multiplication of measured MLSS at steady state in the SBR and reactor volume (Eq. (5-29)). Once simulated solids mass reaches target TSS mass, all the excessive solids generated in each cycle are wasted through the wasting stage to calculate SRT (Eq. (5-28)). The underlying assumptions are that effluent TSS is minimal, and no sludge waste until TSS reaches target mass. Eq. (5-29) - Eq. (5-31) are substituted into Eq. (5-28) to calculate for simulated SRT.

$$SRT = \frac{M_{XTSS,total}}{M_{XTSS,wasted} \times n_{cycle}} \quad \text{Eq. (5-28)}$$

$$M_{XTSS,total} = X_{TSS,measured} \times V_{total} \quad \text{Eq. (5-29)}$$

$$M_{XTSS,wasted} = \min(0, M_{XTSS,film,total} - M_{XTSS,target,flocs}) + X_{TSS,1} \times V_{wastage,compartment,1} \quad \text{Eq. (5-30)}$$

$$M_{XTSS,target,flocs} = V_{flocs} \times X_{TSS,target} \quad \text{Eq. (5-31)}$$

Where $X_{TSS,wasted}$ is the wasted TSS concentration (M/L^3); V_{wasted} is the wasted volume (L); SRT is solids retention time (T); $M_{XTSS,total}$ is the total mass of TSS in the reactor (M); $M_{XTSS,wasted}$ is the mass of TSS removed in one wasting phase (M); n_{cycle} is the number of cycle of one day; $X_{TSS,measured}$ is the measured

TSS concentration in the SBR (M/L^3); V_{total} is the reaction volume of SBR (L^3); $M_{XTSS,film,total}$ is total TSS mass from flocs in the reactor (M); $M_{XTSS,target,flocs}$ is the target TSS mass from flocs in the reactor (M).

5.2.2. Sensitivity analysis

A sensitivity analysis was used to evaluate the relative importance of parameters and minimize the efforts for calibration (Petersen et al., 2002). Eq. (5-32) was used to assess the sensitivity (SEN) of each output variable (y) to a 10% change of default value of each input parameter (ρ) (Van Veldhuizen et al., 1999):

$$\boldsymbol{SEN_{i,j}} = \frac{\boldsymbol{dy_j/y_j}}{\boldsymbol{d\rho_i/\rho_i}} \qquad \text{Eq. (5-32)}$$

Where dρ is the change in the input parameter value ρ; dy is the change in the output variable y; i is the i^{th} input parameter; j is the j^{th} output variable. The influence of a parameter on the model output was interpreted as follows (Petersen et al., 2002): (1) $|SEN| < 0.25$ indicates that a parameter has limited influence on the model output, (2) $0.25 \leq |SEN| < 1$ means that a parameter is influential; (3) $1 \leq |SEN| < 2$ means that a parameter is very influential; (4) $|SEN| \geq 2$ means that a parameter is extremely influential.

Input parameters of sensitivity analysis included all biokinetic, stoichiometric, and floc-related parameters. Sensitivity analysis was conducted for pseudo-steady-state and dynamic simulations. For pseudo-steady-state simulation, sensitivity analysis was used to study the impact of input parameters on long-term effluent performance, including soluble chemical oxygen demand (sCOD), NH_4-N, NO_2-N, NO_3-N, and PO_4-P. For dynamic simulation, sensitivity analysis was used to study the impact of input parameters on the turning points of each substrate in one SBR dynamic cycle, since accurately simulating these turning points of each substrate in one cycle helped interoperate the mechanisms of each substrate transformation in one cycle. Bai et al. (2022) shows that phosphorus release happened in the anaerobic phase. Therefore, the peak value of PO_4-P at the end of the anaerobic phase was a turning point for PO_4-P. In the aerobic phase, ammonia was oxidized to minimal by nitrification, and phosphorus was reduced to minimal by PAO phosphorus

uptake. Therefore, the times for PO_4-P and NH_4-N to be reduced to a minimum in the aerobic phase were turning points for PO_4-P and NH_4-N. Nitrite was generated by AOB nitrification and reduced by NOB nitrification. Therefore, the NO_2-N peak value and the time for NO_2-N to be reduced to minimum were turning points for NO_2-N.

5.2.3. Model calibration and validation

5.2.3.1. Data used for calibration and validation

Data used for model calibration included substrate profiles (sCOD, NH_4-N, NO_2-N, NO_3-N, and PO_4-P) of dynamic tests and six activity tests in Bai et al. (2022). In brief, an SBR with a working volume of 18 L was operated at 10 ± 1 ℃ and a DO of 0.3 ± 0.1 mg/L for 160 days. After the SBR came to a steady state, triplicate dynamic tests were conducted in the SBR. The cycle time was 8h with 0-1 h anaerobic, 1-7 h aerobic, and 7-8 h settling and decanting. 200 mL of mixed liquor was wasted at the end of the aerobic phase, resulting in a SRT of 30 days. The volume exchange ratio was 50%, resulting in a hydraulic retention time (HRT) of 16 hours. Synthetic wastewater was used as influent with a COD of 354 ± 15 mg COD/L (including VFA of 191.5 mg COD/L, readily biodegradable COD of 150 mg COD/L, and soluble unbiodegradable COD of 12.5 mg COD/L), NH_4-N of 30 ± 1.4 mg/L, PO_4-P of 6.5 ± 0.3 mg/L, and soluble biodegradable organic nitrogen of 19 ± 1 mg N/L. For six activity tests, Tests 1-3 were conducted under anoxic conditions to study the denitrification of OHOs, DGAOs, and DPAOs. Tests 4-6 were conducted at a DO of 0.3 mg/L to quantify the denitrification pathways by OHOs, DGAOs, and DPAOs in the aerobic phase. The detailed descriptions of these tests can be found in Bai et al. (2022). Floc size and floc density were tested at the end of dynamic tests.

Data used for model validation was dynamic tests under different DO setpoints in the SBR. After the six activity tests, another triplicate dynamic tests were conducted in the same SBR under the same conditions,

except for DO setpoints. DO concentrations were changed to 0.13 ± 0.1 and 0.055 ± 0.05 mg/L from 1 to 3.5 hour and from 3.5 to 7 hour in the aerobic phase. During the dynamic tests, 10 mL of mixed liquor samples were taken at intervals of 10 min for the first two hours and 30 min for the rest of time. Mixed liquor samples were taken to measure sCOD, NH_4-N, NO_2-N, NO_3-N, PO_4-P, soluble Total Kjeldahl Nitrogen (sTKN), PHA, and glycogen. MLSS and MLVSS were measured by taking mixed liquor at the end of the aerobic phase.

5.2.3.2. Calibration process

Model calibration was conducted by following a logical and hierarchical step iteratively. Based on the calibration protocols from many studies, the calibration of a biofilm model was to adjust the following parameters sequentially: influent characteristics, physical parameters of the reactor (tank volume, flow rates, etc.), floc-related parameters, sensitive kinetic parameters, and sensitive stoichiometric values (Hulsbeek et al., 2002; Langergraber et al., 2004; Melcer, 2004; Rittmann et al., 2018; Vanrolleghem et al., 2003). After calibration, all the adjusted parameters should remain within realistic ranges. The detailed descriptions of influent characteristics and physical parameters are illustrated in Appendix C-2.

5.2.3.2.1. Floc-related parameters

The change of floc-related parameters was based on sensitivity analysis results (Table 5-1). Floc-related parameters were distinguished as measurable, calculable, constant, and variable parameters. The descriptions of the measurable, calculable, and constant parameters are in Appendix C-2.3.

For variable parameters, boundary layer thickness (Z_{BL}) showed minor influence based on sensitivity analysis (Table 5-1), therefore, this parameter was set as default in the calibration and although it can be adjusted if necessary. The model was found to be insensitive to the empirical reduction factor for diffusion in the floc (f_d) but could affect the distribution of oxygen in flocs, resulting in the impact on nitrification

and denitrification in the SNDPR system. This was therefore also set at the default value for calibration but could be adjusted if necessary.

Overall, floc-related parameters which can be measured or calculated should use measured or calculated values, and other floc-related parameters should stay default at the initial calibration. Suppose the adjustment of kinetics and stoichiometries can not pass both calibration and validation exercises. In that case, floc-related parameters (empirical reduction factor of diffusion rate in floc and boundary layer thickness), kinetics, and stoichiometries should be adjusted again until calibration and validation are satisfied.

5.2.3.2.2. Sensitive kinetics and stoichiometries

The fourth step is to adjust kinetics and stoichiometries based on sensitivity analysis results (Table 5-1) and expert knowledge. Since this is a floc model, both half-saturation coefficients in the bulk and biofilm should be the same as intrinsic half-saturation coefficients. Therefore, the diffusion factor for half-saturation coefficients was set to be 1, and the intrinsic half-saturation coefficients are assumed to be 1/10 of default values (extant half-saturation coefficients) (Rittmann et al., 2018; Shaw et al., 2015).

The philosophy of calibration is to separate individual processes based on substrate profiles in the anaerobic/aerobic phase as much as possible to avoid error propagation. Figure 5-2 shows the logical procedures for parameters (kinetics and stochiometric parameters) calibration. The rationale for adjusting corresponding parameters in each step can be found in Table C-2. After the change of corresponding parameters in each step, the model was run for 90 days (3 SRTs) to finalize the results.

The potential for correlation between the maximum growth rate and intrinsic half-saturation coefficient of oxygen for each microorganism was identified. Hence, the data from Tests 1 to 3, anoxic conditions were established, were employed to estimate the maximum growth rates as the half-saturation coefficient of oxygen was not impactful. Then the intrinsic half-saturation coefficient of oxygen was estimated with the

data from Tests 4 to 6, which were operated under aerobic conditions. Therefore, the maximum growth rate and intrinsic half-saturation coefficient of oxygen of OHOs, PAOs, and GAOs were estimated separately to avoid correlation. As for AOB and NOB, the maximum growth rate and intrinsic half-saturation coefficient of oxygen were calibrated together, and then calibrated parameters were validated under different DO setpoints to minimize correlation.

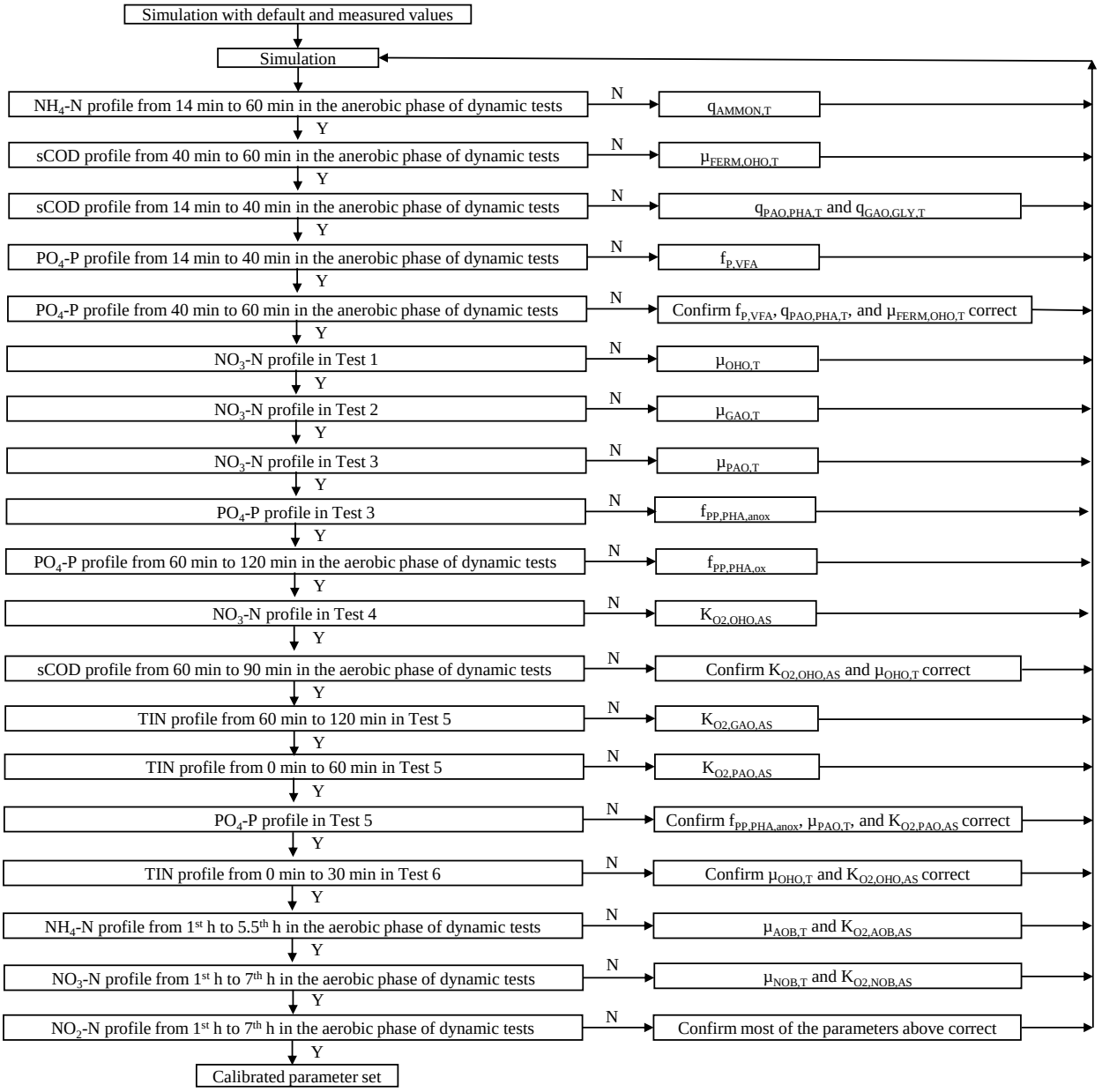

Figure 5-2. Calibration procedure for kinetics and stoichiometries for the floc model.

5.2.3.3. Validation process

After model calibration, a set of parameters was generated and used to fit an independent data set in section 2.3.1. The substrate profiles were compared with simulated results. If the parameter set generated from the calibration does not fit well with the validation data set, adjusting the parameters based on the calibration process should be conducted until both calibration and validation data sets are fitted.

5.2.4. Analysis methods

DO, temperature, pH, sCOD, NH_4-N, NO_2-N, NO_3-N, PO_4-P, sTKN, soluble total nitrogen (sTN), MLSS, MLVSS, PHA, and glycogen were measured using the same methods in Bai et al. (2022).

Floc size distribution was measured using a laser diffraction particle size analyzer (Anton Paar PSA 1190, Anton Paar Malaysia Sdn Bhd, Petaling Jaya, Malaysia). After the homogenization of mixed liquor, the mixed liquor samples were added into the circulation tank filled with deionized water until an obscuration level of 12–14% was achieved. The floc size distribution with mean size, D_{10}, D_{50}, and D_{90} based on volume fraction can be obtained.

As for floc density, a free-settling test was conducted to get terminal settling velocity (Chung & Lee, 2003). Afterwards, Stokes' law was used to calculate floc density in Eq. (5-33). In detail, a glass cylinder with a ruler at one side was used for the free-settling test. After obtaining the average floc size, 15 flocs with the same size as the average floc size were identified using a microscope and dropped to the cylinder from the top one by one. A camera was used to record the movement of flocs.

$$\rho_F - \rho = \frac{18V\eta}{d_f^2 g} \quad \text{Eq. (5-33)}$$

Where ρ_F (kg/m^3) and ρ (1000 kg/m^3) are the floc density and water density, respectively; g (9.8m/s^2) is the gravitational acceleration; d_f (m) is the floc diameter; V (m/s) is the terminal velocity; η (Ns/m^2) is the dynamic viscosity of the liquid phase of the suspension.

5.2.5. Fitness evaluation

Evaluating fitness between simulated values and measured values of a dynamic simulation was performed based on R^2 (Eq. (5-34)), mean square relative error (MSRE) (Eq. (5-35)), and residual analysis (Eq. (5-36)) (Rieger et al., 2012). R^2 is in the range of $-\infty$ to 1, with R^2=1 being the optimal value. MRSE is between 0 and ∞, with MRSE=0 being the optimal value. The drawback of R^2 is that if measured values are around a constant value (e.g., $\sum_i \left(y_{m,i} - \bar{y}\right)^2$ is small), a small variation between simulated and measured values can reduce R^2 significantly. However, MRSE can evaluate the above-mentioned scenarios. Residual was calculated by the difference between the measured and simulated values for each substrate with the expectation of random distribution near zero to be optimal.

$$R^2 = 1 - \frac{SS_{res}}{SS_{tot}} = 1 - \frac{\sum_i \left(y_{m,i} - y_{s,i}\right)^2}{\sum_i \left(y_{m,i} - \bar{y}\right)^2} \quad \text{Eq. (5-34)}$$

$$MRSE = \frac{1}{n} \sum_i \left(\frac{y_{m,i} - y_{s,i}}{y_{m,i}}\right)^2 \quad \text{Eq. (5-35)}$$

$$Residual = y_{m,i} - y_{s,i} \quad \text{Eq. (5-36)}$$

Where MRSE is mean square relative error; n is total measured points; i is the ith measured point; $y_{m,i}$ is the value of the ith measured point; $y_{s,i}$ is the value of the ith simulated point; $\bar{y}$ is the average value of all measured points; SS_{res} is the sum of squares of residuals; SS_{tot} is the total sum of squares.

5.3. Results and discussion

5.3.1. Sensitivity analysis

Sensitivity analysis was conducted to study the significance of each parameter to corresponding output variables and to determine the parameters that should be paid more attention during calibration. Table 5-1 illustrates sensitivity analysis of each input parameter with a 10% increase on corresponding output variables. Even though sensitivity analysis was conducted for 10 output variables, Table 5-1 only lists 6 output variables since the SEN values of effluent sCOD, NH_4-N, NO_2-N, and PO_4-P were always below 0.25 (limited influence). Among all the parameters, 21, 1, and 4 parameters were determined to be influential, very influential, and extremely influential, respectively. Overall, these sensitive parameters might be carefully adjusted during calibration to fit the profiles of each substrate in the dynamic tests.

The sensitivity analysis of floc-related parameters was conducted to understand the parameters that need more attention during calibration. Table 5-1 shows that among all floc-related parameters, only boundary layer thickness (Z_{BL}) has a minor impact on the peak value of NO_2-N. Therefore, during calibration floc-related parameters that could be measured were measured first, and then Z_{BL} might need to be adjusted if adjusting other parameters could not satisfy calibration.

The response of the peak value of PO_4-P at the end of anaerobic phase was assessed to understand the sensitive parameters for phosphorus release in the anaerobic phase. Table 5-1 illustrates that the ratio of P released per VFA stored ($f_{P,VFA}$) (112%) in the process of PHA storage from VFAs by PAOs was the only very influential parameter. With the increase of this parameter, the phosphorus value at the end of the anaerobic phase increased significantly. The other three OHO yield parameters ($Y_{OHO,VFA,anox}$, $Y_{OHO,SB,ox}$, and $Y_{OHO,SB,ana}$) had a slight influence since these yields can impact the competition between OHOs and PAOs for carbon sources. Overall, $f_{P,VFA}$ was significantly influential on the peak value of PO_4-P at the end

of the anaerobic phase, which implies that $f_{P,VFA}$ should be adjusted to match the phosphorus profile in the anaerobic phase during calibration.

Sensitivity analysis was conducted for the response of the time for PO_4-P reduce to minimal in order to identify the parameters that needed to be adjusted in order to match the phosphorus profile in the aerobic phase. Table 5-1 indicates that four PAO-related stoichiometries and kinetics ($f_{P,VFA}$, $f_{PP,PHA,ox}$, μ_{PAO}, and $Y_{PAO,PHA,ox}$) were influential with $f_{P,VFA}$ (71%) and the ratio of PP stored per PHA consumed under aerobic conditions ($f_{PP,PHA,ox}$) (-51%) as the top two sensitive parameters. With the increase of $f_{P,VFA}$, the PO_4-P concentration increased, resulting in more time for PO_4-P reduction to be minimal. However, $f_{PP,PHA,ox}$ means the amount of P uptake per unit of PHA consumed in the aerobic phase, indicating that the higher the value of $f_{PP,PHA,ox}$, the less time is needed for PO_4-P reduction to become minimal in the aerobic phase. Therefore, $f_{P,VFA}$ should be adjusted first based on the phosphorus profile in the anaerobic phase, and then $f_{PP,PHA,ox}$ should be adjusted to match the phosphorus profile in the aerobic phase.

The response of the time for NH_4-N reduction to be minimal was analyzed to find out the sensitive parameters for ammonia reduction in the aerobic phase in the SBR. Table 5-1 shows that the influential parameters were maximum specific growth rate of AOBs (μ_{AOB}) (-66%) and yield of AOBs on NH_x (Y_{AOB}) (52%) for this response. These two parameters are in the process of AOB growth. Therefore, μ_{AOB} and Y_{AOB} need to be paid more attention during calibration for the NH_4-N profile.

Sensitivity analysis on the response of effluent NO_3-N was conducted to study the influential parameters. Table 5-1 suggests that the yield of OHOs on readily biodegradable substrate under aerobic conditions ($Y_{OHO,SB,ox}$) (-39%) was the only influential parameter for this response. $Y_{OHO,SB,ox}$ is in the process of OHO growth under aerobic conditions, which can also perform denitrification under low DO conditions, impacting effluent NO_3-N. In addition, intrinsic half-saturation coefficients of oxygen of OHOs, PAOs, and GAOs were observed to be not influential for effluent NO_3-N. However, those parameters should have an impact on effluent NO_3-N since they can impact the denitrification rate (Jimenez et al., 2010). The level of

impact is dependent on the values of these parameters. Overall, $Y_{OHO,SB,ox}$ and intrinsic half-saturation coefficients of oxygen of OHOs, PAOs, and GAOs should be adjusted to fit the NO_3-N profile.

The response of the time for NO_2-N to reduce to be minimal was studied to find out the influential parameters. Table 5-1 implies that the maximum specific growth rate of NOBs (μ_{NOB}) (-63%) and the yield of NOBs on NO_2 (Y_{NOB}) (54%) were influential since these parameters are in the NOB nitrification process, which reduces NO_2-N. Therefore, μ_{NOB} and Y_{NOB} should be adjusted to match the NO_2-N profile.

The response of the peak value of NO_2-N was analyzed based on sensitivity analysis to identify the parameters that are influential for this response. Based on Table 5-1, most of the parameters had an impact, indicating the complexity for calibration. Among these parameters, four were extremely influential, including μ_{NOB} (-464%), Y_{NOB} (357%), the maximum specific growth rate of AOBs (μ_{AOB}) (393%), and the yield of AOBs on NH_x (Y_{AOB}) (-393%). These four parameters are all involved in the process of AOB and NOB nitrification, and nitrite is the intermediate product. Other parameters had a marginal impact. Therefore, the NO_2-N profile should be last for calibration, and μ_{NOB}, μ_{AOB}, Y_{NOB}, and Y_{AOB} are likely to be adjusted during calibration to fit the NO_2-N profile.

Table 5-1. Sensitivity analysis of the parameters in the floc model.

Parameters	Symbol	P peak value at the end of the anaerobic phase (mg/L)	Time for P reduce to minimal (min)	Time for NH_4-N reduce to minimal (min)	Effluent NO_3-N (mg/L)	Time for N O_2-N reduce to minimal (min)	NO_2-N peak value (mg/L)
Floc properties							
Boundary layer thickness	z_{BL}						-36%
OHOs							
Decay rate of OHOs	b_{OHO}						-36%
Reduction factor for anoxic growth of OHOs	$\eta_{OHO,anox}$						-36%
Half-saturation of O_2 for OHOs	$K_{O2,OHO}$						-36%
PAOs							
Maximum specific growth rate of PAOs	$\mu_{max,PAO}$		-31%				
Decay rate of PAOs	b_{PAO}						-36%
Rate of PAOs maintenance on PHA	b_{PHA}						-36%
Reduction factor for anoxic growth of PAOs	$\eta_{PAO,anox}$						-36%
Reduction factor for anoxic maintenance of PAOs on PHA	$\eta_{bPHA,anox}$						-36%
Half-saturation of PHA for PAOs	K_{PHA}						-36%
Half-saturation of O_2 for PAOs	$K_{O2,PAO}$						-36%
AOBs							
Maximum specific growth rate of AOBs	$\mu_{max,AOB}$			-66%			393%
Decay rate of AOBs	b_{AOB}						-71%
Half-saturation of NH_x for AOBs	$K_{NHx,AOB}$						-36%
Half-saturation of O_2 for AOBs	$K_{O2,AOB}$						-71%
NOBs							
Maximum specific growth rate of NOBs	$\mu_{max.NOB}$					-63%	-464%
Decay rate of NOBs	b_{NOB}						36%

Half-saturation of O_2 for NOBs	$K_{O2,NOB}$						36%
Stoichiometric yields							
Yield of OHOs on VFA under anoxic conditions	$Y_{OHO,VFA,anox}$	-26%					-36%
Yield of OHOs on readily biodegradable substrate under aerobic conditions	$Y_{OHO,SB,ox}$	26%			-39%	-25%	-71%
Yield of OHOs on readily biodegradable substrate under anaerobic conditions	$Y_{OHO,SB,ana}$	-26%					
Yield of PAOs on PHA under aerobic conditions	$Y_{PAO,PHA,ox}$		31%				-36%
Ratio of PP stored per PHA consumed under aerobic conditions	$f_{PP,PHA,ox}$		-51%				36%
Ratio of P released per VFA stored	$f_{P,VFA}$	112%	71%				-71%
Yield of AOBs on NH_x	Y_{AOB}			52%			-393%
Yield of NOBs on NO_2	Y_{NOB}					54%	357%

Note: positive means with the increase of parameter value the corresponding response increases; negative means with the increase of parameter value the corresponding response decreases.

This table does not show the absolute value below 0.25, which is defined as limited influence.

5.3.2. Floc model calibration and validation

5.3.2.1. Model calibration

For model calibration, the data sets of dynamic tests and six activity tests from Bai et al. (2022) were chosen. The detailed calibration procedures are illustrated in Section 5.2.3.2 and shown in Figure 5-2. The chosen parameters that need to be calibrated were confirmed based on sensitivity analysis results. The NH_4-N, sCOD, and PO_4-P profiles of the anaerobic phase in dynamic tests and six activity tests were used to calibrate specific parameters since each substrate profile corresponded to specific biological reactions. Afterwards, the NH_4-N, NO_2-N, and NO_3-N profiles of the aerobic phase in dynamic tests were used to confirm prior calibrated parameters and calibrate other parameters, since more complex biological reactions were responsible for these substrates. The calibrated parameters were listed in Table 5-2. Overall, the calibration strategy was to separate biological reactions as much as possible so that few parameters were calibrated together.

The value of q_{AMMON} was estimated by fitting with the NH_4-N profile from 14 min to 60 min in the anaerobic phase of dynamic tests. Figure 5-3A shows that ammonia concentrations were linearly increased from 14 min to 60 min. The increase of ammonia was only due to ammonification of the yeast extract (Bai et al., 2022). The value of q_{AMMON} was estimated to be 0.0015 d^{-1}, which was far below the default value of 0.05 d^{-1}. The estimated ammonification rate in many studies has varied significantly, ranging from 0.0003 to 0.102 d^{-1}, due to variable wastewater composition (Görgün et al., 2007; Mannina et al., 2011). Overall, the ammonification rate is dependent on wastewater composition, and was estimated to be 0.0015 d^{-1} in this study.

The values of $q_{PAO,PHA}$ and $q_{GAO,GLY}$ were estimated based on the sCOD profile from 14 min to 40 min in the anaerobic phase of dynamic tests. Figure 5-3B shows the linear reduction of sCOD from 14 min to 40 min. The reduction of sCOD contributed to the storage of VFAs by PAOs and GAOs (Bai et al., 2022). In order

to fit the sCOD profile, $q_{PAO,PHA}$ was maintained at a default value (4 d^{-1}), and $q_{GAO,GLY}$ was adjusted from 4 to 3 d^{-1}. Several studies have found that $q_{GAO,GLY}$ was 4 d^{-1} and 5.7 d^{-1} at GAO-rich systems (Filipe et al., 2001; Zeng et al., 2003b), while this system was a PAO-rich system (Bai et al., 2022), leading to a reduction of $q_{GAO,GLY}$ to 3 d^{-1}. Overall, the value of $q_{GAO,GLY}$ could depend on the relative abundance of GAOs in the system and was estimated to be 3 d^{-1} at a PAO-rich system.

The value of $f_{P,VFA}$ was calibrated based on the PO_4-P profile from 14 min to 40 min in the anaerobic phase of dynamic tests. Figure 5-3B shows the increase of phosphorus along with the reduction of sCOD. The increase of phosphorus was due to PO_4-P release by PAOs with the storage of VFAs (Bai et al., 2022). The value of $f_{P,VFA}$ is the ratio of phosphorus release to VFA uptake and was estimated to be 0.4 g P/g COD, which is similar to the value (0.5 g P/g COD) measured in a pure PAO system (Smolders et al., 1994). Many studies have demonstrated the necessity of adjusting parameters related to PAOs, which might be due to the lack of consideration of GAOs (Barnard et al., 2017; De Kreuk et al., 2007). Overall, $f_{P,VFA}$ is a frequently adjusted parameter and was estimated to be 0.4 g P/g COD in this study.

The value of $\mu_{max,OHO}$ was estimated based on the NO_3-N profile in Test 1 under anoxic conditions. Figure 5-3C shows the linear reduction of NO_3-N, which was due to dentification by OHOs using hydrolyzed carbon (Bai et al., 2022). Since Test 1 was conducted under anoxic conditions with sufficient NO_3-N, the sensitive parameter in the OHO denitrification was $\mu_{max,OHO}$, which was adjusted to 4.5 d^{-1} to have a good fit for nitrate concentrations in Test 1.

The value of $\mu_{max,PAO}$ was calibrated based on the NO_3-N profile in Test 3 under anoxic conditions. Figure 5-3E shows the linear reduction of NO_3-N, which contributed to denitrification by OHOs, GAOs, and PAOs (Bai et al., 2022). Figures 5-3C and 5-3D show perfect prediction in Tests 1 and 2, leading to the verification of parameters in OHO and GAO denitrification. Therefore, Test 3 could be used to calibrate parameters in PAO denitrification, and $\mu_{max,PAO}$ was estimated to be 0.5 d^{-1}.

The value of $f_{PP,PHA,ox}$ was calibrated based on the PO_4-P profile from 1h to 2h in the aerobic phase of dynamic tests. Figure 5-3B shows the linear reduction of PO_4-P from 1h to 2h due to PO_4-P uptake by PAOs (Bai et al., 2022). After calibrating $\mu_{max,PAO}$, $f_{PP,PHA,ox}$ was the most sensitive parameter for this process based on sensitivity analysis and estimated to be 0.62 g P/g COD, which is close to the value (0.48 g P/g COD) measured from a pure PAO system (Smolders et al., 1994). Overall, it was necessary to adjust $f_{PP,PHA,ox}$ to fit the PO_4-P profile in the aerobic phase and was estimated to be 0.62 g P/g COD in this study.

Intrinsic $K_{O2,OHO}$ was estimated based on the NO_3-N profile in Test 4. Figure 5-3F shows NO_3-N concentrations were around 11.3 mg N/L, indicating that the increased amount of NO_3-N due to nitrification was equal to the decreased amount through OHO denitrification using hydrolyzed carbon (Bai et al., 2022). Since $\mu_{max,OHO}$ had been calibrated, the sensitive parameter in the OHO denitrification was intrinsic $K_{O2,OHO}$, which was calibrated to be 0.03 mg/L, which is comparable with the value of 0.05 mg/L in Manser et al. (2005). Overall, compared with the value in other studies, intrinsic $K_{O2,OHO}$ of 0.03 mg/L was a reasonable estimation, which is essential for OHO denitrification in SNDPR systems.

Intrinsic $K_{O2,GAO}$ was estimated based on the TIN profile from 60 min to 120 min in Test 5. Figure 5-3G shows NO_3-N concentrations were around 12 mg N/L, indicating the equivalent amount of increase and decrease. The reduction of NO_3-N was due to OHO denitrification using hydrolyzed carbon and DGAO denitrification (Bai et al., 2022). Since OHO denitrification had been calibrated using the NO_3-N profile of Test 4, the TIN profile from 60 min to 120 min in Test 5 was used to calibrate DGAO denitrification, in which intrinsic $K_{O2,GAO}$ was the sensitive parameter based on sensitivity analysis. Intrinsic $K_{O2,GAO}$ was calibrated to be 0.1 mg/L. Overall, intrinsic $K_{O2,GAO}$ was important to GAO denitrification and was calibrated to be 0.1 mg/L.

Intrinsic $K_{O2,PAO}$ was estimated based on the NO_3-N and PO_4-P profiles from 0 min to 60 min in Test 5. Figure 5-3G shows the reduction of both NO_3-N and PO_4-P from 0 min to 60 min in Test 5, which was due to DPAO denitrification (Bai et al., 2022). The intrinsic $K_{O2,PAO}$ was estimated to fit both NO_3-N and PO_4-

P profiles with a value of 0.07 mg/L, which is consistent with the value of 0.091 mg/L from Keene et al. (2017). Compared with intrinsic $K_{O2,GAO}$, intrinsic $K_{O2,PAO}$ was less, indicating that PAOs could be the dominant bacteria at low DO concentrations, which has been demonstrated in several studies (Carvalheira et al., 2014; Lemaire et al., 2006). Overall, the calibrated intrinsic $K_{O2,PAO}$ of 0.07 mg/L was reasonable in this study.

Intrinsic $K_{O2,AOB}$ and $\mu_{max,AOB}$ were calibrated based on the NH_4-N profile from 1h to 5.5h in the aerobic phase of dynamic tests. Figure 5-3A shows the linear reduction of NH_4-N from 1h to 5.5h due to AOB nitrification (Bai et al., 2022). Based on sensitivity analysis, $\mu_{max,AOB}$ was a sensitive parameter for AOB nitrification. In addition, due to the low DO concentration in the aerobic phase, intrinsic $K_{O2,AOB}$ was deemed to be sensitive. Intrinsic $K_{O2,AOB}$ and $\mu_{max,AOB}$ were calibrated to be 0.08 mg/L and 0.6 d^{-1}. Even though these two parameters show correlation, the accurate estimation of these two parameters can be conducted by using two independent NH_4-N data sets, which were generated under different DO conditions. Several studies have shown that intrinsic $K_{O2,AOB}$ is in the range of 0.03-0.07 mg/L (Blackburne et al., 2008; Sliekers et al., 2005; Wu et al., 2017), which is close to the estimated value (0.08 mg/L) in this study. Bai et al. (2022) found that *Nitrosomonas* was the dominant AOB in the system, which was regarded as a typical K-strategist with high substrate affinities (Gieseke et al., 2001; Schramm et al., 1999). This further demonstrated the validity of low intrinsic $K_{O2,AOB}$ in this study. Overall, low intrinsic $K_{O2,AOB}$ (0.08 mg/L) demonstrated that systems operated under low DO conditions were in favor of the accommodation of K-strategist bacteria.

Intrinsic $K_{O2,NOB}$ and $\mu_{max,NOB}$ were calibrated based on the NO_3-N profile from 1h to 5.5h in the aerobic phase of dynamic tests. Figure 5-3A shows a slow increase from 1h to 2h due to NOB nitrification and substantial denitrification, and a linear increase from 2h to 5.5h due to NOB nitrification (Bai et al., 2022). Since all the parameters for OHOs, PAOs, and GAOs which were responsible for denitrification in the aerobic phase had been calibrated, the NO_3-N profile was used to calibrate parameters in NOB nitrification. Intrinsic $K_{O2,NOB}$, which had a significant impact on NOB nitrification, was calibrated to be 0.18 mg/L. The

value of $\mu_{max,NOB}$ was not adjusted; it was maintained as a default value of 0.65 d^{-1}. Even though these two parameters (intrinsic $K_{O2,NOB}$ and $\mu_{max,NOB}$) are correlated, the estimation of these two parameters was iterating constantly until the model can match two independent NO_3-N profiles from different DO setpoints, which is shown in Section 5.2.3.1. Intrinsic $K_{O2,NOB}$ of 0.18 mg/L is consistent with that in Wu et al. (2017) (0.19 mg/L). The dominant NOB was *Nitrospira* in this system, which was regarded as a K-strategist with $K_{O2,NOB}$ registering between 0.09 and 0.14 mg/L (Ushiki et al., 2017). Overall, intrinsic $K_{O2,NOB}$ (0.18 mg/L) was higher than intrinsic $K_{O2,AOB}$ (0.08 mg/L), indicating that AOB could be the dominant bacteria under low DO conditions.

R^2 and MSRE were calculated for each substrate to illustrate the fitness of simulated values and measured values (Table 5-3). It is shown that the R^2 for all the substrates was above 90%, except for the NO_2-N profile in dynamic tests (13%), the NO_3-N profile in Test 2 (84%), and the NO_3-N profile in Test 4 (-2553%). The reason for the low R^2 of the NO_2-N profile in dynamic tests and the NO_3-N profile in Test 4 was that the variation of each data set (NO_2-N and NO_3-N maintained around 0.3 and 0.33 mg N/L) was small, resulting in a small number of SS_{tot}. However, based on MSRE, all the numbers were below 1.5, indicating a successful calibration. Overall, after calibration, the simulation results matched well with measured values based on R^2 and MSRE.

The residual plot of each substrate was drawn to show the fitness of each substrate in the model calibration exercise. Figures 5-4A and 5-4B show that most of the residual errors of substrate were randomly distributed, except for PO_4-P and sCOD in the dynamic tests, and PO_4-P in Tests 5 and 6. Even though the residuals show that the calibrated model consistently overpredicted PO_4-P in the dynamic tests, Test 5, and Test 6, the predicted reduction rates for these substrates were similar to the measured reduction rates, indicating that the calibrated model captured the trend for these substrates. Overall, considering 14 substrates of interest were fitted, it was a success for model calibration.

Simulated SRT was compared with actual SRT to confirm the reliability of the calibrated model. Simulated SRT (29 days) was similar to the actual SRT (30 days) in the SBR. Therefore, the calibrated model was not only able to describe the nutrient transformation in the SBR, but also able to predict accurate SRT in the SBR, thus further confirming the reliability of the calibrated model.

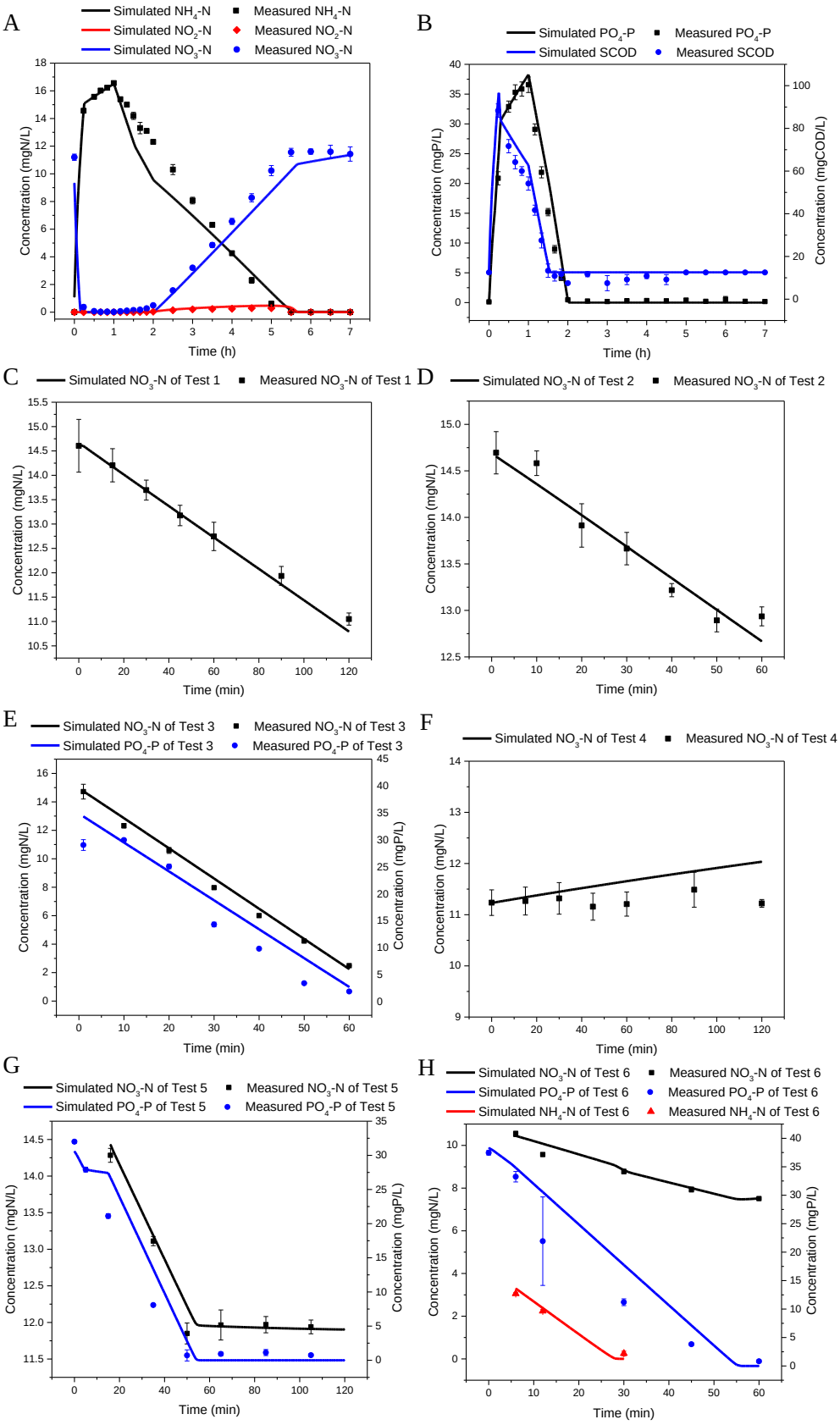
A
Simulated NH4-N
Measured NH4-N
Simulated NO2-N
Measured NO2-N
Simulated NO3-N
Measured NO3-N
Concentration (mgN/L)
Time (h)
B
Simulated PO4-P
Measured PO4-P
Simulated SCOD
Measured SCOD
Concentration (mgP/L)
Concentration (mgCOD/L)
Time (h)
C
Simulated NO3-N of Test 1
Measured NO3-N of Test 1
Concentration (mgN/L)
Time (min)
D
Simulated NO3-N of Test 2
Measured NO3-N of Test 2
Concentration (mgN/L)
Time (min)
E
Simulated NO3-N of Test 3
Measured NO3-N of Test 3
Simulated PO4-P of Test 3
Measured PO4-P of Test 3
Concentration (mgN/L)
Concentration (mgP/L)
Time (min)
F
Simulated NO3-N of Test 4
Measured NO3-N of Test 4
Concentration (mgN/L)
Time (min)
G
Simulated NO3-N of Test 5
Measured NO3-N of Test 5
Simulated PO4-P of Test 5
Measured PO4-P of Test 5
Concentration (mgN/L)
Concentration (mgP/L)
Time (min)
H
Simulated NO3-N of Test 6
Measured NO3-N of Test 6
Simulated PO4-P of Test 6
Measured PO4-P of Test 6
Simulated NH4-N of Test 6
Measured NH4-N of Test 6
Concentration (mgN/L)
Concentration (mgP/L)
Time (min)

Figure 5-3. Model calibration performance with measured data and model simulated data for A) NH_4-N, NO_2-N, and NO_3-N in the dynamic tests; B) PO_4-P and sCOD in the dynamic tests; C) NO_3-N in the Test 1; D) NO_3-N in the Test 2; E) NO_3-N and PO_4-P in the Test 3; F) NO_3-N in the Test 4; G) NO_3-N and PO_4-P in the Test 5; H) NH_4-N, NO_3-N, and PO_4-P in the Test 6.

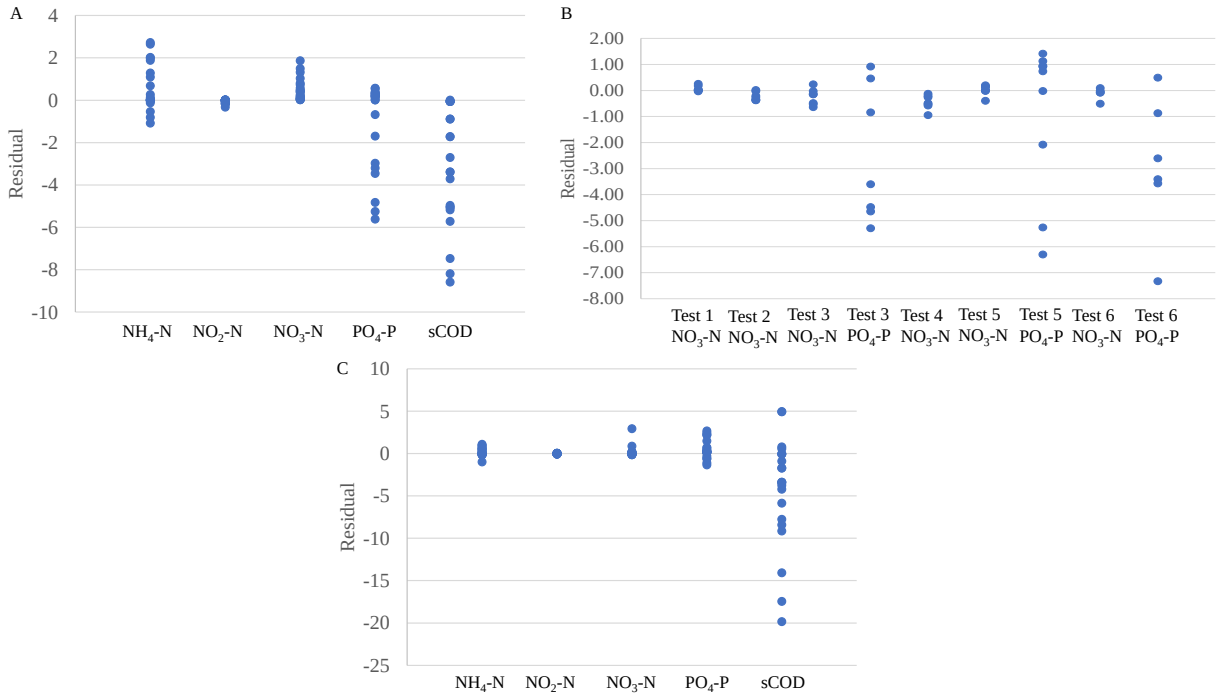

Figure 5-4. Residual plot for each substrate during model calibration (A and B) and validation (C).

Table 5-2. The calibrated model parameters in the study at temperature of 20 ℃.

Parameter	Meaning	Unit	Default value	Adjusted value
OHO				
q_{AMMON}	Rate of ammonification	d^{-1}	0.05	0.0015
$\mu_{max,OHO}$	Maximum growth rate of OHOs	d^{-1}	4	4.5
$K_{O2,OHO}$	Intrinsic half-saturation coefficient of oxygen of OHOs	mg/L	0.015	0.03
$K_{NO2,OHO}$	Intrinsic half-saturation coefficient of nitrite of OHOs	mg/L	0.005	0.05
PAO				
$K_{O2,PAO}$	Intrinsic half-saturation coefficient of oxygen of PAOs	mg/L	0.005	0.07
$f_{P,VFA}$	Ratio of P released per VFA stored	gXPP/gCOD	0.65	0.4
$\mu_{max,PAO}$	Maximum growth rate of PAOs	d^{-1}	1	0.5
$f_{PP,PHA,ox}$	Ratio of PP stored per PHA consumed under aerobic conditions	gXPP/gCOD	0.92	0.62
GAO				
$K_{O2,GAO}$	Intrinsic half-saturation coefficient of oxygen of GAOs	mg/L	0.02	0.1
$q_{GAO,GLY}$	Rate of VFA storage into glycogen for GAOs	d^{-1}	4	3
AOB				
$K_{O2,AOB}$	Intrinsic half-saturation coefficient of oxygen of AOB	mg/L	0.025	0.08
$\mu_{max,AOB}$	Maximum growth rate of AOB	d^{-1}	0.85	0.6
NOB				
$K_{O2,NOB}$	Intrinsic half-saturation coefficient of oxygen of NOB	mg/L	0.025	0.18

Table 5-3. The evaluation of fitness for model calibration and validation.

Data profile	R^2	MSRE
Calibration data set		
The NH_4-N profile in dynamic tests	97%	0.12
The NO_2-N profile in dynamic tests	13%	0.25
The NO_3-N profile in dynamic tests	98%	0.48
The sCOD profile in dynamic tests	97%	0.55
The PO_4-P profile in dynamic tests	97%	0.06
The NO_3-N profile in Test 1	99%	0.0001
The NO_3-N profile in Test 2	84%	0.0004
The NO_3-N profile in Test 3	99%	0.004
The PO_4-P profile in Test 3	90%	0.32
The NO_3-N profile in Test 4	-2553%	0.002
The NO_3-N profile in Test 5	96%	0.0002
The PO_4-P profile in Test 5	94%	1.46
The NO_3-N profile in Test 6	95%	0.0006
The PO_4-P profile in Test 6	93%	0.39
The NH_4-N profile in Test 6	96%	0.33
Validation data set		
The NH_4-N profile in dynamic tests with different DO	98%	0.001
The NO_2-N profile in dynamic tests with different DO	-625%	0.51
The NO_3-N profile in dynamic tests with different DO	93%	0.53
The sCOD profile in dynamic tests with different DO	90%	0.46
The PO_4-P profile in dynamic tests with different DO	99%	0.18

Note: MSRE: mean square relative error

5.3.2.2. Model validation

Model validation was conducted to confirm whether the calibrated model can be used to predict an independent data set from a different condition. The data used for model validation was generated from independent dynamic tests, which were similar to the dynamic tests for model calibration except that DO was set at 0.13 and 0.055 mg/L at the first 1.5 hours of aerobic zone and for the remaining time. The change of DO setpoints can be used to validate all parameters, especially the intrinsic half-saturation coefficients of oxygen of each microorganism. Overall, the data sets generated at different DO setpoints can be used for model validation.

The NH_4-N profile (Figure 5-5A) was used to validate the parameters in ammonification and AOB nitrification. The prefect fitness of NH_4-N concentrations from 14 min to 60 min in the anaerobic phase verified the demonstrated the validation of ammonification rate. In the aerobic phase, the two-stage NH_4-N reduction was observed due to two different DO setpoints (0.13 and 0.055 mg/L), which can be used to verify intrinsic $K_{O2,AOB}$ and $\mu_{max,AOB}$. All these changes were perfectly captured by the model with R^2 of 98% and MSRE of 0.001. Overall, ammonia-related parameters (intrinsic $K_{O2,AOB}$ and $\mu_{max,AOB}$) were validated based on R^2 and MSRE.

The sCOD and PO_4-P profiles were analyzed together to valid the calibrated parameters related to fermentation and PO_4-P release and uptake by PAOs. Figure 5-5B shows great fitness for sCOD from 30 min to 60 min, PO_4-P from 30 min to 60min, and PO_4-P from 60 min to 150 min, which corresponded to fermentation, PO_4-P release by PAOs, and PO_4-P uptake by PAOs, respectively. In addition, R^2 and MSRE were more than 90% and less than 0.5 for both sCOD and PO_4-P, which further indicated goodness of fit for simulated and measured data. Therefore, parameters in fermentation and PAO-related processes were validated, especially, $f_{P,VFA}$, $\mu_{max,PAO}$, $f_{PP,PHA,ox}$, $q_{GAO,GLY}$, and intrinsic $K_{O2,PAO}$.

The NO_2-N and NO_3-N profiles were analyzed together to confirm the parameters in nitrification by AOB and NOB and denitrification by OHOs, GAOs, and PAOs. Figure 5-5A shows that TIN was reduced in the

aerobic phase, indicating the existence of SND. The NO_2-N and NO_3-N profiles reflected the most complicated processes since NO_2-N and NO_3-N were related to both nitrification by AOB and NOB and denitrification by OHOs, PAOs, and GAOs. Therefore, the great fitness of NO_2-N and NO_3-N (NO_3-N: R^2=93% and MSRE=0.53; NO_2-N: MSRE=0.51) demonstrated the validation of parameters in nitrification and denitrification processes; especially intrinsic $K_{O2,NOB}$, $K_{O2,OHO}$, $K_{O2,GAO}$, and $K_{O2,PAO}$.

Residual plots were outlined to evaluate goodness of fit for model validation. Figure 5-4C shows the residuals of most of the substrates were evenly distributed near zero, except for sCOD. The validated model overpredicted sCOD. Viewed collectively, validated model can reflect the nutrient transformation, which can be used to quantitatively study the nutrient removal pathways in the system.

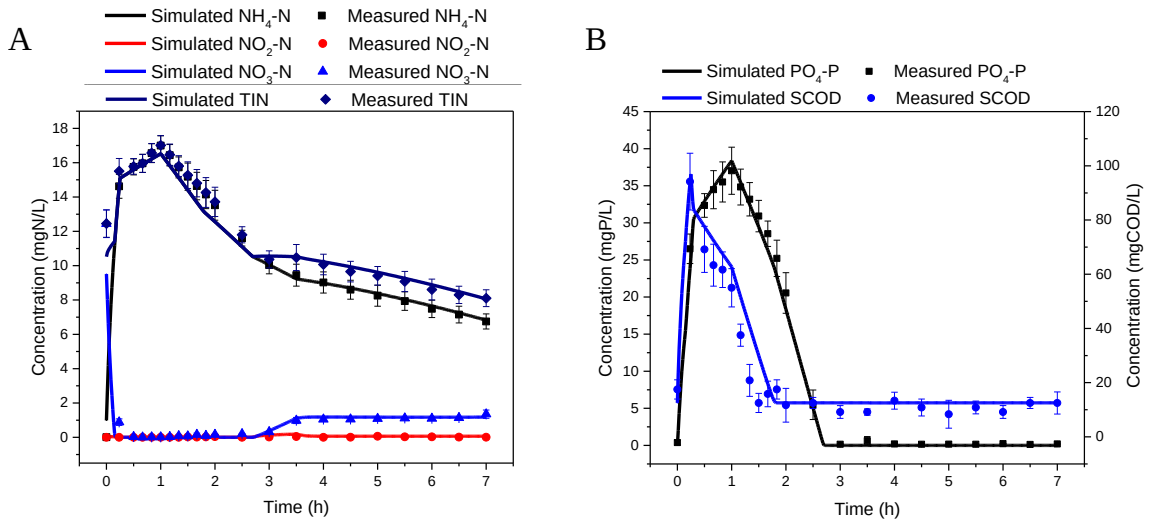

Figure 5-5. Model validation performance with measured data and model simulated data for A) NH_4-N, NO_2-N, NO_3-N, and TIN in the dynamic tests; B) PO_4-P and sCOD in the dynamic tests.

5.3.3. C, N, and P removal mechanisms based on modeling results

After the model calibration and validation, the validated model was used to illustrate carbon, nitrogen, and phosphorus transformation in the dynamic tests to better understand SNDPR at low temperatures. Table 5-4 shows the consumption or generation mass of each substrate (VFAs, rbCOD, NH_4-N, NO_2-N, NO_3-N,

organic nitrogen, and PO_4-P) through each biological process. By understanding the transformation of each substrate, it is possible to optimize the SNDPR system at low temperatures.

Mass balance of each substrate was analyzed to confirm whether the mass balance closure of each substrate was achieved. Table 5-5 shows the relative error of each substate. The absolute value of each relative error was less than 7%, which was within the acceptable range. Therefore, the value of mass change from each biological reaction was reliable, leading to the trustworthy analysis of carbon, nitrogen, and phosphorus transformation in the dynamic tests.

The analysis of mass change of VFAs from each biological process was conducted to study the transformation of VFAs and determine which process was dominant in terms of VFA consumption. Table 5-4 shows the mass change of VFAs from each biological process in the anaerobic and aerobic phases. Almost 100% of VFAs was consumed in the anaerobic phase. In the anaerobic phase, VFAs were used for OHO denitrification first, which accounted for 13% of total VFA consumption. Then, VFAs were used for PAO and GAO storage, which accounted for 85% and 2% of total VFA consumption, revealing PAO storage as the dominant process. In addition, extra VFAs were generated from rbCOD fermentation, which were mostly stored by PAOs. Overall, the dominant process of VFA consumption was PAO storage, indicating the dominant bacteria of PAOs.

The analysis of mass change of rbCOD from each biological process was used to study the transformation of rbCOD in the dynamic tests and verify whether rbCOD was used for SND in the aerobic phase. Table 5-4 shows that rbCOD was consumed by 441 mg COD and 894 mg COD in the anaerobic and aerobic phases, respectively, which indicated that most of the rbCOD was consumed in the aerobic phase. In the anaerobic phase, rbCOD (441 mg COD) was used for fermentation to generate VFAs. In the aerobic phase, the residual rbCOD from the anaerobic phase (894 mg COD) was consumed in the first hour for OHO aerobic growth (93% of consumed rbCOD) and OHO denitrification via nitrite (5% of consumed rbCOD). This indicated that rbCOD participated in SND in the aerobic phase. From 2 h to 7 h, rbCOD (1023 mg COD)

was generated through hydrolysis and consumed through OHO aerobic growth (92%), OHO denitrification via nitrite (7%), and OHO denitrification via nitrate (1%). Overall, most of the rbCOD was used for fermentation and OHO aerobic growth, and a small percentage of rbCOD was used for denitrification with nitrite as the electron acceptor.

The analysis of mass change of NH_4-N from each biological process (Table 5-4) was used to study the transformation of NH_4-N in the anaerobic and aerobic phases and explain the reason for underestimation of NH_4-N from 1 h to 2 h in the aerobic phase as shown in Figure 5-3A. In the system, NH_4-N increased through ammonification and decreased through bacteria growth and AOB nitrification. In the anaerobic phase, the amount of NH_4-N (37 mg N) produced through ammonification was greater than that reduced through bacteria growth (18 mg N), leading to the net NH_4-N increase. In the aerobic phase, from 1 h to 2 h, NH_4-N was used for cell growth and AOB nitrification, which accounted for 98 and 62 mg N. High percentage of NH_4-N used for cell growth (including processes of OHO and PAO aerobic growth, and OHO and PAO denitrification) was the reason for underestimation of NH_4-N. From 2 h to 5.5 h, all residual NH_4-N (170 mg N) combined with the NH_4-N generated from ammonification (97 mg N) were used for cell growth (37 mg N) and AOB nitrification (231 mg N). During this period, the percentage of NH_4-N used for cell growth was significantly reduced compared to that from 1 h to 2 h, which was due to limited PAO aerobic growth and denitrification as well as reduced OHO aerobic growth and denitrification. From 5.5 h to 7 h, all the NH_4-N generated from ammonification (40 mg N) was used for cell growth (14 mg N) and AOB nitrification (27 mg N). Overall, NH_4-N was generated from ammonification and consumed by cell growth and AOB nitrification, which were 73%, 61%, and 116% of influent NH_4-N, respectively. The high percentage of NH_4-N used for cell growth was the reason for underestimation of NH_4-N from 1 h to 2 h in the aerobic phase.

The analysis of mass change of NO_2-N from each biological process (Table 5-4) was used to confirm whether denitrification in the aerobic phase was through NO_2-N. Bai et al. (2022) indicated that there was OHO denitrification from 1 h to 1.5 h and PAO denitrification from 1 h to 2 h, which was consistent with

the simulation results. From 1 h to 1.5 h, 28 mg N of NO_2-N was generated through AOB nitrification and used for OHO denitrification via nitrite (11 mg N) and PAO denitrification via nitrite (15 mg N). From 1.5 h to 2 h, 33 mg N of generated NO_2-N was used for PAO denitrification via nitrite (26 mg N) and OHO denitrification via nitrite (3 mg N). Several studies have also found that nitrite instead of nitrate was the electron acceptor for OHO denitrification and PAO denitrification in the SNDPR system, indicating nitrite was easier to be used for denitrification than nitrate (Yan et al., 2019; Zaman et al., 2021). Therefore, it has been demonstrated that NO_2-N was the dominant electron acceptor for denitrification in the aerobic phase.

The analysis of mass change of NO_3-N from each biological process (Table 5-4) was used to study the transformation of NO_3-N in the aerobic phase and investigate whether there was denitrification via nitrate in the aerobic phase. In the aerobic phase from 1 h to 2 h, there was limited amount of NO_3-N accumulation. All the NO_3-N generated through NOB nitrification (17 mg N) was consumed through OHO (3 mg N) and DPAO (12 mg N) denitrification via nitrate with DPAO denitrification as the dominant process. Even though nitrite was the dominant electron acceptor for denitrification (56 mg N), nitrate was also used for denitrification (15 mg N). From 5.5 h to 7 h, all the NO_3-N generated through NOB nitrification was consumed by OHO denitrification through hydrolyzed carbon and PAO anoxic maintenance. Overall, denitrification via nitrate was also active in the aerobic phase.

The analysis of PO_4-P uptake in the aerobic phase can help understand the percentage of PO_4-P uptake by PAO aerobic growth and PAO denitrification. Table 5-4 shows that, in the aerobic phase, the mass changes of PO_4-P through PAO aerobic growth, PAO denitrification via nitrite, and PAO denitrification via nitrate were 588, 84, and 17 mg P, respectively, which were 85%, 12%, and 2% of total PO_4-P uptake, respectively. Overall, PAO aerobic growth was the main process responsible for PO_4-P uptake, and PAO denitrification was mainly processed through nitrite.

Table 5-4. The mass change of each interested substrate from each biological reaction in the anaerobic and aerobic phases of the dynamic tests.

	The anaerobic phase (mg)								The aerobic phase (mg)							
Process	VFA	rbCOD	X_B	OrgN	NH_4-N	NO_2-N	NO_3-N	PO_4-P	VFA	rbCOD	X_B	OrgN	NH_4-N	NO_2-N	NO_3-N	PO_4-P
OHO growth on VFAs, O_2									-16							
OHO growth on VFAs, NO_2	-164					-53			-1					-0.3		
OHO growth on VFAs, NO_3	-109					53	-53									
PAO's PHA storage from VFAs	-1756							702	-5							2
GAO's GLY storage from VFAs	-44															
S_B fermentation with high VFA (OHO growth, anaerobic)	34	-62														
S_B fermentation with low VFA (OHO growth, anaerobic)	358	-448							17	-21						
OHO growth on SB, O_2										-1947						
OHO growth on SB, NO_2		-3				-1				-121				-33		
OHO growth on SB, NO_3		-2				1	-1			-19				8	-8	
X_B hydrolysis		74	-74	5						1215	-1215	78				
Bacteria growth					-18			-4					-149			-30
Bacteria decay			75					9			1214		1			8
AOB nitrification and growth													-319	315		
$S_{N,B}$ ammonification				-37	37							-163	163			
NO_2 assimilative reduction													9	-7		
Denitrification by PAO from nitrate to nitrite						26	-26	-35						13	-13	-17
Denitrification by PAO from nitrite to nitrogen gas						-26		-52						-42		-84
PAO anoxic maintenance, NO_3						3	-3							8	-8	
PAO anoxic maintenance, NO_2						-3								-27		
NOB nitrification and growth														-233	233	
PAO aerobic growth																-588
$S_{P,B}$ conversion to PO_4								1								24
Sum	-1680	-441	1	-32	19	0	-83	622	-5	-894	-1	-85	-295	1	205	-685

Note: the negative value means decrease; the positive value means increase.

Table 5-5. Mass balance of each substrate in the dynamic tests.

	VFA	rbCOD	X_B	OrgN	NH_4-N	NO_2-N	NO_3-N	PO_4-P
Mass change from biological reactions (mg)	-1685	-1335	0	-117	-276	1	122	-62
Mass in from influent (mg)	1723	1351	0	171	270	0	0	59
Mass decant from the system (mg)	0	0	0	-54	0	0	-102	0
Relative error (%)	2%	1%		0%	-2%		16%	-7%

Note: the negative value means decrease; the positive value means increase.

5.3.4. Microorganism and dissolved oxygen concentration profiles within the floc

The concentrations of microorganisms in each layer were investigated to study microorganism distribution within a floc. Figures 5-6 a and b show the distribution of AOB, NOB, OHOs, PAOs, and GAOs within a floc. Nitrifiers (AOB and NOB) were maintained at a low level and showed even distribution within the floc. Bai et al. (2022) also demonstrated that AOB and NOB were at a low level with the relative abundances of 0.5% and 0.4%, respectively. The even distribution of nitrifiers can be attributed to the relatively consistent dissolved oxygen concentrations within the floc for 75% of time in the aerobic phase as shown in Figure 5-6 c. With the increase in depth, the OHO concentration was reduced, and PAO and GAO concentrations increased. The relative high amount of PAOs resulted in more denitrification in the aerobic phase through DPAO denitrification when compared to OHO denitrification. Compared with PAOs and OHOs, GAOs were estimated to be present at low levels, which was also demonstrated in Bai et al. (2022). Due to the low level of GAOs, denitrification by GAOs was estimated to be minimal, which was consistent with the results from Bai et al. (2022). Overall, the microorganism distribution within a floc was demonstrated with PAOs as the dominant bacteria.

Dissolved oxygen profiles in each layer (Figure 5-6 c) were studied since DO could be considered as the dominant parameter determining SND in the aerobic phase. The differences in DO between the bulk and inner layer were 0.22, 0.15, 0.08, and 0.04 mg/L for the periods from 60min to 90min, 90min to 120min, 120min to 330min, and 330min to 420min, respectively. The gradual reduction of DO difference was

attributed to the elimination of rbCOD, PO_4-P, and NH_4-N in the aerobic phase with time. In the first two time intervals, the DO concentration in the bulk was 0.3 mg/L, however, the DO concentrations in the inner layer were 0.08 and 0.15 mg/L, respectively. The low DO concentration in the inner layer created conditions that were favourable for SND. Bai et al. (2022) demonstrated that SND in the aerobic phase was due to OHO denitrification using residual rbCOD and DPAO denitrification. When rbCOD and PO_4-P were reduced to minimal, the DO concentration in the inner layer was increased to 0.22 mg/L, which did not exhibit denitrification performance. Therefore, due to the existence of rbCOD and PO_4-P at the beginning of the aerobic phase the DO in the inner layers of the floc was reduced, resulting in the existence of SND in the aerobic phase.

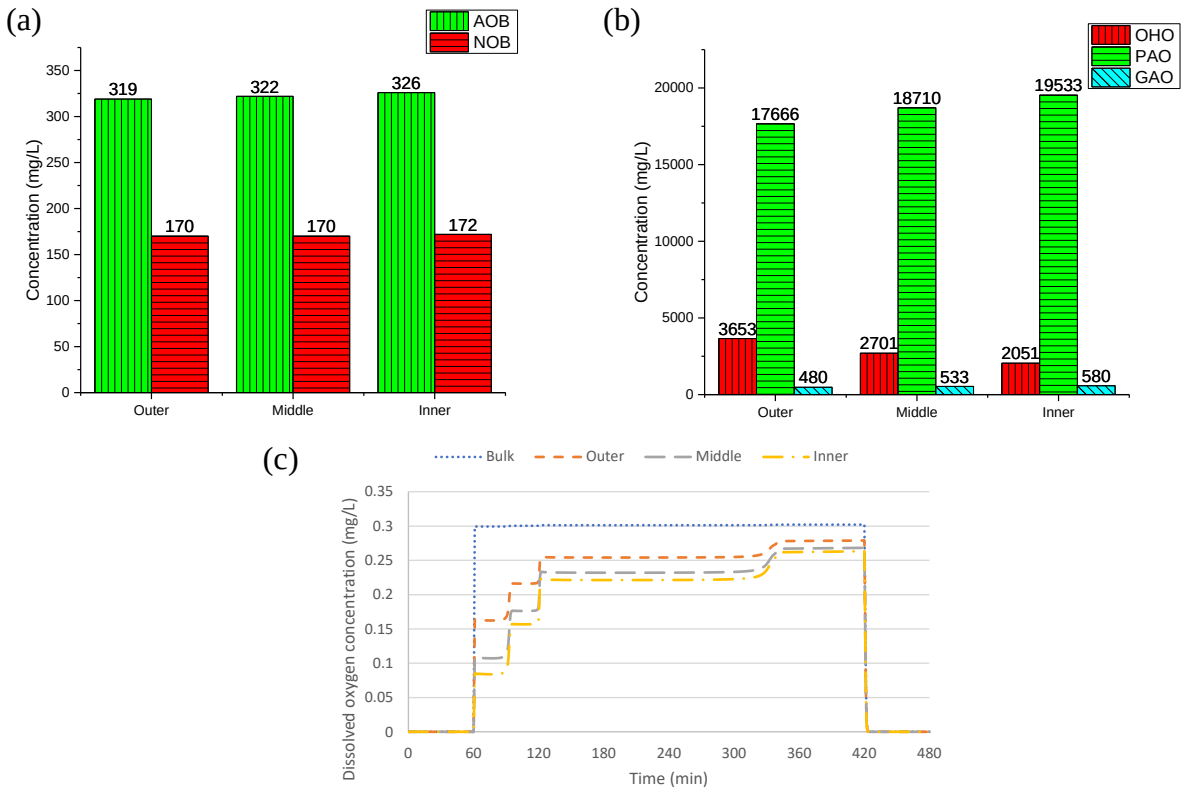

Figure 5-6. Microorganism and dissolved oxygen concentration profiles in each layer.

5.4. Conclusions

A comprehensive floc model, including PAOs and GAOs, intrinsic half-saturation coefficients, and explicit external mass transfer terms, successfully predicted the performance of SNDPR at 10°C. Among all floc-related parameters, the boundary layer thickness was found to have a minor influence on nitrite removal, indicating limited influence of floc-related parameters. Several new parameters were regarded as sensitive parameters, which included $f_{P,VFA}$, $f_{PP,PHA,ox}$, and intrinsic K_O of AOB, NOB, OHOs, PAOs, and GAOs. The sensitive intrinsic K_O values of each microorganism implied nitrification and denitrification rates in the aerobic phase would be highly impacted in the SNDPR systems. After model validation, intrinsic K_O values of AOB, NOB, OHOs, PAOs, and GAOs were estimated to be 0.08, 0.18, 0.03, 0.1, and 0.07 mg/L, respectively. Low intrinsic $K_{O2,AOB}$ (0.08 mg/L) and $K_{O2,NOB}$ (0.18 mg/L) values demonstrated SNDPR systems were benefiting for K-strategy nitrifiers growth accommodation with low half-saturation coefficients. The intrinsic $K_{O2,PAO}$ value (0.07 mg/L) was higher than the intrinsic $K_{O2,OHO}$ value (0.03 mg/L), which resulted in more denitrification by PAOs in the aerobic phase. Based on model analysis, 87% of VFAs were stored by PAOs and GAOs, leading to successful SNDPR. 85% of PO_4-P was taken up through PAO aerobic growth, and PAO denitrification via nitrite was responsible for 12% of PO_4-P uptake. It could be expected that with the reduction of oxygen more PO_4-P would be taken up through PAO denitrification, while the nitrification rate would reduce, thereby leading to an increased ammonia residual in the effluent. Regarding to SND, nitrite was the dominant electron acceptor for denitrification by PAOs (75%) and OHOs (25%), indicating NO_2-N was easier to be used by PAOs and OHOs for denitrification than by NOB for nitrification. SND through nitrite further demonstrated the existence of short-cut nitritation and denitritation. Microbial and dissolved oxygen profiles within the floc demonstrated that PAOs were the dominant bacteria and SND in the aerobic phase was due to low DO values in the inner layer at the beginning of the aerobic phase. This study was the first to design a comprehensive floc model that incorporated PAOs and GAOs, intrinsic half-saturation coefficients of each microorganism, external mass transfer terms, internal diffusion,

and intra-floc movement, to simulate SNDPR. A set of intrinsic half-saturation coefficients of oxygen of each microorganism was estimated for the first time.

Chapter 6 Conclusions and recommendations

6.1. Conclusions

The SNDPR performance when treating a complex synthetic wastewater at 10℃.

A detailed study of nitrogen removal pathways in the SNDPR system, when operated with a complex synthetic wastewater under low temperature (10 ℃) and dissolved oxygen (0.3 mg/L) conditions, was conducted using experimental methods that included characterization of the microbial community. The results indicated:

- SNDPR was achieved with stable TIN and PO_4-P removal efficiencies of 62.6% and 97%, respectively.
- Dynamic tests showed two-stage sCOD reduction and phosphorus release in the anaerobic phase due to fermentation of a complex carbon source (yeast extract) by genera *Lactococcus* and *Tetrasphaera* that had relative abundances of 1% ± 0.1% and 1.2% ± 0.6, respectively.
- The high level of PAO activity was supported by the observed ratios of P released to sCOD uptake, P release to PHA generation, PHA generation to glycogen consumption, and PHA generation to COD storage in the anaerobic phase, and the ratios of phosphorus uptake to PHA oxidized and glycogen replenishment to PHA consumption in the aerobic phase.
- PAO activity was attributed to the presence of *Dechloromonas* (9.5% ± 0.9%), *Zoogloea* (2.3% ± 0.3%), and *Paracoccus* (0.3% ± 0.01%) as DPAOs and *Ca.* Accumulibacter (3.5% ± 0.3%) and *Tetrasphaera* (1.2% ± 0.6%) as PAOs.
- AOB nitritation and NOB nitratation were active in the aerobic phase at a DO of 0.3 mg/L and temperature of 10 ℃ with *Nitrosomonas, Nitrotoga,* and *Nitrospira* as the predominant AOBs and NOBs.
- SND occurred in the first 2 hours of the aerobic phase to yield an overall SND efficiency of 31%. This was attributed to the activity of denitrifying OHOs using residual rbCOD from the anaerobic

phase and DPAO denitrification that removed 15% ± 1% and 12% ± 1% of influent total nitrogen, respectively.

- The limited DGAO activity that was observed in the presence of *Ca.* Competibacter (10.4% ± 0.6%), was attributed to low temperature (10 ℃) operation.

Overall, this research was the few researches that investigated the SNDPR process at 10℃ by using a complex synthetic wastewater, investigated the nitrogen removal pathways in the aerobic phase using an experimental method, and integrated microbial community analysis with experimental findings. The results demonstrate that operating the system at 10℃ resulted in a PAO-rich system that achieved substantial SNDPR with TIN and PO_4-P removal efficiencies of 62.6% and 97%, respectively. The main nitrogen removal pathways in the aerobic phase involved OHO supported denitrification using residual rbCOD from the anaerobic phase and DPAO denitrification, which could be enhanced by reducing the DO to a lower level.

The SNDPR performance when treating real municipal wastewater at 10℃ with a long SRT.

A detailed study of the performance of SNDPR when treating real municipal wastewater at 10℃ in the AO and AOA configurations was conducted, and microbial community analysis was conducted to support all the findings from experiment. The results indicated:

- The AO configuration could not achieve SNDPR when treating real municipal wastewater since most of the influent rbCOD was used for denitrification, resulting in limited PHA accumulation.
- The operational conditions that have demonstrated successful SNDPR to treat synthetic wastewaters did not achieve SNDPR when treating real municipal wastewaters. Therefore, more careful should be paid when adopting conclusions from synthetic wastewaters to real municipal wastewaters.

- The AOA configuration achieved improved SNDPR as compared to the AO configuration with TN removal, TP removal, and SND efficiencies of 91.1%, 92.4%, and 28.5%, respectively.
- More fermentation-related bacteria were present in the system when treating real municipal wastewater as compared to complex synthetic wastewater, which was benefit for the generation of fermented VFAs and EBPR.
- Stoichiometric ratios suggested that a PAO-rich system was generated in the AOA configuration, which was verified by microbial community analysis with *Dechloromonas* and *Ca.* Accumulibacter as dominant DPAOs and PAOs.
- SND was achieved in the first 2 hours of the aerobic phase, which was contributed to DPAO denitrification.
- The main nitrogen removal pathways were denitrification by DPAOs in the aerobic phase and denitrifying OHOs using hydrolyzed carbon in the anoxic phase, which accounted for 16% and 56% of influent nitrogen.
- The inactive denitrification by DGAOs in the aeorbic phase was not due to the absense of *Ca.* Competibacter, a known DGAO, but might due to the low temperature (10℃).

Overall, this research was the first to 1) investigate the performance of SNDPR when real municipal wastewater was treated under low temperature conditions (10℃); 2) investigate whether operational conditions that have been successfully employed to treat synthetic wastewaters can also be applied to real municipal wastewaters; 3) compare the performance of SNDPR when operated in different process configurations (AO and AOA). The results of this study demonstrate that SNDPR can be achieved at 10℃ in the AOA configuration to treat real municipal wastewater. More careful should be paid when adopting conclusions from synthetic wastewaters to real municipal wastewaters. The AOA configuration was more effective than the AO configuration to achieve SNDPR when treating real municipal wastewater at 10℃.

A comprehensive floc model developed to study the SNDPR performance when treating a complex synthetic wastewater at 10 ℃.

A comprehensive floc model, including PAOs and GAOs, intrinsic half-saturation coefficients, and explicit external mass transfer terms, was developed, calibrated, and validated to describe SNDPR at low temperatures. The results indicated:

- Among all floc-related parameters, boundary layer thickness had minor influence on nitrite. Several new parameters ($f_{P,VFA}$, $f_{PP,PHA,ox}$, and intrinsic half-saturation coefficients of oxygen of AOB, NOB, OHOs, PAOs, and GAOs) were regarded as sensitive parameters.
- After model validation, intrinsic K_O values of AOB, NOB, OHOs, PAOs, and GAOs were estimated to be 0.08, 0.18, 0.03, 0.1, and 0.07 mg/L, respectively.
- Low DO environment was benefit for the accommodation of K-strategy nitrifiers, which was indicated by low intrinsic K_O values of AOB (0.08 mg/L) and NOB (0.18 mg/L).
- The intrinsic $K_{O2,PAO}$ (0.07 mg/L) was higher than intrinsic $K_{O2,OHO}$ (0.03 mg/L), resulted in more denitrification by PAOs in the aerobic phase.
- Based on model analysis, 87% of VFAs were stored by PAOs and GAOs, leading to successful PO_4-P uptake through PAO aerobic growth (85%) and PAO denitrification via nitrite (12%).
- Regarding to SND, nitrite was the dominant electron acceptor for denitrification by PAOs (75%) and OHOs (25%), indicating NO_2-N was easier to be used by PAOs and OHOs for denitrification than by NOB for nitrification. The simulation results demonstrate the existence of short-cut nitritation and denitritation, which could save energy and carbon source for nitrogen removal.
- Microbial and dissolved oxygen profiles within the floc demonstrated that PAOs were the dominant bacteria and SND in the aerobic phase was due to low DO concentrations in the inner layer of the floc at the beginning of the aerobic phase.

Overall, this study was the first to design a comprehensive floc model that incorporated PAOs and GAOs, intrinsic half-saturation coefficients of each microorganism, external mass transfer terms, internal diffusion, and intra-floc movement, to simulate SNDPR. The results of this study reveal that the developed novel comprehensive floc model can be successfully used to predict SNDPR with the estimation of a set of intrinsic half-saturation coefficients of each microorganism. The model can be further used to optimize SNDPR under different conditions.

6.2. Recommendations

The following recommendations are suggested for future studies of SNDPR.

This study calibrated and validated the floc model to describe SNDPR when treating synthetic wastewater. However, the validated floc model was not tested to describe SNDPR when treating real municipal wastewater. Therefore, future studies should investigate whether the validated floc model can predict SNDPR when real municipal wastewater is applied.

After the validation of the floc model to simulate SNDPR to treat real municipal wastewater, the validated floc model can be used to study the impact of various operational parameters (DO concentration, temperature, SRT, and HRT) on SNDPR, and find out the optimal operational parameters. Then experiment can be used to verify the performance of SNDPR using the optimal operational parameters.

This study demonstrated successful SNDPR when treating real municipal wastewater in the AOA configuration. However, the cycle time and SRT were long. Moving bed biofilm reactor (MBBR) can increase the biomass in the system, which can reduce the cycle time and SRT. Therefore, future studies should study SNDPR with the implementation of MBBR.

This study demonstrated successful SNDPR under dry weather conditions. However, wet weather conditions, which are characterized by high flow rate and low substrate concentration, show challenges for

SNDPR. Therefore, future studies should focus on the development of an automatic control system for SNDPR to meet the requirement under each condition.

This study demonstrated successful SNDPR when using normal suspended sludge. It is known that with the increase of the floc size SNDPR can be enhanced. The Nereda process, which develops aerobic granular sludge, exhibits SNDPR in the SBR. However, the development of granular sludge in the continuous flow has not been fully understood. Therefore, future studies can investigate the performance of SNDPR in the continuous flow with the implementation of granular sludge.

This study demonstrated successful SNDPR in the lab scale. However, there are still many challenges before full-scale application. In order to scale up this technology, future studies should address issues like maintaining mixing, probe installation location, process monitoring, process control logic, maintenance, wet weather management, etc.

References

Abeling, U., Seyfried, C. 1993. Anaerobic-aerobic treatment of potato-starch wastewater. *Water Science and Technology*, 28 (2), 165-176.

Arnaldos, M., Amerlinck, Y., Rehman, U., Maere, T., Van Hoey, S., Naessens, W., Nopens, I. 2015. From the affinity constant to the half-saturation index: understanding conventional modeling concepts in novel wastewater treatment processes. *Water Research*, 70, 458-470.

Baeten, J.E., Batstone, D.J., Schraa, O.J., van Loosdrecht, M.C., Volcke, E.I. 2019. Modelling anaerobic, aerobic and partial nitritation-anammox granular sludge reactors-A review. *Water Research*, 149, 322-341.

Baetens, D., Vanrolleghem, P., Van Loosdrecht, M., Hosten, L. 1999. Temperature effects in bio-P removal. *Water Science and Technology*, 39 (1), 215-225.

Bai, X., McKnight, M.M., Neufeld, J.D., Parker, W.J. 2022. Nitrogen removal pathways during simultaneous nitrification, denitrification, and phosphorus removal under low temperature and dissolved oxygen conditions. *Bioresource Technology*, 16, 127177.

Barnard, J.L., Dunlap, P., Steichen, M. 2017. Rethinking the mechanisms of biological phosphorus removal: Barnard et al. *Water Environment Research*, 89 (11), 2043-2054.

Barnard, J.L., Meiring, P. 1988. Dissolved oxygen control in the activated sludge process. *Water Science and Technology*, 20 (4-5), 93-100.

Blackburne, R., Yuan, Z., Keller, J. 2008. Partial nitrification to nitrite using low dissolved oxygen concentration as the main selection factor. *Biodegradation*, 19 (2), 303-312.

Bliss, P.J., Barnes, D. 1986. Modelling nitrification in plant scale activated sludge. *Water Science and Technology*, 18 (6), 139-148.

Booth, R.L. 1979. *Handbook for analytical quality control in water and wastewater laboratories*. USEPA.

Bougard, D., Bernet, N., Cheneby, D., Delgenès, J.-P. 2006. Nitrification of a high-strength wastewater in an inverse turbulent bed reactor: effect of temperature on nitrite accumulation. *Process Biochemistry*, 41 (1), 106-113.

Brdjanovic, D., Logemann, S., van Loosdrecht, M.C., Hooijmans, C.M., Alaerts, G.J., Heijnen, J.J. 1998. Influence of temperature on biological phosphorus removal: process and molecular ecological studies. *Water Research*, 32 (4), 1035-1048.

Bryant, C., Coats, E.R. 2021. Integrating dairy manure for enhanced resource recovery at a WRRF: Environmental life cycle and pilot-scale analyses. *Water Environment Research*, 93 (10), 2034-50.

Burow, L.C., Kong, Y., Nielsen, J.L., Blackall, L.L., Nielsen, P.H. 2007. Abundance and ecophysiology of Defluviicoccus spp., glycogen-accumulating organisms in full-scale wastewater treatment processes. *Microbiology*, 153 (1), 178-185.

Carvalheira, M., Oehmen, A., Carvalho, G., Eusébio, M., Reis, M.A. 2014. The impact of aeration on the competition between polyphosphate accumulating organisms and glycogen accumulating organisms. *Water Research*, 66, 296-307.

Carvalho, G., Lemos, P.C., Oehmen, A., Reis, M.A. 2007. Denitrifying phosphorus removal: linking the process performance with the microbial community structure. *Water Research*, 41 (19), 4383-4396.

Chen, Y., Li, S., Lu, Y., Zhu, G., Cheng, H. 2020. Simultaneous nitrification, denitrification and phosphorus removal (SNDPR) at low atmosphere pressure. *Biochemical Engineering Journal*, 160, 107629.

Cheng, Y., Li, J.-Y., Ren, X., Li, Y., Kou, Y.-Y., Chon, K., Hwang, M.-H., Ko, M.-H. 2021. High efficiency of simultaneous nitrification, denitrification, and organics removal in the real-scale treatment of high C/N ratio food-processing wastewater using micro-aerobic reactors. *Biochemical Engineering Journal*, 108218.

Choi, E., Rhu, D., Yun, Z., Lee, E. 1998. Temperature effects on biological nutrient removal system with weak municipal wastewater. *Water Science and Technology*, 37 (9), 219-226.

Chung, H., Lee, D. 2003. Porosity and interior structure of flocculated activated sludge floc. *Journal of Colloid and Interface Science*, 267 (1), 136-143.

Close, K., Marques, R., Carvalho, V.C., Freitas, E.B., Reis, M.A., Carvalho, G., Oehmen, A. 2021. The storage compounds associated with Tetrasphaera PAO metabolism and the relationship between diversity and P removal. *Water Research*, 204, 117621.

Coats, E.R., Mockos, A., Loge, F.J. 2011. Post-anoxic denitrification driven by PHA and glycogen within enhanced biological phosphorus removal. *Bioresource Technology*, 102 (2), 1019-1027.

Collivignarelli, C., Bertanza, G. 1999. Simultaneous nitrification-denitrification processes in activated sludge plants: Performance and applicability. *Water Science and Technology*, 40 (4-5), 187-194.

Conley, D.J., Paerl, H.W., Howarth, R.W., Boesch, D.F., Seitzinger, S.P., Havens, K.E., Lancelot, C., Likens, G.E. 2009. Controlling eutrophication: nitrogen and phosphorus. *Science*, 323 (5917), 1014-1015.

Cui, D., Li, A., Zhang, S., Pang, C., Yang, J., Guo, J., Ma, F., Wang, J., Ren, N. 2012. Microbial community analysis of three municipal wastewater treatment plants in winter and spring using culture-dependent and culture-independent methods. *World Journal of Microbiology and Biotechnology*, 28 (6), 2341-2353.

Daigger, G.T., Adams, C.D., Steller, H.K. 2007. Diffusion of oxygen through activated sludge flocs: experimental measurement, modeling, and implications for simultaneous nitrification and denitrification. *Water Environment Research*, 79 (4), 375-387.

De Kreuk, M., Picioreanu, C., Hosseini, M., Xavier, J., Van Loosdrecht, M. 2007. Kinetic model of a granular sludge SBR: influences on nutrient removal. *Biotechnology and Bioengineering*, 97 (4), 801-815.

do Canto, C.S.A., Rodrigues, J.A.D., Ratusznei, S.M., Zaiat, M., Foresti, E. 2008. Feasibility of nitrification/denitrification in a sequencing batch biofilm reactor with liquid circulation applied to post-treatment. *Bioresource Technology*, 99 (3), 644-654.

Dotro, G., Jefferson, B., Jones, M., Vale, P., Cartmell, E., Stephenson, T. 2011. A review of the impact and potential of intermittent aeration on continuous flow nitrifying activated sludge. *Environmental Technology*, 32 (15), 1685-1697.

Drewnowski, J., Makinia, J. 2013. Modeling hydrolysis of slowly biodegradable organic compounds in biological nutrient removal activated sludge systems. *Water Science and Technology*, 67 (9), 2067-2074.

Dynamita (2017). Sumo User Manual.

Eaton, A.D., Clesceri, L.S., Greenberg, A.E., Franson, M.A.H. 2005. *Standard methods for the examination of water and wastewater*. American public health association.

Eberl, H., Morgenroth, E., Noguera, D., Picioreanu, C., Rittmann, B., van Loosdrecht, M., Wanner, O. 2006. *Mathematical modeling of biofilms*. IWA publishing.

Erdal, U. 2003. The competition between PAOs and GAOs in EBPR systems at different temperatures and the effects on system performanace. *Water Science and Technology*, 47 (11), 1-8.

Fernández, N., Sierra-Alvarez, R., Field, J.A., Amils, R., Sanz, J.L. 2008. Microbial community dynamics in a chemolithotrophic denitrification reactor inoculated with methanogenic granular sludge. *Chemosphere*, 70 (3), 462-474.

Ferrentino, R., Langone, M., Ancdreottola, G. 2017. Temperature effects on the activity of denitrifying phosphate accumulating microorganisms and sulphate reducing bacteria in anaerobic side-stream reactor. *Journal of Environmental and Bio Research*, 1 (1), 1.

Filipe, C.D., Daigger, G.T. 1999. Evaluation of the capacity of phosphorus-accumulating organisms to use nitrate and oxygen as final electron acceptors: A theoretical study on population dynamics. *Water Environment Research*, 71 (6), 1140-1150.

Filipe, C.D., Daigger, G.T., Grady Jr, C.L. 2001. A metabolic model for acetate uptake under anaerobic conditions by glycogen accumulating organisms: stoichiometry, kinetics, and the effect of pH. *Biotechnology and Bioengineering*, 76 (1), 17-31.

Gabb, D.M., Still, D.A., Ekama, G.A., Jenkins, D., Marais, G.V. 1991. The selector effect on filamentous bulking in long sludge age activated sludge systems. *Water Science and Technology*, 23 (4-6), 867-877.

Gazsó, Z., Házi, F., Kenyeres, I., Váci, L. 2017. Full-scale wastewater treatment plant simulation for real-time optimization. *Water Practice & Technology*, 12 (4), 848-856.

Gieseke, A., Purkhold, U., Wagner, M., Amann, R., Schramm, A. 2001. Community structure and activity dynamics of nitrifying bacteria in a phosphate-removing biofilm. *Applied and Environmental Microbiology*, 67 (3), 1351-1362.

Görgün, E., Insel, G., Artan, N., Orhon, D. 2007. Model evaluation of temperature dependency for carbon and nitrogen removal in a full-scale activated sludge plant treating leather-tanning wastewater. *Journal of Environmental Science and Health, Part A*, 42 (6), 747-756.

Guo, J., Zhang, L., Chen, W., Ma, F., Liu, H., Tian, Y. 2013. The regulation and control strategies of a sequencing batch reactor for simultaneous nitrification and denitrification at different temperatures. *Bioresource Technology*, 133, 59-67.

Haiming, Z., Xiwu, L., Abualhail, S., Jing, S., Qian, G. 2014. Enrichment of PAO and DPAO responsible for phosphorus removal at low temperature. *Environment Protection Engineering*, 40 (1).

Hanaki, K., Wantawin, C., Ohgaki, S. 1990. Nitrification at low levels of dissolved oxygen with and without organic loading in a suspended-growth reactor. *Water Research*, 24 (3), 297-302.

Hauduc, H., Rieger, L., Ohtsuki, T., Shaw, A., Takács, I., Winkler, S., Héduit, A., Vanrolleghem, P., Gillot, S. 2011. Activated sludge modelling: development and potential use of a practical applications database. *Water Science and Technology*, 63 (10), 2164-2182.

He, Q., Wang, H., Chen, L., Gao, S., Zhang, W., Song, J., Yu, J. 2020a. Elevated salinity deteriorated enhanced biological phosphorus removal in an aerobic granular sludge sequencing batch reactor performing simultaneous nitrification, denitrification and phosphorus removal. *Journal of Hazardous Materials*, 390, 121782.

He, Q., Wang, H., Chen, L., Gao, S., Zhang, W., Song, J., Yu, J. 2020b. Robustness of an aerobic granular sludge sequencing batch reactor for low strength and salinity wastewater treatment at ambient to winter temperatures. *Journal of Hazardous Materials*, 384, 121454.

He, Q., Zhang, S., Zou, Z., Zheng, L.-a., Wang, H. 2016. Unraveling characteristics of simultaneous nitrification, denitrification and phosphorus removal (SNDPR) in an aerobic granular sequencing batch reactor. *Bioresource Technology*, 220, 651-655.

Hellinga, C., Schellen, A., Mulder, J.W., van Loosdrecht, M.v., Heijnen, J. 1998. The SHARON process: an innovative method for nitrogen removal from ammonium-rich waste water. *Water Science and Technology*, 37 (9), 135-142.

Henze, M., Comeau, Y. 2008. *Biological wastewater treatment: Principles modelling and design*. IWA publishing.

Henze, M., Gujer, W., Mino, T., Van Loosdrecht, M. 2000. *Activated sludge models ASM1, ASM2, ASM2d and ASM3*. IWA publishing.

Henze, M., van Loosdrecht, M.C., Ekama, G.A., Brdjanovic, D. 2008. *Biological wastewater treatment*. IWA publishing.

Huang, Z., Gedalanga, P.B., Asvapathanagul, P., Olson, B.H. 2010. Influence of physicochemical and operational parameters on Nitrobacter and Nitrospira communities in an aerobic activated sludge bioreactor. *Water Research*, 44 (15), 4351-4358.

Huang, Z., Qie, Y., Wang, Z., Zhang, Y., Zhou, W. 2015. Application of deep-sea psychrotolerant bacteria in wastewater treatment by aerobic dynamic membrane bioreactors at low temperature. *Journal of Membrane Science*, 475, 47-56.

Hulsbeek, J., Kruit, J., Roeleveld, P., Van Loosdrecht, M. 2002. A practical protocol for dynamic modelling of activated sludge systems. *Water Science and Technology*, 45 (6), 127-136.

Igos, E., Besson, M., Gutierrez, T.N., de Faria, A.B.B., Benetto, E., Barna, L., Ahmadi, A., Spérandio, M. 2017. Assessment of environmental impacts and operational costs of the implementation of an innovative source-separated urine treatment. *Water Research*, 126, 50-59.

Jenkins, D., Richard, M.G., Daigger, G.T. 1993. Manual on the causes and control of activated sludge bulking and foaming (2nd ed.), Lewis Publishers, Michigan.

Ji, J., Peng, Y., Wang, B., Li, X., Zhang, Q. 2020. A novel SNPR process for advanced nitrogen and phosphorus removal from mainstream wastewater based on anammox, endogenous partial-denitrification and denitrifying dephosphatation. *Water Research*, 170, 115363.

Jia, W., Wang, Q., Zhang, J., Yang, W., Zhou, X. 2016. Nutrients removal and nitrous oxide emission during simultaneous nitrification, denitrification, and phosphorus removal process: effect of iron. *Environmental Science and Pollution Research*, 23 (15), 15657-15664.

Jimenez, J., Dursun, D., Dold, P., Bratby, J., Keller, J., Parker, D. 2010. Simultaneous nitrification-denitrification to meet low effluent nitrogen limits: Modeling, performance and reliability. *Proceedings of the Water Environment Federation*, 2010 (15), 2404-2421.

Ju, L.K., Huang, L., Trivedi, H. 2007. Simultaneous Nitrification, Denitrification, and Phosphorus Removal in Single-Tank Low-Dissolved-Oxygen Systems Under Cyclic Aeration. *Water Environment Research*, 79 (8), 912-920.

Kampschreur, M.J., Temmink, H., Kleerebezem, R., Jetten, M.S., van Loosdrecht, M.C. 2009. Nitrous oxide emission during wastewater treatment. *Water research*, 43 (17), 4093-4103.

Kärrman, E. 2001. Strategies towards sustainable wastewater management. *Urban Water*, 3 (1-2), 63-72.

Keene, N.A., Reusser, S.R., Scarborough, M.J., Grooms, A.L., Seib, M., Santo Domingo, J., Noguera, D.R. 2017. Pilot plant demonstration of stable and efficient high rate biological nutrient removal with low dissolved oxygen conditions. *Water Research*, 121, 72-85.

Kuba, T., Murnleitner, E., Van Loosdrecht, M., Heijnen, J. 1996. A metabolic model for biological phosphorus removal by denitrifying organisms. *Biotechnology and Bioengineering*, 52 (6), 685-695.

Kuba, T., Van Loosdrecht, M., Brandse, F., Heijnen, J. 1997. Occurrence of denitrifying phosphorus removing bacteria in modified UCT-type wastewater treatment plants. *Water Research*, 31 (4), 777-786.

Kunapongkiti, P., Rongsayamanont, C., Nayramitsattha, P., Limpiyakorn, T. 2020. Application of cell immobilization technology to promote nitritation: A review. *Environmental Engineering Research*, 25 (6), 807-818.

Kunst, S., Reins, M. 1994. Practical investigations on bulking and foaming in activated sludge plants with biological phosphorus removal. *Water Science and Technology*, 29 (7), 289-294.

Langergraber, G., Rieger, L., Winkler, S., Alex, J., Wiese, J., Owerdieck, C., Ahnert, M., Simon, J., Maurer, M. 2004. A guideline for simulation studies of wastewater treatment plants. *Water Science and Technology*, 50 (7), 131-138.

Layer, M., Villodres, M.G., Hernandez, A., Reynaert, E., Morgenroth, E., Derlon, N. 2020. Limited simultaneous nitrification-denitrification (SND) in aerobic granular sludge systems treating municipal wastewater: Mechanisms and practical implications. *Water Research X*, 7, 100048.

Lemaire, R., Meyer, R., Taske, A., Crocetti, G.R., Keller, J., Yuan, Z. 2006. Identifying causes for N2O accumulation in a lab-scale sequencing batch reactor performing simultaneous nitrification, denitrification and phosphorus removal. *Journal of Biotechnology*, 122 (1), 62-72.

Li, B., Bishop, P.L. 2004. Micro-profiles of activated sludge floc determined using microelectrodes. *Water Research*, 38 (5), 1248-1258.

Li, B., Irvin, S. 2007. The comparison of alkalinity and ORP as indicators for nitrification and denitrification in a sequencing batch reactor (SBR). *Biochemical Engineering Journal*, 34 (3), 248-255.

Li, C., Liu, S., Ma, T., Zheng, M., Ni, J. 2019. Simultaneous nitrification, denitrification and phosphorus removal in a sequencing batch reactor (SBR) under low temperature. *Chemosphere*, 229, 132-141.

Li, X., Sun, S., Badgley, B.D., Sung, S., Zhang, H., He, Z. 2016. Nitrogen removal by granular nitritation–anammox in an upflow membrane-aerated biofilm reactor. *Water Research*, 94, 23-31.

Li, D., Wei, Z., Li, S., Lao, H., Wang, W., Zeng, H., Zhang, J. 2021. Performance and operational strategy of simultaneous nitrification, denitrification, and phosphorus removal system under the condition of low organic loading rate in wet weather. *Chemosphere*, 270, 129464.

Li, X., Xiao, Y., Liao, D., Zheng, W., Yi, T., Yang, Q., Zeng, G. 2011. Granulation of simultaneous partial nitrification and anammox biomass in one single SBR system. *Applied Biochemistry and Biotechnology*, 163 (8), 1053-1065.

Li, Y., He, Y., Ohandja, D., Ji, J., Li, J., Zhou, T. 2008. Simultaneous nitrification–denitrification achieved by an innovative internal-loop airlift MBR: Comparative study. *Bioresource Technology*, 99 (13), 5867-5872.

Lishman, L., Smyth, S.A., Sarafin, K., Kleywegt, S., Toito, J., Peart, T., Lee, B., Servos, M., Beland, M., Seto, P. 2006. Occurrence and reductions of pharmaceuticals and personal care products and estrogens by municipal wastewater treatment plants in Ontario, Canada. *Science of the Total Environment*, 367 (2-3), 544-558.

Liu, F., Hu, X., Zhao, X., Guo, H., Zhao, Y. 2019. Microbial community structures' response to seasonal variation in a full-scale municipal wastewater treatment plant. *Environmental Engineering Science*, 36 (2), 172-179.

Liu, Y., Shi, H., Xia, L., Shi, H., Shen, T., Wang, Z., Wang, G., Wang, Y. 2010. Study of operational conditions of simultaneous nitrification and denitrification in a Carrousel oxidation ditch for domestic wastewater treatment. *Bioresource Technology*, 101 (3), 901-906.

Liu, G., Wu, X., Li, D., Jiang, L., Huang, J., Zhuang, L. 2021. Long-Term Low Dissolved Oxygen Operation Decreases N2O Emissions in the Activated Sludge Process. *Environmental Science & Technology*, 55 (10), 6975-6983.

Lopez-Vazquez, C.M., Hooijmans, C.M., Brdjanovic, D., Gijzen, H.J., van Loosdrecht, M.C. 2009a. Temperature effects on glycogen accumulating organisms. *Water Research*, 43 (11), 2852-2864.

Lopez-Vazquez, C.M., Oehmen, A., Hooijmans, C.M., Brdjanovic, D., Gijzen, H.J., Yuan, Z., van Loosdrecht, M.C. 2009b. Modeling the PAO–GAO competition: effects of carbon source, pH and temperature. *Water Research*, 43 (2), 450-462.

Lopez-Vazquez, C.M., Song, Y.I., Hooijmans, C.M., Brdjanovic, D., Moussa, M.S., Gijzen, H.J., van Loosdrecht, M.C. 2008. Temperature effects on the aerobic metabolism of glycogen-accumulating organisms. *Biotechnology and Bioengineering*, 101 (2), 295-306.

Mannina, G., Di Bella, G., Viviani, G. 2011. An integrated model for biological and physical process simulation in membrane bioreactors (MBRs). *Journal of Membrane Science*, 376(1-2), 56-69.

Manser, R., Gujer, W., Siegrist, H. 2005. Consequences of mass transfer effects on the kinetics of nitrifiers. *Water Research*, 39 (19), 4633-4642.

Mao, Y., Xia, Y., Zhang, T. 2013. Characterization of Thauera-dominated hydrogen-oxidizing autotrophic denitrifying microbial communities by using high-throughput sequencing. *Bioresource Technology*, 128, 703-710.

Marques, R., Ribera-Guardia, A., Santos, J., Carvalho, G., Reis, M.A., Pijuan, M., Oehmen, A. 2018. Denitrifying capabilities of Tetrasphaera and their contribution towards nitrous oxide production in enhanced biological phosphorus removal processes. *Water Research*, 137, 262-272.

Mehrani, M.-J., Sobotka, D., Kowal, P., Ciesielski, S., Makinia, J. 2020. The occurrence and role of Nitrospira in nitrogen removal systems. *Bioresource Technology*, 303, 122936.

Melcer, H. 2004. *Methods for wastewater characterization in activated sludge modelling*. IWA publishing.

Metcalf, Eddy, Abu-Orf, M., Bowden, G., Burton, F.L., Pfrang, W., Stensel, H.D., Tchobanoglous, G., Tsuchihashi, R., AECOM. 2014. *Wastewater Engineering: Treatment and Resource Recovery*. McGraw Hill Education.

Min, D., Doxey, A.C., Neufeld, J.D. 2021. AXIOME3: Automation, eXtension, and Integration Of Microbial Ecology. *GigaScience*, 10 (2), giab006.

Mobarry, B.K., Wagner, M., Urbain, V., Rittmann, B.E., Stahl, D.A. 1996. Phylogenetic probes for analyzing abundance and spatial organization of nitrifying bacteria. *Applied and Environmental Microbiology*, 62 (6), 2156-2162.

Münch, E.V., Lant, P., Keller, J. 1996. Simultaneous nitrification and denitrification in bench-scale sequencing batch reactors. *Water Research*, 30 (2), 277-284.

Ni, B.-J., Sheng, G.-P., Li, X.-Y., Yu, H.-Q. 2010. Quantitative simulation of the granulation process of activated sludge for wastewater treatment. *Industrial & Engineering Chemistry Research*, 49 (6), 2864-2873.

Nogueira, B.L., Pérez, J., van Loosdrecht, M.C., Secchi, A.R., Dezotti, M., Biscaia Jr, E.C. 2015. Determination of the external mass transfer coefficient and influence of mixing intensity in moving bed biofilm reactors for wastewater treatment. *Water Research*, 80, 90-98.

Oehmen, A., Carvalho, G., Freitas, F., Reis, M.A. 2010a. Assessing the abundance and activity of denitrifying polyphosphate accumulating organisms through molecular and chemical techniques. *Water Science and Technology*, 61 (8), 2061-2068.

Oehmen, A., Lopez-Vazquez, C., Carvalho, G., Reis, M., Van Loosdrecht, M. 2010b. Modelling the population dynamics and metabolic diversity of organisms relevant in anaerobic/anoxic/aerobic enhanced biological phosphorus removal processes. *Water Research*, 44 (15), 4473-4486.

Oehmen, A., Vives, M.T., Lu, H., Yuan, Z., Keller, J. 2005a. The effect of pH on the competition between polyphosphate-accumulating organisms and glycogen-accumulating organisms. *Water Research*, 39 (15), 3727-3737.

Oehmen, A., Yuan, Z., Blackall, L.L., Keller, J. 2005b. Comparison of acetate and propionate uptake by polyphosphate accumulating organisms and glycogen accumulating organisms. *Biotechnology and Bioengineering*, 91 (2), 162-168.

Oehmen, A., Zeng, R.J., Yuan, Z., Keller, J. 2005c. Anaerobic metabolism of propionate by polyphosphate-accumulating organisms in enhanced biological phosphorus removal systems. *Biotechnology and Bioengineering*, 91 (1), 43-53.

Ou, D., Li, W., Li, H., Wu, X., Li, C., Zhuge, Y. 2018. Enhancement of the removal and settling performance for aerobic granular sludge under hypersaline stress. *Chemosphere*, 212, 400-407.

Pan, M., Huang, X., Wu, G., Hu, Y., Yang, Y., Zhan, X. 2017. Performance of Denitrifying Phosphate Removal via Nitrite from Slaughterhouse Wastewater Treatment at Low Temperature. *Water*, 9 (11), 818.

Paredes, D., Kuschk, P., Mbwette, T., Stange, F., Müller, R., Köser, H. 2007. New aspects of microbial nitrogen transformations in the context of wastewater treatment–a review. *Engineering in Life Sciences*, 7 (1), 13-25.

Park, H.-D., Noguera, D.R. 2008. Nitrospira community composition in nitrifying reactors operated with two different dissolved oxygen levels. *Journal of Microbiology and Biotechnology*, 18 (8), 1470-1474.

Pérez, J., Picioreanu, C., Van Loosdrecht, M. 2005. Modeling biofilm and floc diffusion processes based on analytical solution of reaction-diffusion equations. *Water Research*, 39 (7), 1311-1323.

Petersen, B., Vanrolleghem, P.A., Gernaey, K., Henze, M. 2002. Evaluation of an ASM1 model calibration procedure on a municipal–industrial wastewater treatment plant. *Journal of Hydroinformatics*, 4 (1), 15-38.

Pochana, K., Keller, J. 1999. Study of factors affecting simultaneous nitrification and denitrification (SND). *Water Science and Technology*, 39 (6), 61-68.

Pochana, K., Keller, J., Lant, P. 1999. Model development for simultaneous nitrification and denitrification. *Water Science and Technology*, 39 (1), 235-243.

Quince, C., Lanzen, A., Davenport, R.J., Turnbaugh, P.J. 2011. Removing noise from pyrosequenced amplicons. *BMC Bioinformatics*, 12 (1), 1-18.

Rajeshwari, K., Balakrishnan, M., Kansal, A., Lata, K., Kishore, V. 2000. State-of-the-art of anaerobic digestion technology for industrial wastewater treatment. *Renewable and Sustainable Energy Reviews*, 4 (2), 135-156.

Reddy, C., Beveridge, T.J., Breznak, J.A., Marzluf, G. 2007. *Methods for general and molecular microbiology*. American Society for Microbiology Press.

Rieger, L., Gillot, S., Langergraber, G., Ohtsuki, T., Shaw, A., Takacs, I., Winkler, S. 2012. *Guidelines for using activated sludge models*. IWA publishing.

Rittmann, B.E., Boltz, J.P., Brockmann, D., Daigger, G.T., Morgenroth, E., Sørensen, K.H., Takács, I., Van Loosdrecht, M., Vanrolleghem, P.A. 2018. A framework for good biofilm reactor modeling practice (GBRMP). *Water Science and Technology*, 77 (5), 1149-1164.

Rubilar, O., Munoz, P., Ruiz, G., Chamy, R., Vergara, C., Jeison, D. 2005. Partial nitrification of high ammonia concentration wastewater as a part of a shortcut biological nitrogen removal process. *Process Biochemistry*, 40 (5), 1715-1719.

Rubio-Rincón, F., Lopez-Vazquez, C., Welles, L., Van Loosdrecht, M., Brdjanovic, D. 2017. Cooperation between Candidatus Competibacter and Candidatus Accumulibacter clade I, in denitrification and phosphate removal processes. *Water Research*, 120, 156-164.

Ruiz, G., Jeison, D., Chamy, R. 2003. Nitrification with high nitrite accumulation for the treatment of wastewater with high ammonia concentration. *Water Research*, 37 (6), 1371-1377.

Salehi, S., Cheng, K.Y., Heitz, A., Ginige, M.P. 2019. Simultaneous nitrification, denitrification and phosphorus recovery (SNDPr)-An opportunity to facilitate full-scale recovery of phosphorus from municipal wastewater. *Journal of Environmental Management*, 238, 41-48.

Sarioglu, M., Sayi-Ucar, N., Cokgor, E., Orhon, D., Van Loosdrecht, M., Insel, G. 2017. Dynamic modeling of nutrient removal by a MBR operated at elevated temperatures. *Water Research*, 123, 420-428.

Saunders, A.M., Albertsen, M., Vollertsen, J., Nielsen, P.H. 2016. The activated sludge ecosystem contains a core community of abundant organisms. *The ISME journal*, 10 (1), 11-20.

Schramm, A., de Beer, D., van den Heuvel, J.C., Ottengraf, S., Amann, R. 1999. Microscale distribution of populations and activities of Nitrosospira and Nitrospira spp. along a macroscale gradient in a nitrifying bioreactor: quantification by in situ hybridization and the use of microsensors. *Applied and Environmental Microbiology*, 65 (8), 3690-3696.

Shaw, A., Takács, I., Pagilla, K., Murthy, S. 2013. A new approach to assess the dependency of extant half-saturation coefficients on maximum process rates and estimate intrinsic coefficients. *Water Research*, 47 (16), 5986-5994.

Shaw, A., Takacs, I., Pagilla, K., Riffat, R., DeClippeleir, H., Wilson, C., Murthy, S. 2015. Toward universal half-saturation coefficients: Describing extant KS as a function of diffusion. *Water Environment Research*, 87 (5), 387-391.

Sliekers, A.O., Haaijer, S.C., Stafsnes, M.H., Kuenen, J.G., Jetten, M.S. 2005. Competition and coexistence of aerobic ammonium-and nitrite-oxidizing bacteria at low oxygen concentrations. *Applied Microbiology and Biotechnology*, 68 (6), 808-817.

Smolders, G., Van der Meij, J., Van Loosdrecht, M., Heijnen, J. 1994. Stoichiometric model of the aerobic metabolism of the biological phosphorus removal process. *Biotechnology and Bioengineering*, 44 (7), 837-848.

Soler-Jofra, A., Wang, R., Kleerebezem, R., van Loosdrecht, M.C., Pérez, J. 2019. Stratification of nitrifier guilds in granular sludge in relation to nitritation. *Water Research*, 148, 479-491.

Sun, S.-P., Nàcher, C.P.i., Merkey, B., Zhou, Q., Xia, S.-Q., Yang, D.-H., Sun, J.-H., Smets, B.F. 2010. Effective biological nitrogen removal treatment processes for domestic wastewaters with low C/N ratios: a review. *Environmental Engineering Science*, 27 (2), 111-126.

Thomas, M., Wright, P., Blackall, L., Urbain, V., Keller, J. 2003. Optimisation of Noosa BNR plant to improve performance and reduce operating costs. *Water Science and Technology*, 47 (12), 141-148.

Tian, Q., Zhuang, L., Ong, S.K., Wang, Q., Wang, K., Xie, X., Zhu, Y., Li, F. 2017a. Phosphorus (P) recovery coupled with increasing influent ammonium facilitated intracellular carbon source storage and simultaneous aerobic phosphorus & nitrogen removal. *Water Research*, 119, 267-275.

Tian, W., Ma, C., Lin, Y., Welles, L., Lopez-Vazquez, C., van Loosdrecht, M. 2017b. Enrichment and characterization of a psychrophilic 'Candidatus Accumulibacter phosphatis' culture. *International Biodeterioration & Biodegradation*, 124, 267-275.

Tsushima, I., Yoochatchaval, W., Yoshida, H., Araki, N., Syutsubo, K. 2010. Microbial community structure and population dynamics of granules developed in expanded granular sludge bed (EGSB) reactors for the anaerobic treatment of low-strength wastewater at low temperature. *Journal of Environmental Science and Health Part A*, 45 (6), 754-766.

Turk, O., Mavinic, D. 1986. Preliminary assessment of a shortcut in nitrogen removal from wastewater. *Canadian Journal of Civil Engineering*, 13 (6), 600-605.

Tyagi, R., Du, Y., Bhamidimarri, R. 1996. Dynamic behavior of the activated sludge process under shock loading: application of the floc model. *Water Research*, 30 (7), 1605-1616.

Ushiki, N., Jinno, M., Fujitani, H., Suenaga, T., Terada, A., Tsuneda, S. 2017. Nitrite oxidation kinetics of two Nitrospira strains: the quest for competition and ecological niche differentiation. *Journal of Bioscience and Bioengineering*, 123 (5), 581-589.

Van de Graaf, A.A., de Bruijn, P., Robertson, L.A., Jetten, M.S., Kuenen, J.G. 1996. Autotrophic growth of anaerobic ammonium-oxidizing micro-organisms in a fluidized bed reactor. *Microbiology*, 142 (8), 2187-2196.

Van Veldhuizen, H., van Loosdrecht, M.C., Heijnen, J. 1999. Modelling biological phosphorus and nitrogen removal in a full scale activated sludge process. *Water Research*, 33 (16), 3459-3468.

Vanrolleghem, P.A., Insel, G., Petersen, B., Sin, G., De Pauw, D., Nopens, I., Dovermann, H., Weijers, S., Gernaey, K. 2003. A comprehensive model calibration procedure for activated sludge models. *Proceedings of the Water Environment Federation*, 2003 (9), 210-237.

Varga, E., Hauduc, H., Barnard, J., Dunlap, P., Jimenez, J., Menniti, A., Schauer, P., Lopez Vazquez, C.M., Gu, A.Z., Sperandio, M. 2018. Recent advances in bio-P modelling–a new approach verified by full-scale observations. *Water Science and Technology*, 78 (10), 2119-2130.

Wang, C., Zeng, Y., Lou, J., Wu, P. 2007. Dynamic simulation of a WWTP operated at low dissolved oxygen condition by integrating activated sludge model and a floc model. *Biochemical Engineering Journal*, 33 (3), 217-227.

Wang, D., Li, X., Yang, Q., Zheng, W., Cao, J., Zeng, G., Yue, X., Shen, T., Zeng, T., Ding, Y. 2009. Effect and mechanism of carbon sources on phosphorus uptake by microorganisms in sequencing batch reactors with the single-stage oxic process. *Science in China Series B: Chemistry*, 52 (12), 2358.

Wang, Q., Jia, W., Zhang, J., Li, C., Yang, W. 2016a. Nutrients removal and nitrous oxide emission during simultaneous nitrification, denitrification, and phosphorus removal process: impact of temperature. *Desalination and Water Treatment*, 57 (54), 26187-26195.

Wang, Q., Yu, D., Wang, X., Chu, G., He, T., Zhao, J. 2021. Development of novel denitrifying nitrite accumulation and phosphorus removal (DNAPR) process for offering an alternative pretreatment to achieve mainstream Anammox. *Bioresource Technology*, 319, 124164.

Wang, S., Li, Z., Wang, D., Li, Y., Sun, L. 2020. Performance and population structure of two carbon sources granular enhanced biological phosphorus removal systems at low temperature. *Bioresource Technology*, 300, 122683.

Wang, X., Wang, S., Xue, T., Li, B., Dai, X., Peng, Y. 2015. Treating low carbon/nitrogen (C/N) wastewater in simultaneous nitrification-endogenous denitrification and phosphorous removal (SNDPR) systems by strengthening anaerobic intracellular carbon storage. *Water Research*, 77, 191-200.

Wang, X., Wang, S., Zhao, J., Dai, X., Li, B., Peng, Y. 2016b. A novel stoichiometries methodology to quantify functional microorganisms in simultaneous (partial) nitrification-endogenous denitrification and phosphorus removal (SNEDPR). *Water Research*, 95, 319-329.

Wang, X., Wang, S., Zhao, J., Dai, X., Peng, Y. 2016c. Combining simultaneous nitrification-endogenous denitrification and phosphorus removal with post-denitrification for low carbon/nitrogen wastewater treatment. *Bioresource Technology*, 220, 17-25.

Wang, X., Zeng, R.J., Dai, Y., Peng, Y., Yuan, Z. 2008. The denitrification capability of cluster 1 Defluviicoccus vanus-related glycogen-accumulating organisms. *Biotechnology and Bioengineering*, 99 (6), 1329-1336.

Wanner, O. 1996. Modelling of biofilms. *Biofouling*, 10 (1-3), 31-41.

Welles, L., Tian, W., Saad, S., Abbas, B., Lopez-Vazquez, C., Hooijmans, C., Van Loosdrecht, M., Brdjanovic, D. 2015. Accumulibacter clades Type I and II performing kinetically different glycogen-accumulating organisms metabolisms for anaerobic substrate uptake. *Water Research*, 83, 354-366.

Wen, Y., Jin, Y., Wang, J., Cai, L. 2015. MiSeq sequencing analysis of bacterial community structures in wastewater treatment plants. *Polish Journal of Environmental Studies*, 24 (4).

Winkler, M., Coats, E.R., Brinkman, C.K. 2011. Advancing post-anoxic denitrification for biological nutrient removal. *Water Research*, 45 (18), 6119-6130.

Wu, J., Li, Y., Zhang, M. 2017. Activated sludge floc morphology and nitrifier enrichment can explain the conflicting reports on the oxygen half-saturation index for ammonium oxidizing bacteria (AOB) and nitrite oxidizing bacteria (NOB). *Journal of Chemical Technology & Biotechnology*, 92 (10), 2673-2682.

Xu, G., Zhou, Y., Yang, Q., Lee, Z.M.-P., Gu, J., Lay, W., Cao, Y., Liu, Y. 2015. The challenges of mainstream deammonification process for municipal used water treatment. *Applied Microbiology and Biotechnology*, 99 (6), 2485-2490.

Yan, L., Liu, S., Liu, Q., Zhang, M., Liu, Y., Wen, Y., Chen, Z., Zhang, Y., Yang, Q. 2019. Improved performance of simultaneous nitrification and denitrification via nitrite in an oxygen-limited SBR by alternating the DO. *Bioresource Technology*, 275, 153-162.

Yang, M., Ma, F., Xie, Y., Li, L., Xue, Y. 2021. The SBR start-up performing simultaneous removal of organics, nitrogen and phosphorus from aniline wastewater: Pollutant removal efficiency and microbial community succession. *Environmental Pollutants and Bioavailability*, 33 (1), 104-112.

Yilmaz, G., Lemaire, R., Keller, J., Yuan, Z. 2008. Simultaneous nitrification, denitrification, and phosphorus removal from nutrient-rich industrial wastewater using granular sludge. *Biotechnology and Bioengineering*, 100 (3), 529-541.

Yuan, C., Wang, B., Peng, Y., Li, X., Zhang, Q., Hu, T. 2020. Enhanced nutrient removal of simultaneous partial nitrification, denitrification and phosphorus removal (SPNDPR) in a single-stage anaerobic/micro-aerobic sequencing batch reactor for treating real sewage with low carbon/nitrogen. *Chemosphere*, 257, 127097.

Yuan, Q., Sparling, R., Oleszkiewicz, J. 2011. VFA generation from waste activated sludge: effect of temperature and mixing. *Chemosphere*, 82 (4), 603-607.

Zaman, M., Kim, M., Nakhla, G. 2021. Simultaneous nitrification-denitrifying phosphorus removal (SNDPR) at low DO for treating carbon-limited municipal wastewater. *Science of The Total Environment*, 760, 143387.

Zeng, R.J., Lemaire, R., Yuan, Z., Keller, J. 2003a. Simultaneous nitrification, denitrification, and phosphorus removal in a lab-scale sequencing batch reactor. *Biotechnology and Bioengineering*, 84 (2), 170-178.

Zeng, R.J., Van Loosdrecht, M.C., Yuan, Z., Keller, J. 2003b. Metabolic model for glycogen-accumulating organisms in anaerobic/aerobic activated sludge systems. *Biotechnology and Bioengineering*, 81 (1), 92-105.

Zeng, R.J., Yuan, Z., Keller, J. 2003c. Enrichment of denitrifying glycogen-accumulating organisms in anaerobic/anoxic activated sludge system. *Biotechnology and Bioengineering*, 81 (4), 397-404.

Zhang, W., Hou, F., Peng, Y., Liu, Q., Wang, S. 2014. Optimizing aeration rate in an external nitrification–denitrifying phosphorus removal (ENDPR) system for domestic wastewater treatment. *Chemical Engineering Journal*, 245, 342-347.

Zhao, W., Huang, Y., Wang, M., Pan, C., Li, X., Peng, Y., Li, B. 2018. Post-endogenous denitrification and phosphorus removal in an alternating anaerobic/oxic/anoxic (AOA) system treating low carbon/nitrogen (C/N) domestic wastewater. *Chemical Engineering Journal*, 339, 450-458.

Zhu, C.-Y., Wang, J.-F., Li, Q.-S., Wang, L.-L., Tang, G.-H., Cui, B.-S., Bai, J. 2021. Integration of CW-MFC and anaerobic granular sludge to explore the intensified ammonification-nitrification-denitrification processes for nitrogen removal. *Chemosphere*, 278, 130428.

Appendix A

Appendix A-1. Calculations

The detailed calculation equations for values in Chapter 3 are illustrated in the following.

$$\text{COD}_{\text{intra}}\ \text{efficiency} = 1 - \frac{\text{COD}_{\text{dn}}}{\text{COD}_{\text{consum}}} = 1 - \frac{\frac{2.86}{1-0.45} \times \left(\frac{11.2}{2}\right)}{\frac{350+12.5}{2} - 54.17} = 77\%$$

$$\text{Calculated N used for cell synthesis} = \frac{\text{MLVSS}}{\text{MW of biomass}} \times \text{MW of nitrogen} \times V_{\text{waste}} = (4215\ \text{mg/L} \div 115\ \text{g/mol}) \times 14\ \text{g/mol} \times 0.2\ \text{L}) = 103\ \text{mg N}$$

The detailed calculations to get the values in Table 3-2 are shown below.

N mass used for cell synthesis = particulate organic N concentration of MLSS × wasting volume

$$= 434.4 \frac{\text{mg N}}{\text{L}} \times 0.2\text{L} = 86.9\ \text{mg N}$$

N mass decant from the system = TN concentration in the effluent × decanting volume

$$= (6 + 11.43) \frac{\text{mg N}}{\text{L}} \times 9\text{L} = 156.8\ \text{mgN}$$

N mass denitrified in the anaerobic zone

$$= NO_x \text{ concentration in the effluent} \times \text{remaining volume after decanting}$$

$$= (11.43) \frac{\text{mg N}}{\text{L}} \times 9\text{L} = 102.8\ \text{mg N}$$

Nitrogen removal amount due to DPAOs = SNRR × MLVSS × reactor volume × time period =

$$0.74\frac{\text{mg N}}{\text{gVSS·h}} \times \frac{4.215\text{g VSS}}{\text{L}} \times 18\text{L} \times 1\text{h} = 56.1\text{ mg N}$$

Where, the time period for DPAOs using PHA refers to the time over which phosphorus was depleted under aerobic phase in a typical cycle, which was 1h as shown in Figure 3-3.

Nitrogen removal amount due to denitrifying OHOs using residual rbCOD

$$= \text{SNRR} \times \text{MLVSS} \times \text{reactor volume} \times \text{time period}$$

$$= 1.84\frac{\text{mgN}}{\text{gVSS·h}} \times \frac{4.215\text{gVSS}}{\text{L}} \times 18\text{L} \times \frac{1}{60}\frac{\text{h}}{\text{min}} \times 30\text{min} = 69.8\text{ mgN}$$

Where, the time period for denitrifying OHOs using residual rbCOD refers to the time over which sCOD was depleted under aerobic phase in a typical cycle, which was 0.5 h as shown in Figure 3-3.

Calculated N mass in from influent

= N mass used for cell synthesis + N mass decant from the system

+ N mass denitrified in the anaerobic zone

+ N mass removed through denitrifying OHO denitrification using residual rbCOD in the aerobic zone

+ N mass removed through DPAO denitrification in the aerobic zone

$$= 86.88 + 156.8 + 102.8 + 69.8 + 56.1 = 472\text{ mgN}$$

$$\text{Relative error} = \frac{\text{calculated N mass in from influent}}{\text{N mass in from influent}} - 1 = \frac{472}{441} - 1 = 7\%$$

Appendix A-2. Figures and Tables

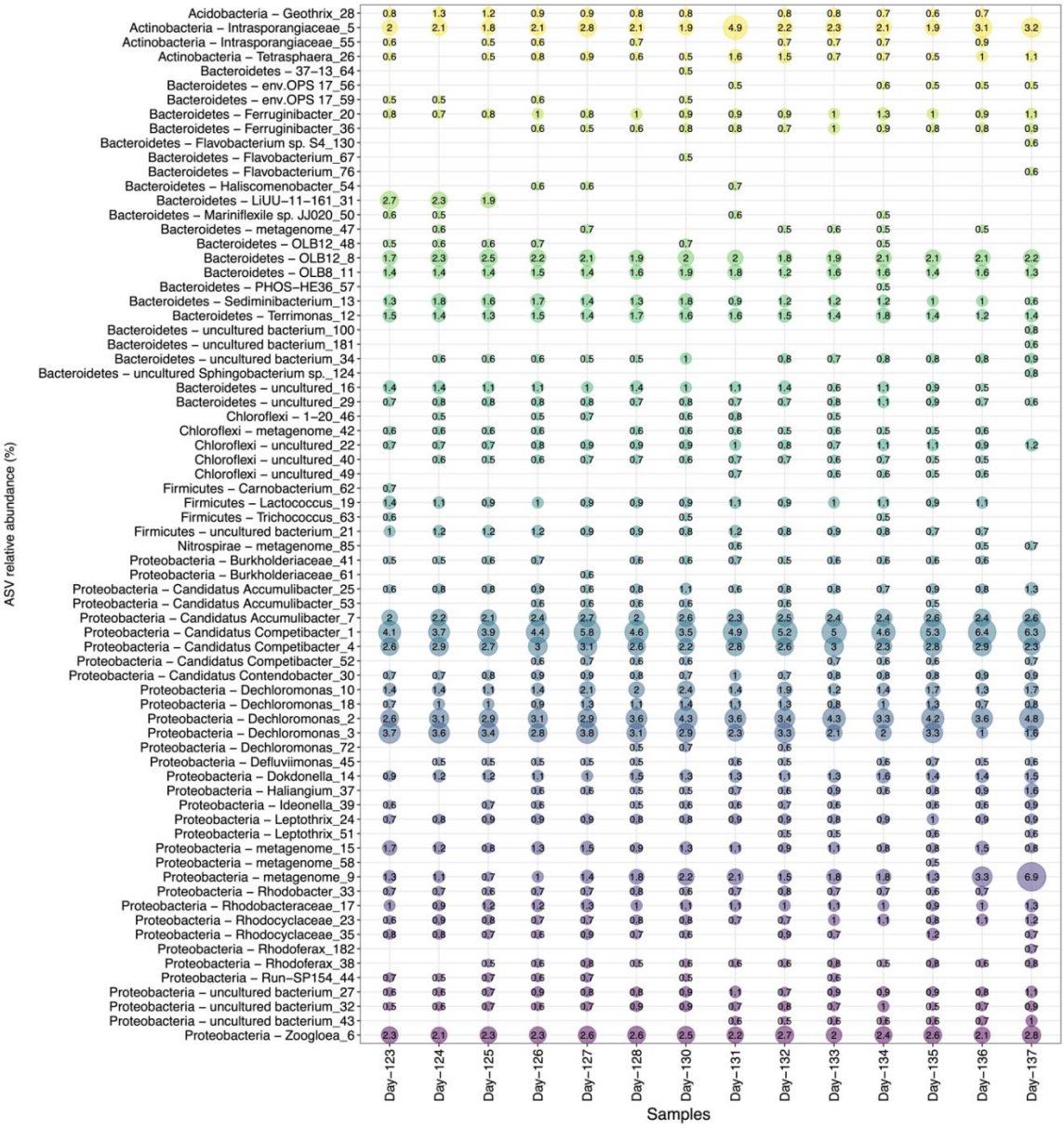

Figure A-1. Relative abundance of individual amplicon sequence variants (ASVs) detected in the system from day 123 to day 137 of operation. The ASVs are only shown on the plot if greater than 0.5% relative abunadnce (RA) within the microbial community. Individual ASVs were assigned to the lowest possible

taxonomic level based on the nucleotide sequence. The phylum for each ASV is also indicated before the additional taxonomy assignment on the y-axis, with the numbers inside circles representing the % RA.

Appendix A-3. Definition of each term in FAPROTAX

The main functionalities in FAPROTAX are listed below. The description of each functionality is based on electron donor, electron acceptor, whether aerobic, whether exclusively prokaryotic, and whether light dependent. Some of the functionalities are the combination of several functionalities and specific microorganisms.

aerobic_ammonia_oxidation elements:N,O; main_element:N; electron_donor:N; electron_acceptor:O; aerobic:yes; exclusively_prokaryotic:yes; light_dependent:no

aerobic_chemoheterotrophy elements:C,O; main_element:C; electron_donor:C; electron_acceptor:O; aerobic:yes; exclusively_prokaryotic:no; light_dependent:no
other than lignin, chitin, xylan, cellulose, methanol, methane, aromatic hydrocarbons

aerobic_nitrite_oxidation elements:N,O; main_element:N; electron_donor:N; electron_acceptor:O; aerobic:yes; exclusively_prokaryotic:yes; light_dependent:no

chemoheterotrophy elements:C; main_element:C; electron_donor:C; electron_acceptor:variable; aerobic:variable; exclusively_prokaryotic:no; light_dependent:no
add_group:aerobic_chemoheterotrophy
add_group:fermentation
add_group:cellulolysis
add_group:xylanolysis

add_group:chitinolysis

add_group:ligninolysis

add_group:methylotrophy

add_group:acetoclastic_methanogenesis

add_group:methanogenesis_by_disproportionation_of_methyl_groups

add_group:methanogenesis_using_formate

add_group:oil_bioremediation

add_group:aromatic_compound_degradation

add_group:hydrocarbon_degradation

add_group: Its own specific microorganisms

chlorate_reducers elements:C; main_element:C; electron_donor:variable; electron_acceptor:Cl; aerobic:variable; exclusively_prokaryotic:no; light_dependent:no

denitrification elements:N; main_element:N; electron_donor:variable; electron_acceptor:N; aerobic:no; exclusively_prokaryotic:no; light_dependent:no

dissimilatory reduction of fixed nitrogen compounds (NO3, NO2, N2O ...) to dinitrogen

add_group:nitrate_denitrification

add_group:nitrite_denitrification

add_group:nitrous_oxide_denitrification

add_group: Its own specific microorganisms

fermentation elements:C; main_element:C; electron_donor:C; electron_acceptor:none; aerobic:no; exclusively_prokaryotic:no; light_dependent:no

nitrate_denitrification elements:N; main_element:N; electron_donor:variable; electron_acceptor:N; aerobic:no; exclusively_prokaryotic:no; light_dependent:no

dissimilatory reduction of NO3 to N2

nitrate_reduction elements:N; main_element:N; electron_donor:variable; electron_acceptor:N; aerobic:variable; exclusively_prokaryotic:no; light_dependent:no

assimilatory or dissimilatory

add_group:nitrate_respiration

add_group: Its own specific microorganisms

nitrate_respiration elements:N; main_element:N; electron_donor:variable; electron_acceptor:N; aerobic:no; exclusively_prokaryotic:no; light_dependent:no

dissimilatory nitrate respiration

add_group:nitrate_denitrification

add_group:nitrate_ammonification

add_group: Its own specific microorganisms

nitrification elements:N,O; main_element:N; electron_donor:N; electron_acceptor:O; aerobic:yes; exclusively_prokaryotic:yes; light_dependent:no

add_group:aerobic_ammonia_oxidation

add_group:aerobic_nitrite_oxidation

nitrite_denitrification elements:N; main_element:N; electron_donor:variable; electron_acceptor:N; aerobic:no; exclusively_prokaryotic:no; light_dependent:no

add_group:nitrate_denitrification

add_group: Its own specific microorganisms

nitrite_respiration elements:N; main_element:N; electron_donor:variable; electron_acceptor:N; aerobic:no; exclusively_prokaryotic:no; light_dependent:no

add_group:nitrite_ammonification

add_group:nitrite_denitrification

add_group:anammox

add_group: Its own specific microorganisms

nitrogen_respiration elements:N; main_element:N; electron_donor:variable; electron_acceptor:N; aerobic:no; exclusively_prokaryotic:no; light_dependent:no

dissimilatory reduction of nitrogen compounds

add_group:nitrate_respiration

add_group:nitrite_respiration

add_group:denitrification

add_group:nitrate_ammonification

add_group:nitrite_ammonification

add_group:anammox

nitrous_oxide_denitrification elements:N; main_element:N; electron_donor:variable; electron_acceptor:N; aerobic:no; exclusively_prokaryotic:no; light_dependent:no

add_group:nitrite_denitrification # assuming that all nitite denitrifiers are also N2O denitrifiers

add_group: Its own specific microorganisms

phototrophy elements:variable; main_element:variable; electron_donor:variable; electron_acceptor:C; aerobic:variable; exclusively_prokaryotic:no; light_dependent:yes

add_group:photoautotrophy

add_group:photoheterotrophy

photoheterotrophy elements:C; main_element:C; electron_donor:C; electron_acceptor:C; aerobic:variable; exclusively_prokaryotic:yes; light_dependent:yes

add_group:aerobic_anoxygenic_phototrophy

add_group: Its own specific microorganisms

Appendix B

Appendix B-1. Synthetic wastewater composition

The composition of the synthetic wastewater contained (per liter): 128 mg sodium acetate (100 mg COD/L), 3.8 mg NH_4Cl (1 mg/L of NH_4-N), 9.5 mg KH_2PO_4 (2 mg/L of PO_4-P), 15 mg $MgSO_4$, 300 mg $NaHCO_3$, 10 mg $CaCl_2$, and trace elements I and II with 1mL/L. Trace elements I and II were the same as (Van de Graaf et al., 1996). Trace element I included EDTA (5.0 g/L) and $FeSO_4 \cdot 7H_2O$ (9.15 g/L). Trace element II included EDTA (15.0 g/L), $ZnSO_4 \cdot 7H_2O$ (0.430 g/L), $C_O(NO_3) \cdot 6H_2O$ (0.294 g/L), $MnCl_4 \cdot 4H_2O$ (0.990 g/L), $CuSO_4 \cdot 5H_2O$ (0.250 g/L), $(NH_4)_6MO_7O_{24}$ (0.177 g/L), $NiCl_2 \cdot 6H_2O$ (0.190 g/L), Na_2SeO_3 (0.105 g/L), and H_3BO_3 (0.0111 g/L). Overall, the synthetic wastewater contained a VFA of 100 mg COD/L, NH_4-N of 1 mg/L, and PO_4-P of 2 mg/L.

Appendix B-2. Calculations

The detailed calculation equations for values in Chapter 4 are illustrated in the following.

$$\mathrm{COD_{intra}\ efficiency} = 1 - \frac{\mathrm{COD_{dn}}}{\mathrm{COD_{consum}}} = 1 - \frac{\frac{2.86}{1-0.45} \times \left(\frac{0.1}{2}\right)}{\frac{110+22.5}{2} - 27.5} = 98\%$$

$$\text{Calculated N used for cell synthesis} = \frac{\mathrm{MLVSS}}{\mathrm{MW\ of\ biomass}} \times \mathrm{MW\ of\ nitrogen} \times \mathrm{V_{waste}} = (3160\ \mathrm{mg/L} \div 115\ \mathrm{g/mol}) \times 14\ \mathrm{g/mol} \times 0.2\ \mathrm{L}) = 77\ \mathrm{mg\ N}$$

The detailed calculations to get the values in Table 4-1 are shown below.

N mass used for cell synthesis = particulate organic N concentration of MLSS × wasting volume

$$= 328.07 \frac{\text{mg N}}{\text{L}} \times 0.2\text{L} = 66 \text{ mg N}$$

N mass decant from the system = TN concentration in the effluent × decanting volume

$$= (0.1 + 1.74) \frac{\text{mg N}}{\text{L}} \times 9\text{L} = 17 \text{ mgN}$$

N mass denitrified in the anaerobic zone

$= NO_x$ concentration in the effluent × remaining volume after decanting

$$= (0.1) \frac{\text{mg N}}{\text{L}} \times 9\text{L} = 1 \text{ mg N}$$

Nitrogen removal amount due to DPAOs = SNRR × MLVSS × reactor volume × time period =

$0.6 \frac{\text{mg N}}{\text{gVSS·h}} \times \frac{3.16\text{g VSS}}{\text{L}} \times 18\text{L} \times 1.5\text{h} = 51 \text{ mg N}$

Where, the time period for DPAOs using PHA refers to the time over which phosphorus was depleted under aerobic phase in a typical cycle, which was 1.5h as shown in Figure 4-2D.

N mass removal amount through denitrifying OHOs using hydrolyzed carbon in the post anoxic phase = (TN at the start of the post anoxic phase – TN at the end of the post anoxic phase) × reactor volume = (10.69-0.63) mg N/L × 18 L= 181 mg N

Calculated N mass in from influent

$=$ N mass used for cell synthesis $+$ N mass decant from the system

$+$ N mass denitrified in the anaerobic zone

$+$ N mass removed through DPAO denitrification in the aerobic zone

$+$ N mass removed through denitrifying OHOs using hydrolyzed carbon in the post anoxic phase

$= 66 + 17 + 1 + 51 + 181 = 316$ mgN

$$\text{Relative error} = \frac{\text{calculated N mass in from influent}}{\text{N mass in from influent}} - 1 = \frac{316}{324} - 1 = -3\%$$

Appendix B-3. Figures and Tables

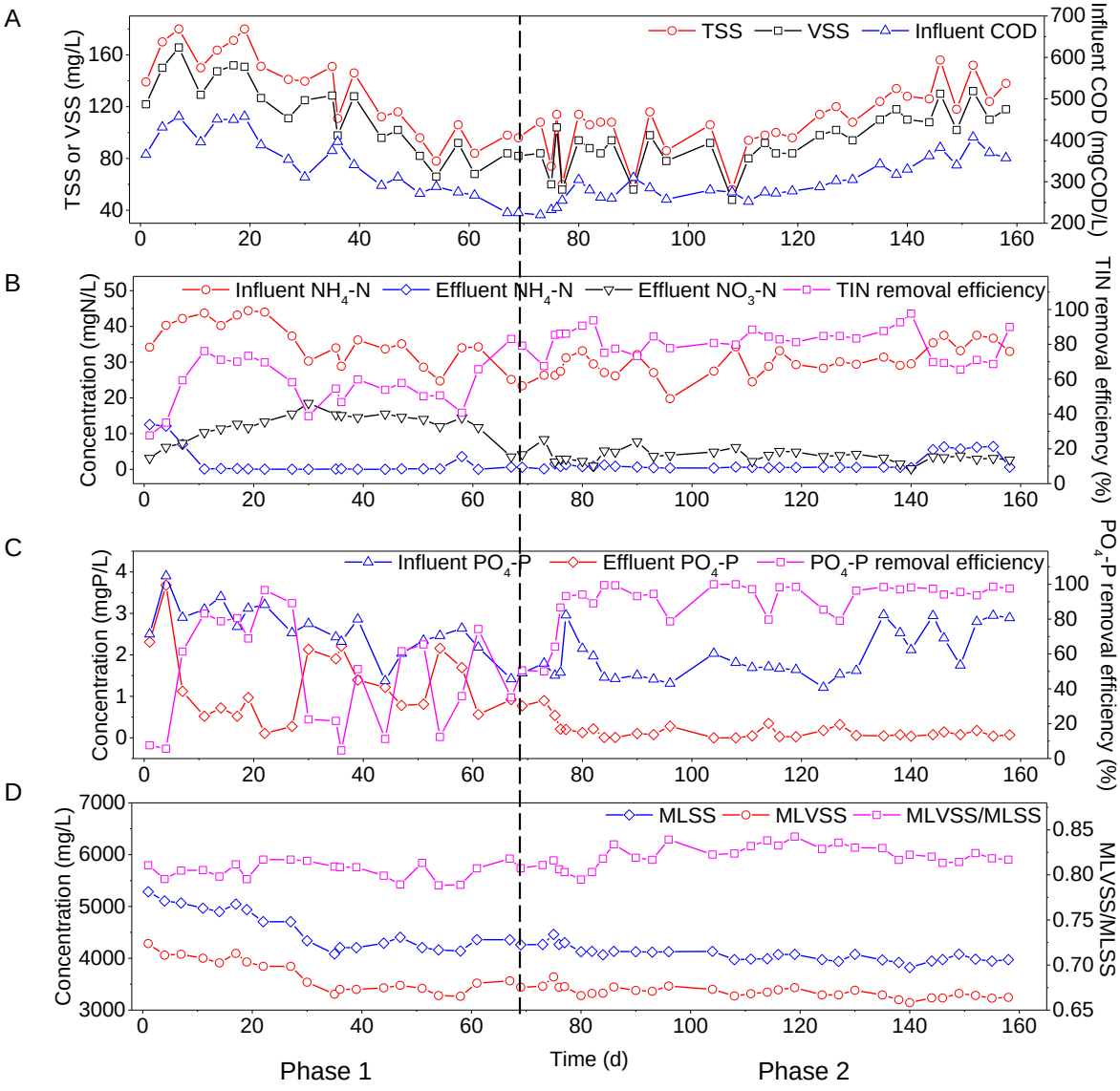

Figure B-1. The performance of SBR (A: influent TSS, VSS, COD; B: influent NH4-N, effluent NH4-N, effluent NO_3-N, TIN removal efficiency; C: influent PO_4-P, effluent PO_4-P, PO_4-P removal efficiency; D: MLSS, MLVSS, MLVSS/MLSS) in Phases 1 and 2 at a DO of 0.3 mg/L and 10°C.

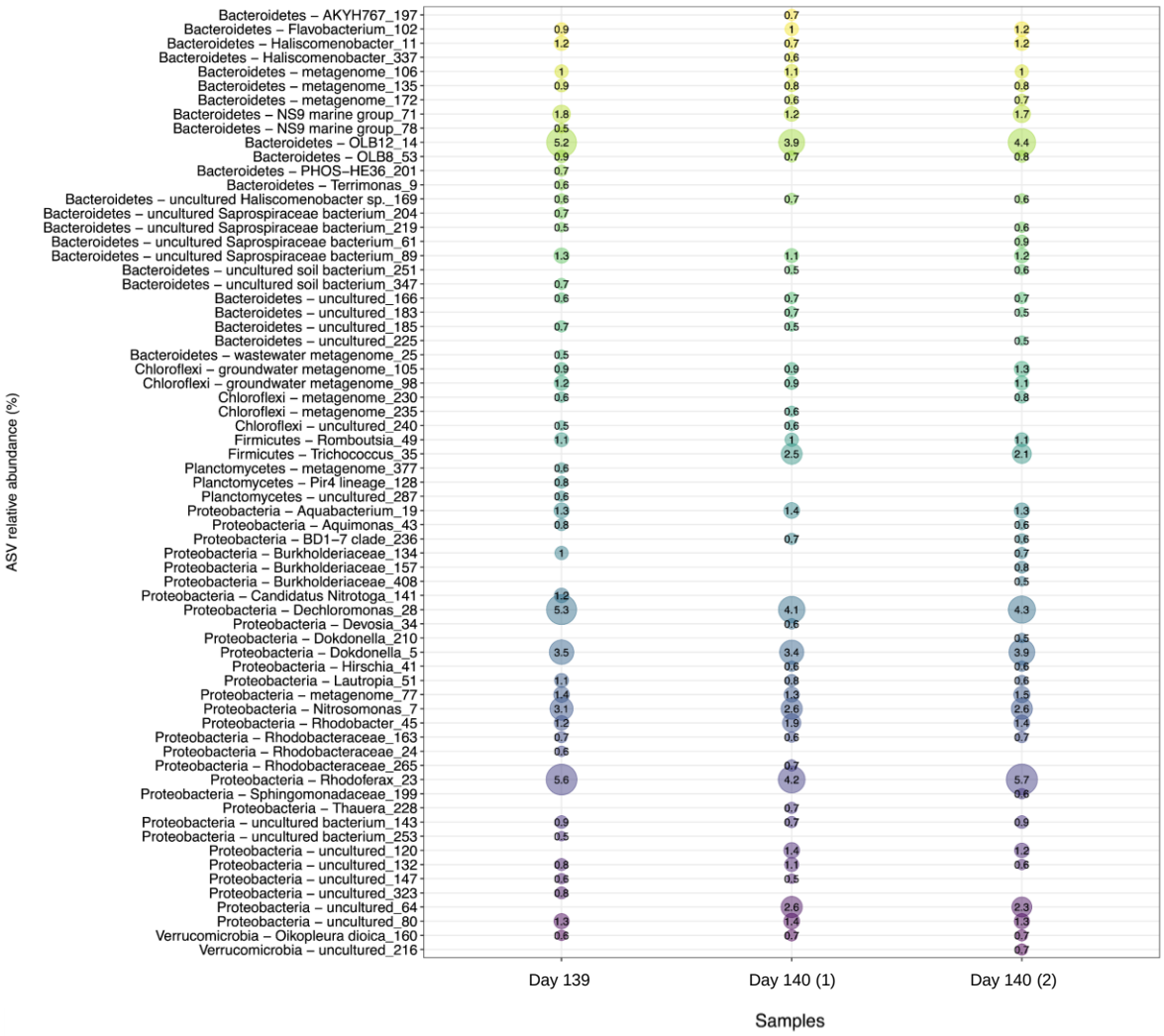

Figure B-2. Relative abundance of individual amplicon sequence variants (ASVs) detected in the dynamic tests in Period 2. The ASVs are only shown on the plot if greater than 0.5% relative abunadnce (RA) within the microbial community. Individual ASVs were assigned to the lowest possible taxonomic level based on the nucleotide sequence. The phylum for each ASV is also indicated before the additional taxonomy assignment on the y-axis, with the numbers inside circles representing the % RA.

Appendix C

Appendix C-1. Detailed biological processes for carbon, nitrogen and phosphorus transformation in the model

Figure C-1A presents the processes impacting carbon species. Bacterial decay can generate particulate biodegradable organics (X_B) and endogenous decay products (X_E), which can be hydrolyzed/converted to rbCOD (S_B) and particulate biodegradable organics later on. Particulate biodegradable organics can be hydrolyzed to rbCOD by all bacteria under all conditions. rbCOD can be fermented to VFAs (S_{VFA}) by OHOs and PAOs. Both VFAs and rbCOD can be used for OHO growth under aerobic and anoxic conditions. Under the anaerobic conditions, VFAs can be stored by PAOs as PHA (X_{PHA}) and by GAOs as glycogen (X_{GLY}). Under the anoxic conditions, stored PHA and glycogen can be used for denitrification to reduce nitrate and nitrite and maintenance by PAOs and GAOs, respectively. Under aerobic conditions, PHA and glycogen can be oxidized for PAO and GAO growth and maintenance.

Figure C-1B shows the processes related to nitrogen species. Cell decay can generate particulate biodegradable organic nitrogen ($X_{N,B}$) and ammonia (S_{NHx}). Particulate biodegradable organic nitrogen can be hydrolyzed to soluble biodegradable organic nitrogen ($S_{N,B}$). Ammonification can convert soluble biodegradable nitrogen to ammonia. Ammonia can be oxidized to nitrite (S_{NO2}) and then nitrate (S_{NO3}) by AOBs and NOBs. At the same time, nitrate can be reduced to nitrite through denitrification by OHOs, PAOs, and GAOs using rbCOD/VFAs, PHA, and glycogen, respectively, and PAO and GAO anoxic maintenance through nitrate. Nitrite can be reduced to nitrogen gas through denitrification by OHOs, PAOs, and GAOs using rbCOD/VFAs, PHA, and glycogen, respectively, and PAO and GAO anoxic maintenance through nitrite. Both nitrate and nitrite can be reduced to ammonia through nitrite and nitrate assimilative reduction.

Figure C-1C shows the processes related to phosphorus species. Cell decay can generate particulate biodegradable organic phosphorus ($X_{P,B}$), which can be hydrolyzed to soluble biodegradable organic

phosphorus ($S_{P,B}$). The hydrolyzed soluble biodegradable organic phosphorus can be converted to orthophosphate (S_{PO4}). Under the anaerobic conditions, orthophosphate is released from polyP (X_{PP}) by PAOs. Under the anoxic and aerobic conditions, orthophosphate is taken up by PAOs to replenish polyP.

Appendix C-2. Influent characteristics, physical parameters, and floc-related parameters in the floc model

Appendix C-2.1. Influent characteristics

The influent characteristics for dynamic tests included VFAs of 191.5 mg COD/L, readily biodegradable substrate of 150 mg COD/L, soluble unbiodegradable substrate of 12.5 mg COD/L, ammonia of 30 mg N/L, soluble biodegradable organic nitrogen of 19 mg N/L, orthophosphate of 6.5 mg P/L, calcium of 150 mg/L, magnesium of 15 mg/L, and potassium of 16 mg/L.

Appendix C-2.2. Physical parameters

The second step is to assure that the physical parameters are the same as those in the experiment. The detailed value of each parameter for dynamic tests is shown in Table C-1. The physical parameters setting of activity tests was different from that of dynamic tests. For activity test 1, all the physical parameters were the same except cycle length and reaction phase length were extended for another two hours. The DO concentration was set to be zero in these two hours. For activity tests 2 and 3, sludge was taken at the 1st hour of cycle and washed six times to eliminate all residual soluble substrates. Then $NaNO_3$ was added to achieve NO_3-N of 14.7 mg N/L as measured for Test 2, and $NaNO_3$ and PO_4 were added to achieve NO_3-N of 14.7 mg N/L and PO_4-P of 30 mg P/L as measured for Test 3. The ways to achieve these processes in Sumo were to stop dynamic cycle test simulation at the 1st hour, save all the substrate (soluble and particle) concentrations, set all the kinetics with the unit of 1/d to zero to stop all the biological reactions, add another

influent with no substrate concentrations but deionized water, and run the model for 6 cycles to mimic sludge wash using deionized water. By doing these steps, all the soluble substrates were minimized but the particulate substrates were remained at the same level as before. After all these steps, all the kinetics with the unit of 1/d were set back to previous values. Then two influents (one with NO_3-N and the other with NO_3-N and PO_4-P) were fed to SBR with the feeding time of 1s at the beginning for Test 2 and Test 3, respectively to achieve corresponding substrate concentrations. Then the model was run under anoxic conditions for 1 hour to mimic activity tests 2 and 3.

For Test 4, the SBR cycle setup was extended for two more hours at the same DO concentration (0.3 mg/L). For Test 5, the influent added to the SBR was changed to include VFA of 191.5 mg COD/L, soluble unbiodegradable COD of 12.5 mg COD/L, and PO_4-P of 6.5 mg P/L. After feeding, the SBR went through one hour of anaerobic phase, then went through two hours of aeration at a DO of 0.3 mg/L. At the beginning of the aerobic phase, a stream of NO_3-N was added into the reactor within 1s to achieve NO_3-N of 14.5 mg N/L as measured in the SBR. For Test 6, the influent was the same as the influent for dynamic tests except for no ammonia addition. After feeding, the SBR went through one hour of anaerobic phase, then went through one hour of aerobic phase at a DO of 0.3 mg/L. At the beginning of the aerobic phase, NO_3-N and NH_4-N were added into the reactor within 1s to achieve NO_3-N of 10.6 mg N/L and NH_4-N of 3.3 mg N/L as measured in the SBR.

Appendix C-2.3. Floc-related parameters

For measurable parameters, settled floc level at decanted water level ($h_{settled,floc}$), floc density (ρ_F), and average floc radius (Z_F) were measured to be 7.6 ± 0.4 cm, 1120 ± 21 kg/m^3, and 110 ± 10 μm. In the floc model, the distribution of floc size was not considered due to its irrelevant to the simulation goals.

For calculable parameter, dry matter content of flocs ($X_{TSS,F}$) was calculated to be 0.025 kg/kg based on the relationship with floc density and measured MLSS at the steady state in the SBR as illustrated in Eq. (5-23).

For constant parameters, water between settled floc (free water) ($V_{water,floc}$), internal solids transfer rate in floc (D_X), slope of switching function around $X_{TSStarget}$ (sl), and TSS controller displacement rate gain of solids between floc layers ($r_{dpm,max}$) were set as default values. In addition, a floc was assumed to have three layers including top, middle, and bottom layer (near core of the floc) in the model. Since the system was a flocculant sludge system, all TSS was in flocs, and no TSS was present in the bulk phase. Therefore, specific attachment rate of solids to floc (r_{attach}) was set as default value, and detachment rate gain of solids from floc (r_{detach}) was set to zero, leading to minimal TSS in the bulk phase during the simulation.

Appendix C-3. Figures and Tables

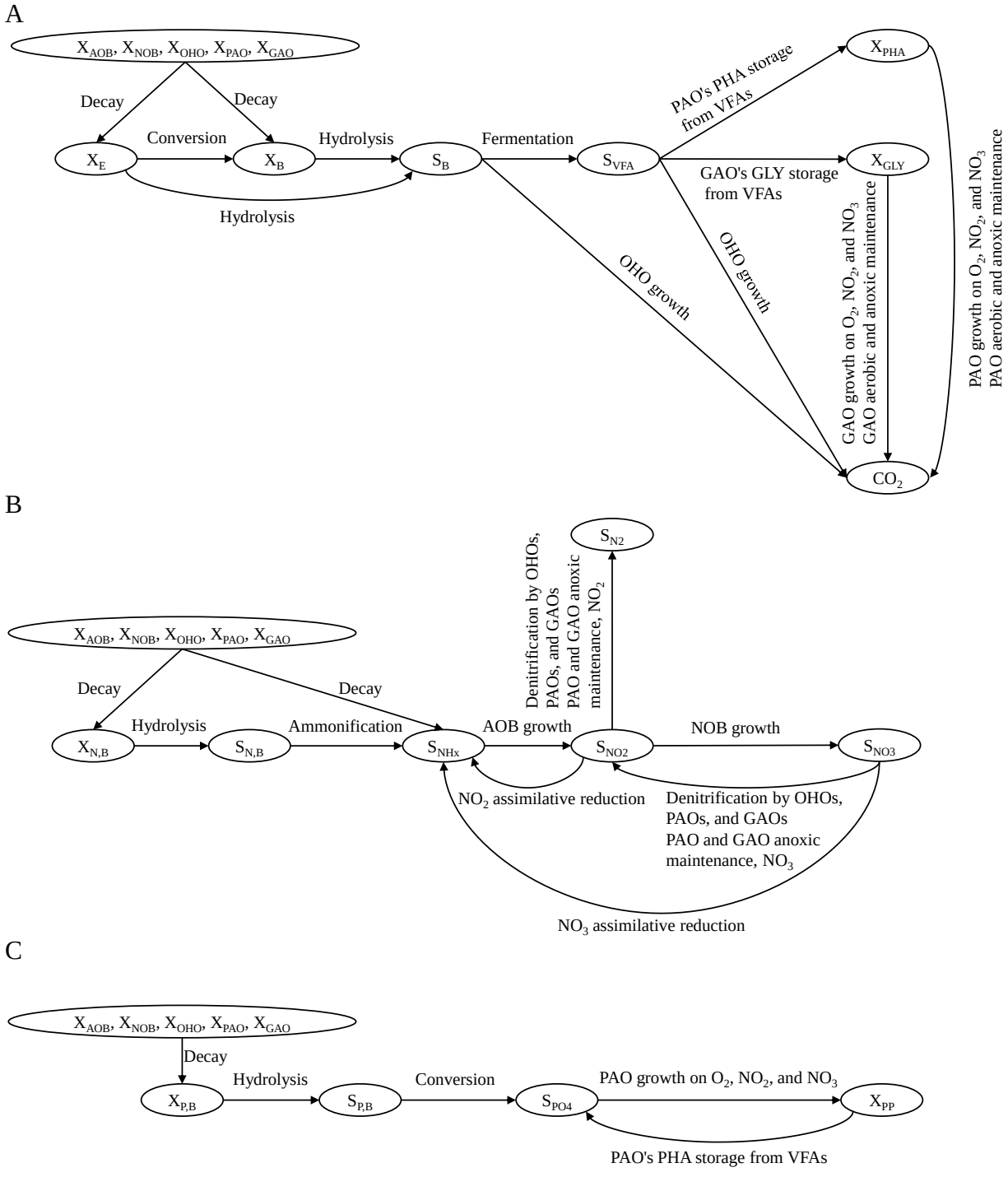

Figure C-1. The transformation of carbon (A), nitrogen (B), and phosphorus (C) species in Sumo2.

Table C-1. Physical parameters in the SBR.

Parameter	Value	Unit
Influent flow rate	0.86	m^3/d
Influent addition time	15	min
Temperature	10	℃
SBR surface area	0.06	m^3
Tank depth	0.04	m
Initial volume	0.009	m^3
Cycle length	8	h
Reaction phase length	7	h
Settle phase length	0.75	h
Decant phase length	0.2	h
Wasting phase length	0.05	h
Decant height	0.15	m
Effluent solids concentration	0	g/m^3
Diffuser distance from tank bottom	0.01	m
Covered fraction of reactor surface	100	%

Table C-2. The rational for adjusting corresponding parameters in each step during calibration.

Data profile range	Related mechanisms	Important parameters	Step
NH_4-N profile from 14min to 60 min in the anaerobic phase of dynamic tests	NH_4-N increase due to SN,B ammonification	q_{AMMON}	1
sCOD profile from 40 min to 60 min in the anaerobic phase of dynamic tests	• sCOD reduction due to SB fermentation with low VFA (OHO growth, anaerobic) and PAO's PHA storage from VFAs • SB fermentation with low VFA (OHO growth, anaerobic) is the limiting process	$\mu_{FERM,OHO}$	2
sCOD profile from 14 min to 40 min in the anaerobic phase of dynamic tests	sCOD reduction due to PAO's PHA storage from VFAs and GAO's GLY storage from VFAs	$q_{PAO,PHA}$ and $q_{GAO,GLY}$	3
PO_4-P profile from 14 min to 40 min in the anaerobic phase of dynamic tests	PO_4-P increase due to PAO's PHA storage from VFAs	$f_{P,VFA}$ $q_{PAO,PHA}$	4
PO_4-P profile from 40 min to 60 min in the anaerobic phase of dynamic tests	• PO_4-P increase due to PAO's PHA storage from VFAs and S_B fermentation with low VFA (OHO growth, anaerobic) • SB fermentation with low VFA (OHO growth, anaerobic) is the limiting process	$f_{P,VFA}$ $q_{PAO,PHA}$ $\mu_{FERM,OHO}$	5
NO_3-N profile in Test 1 under anoxic conditions	• NO_3-N reduction due to OHO growth on S_B, NO_3 and XB hydrolysis • XB hydrolysis is the limiting process	$\mu_{max,OHO}$	6
NO_3-N profile in Test 2 under anoxic conditions	NO_3-N reduction due to OHO growth on S_B, NO_3, XB hydrolysis, and GAO growth on GLY, NO_3	$\mu_{max,GAO}$	7
NO_3-N profile in Test 3 under anoxic conditions	NO_3-N reduction due to OHO growth on S_B, NO_3, XB hydrolysis, GAO growth on GLY, NO_3, and PAO growth on PHA, NO_3	$\mu_{max,PAO}$	8
PO_4-P profile in Test 3 under anoxic conditions	PO_4-P reduction due to PAO growth on PHA, NO_3	$f_{PP,PHA,anox}$	9
PO_4-P profile from 1 h to 2 h in the aerobic phase of dynamic tests	PO_4-P reduction due to PAO growth on PHA, O_2 and PAO growth on PHA, NO_3	$f_{PP,PHA,ox}$	10
NO_3-N profile in Test 4 under aerobic conditions	Stable NO_3-N due to SN,B ammonification, AOB growth, NOB growth, OHO growth on S_B, NO_3, and XB hydrolysis	$K_{O2,OHO}$	11
sCOD profile from 1 h to 1.5 h in the aerobic zone	sCOD reduction due to OHO growth on S_B, O_2 and OHO growth on S_B, NO_3	$\mu_{max,HO}$ and $K_{O2,OHO}$	12

TIN profile from 60 min to 120 min in Test 5 under aerobic conditions	Stable TIN due to no GAO growth on GLY, NO_3	$K_{O2,GAO}$	13
TIN profile from 0 min to 60 min in Test 5 under aerobic conditions	TIN reduction due to PAO growth on PHA, NO_3	$K_{O2,PAO}$	14
PO_4-P profile in Test 5 under aerobic conditions	PO_4-P reduction due to PAO growth on PHA, NO_3	$f_{PP,PHA,anox}$, $\mu_{max,PAO}$, and $K_{O2,PAO}$	15
TIN profile from 0 min to 30 min in Test 6 under aerobic conditions	TIN reduction due to PAO growth on PHA, NO_3 and OHO growth on S_B, NO_3	$\mu_{max,OHO}$ and $K_{O2,OHO}$	16
NH_4-N profile from 1 h to 5.5 h in the aerobic phase of dynamic tests	NH_4-N reduction due to bacteria growth and AOB growth	$\mu_{max,AOB,}$ and $K_{O2,AOB}$	17
NO_3-N profile from 1 h to 7 h in the aerobic phase of dynamic tests	NO_3-N increase due to NOB growth, OHO growth on S_B, NO_3, GAO growth on GLY, NO_3, and PAO growth on PHA, NO_3	$\mu_{max,NOB}$ and $K_{O2,NOB}$	18
NO_2-N profile from 1 h to 7 h in the aerobic phase of dynamic tests	Nitrite profile is related to most of the processes above	Confirm all of the parameters above	19

Table C-3. The stoichiometric matrix of Sumo2.

j	Symbol	Name	S_{VFA}	S_B	C_B	X_B	X_{PHA}	X_{GLY}	X_{OHO}	X_{PAO}	X_{GAO}	X_{AOB}	X_{NOB}
1	R1	OHO growth on VFAs, O_2	$-1/Y_{OHO,VFA,ox}$						1				
2	R2	OHO growth on VFAs, NO_2	$-1/Y_{OHO,VFA,anox}$						1				
3	R3	OHO growth on VFAs, NO_3	$-1/Y_{OHO,VFA,anox}$						1				
4	R4	OHO growth on S_B, O_2		$-1/Y_{OHO,SB,ox}$					1				
5	R5	OHO growth on S_B, NO_2		$-1/Y_{OHO,SB,anox}$					1				
6	R6	OHO growth on S_B, NO_3		$-1/Y_{OHO,SB,anox}$					1				
7	R7	S_B fermentation with low VFA (OHO growth, anaerobic)	$(1-Y_{OHO,SB,ana}-Y_{OHO,H2,ana,low})/Y_{OHO,SB,ana}$	$-1/Y_{OHO,SB,ana}$					1				
8	R8	OHO decay				$1-f_E$			-1				
9	R9	OHO anaerobic decay				$1-f_E$			-1				
10	r10	PAO growth on PHA, O_2					$-1/Y_{PAO,PHA,ox}$			1			
11	r11	PAO growth on PHA, NO_2					$-1/Y_{PAO,PHA,anox}$			1			
12	r12	PAO growth on PHA, NO_3					$-1/Y_{PAO,PHA,anox}$			1			
13	R13	PAO's PHA storage from VFAs	-1				1						
14	R14	PAO aerobic maintenance					-1						
15	R15	S_B fermentation with low VFA (PAO growth, anaerobic)	$(1-Y_{PAO,SB,ana}-Y_{PAO,H2,ana,low})/Y_{PAO,SB,ana}$	$-1/Y_{PAO,SB,ana}$						1			
16	R16	PAO decay	X_{PHA}/X_{PAO}			$1-f_E$	$-X_{PHA}/X_{PAO}$			-1			
17	R17	PAO anaerobic decay	X_{PHA}/X_{PAO}			$1-f_E$	$-X_{PHA}/X_{PAO}$			-1			
18	R18	GAO growth on GLY, O_2						$-1/Y_{GAO,GLY,ox}$			1		

19	**R19**	GAO growth on GLY, NO_2						$-1/Y_{GAO,GLY,anox}$			1			
20	**R20**	GAO growth on GLY, NO_3						$-1/Y_{GAO,GLY,anox}$			1			
21	**R21**	GAO's GLY storage from VFAs	-1					1						
22	**R22**	GAO aerobic maintenance						-1						
23	**R23**	GAO decay	X_{GLY}/X_{GAO}			$1-f_E$		$-X_{GLY}/X_{GAO}$			-1			
24	**R24**	AOB growth										1		
25	**R25**	AOB decay				$1-f_E$						-1		
26	**R26**	NOB growth											1	
27	**R27**	NOB decay				$1-f_E$							-1	
28	**R28**	XB hydrolysis		1		-1								
29	**R29**	SN,B ammonification												
30	**R30**	$S_{P,B}$ conversion to PO_4												

Table C-4. The stoichiometric matrix of Sumo2 (continue).

j	Symbol	Name	S_{NHx}	S_{NO2}	S_{NO3}	$S_{N,B}$	$X_{N,B}$	S_{PO4}	X_{PP}	$S_{P,B}$	$X_{P,B}$	S_{O2}
1	R1	OHO growth on VFAs, O_2	$-i_{N,BIO}$					$-i_{P,BIO}$				$-(1-Y_{OHO,VFA,ox})/Y_{OHO,VFA,ox}$
2	R2	OHO growth on VFAs, NO_2	$-i_{N,BIO}$	$-(1-Y_{OHO,VFA,anox})/(EEQ_{N2,NO2}*Y_{OHO,VFA,anox})$				$-i_{P,BIO}$				
3	R3	OHO growth on VFAs, NO_3	$-i_{N,BIO}$	$(1-Y_{OHO,VFA,anox})/(EEQ_{NO2,NO3}*Y_{OHO,VFA,anox})$	$-(1-Y_{OHO,VFA,anox})/(EEQ_{NO2,NO3}*Y_{OHO,VFA,anox})$			$-i_{P,BIO}$				
4	R4	OHO growth on S_B, O_2	$-i_{N,BIO}$					$-i_{P,BIO}$				$-(1-Y_{OHO,SB,ox})/Y_{OHO,SB,ox}$
5	R5	OHO growth on S_B, NO_2	$-i_{N,BIO}$	$-(1-Y_{OHO,SB,anox})/(EEQ_{N2,NO2}*Y_{OHO,SB,anox})$				$-i_{P,BIO}$				
6	R6	OHO growth on S_B, NO_3	$-i_{N,BIO}$	$(1-Y_{OHO,SB,anox})/(EEQ_{NO2,NO3}*Y_{OHO,SB,anox})$	$-(1-Y_{OHO,SB,anox})/(EEQ_{NO2,NO3}*Y_{OHO,SB,anox})$			$-i_{P,BIO}$				
7	R7	S_B fermentation with low VFA (OHO growth, anaerobic)	$-i_{N,BIO}$					$-i_{P,BIO}$				
8	R8	OHO decay	$-f_E*(i_{N,XE}-i_{N,BIO})$				$(1-f_E)*i_{N,BIO}$				$(1-f_E)*i_{P,BIO}$	
9	R9	OHO anaerobic decay	$-f_E*(i_{N,XE}-i_{N,BIO})$				$(1-f_E)*i_{N,BIO}$				$(1-f_E)*i_{P,BIO}$	
10	r10	PAO growth on PHA, O_2	$-i_{N,BIO}$					$-f_{PP,PHA,ox}/Y_{PAO,PHA,ox}-i_{P,BIO}$	$f_{PP,PHA,ox}/Y_{PAO,PHA,ox}$			$-(1-Y_{PAO,PHA,ox})/Y_{PAO,PHA,ox}$
11	r11	PAO growth on PHA, NO_2	$-i_{N,BIO}$	$-(1-Y_{PAO,PHA,anox})/(EEQ_{N2,NO2}*Y_{PAO,PHA,anox})$				$-f_{PP,PHA,anox}/Y_{PAO,PHA,anox}-i_{P,BIO}$	$f_{PP,PHA,anox}/Y_{PAO,PHA,anox}$			
12	r12	PAO growth on PHA, NO_3	$-i_{N,BIO}$	$(1-Y_{PAO,PHA,anox})/(EEQ_{NO2,NO3}*Y_{PAO,PHA,anox})$	$-(1-Y_{PAO,PHA,anox})/(EEQ_{NO2,NO3}*Y_{PAO,PHA,anox})$			$-f_{PP,PHA,anox}/Y_{PAO,PHA,anox}-i_{P,BIO}$	$f_{PP,PHA,anox}/Y_{PAO,PHA,anox}$			

13	**R13**	PAO's PHA storage from VFAs						$f_{P,VFA}$	$-f_{P,VFA}$			
14	**R14**	PAO aerobic maintenance										-1
15	**R15**	S_B fermentation with low VFA (PAO growth, anaerobic)	$-i_{N,BIO}$					$-i_{P,BIO}$				
16	**R16**	PAO decay	$-f_E*(i_{N,XE}-i_{N,BIO})$				$(1-f_E)*i_{N,BIO}$	X_{PP}/X_{PAO}	$-X_{PP}/X_{PAO}$		$(1-f_E)*i_{P,BIO}$	
17	**R17**	PAO anaerobic decay	$-f_E*(i_{N,XE}-i_{N,BIO})$				$(1-f_E)*i_{N,BIO}$	X_{PP}/X_{PAO}	$-X_{PP}/X_{PAO}$		$(1-f_E)*i_{P,BIO}$	
18	**R18**	GAO growth on GLY, O_2	$-i_{N,BIO}$					$-i_{P,BIO}$				$-(1-Y_{GAO,GLY,ox})/Y_{GAO,GLY,ox}$
19	**R19**	GAO growth on GLY, NO_2	$-i_{N,BIO}$	$-(1-Y_{GAO,GLY,anox})/(EEQ_{N2,NO2}*Y_{GAO,GLY,anox})$				$-i_{P,BIO}$				
20	**R20**	GAO growth on GLY, NO_3	$-i_{N,BIO}$	$(1-Y_{GAO,GLY,anox})/(EEQ_{NO2,NO3}*Y_{GAO,GLY,anox})$	$-(1-Y_{GAO,GLY,anox})/(EEQ_{NO2,NO3}*Y_{GAO,GLY,anox})$			$-i_{P,BIO}$				
21	**R21**	GAO's GLY storage from VFAs										
22	**R22**	GAO aerobic maintenance										-1
23	**R23**	GAO decay	$-f_E*(i_{N,XE}-i_{N,BIO})$				$(1-f_E)*i_{N,BIO}$				$(1-f_E)*i_{P,BIO}$	
24	**R24**	AOB growth	$-1/Y_{AOB}-i_{N,BIO}$	$1/Y_{AOB}$				$-i_{P,BIO}$				$-(EEQ_{NO2}-Y_{AOB})/Y_{AOB}$

25	**R25**	AOB decay	$-f_E*(i_{N,XE}-i_{N,BIO})$				$(1-f_E)*i_{N,BIO}$				$(1-f_E)*i_{P,BIO}$	
26	**R26**	NOB growth	$-i_{N,BIO}$	$-1/Y_{NOB}$	$1/Y_{NOB}$			$-i_{P,BIO}$				$-(EEQ_{NO2,NO3}-Y_{NOB})/Y_{NOB}$
27	**R27**	NOB decay	$-f_E*(i_{N,XE}-i_{N,BIO})$				$(1-f_E)*i_{N,BIO}$				$(1-f_E)*i_{P,BIO}$	
28	**R28**	XB hydrolysis				$X_{N,B}/X_B$	$-X_{N,B}/X_B$			$X_{P,B}/X_B$	$-X_{P,B}/X_B$	
29	**R29**	SN,B ammonification	1			-1						
30	**R30**	$S_{P,B}$ conversion to PO_4						1		-1		

Table C-5. Definition of components

	Components
Symbol	**Name**
$\mathbf{S_{VFA}}$	Volatile fatty acids (VFA)
$\mathbf{S_B}$	Readily biodegradable substrate (non-VFA)
$\mathbf{C_B}$	Colloidal biodegradable substrate
$\mathbf{X_B}$	Slowly biodegradable substrate
$\mathbf{X_{PHA}}$	Stored polyhydroxyalkanoates (PHA)
$\mathbf{X_{GLY}}$	Stored glycogen (GLY)
$\mathbf{X_{OHO}}$	Ordinary heterotrophic organisms (OHO)
$\mathbf{X_{PAO}}$	Phosphorus accumulating organisms (PAO)
$\mathbf{X_{GAO}}$	Glycogen accumulating organisms (GAO)
$\mathbf{X_{AOB}}$	Aerobic ammonia oxidizers (AOB)
$\mathbf{X_{NOB}}$	Nitrite oxidizers (NOB)
$\mathbf{S_{NHx}}$	Total ammonia (NH_x)
$\mathbf{S_{NO2}}$	Nitrite (NO_2)
$\mathbf{S_{NO3}}$	Nitrate (NO_3)
$\mathbf{S_{N,B}}$	Soluble biodegradable organic N (from SB)
$\mathbf{X_{N,B}}$	Particulate biodegradable organic N (from X_B)
$\mathbf{S_{PO4}}$	Orthophosphate (PO_4)
$\mathbf{X_{PP}}$	Stored polyphosphate (PP)
$\mathbf{S_{P,B}}$	Soluble biodegradable organic P (from SB)
$\mathbf{X_{P,B}}$	Particulate biodegradable organic P (from X_B)
$\mathbf{S_{O2}}$	Dissolved oxygen (O_2)

Table C-6. Process rate expressions of Sumo2

j	Symbol	Name	Rate
1	R1	OHO growth on VFAs, O_2	$\mu_{OHO,T}*X_{OHO}*Msat_{SVFA,KVFA}*Msat_{SO2,KO2,OHO}*Msat_{SNHx,KNHx,BIO}*Msat_{SPO4,KPO4,BIO}*Msat_{SCAT,KCAT}*Msat_{SAN,KAN}*Msat_{SCa,KCa}*Msat_{SMg,KMg}*Bellinh_{pH}$
2	R2	OHO growth on VFAs, NO_2	$\mu_{OHO,T}*X_{OHO}*\eta_{OHO,anox}*Msat_{SVFA,KVFA}*Msat_{SNO2,KNO2,OHO}*Minh_{SO2,KO2,OHO}*Msat_{SNHx,KNHx,BIO}*Msat_{SPO4,KPO4,BIO}*Msat_{SCAT,KCAT}*Msat_{SAN,KAN}*Msat_{SCa,KCa}*Msat_{SMg,KMg}*Bellinh_{pH}$
3	R3	OHO growth on VFAs, NO_3	$\mu_{OHO,T}*X_{OHO}*\eta_{OHO,anox}*Msat_{SVFA,KVFA}*Msat_{SNO3,KNO3,OHO}*Minh_{SO2,KO2,OHO}*Minh_{SNO2,KNO2,OHO}*Msat_{SNHx,KNHx,BIO}*Msat_{SPO4,KPO4,BIO}*Msat_{SCAT,KCAT}*Msat_{SAN,KAN}*Msat_{SCa,KCa}*Msat_{SMg,KMg}*Bellinh_{pH}$
4	R4	OHO growth on S_B, O_2	$\mu_{OHO,T}*X_{OHO}*Msat_{SB,KSB}*Minh_{SVFA,KVFA}*Msat_{SO2,KO2,OHO}*Msat_{SNHx,KNHx,BIO}*Msat_{SPO4,KPO4,BIO}*Msat_{SCAT,KCAT}*Msat_{SAN,KAN}*Msat_{SCa,KCa}*Msat_{SMg,KMg}*Bellinh_{pH}$
5	R5	OHO growth on S_B, NO_2	$\mu_{OHO,T}*X_{OHO}*\eta_{OHO,anox}*Msat_{SB,KSB}*Minh_{SVFA,KVFA}*Msat_{SNO2,KNO2,OHO}*Minh_{SO2,KO2,OHO}*Msat_{SNHx,KNHx,BIO}*Msat_{SPO4,KPO4,BIO}*Msat_{SCAT,KCAT}*Msat_{SAN,KAN}*Msat_{SCa,KCa}*Msat_{SMg,KMg}*Bellinh_{pH}$
6	R6	OHO growth on S_B, NO_3	$\mu_{OHO,T}*X_{OHO}*\eta_{OHO,anox}*Msat_{SB,KSB}*Minh_{SVFA,KVFA}*Msat_{SNO3,KNO3,OHO}*Minh_{SO2,KO2,OHO}*Minh_{SNO2,KNO2,OHO}*Msat_{SNHx,KNHx,BIO}*Msat_{SPO4,KPO4,BIO}*Msat_{SCAT,KCAT}*Msat_{SAN,KAN}*Msat_{SCa,KCa}*Msat_{SMg,KMg}*Bellinh_{pH}$
7	R7	S_B fermentation with low VFA (OHO growth, anaerobic)	$\mu_{FERM,OHO,T}*X_{OHO}*Loginh_{SVFA,KVFA,FERM}*Msat_{SB,KSB,ana}*Minh_{SO2,KO2,OHO}*Minh_{SNO2,KNO2,OHO}*Minh_{SNO3,KNO3,OHO}*Msat_{SNHx,KNHx,BIO}*Msat_{SPO4,KPO4,BIO}*Msat_{SCAT,KCAT}*Msat_{SAN,KAN}*Msat_{SCa,KCa}*Msat_{SMg,KMg}*Msat_{SCO2,KCO2,BIO}*Bellinh_{pH}$
8	R8	OHO decay	$b_{OHO,T}*X_{OHO}*(Msat_{SO2,KO2,OHO}+\eta_{b,anox}*Msat_{SNO2,KNO2,OHO}*Minh_{SO2,KO2,OHO}+\eta_{b,anox}*Msat_{SNO3,KNO3,OHO}*Minh_{SNO2,KNO2,OHO}*Minh_{SO2,KO2,OHO})$
9	R9	OHO anaerobic decay	$b_{OHO,T}*X_{OHO}*\eta_{b,ana}*Minh_{SNO2,KNO2,OHO}*Minh_{SNO3,KNO3,OHO}*Minh_{SO2,KO2,OHO}$
10	r10	PAO growth on PHA, O_2	$\mu_{PAO,T}*X_{PAO}*MRsat_{XPHA,XPAO,KPHA}*Msat_{SO2,KO2,PAO}*Msat_{SNHx,KNHx,BIO}*Msat_{SPO4,KPO4,PAO}*Loginh_{XPP,XPAO,max}*Msat_{SCAT,KCAT}*Msat_{SAN,KAN}*Msat_{SCa,KCa,PAO}*Msat_{SMg,KMg,PAO}*Msat_{SK,KK,PAO}*Bellinh_{pH}$
11	r11	PAO growth on PHA, NO_2	$\mu_{PAO,T}*X_{PAO}*\eta_{PAO,anox}*MRsat_{XPHA,XPAO,KPHA}*Msat_{SNO2,KNO2,PAO}*Minh_{SO2,KO2,PAO}*Msat_{SNHx,KNHx,BIO}*Msat_{SPO4,KPO4,PAO}*Msat_{SCAT,KCAT}*Msat_{SAN,KAN}*Msat_{SCa,KCa,PAO}*Msat_{SMg,KMg,PAO}*Msat_{SK,KK,PAO}*Bellinh_{pH}$
12	r12	PAO growth on PHA, NO_3	$\mu_{PAO,T}*X_{PAO}*\eta_{PAO,anox}*MRsat_{XPHA,XPAO,KPHA}*Msat_{SNO3,KNO3,PAO}*Minh_{SO2,KO2,PAO}*Minh_{SNO2,KNO2,PAO}*Msat_{SNHx,KNHx,BIO}*Msat_{SPO4,KPO4,PAO}*Msat_{SCAT,KCAT}*Msat_{SAN,KAN}*Msat_{SCa,KCa,PAO}*Msat_{SMg,KMg,PAO}*Msat_{SK,KK,PAO}*Bellinh_{pH}$
13	R13	PAO's PHA storage from VFAs	$q_{PAO,PHA,T}*X_{PAO}*Msat_{SVFA,KVFA,PAO}*MRsat_{XPP,XPAO,KPP}*Loginh_{XPHA,XPAO,max}$
14	R14	PAO aerobic maintenance	$b_{PHA,T}*X_{PAO}*Msat_{SO2,KO2,PAO}*MRsat_{XPHA,XPAO,KPHA}$
15	R15	S_B fermentation with low VFA (PAO growth, anaerobic)	$\mu_{FERM,PAO,T}*X_{PAO}*Loginh_{SVFA,KVFA,FERM}*Msat_{SB,KSB,ana}*Msat_{SNHx,KNHx,BIO}*Msat_{SPO4,KPO4,BIO}*Msat_{SCAT,KCAT}*Msat_{SAN,KAN}*Msat_{SCa,KCa}*Msat_{SMg,KMg}*Msat_{SCO2,KCO2,BIO}*Bellinh_{pH}*Loginh_{ORP,PAO}$
16	R16	PAO decay	$b_{PAO,T}*X_{PAO}*(MRinh_{XPHA,XPAO,KPHA}*Msat_{SO2,KO2,PAO}+\eta_{bPAO,anox}*MRinh_{XPHA,XPAO,KPHA}*MRinh_{XPP,XPAO,KPP}*(Msat_{SNO2,KNO2,PAO}+Minh_{SNO2,KNO2,PAO}*Msat_{SNO3,KNO3,PAO})*Minh_{SO2,KO2,PAO})$
17	R17	PAO anaerobic decay	$b_{PAO,T}*X_{PAO}*(\eta_{bPAO,ana}*MRinh_{XPP,XPAO,KPP}*Minh_{SNO3,KNO3,PAO}*Minh_{SNO2,KNO2,PAO}*Minh_{SO2,KO2,PAO}+m_{tox,ana})$
18	R18	GAO growth on GLY, O_2	$\mu_{GAO,T}*X_{GAO}*MRsat_{XGLY,XGAO,KGLY}*Msat_{SO2,KO2,GAO}*Msat_{SNHx,KNHx,BIO}*Msat_{SPO4,KPO4,BIO}*Msat_{SCAT,KCAT}*Msat_{SAN,KAN}*Msat_{SCa,KCa}*Msat_{SMg,KMg}*Bellinh_{pH}$
19	R19	GAO growth on GLY, NO_2	$\mu_{GAO,T}*X_{GAO}*\eta_{GAO,anox}*MRsat_{XGLY,XGAO,KGLY}*Msat_{SNO2,KNO2,GAO}*Minh_{SO2,KO2,GAO}*Msat_{SNHx,KNHx,BIO}*Msat_{SPO4,KPO4,BIO}*Msat_{SCAT,KCAT}*Msat_{SAN,KAN}*Msat_{SCa,KCa}*Msat_{SMg,KMg}*Bellinh_{pH}$
20	R20	GAO growth on GLY, NO_3	$\mu_{GAO,T}*X_{GAO}*\eta_{GAO,anox}*MRsat_{XGLY,XGAO,KGLY}*Msat_{SNO3,KNO3,GAO}*Minh_{SNO2,KNO2,GAO}*Minh_{SO2,KO2,GAO}*Msat_{SNHx,KNHx,BIO}*Msat_{SPO4,KPO4,BIO}*Msat_{SCAT,KCAT}*Msat_{SAN,KAN}*Msat_{SCa,KCa}*Msat_{SMg,KMg}*Bellinh_{pH}$
21	R21	GAO's GLY storage from VFAs	$q_{GAO,GLY,T}*X_{GAO}*Msat_{SVFA,KVFA,GAO}*Loginh_{XGLY,XGAO,max}*Logsat_{ORP,GAO}$
22	R22	GAO aerobic maintenance	$b_{GLY,T}*X_{GAO}*Msat_{SO2,KO2,GAO}*MRsat_{XGLY,XGAO,KGLY}$

23	**R23**	GAO decay	$b_{GAO,T}*X_{GAO}*(MRinh_{XGLY,XGAO,KGLY}*Msat_{SO2,KO2,GAO}+\eta_{bGAO,anox}*MRinh_{XGLY,XGAO,KGLY}*Msat_{SNO2,KNO2,GAO}*Minh_{SO2,KO2,GAO}*Minh_{SO2,KO2,GAO}+\eta_{bGAO,anox}*MRinh_{XGLY,XGAO,KGLY}*Msat_{SNO3,KNO3,GAO}*Minh_{SNO2,KNO2,GAO}*Minh_{SO2,KO2,GAO})$
24	**R24**	AOB growth	$\mu_{AOB,T}*X_{AOB}*Msat_{SNHx,KNHx,AOB}*LogsatpH_{CO2,AOB}*Msat_{SO2,KO2,AOB}*Msat_{SPO4,KPO4,BIO}*Msat_{SCAT,KCAT}*Msat_{SAN,KAN}*Msat_{SCa,KCa}*Msat_{SMg,KMg}*MinhpH_{HNO2,AOB}*Bellinh_{pH}$
25	**R25**	AOB decay	$b_{AOB,T}*X_{AOB}*(Msat_{SO2,KO2,AOB}+\eta_{b,anox}*Msat_{SNOx,\mathbf{kin},KNOx,AOB}*Minh_{SO2,KO2,AOB})$
26	**R26**	NOB growth	$\mu_{NOB,T}*X_{NOB}*Msat_{SNO2,KNO2,NOB}*LogsatpH_{CO2,NOB}*Msat_{SO2,KO2,NOB}*Msat_{SNHx,KNHx,BIO}*Msat_{SPO4,KPO4,BIO}*Msat_{SCAT,KCAT}*Msat_{SAN,KAN}*Msat_{SCa,KCa}*Msat_{SMg,KMg}*MinhpH_{NH3,NOB}*Bellinh_{pH}$
27	**R27**	NOB decay	$b_{NOB,T}*X_{NOB}*(Msat_{SO2,KO2,NOB}+\eta_{b,anox}*Msat_{SNOx,\mathbf{kin},KNOx,NOB}*Minh_{SO2,KO2,NOB})$
28	**R28**	XB hydrolysis	$q_{HYD,T}*X_{BIO,kin}*MRsat_{XB,XBIO,KHYD}*(Msat_{SO2,KO2,OHO}+\eta_{HYD,anox}*(Msat_{SNO2,KNO2,OHO}+Msat_{SNO3,KNO3,OHO}*Minh_{SNO2,KNO2,OHO})*Minh_{SO2,KO2,OHO}+\eta_{HYD,ana}*Minh_{SNO3,KNO3,OHO}*Minh_{SNO2,KNO2,OHO}*Minh_{SO2,KO2,OHO})$
29	**R29**	SN,B ammonification	$q_{AMMON,T}*S_{N,B}*X_{BIO,kin}$
30	**R30**	$S_{P,B}$ conversion to PO_4	$q_{SPB,T}*S_{P,B}*X_{BIO,kin}$

Table C-7. Default kinetic parameter values of Sumo2

	Ordinary heterotrophic organism kinetics (OHO)	Type(Kinetic)	
Symbol	**Name**	**Default**	**Unit**
μ_{OHO}	Maximum specific growth rate of OHOs	4.0	d^{-1}
$\mu_{FERM,OHO}$	Fermentation growth rate of OHOs	0.3	d^{-1}
b_{OHO}	Decay rate of OHOs	0.62	d^{-1}
$\eta_{OHO,anox}$	Reduction factor for anoxic growth of OHOs	0.60	unitless
$K_{SB,AS}$	Half-saturation of readily biodegradable substrate for OHOs (AS)	5.0	g COD.m^{-3}
$K_{O2,OHO,AS}$	Half-saturation of O_2 for OHOs (AS)	0.15	g O_2.m^{-3}
$K_{VFA,AS}$	Half-saturation of VFA for OHOs (AS)	0.5	g COD.m^{-3}
$K_{MEOL,OHO,AS}$	Half-saturation of methanol for OHOs (AS)	0.1	g COD.m^{-3}
$K_{NO3,OHO,AS}$	Half-saturation of NO_3 for OHOs (AS)	0.10	g N.m^{-3}
$K_{NO2,OHO,AS}$	Half-saturation of NO_2 for OHOs (AS)	0.05	g N.m^{-3}
$K_{VFA,FERM,AS}$	Half-saturation of VFA in fermentation of OHOs (AS)	50.0	g COD.m^{-3}
$K_{SB,ana,AS}$	Half-saturation of readily biodegradable substrate in fermentation by OHOs (AS)	350.0	g COD.m^{-3}

	Phosphorus accumulating organism kinetics (PAO)	Type(Kinetic)	
Symbol	**Name**	**Default**	**Unit**
μ_{PAO}	Maximum specific growth rate of PAOs	1.00	d^{-1}
$\mu_{FERM,PAO}$	Fermentation growth rate of PAOs	0.45	d^{-1}
$\mu_{PAO,lim}$	Maximum specific growth rate of PAOs under P limited	0.49	d^{-1}
b_{PAO}	Decay rate of PAOs	0.05	d^{-1}
b_{PHA}	Rate of PAOs maintenance on PHA	0.05	d^{-1}
$b_{PP,ana}$	Rate of PAOs maintenance under anaerobic conditions (PP cleavage)	0.01	d^{-1}

$q_{PAO,PHA}$	Rate of VFA storage into PHA for PAOs	4.0	d^{-1}
$\eta_{PAO,anox}$	Reduction factor for anoxic growth of PAOs	0.66	unitless
$\eta_{bPAO,anox}$	Reduction factor for anoxic decay of PAOs	0.50	unitless
$\eta_{bPAO,ana}$	Reduction factor for anaerobic decay of PAOs	0.25	unitless
$\eta_{bPHA,anox}$	Reduction factor for anoxic maintenance of PAOs on PHA	0.66	unitless
$\eta_{bPP,aer}$	Reduction factor for aerobic maintenance of PAOs on PP	0.25	unitless
$\eta_{bPP,anox}$	Reduction factor for anoxic maintenance of PAOs on PP	0.50	unitless
$K_{PO4,PAO,AS}$	Half-saturation of PO_4 for PAOs (AS)	0.50	g $P.m^{-3}$
K_{PHA}	Half-saturation of PHA for PAOs	0.10	g $COD.m^{-3}$
$K_{O2,PAO,AS}$	Half-saturation of O_2 for PAOs (AS)	0.05	g $O_2.m^{-3}$
$K_{NO3,PAO,AS}$	Half-saturation of NO_3 for PAOs (AS)	0.10	g $N.m^{-3}$
$K_{NO2,PAO,AS}$	Half-saturation of NO_2 for PAOs (AS)	0.05	g $N.m^{-3}$
$K_{VFA,PAO,AS}$	Half-saturation of VFA storage for PAOs (AS)	5.0	g $COD.m^{-3}$
K_{PP}	Half-saturation of PP for PAOs	0.01	g $P.m^{-3}$
$Ki_{PP,PAO,max}$	Half-inhibition of maximum PP content of PAOs	99.00	g P.g COD^{-1}
$Ki_{PHA,PAO,max}$	Half-inhibition of maximum PHA content of PAOs	0.60	g COD.g COD^{-1}
$K_{Mg,PAO,AS}$	Half-saturation of Mg (counter-ion in PP storage) for PAOs (AS)	0.001	g $Mg.m^{-3}$
$K_{K,PAO,AS}$	Half-saturation of K (counter-ion in PP storage) for PAOs (AS)	0.001	g $K.m^{-3}$
$K_{Ca,PAO,AS}$	Half-saturation of Ca (counter-ion in PP storage) for PAOs (AS)	0.001	g $Ca.m^{-3}$
$K_{PP,lim}$	Half-saturation of PP (nutrient) for PAOs under PO4 limitation (AS)	0.002	g $P.m^{-3}$
$Ki_{PO4,lim,AS}$	Half-inhibition of PO_4 for PAOs under PO4 limitation (AS)	0.005	g $P.m^{-3}$
$Logsat_{ORP,PAO,Half}$	Logistic half-saturation of ORP switching in fermentation of PAO	-100.0	mV
$Logsat_{ORP,PAO,Slope}$	Logistic slope of ORP switching in fermentation of PAO	0.1	mV^{-1}

	Glycogen accumulating organism kinetics (GAO)	Type(Kinetic)	
Symbol	**Name**	**Default**	**Unit**
μ_{GAO}	Maximum specific growth rate of GAOs	0.55	d^{-1}

b_{GAO}	Decay rate of GAOs	0.05	d^{-1}
b_{GLY}	Rate of GAOs maintenance on glycogen	0.10	d^{-1}
$q_{GAO,GLY}$	Rate of VFA storage into glycogen for GAOs	4.0	d^{-1}
$\eta_{GAO,anox}$	Reduction factor for anoxic growth of GAOs	0.33	unitless
$\eta_{bGAO,anox}$	Reduction factor for anoxic decay of GAOs	0.50	unitless
$\eta_{bGAO,ana}$	Reduction factor for anaerobic decay of GAOs	0.25	unitless
$\eta_{bGLY,anox}$	Reduction factor for anoxic maintenance of GAOs on glycogen	0.33	unitless
$\eta_{bGLY,ana}$	Reduction factor for anaerobic maintenance of GAOs on glycogen	0.10	unitless
K_{GLY}	Half-saturation of glycogen for GAOs (AS)	0.05	g COD.m^{-3}
$K_{O2,GAO,AS}$	Half-saturation of O_2 for GAOs (AS)	0.2	g O_2.m^{-3}
$K_{NO3,GAO,AS}$	Half-saturation of NO_3 for GAOs (AS)	0.10	g N.m^{-3}
$K_{NO2,GAO,AS}$	Half-saturation of NO_2 for GAOs (AS)	0.05	g N.m^{-3}
$Ki_{GLY,GAO,max}$	Half-inhibition of maximum glycogen content of GAOs (AS)	0.5	g COD.g COD^{-1}
$K_{VFA,GAO,AS}$	Half-saturation of VFA storage for GAOs (AS)	5.0	g COD.m^{-3}
$Logsat_{ORP,Half}$	Logistic half-saturation of ORP switching of GAOs	-100.0	mV
$Logsat_{ORP,Slope}$	Logistic slope of ORP switching of GAOs	0.1	mV^{-1}

	Aerobic ammonia oxidizer kinetics (AOB)	Type(Kinetic)	
Symbol	**Name**	**Default**	**Unit**
μ_{AOB}	Maximum specific growth rate of AOBs	0.85	d^{-1}
b_{AOB}	Decay rate of AOBs	0.17	d^{-1}
$K_{NHx,AOB,AS}$	Half-saturation of NH_x for AOBs (AS)	0.7	g N.m^{-3}
$K_{CO2,AOB,sidestream}$	Half-saturation of CO_2 for AOBs (Sidestream)	48.0	g TIC.m^{-3}
$K_{CO2,AOB,AS}$	Half-saturation of CO_2 for AOBs (AS)	12.0	g TIC.m^{-3}
$K_{CO2,AOB,pH,sidestream}$	Half-saturation of bicarbonate for AOBs (Sidestream)	0.0040	mol $[HCO_3^-]$.L^{-1}
$K_{CO2,AOB,pH,AS}$	Half-saturation of bicarbonate for AOBs (AS)	0.0010	mol $[HCO_3^-]$.L^{-1}

$K_{O2,AOB,sidestream}$	Half-saturation of O_2 for AOBs (Sidestream)	0.50	g $O_2.m^{-3}$
$K_{O2,AOB,AS}$	Half-saturation of O_2 for AOBs (AS)	0.25	g $O_2.m^{-3}$
$K_{NOx,AOB,AS}$	Half-saturation of NO_x (anoxic conditions) for AOBs (AS)	0.03	g $N.m^{-3}$
$Ki_{HNO2,AOB,pH,AS}$	Half-inhibition of nitrous acid for AOBs (AS)	9999	mol $[HNO_2].L^{-1}$

	Nitrite oxidizer kinetics (NOB)	Type(Kinetic)	
Symbol	**Name**	**Default**	**Unit**
μ_{NOB}	Maximum specific growth rate of NOBs	0.65	d^{-1}
b_{NOB}	Decay rate of NOBs	0.15	d^{-1}
$K_{NO2,NOB,AS}$	Half-saturation of NO_2 for NOBs (AS)	0.10	g $N.m^{-3}$
$K_{CO2,NOB,AS}$	Half-saturation of CO_2 for NOBs (AS)	1.00	g $CO_2.m^{-3}$
$K_{CO2,NOB,pH,AS}$	Half-saturation of bicarbonate for NOBs (AS)	1.00E-10	mol $[HCO_3^-].L^{-1}$
$K_{O2,NOB,sidestream}$	Half-saturation of O_2 for NOBs (Sidestream)	0.50	g $O_2.m^{-3}$
$K_{O2,NOB,AS}$	Half-saturation of O_2 for NOBs (AS)	0.25	g $O_2.m^{-3}$
$K_{NOx,NOB,AS}$	Half-saturation of NO_x (anoxic conditions) for NOBs (AS)	0.03	g $N.m^{-3}$
$Ki_{NH3,NOB,pH,AS}$	Half-inhibition of NH_3 for NOBs (AS)	9999	mol $[NH_3].L^{-1}$

	Common switches	Type(Kinetic)	
Symbol	**Name**	**Default**	**Unit**
$K_{NHx,BIO,AS}$	Half-saturation of NH_x as nutrient for biomasses (AS)	0.005	g $N.m^{-3}$
$K_{PO4,BIO,AS}$	Half-saturation of PO_4 as nutrient for biomasses (AS)	0.002	g $P.m^{-3}$
$K_{CO2,BIO,AS}$	Half-saturation of CO_2 for biomasses (except NITOs)	1.2	g $TIC.m^{-3}$
$K_{CAT,AS}$	Half-saturation of strong cations (as Na+)	0.1	g $Na.m^{-3}$
$K_{AN,AS}$	Half-saturation of strong anions (as Cl-)	0.1	g $Cl.m^{-3}$
$K_{Mg,BIO,AS}$	Half-saturation of Mg for biomasses (AS)	0.0001	g $Mg.m^{-3}$
$K_{Ca,BIO,AS}$	Half-saturation of Ca for biomasses (AS)	0.0001	g $Ca.m^{-3}$

$\eta_{b,anox}$	Reduction factor for anoxic decay	0.50	unitless
$\eta_{b,ana}$	Reduction factor for anaerobic decay	0.25	unitless
$m_{tox,anox}$	Toxicity factor of anaerobes under anoxic conditions	5.00	unitless
$m_{tox,aer}$	Toxicity factor of anaerobes under aerobic conditions	10.00	unitless
$m_{tox,ana,max}$	Toxicity factor of aerobes under anaerobic conditions (maximum)	10.00	unitless
pH_{low}	pH inhibition low value	3	pHunit
pH_{high}	pH inhibition high value	11	pHunit

	Conversion kinetics	Type(Kinetic)	
Symbol	**Name**	**Default**	**Unit**
q_{HYD}	Rate of hydrolysis	2.0	d^{-1}
$\eta_{HYD,anox}$	Reduction factor for anoxic hydrolysis	0.5	unitless
$\eta_{HYD,ana}$	Reduction factor for anaerobic hydrolysis	0.5000	unitless
q_{FLOC}	Rate of flocculation	50.0	d^{-1}
$K_{FLOC,AS}$	Half-saturation of colloids in flocculation (AS)	0.0010	g COD.g COD^{-1}
$K_{HYD,AS}$	Half-saturation of particulates in hydrolysis (AS)	0.05	g COD.g COD^{-1}
q_{AMMON}	Rate of ammonification	0.05	d^{-1}
q_{SPB}	Rate of soluble biodegradable organic P conversion	0.50	d^{-1}
q_{XE}	Rate of endogenous decay products conversion	0.007	d^{-1}
q_{ASSIM}	Rate of assimilative nutrient production	1.0	d^{-1}
$Ki_{NHx,ASSIM,AS}$	Half-inhibition of NH_x in NO_x assimilative reduction	0.0005	g $N.m^{-3}$
$K_{NO2,ASSIM,AS}$	Half-saturation of NO_2 in NO_2 assimilative reduction (AS)	0.001	g $N.m^{-3}$
$K_{NO3,ASSIM,AS}$	Half-saturation of NO_3 in NO_3 assimilative reduction (AS)	0.001	g $N.m^{-3}$

	Parameters for half saturation coefficients in biofilms	Type(Kinetic)	
Symbol	**Name**	**Default**	**Unit**
$f_{KS,biofilm}$	Diffusion factor for half-saturation coefficients	0.1	unitless

	Temperature dependency	Type(Kinetic)	
Symbol	**Name**	**Default**	**Unit**
$\theta_{\mu,OHO}$	Arrhenius coefficient for OHO growth	1.040	unitless
$\theta_{FERM,OHO}$	Arrhenius coefficient for fermentation (OHO)	1.040	unitless
$\theta_{b,OHO}$	Arrhenius coefficient for OHO decay	1.030	unitless
$\theta_{\mu,MEOLO}$	Arrhenius coefficient for MEOLO growth	1.060	unitless
$\theta_{b,MEOLO}$	Arrhenius coefficient for MEOLO decay	1.030	unitless
$\theta_{\mu,PAO}$	Arrhenius coefficient for PAO growth	1.040	unitless
$\theta_{\mu,PAO,lim}$	Arrhenius coefficient for PAO growth (P limited)	1.040	unitless
$\theta_{FERM,PAO}$	Arrhenius coefficient for fermentation (PAO)	1.040	unitless
$\theta_{q,PAO,PHA}$	Arrhenius coefficient for PHA storage	1.040	unitless
$\theta_{b,PAO}$	Arrhenius coefficient for PAO decay	1.030	unitless
$\theta_{b,PHA}$	Arrhenius coefficient for PHA storage use for maintenance	1.064	unitless
$\theta_{b,PP,ana}$	Arrhenius coefficient for anaerobic PP storage	1.030	unitless
$\theta_{\mu,GAO}$	Arrhenius coefficient for GAO growth	1.072	unitless
$\theta_{q,GAO,GLY}$	Arrhenius coefficient for GLY storage	1.040	unitless
$\theta_{b,GAO}$	Arrhenius coefficient for GAO decay	1.030	unitless
$\theta_{b,GLY}$	Arrhenius coefficient for GLY storage use for maintenance	1.054	unitless
$\theta_{\mu,AOB}$	Arrhenius coefficient for AOB growth	1.072	unitless
$\theta_{b,AOB}$	Arrhenius coefficient for AOB decay	1.030	unitless
$\theta_{\mu,NOB}$	Arrhenius coefficient for NOB growth	1.060	unitless
$\theta_{b,NOB}$	Arrhenius coefficient for NOB decay	1.030	unitless
$\theta_{\mu,AMX}$	Arrhenius coefficient for anammox growth	1.010	unitless
$\theta_{b,AMX}$	Arrhenius coefficient for anammox decay	1.030	unitless
$\theta_{\mu,AMETO}$	Arrhenius coefficient for AMETO growth	1.030	unitless
$\theta_{b,AMETO}$	Arrhenius coefficient for AMETO decay	1.030	unitless

$\theta_{\mu,HMETO}$	Arrhenius coefficient for HMETO growth	1.030	unitless
$\theta_{b,HMETO}$	Arrhenius coefficient for HMETO decay	1.030	unitless
$\theta_{q,FLOC}$	Arrhenius coefficient for flocculation	1.030	unitless
$\theta_{q,HYD}$	Arrhenius coefficient for hydrolysis	1.030	unitless
$\theta_{q,AMMON}$	Arrhenius coefficient for ammonification	1.030	unitless
$\theta_{q,SPB}$	Arrhenius coefficient for PO4 conversion	1.030	unitless
$\theta_{q,XE}$	Arrhenius coefficient endogenous residual conversion	1.030	unitless
$\theta_{q,ASSIM}$	Arrhenius coefficient assimilative kinetics	1.030	unitless
$\theta_{q,Fe2,OX}$	Arrhenius coefficient for ferrous iron oxidation kinetics	1.040	unitless
$\theta_{q,HFO,RED}$	Arrhenius coefficient for ferric iron reduction kinetics	1.040	unitless
T_{base}	Arrhenius base temperature	20.0	C^o

	Stoichiometric yields	Type(Stoichiometric)	
Symbol	**Name**	**Default**	**Unit**
$Y_{OHO,VFA,ox}$	Yield of OHOs on VFA under aerobic conditions	0.60	g X_{OHO}.g S_{VFA}^{-1}
$Y_{OHO,VFA,anox}$	Yield of OHOs on VFA under anoxic conditions	0.45	g X_{OHO}.g S_{VFA}^{-1}
$Y_{OHO,SB,ox}$	Yield of OHOs on readily biodegradable substrate under aerobic conditions	0.67	g X_{OHO}.g S_B^{-1}
$Y_{OHO,SB,anox}$	Yield of OHOs on readily biodegradable substrate under anoxic conditions	0.54	g X_{OHO}.g S_B^{-1}
$Y_{OHO,SB,ana}$	Yield of OHOs on readily biodegradable substrate under anaerobic conditions	0.10	g X_{OHO}.g S_B^{-1}
$Y_{OHO,H2,ana,high}$	Yield of H2 production in fermentation with high VFA concentration (OHO)	0.35	g S_{H2}.g S_B^{-1}
$Y_{OHO,H2,ana,low}$	Yield of H2 production in fermentation with low VFA concentration (OHO)	0.1	g S_{H2}.g S_B^{-1}
$Y_{OHO,SMEOL,ox}$	Yield of OHOs on methanol under aerobic conditions	0.40	g X_{OHO}.g S_{MEOL}^{-1}
Y_{MEOLO}	Yield of MEOLOs on methanol	0.40	g X_{MEOLO}.g S_{MEOL}^{-1}
$Y_{PAO,PHA,ox}$	Yield of PAOs on PHA under aerobic conditions	0.639	g X_{PAO}.g X_{PHA}^{-1}
$Y_{PAO,PHA,anox}$	Yield of PAOs on PHA under anoxic conditions	0.52	g X_{PAO}.g X_{PHA}^{-1}
$Y_{PAO,SB,ana}$	Yield of PAOs on readily biodegradable substrate under anaerobic conditions	0.10	g X_{PAO}.g S_B^{-1}

$Y_{PAO,H2,ana,high}$	Yield of H2 production in fermentation with high VFA concentration (PAO)	0.35	g S_{H2}.g S_B^{-1}
$Y_{PAO,H2,ana,low}$	Yield of H2 production in fermentation with low VFA concentration (PAO)	0.1	g S_{H2}.g S_B^{-1}
$f_{PP,PHA,ox}$	Ratio of PP stored per PHA consumed under aerobic conditions	0.92	g X_{PP}.g X_{PHA}^{-1}
$f_{PP,PHA,anox}$	Ratio of PP stored per PHA consumed under anoxic conditions	0.55	g X_{PP}.g X_{PHA}^{-1}
$f_{P,VFA}$	Ratio of P released per VFA stored	0.65	g X_{PP}.g S_{VFA}^{-1}
$i_{TSS,PP}$	TSS content of PP	3.5	g X_{TSS}.g X_{PP}^{-1}
$Y_{GAO,GLY,ox}$	Yield of GAOs on glycogen under aerobic conditions	0.6	g X_{GAO}.g X_{GLY}^{-1}
$Y_{GAO,GLY,anox}$	Yield of GAOs on glycogen under anoxic conditions	0.5	g X_{GAO}.g X_{GLY}^{-1}
Y_{AOB}	Yield of AOBs on NH_x	0.15	g X_{AOB}.g S_{NHx}^{-1}
Y_{NOB}	Yield of NOBs on NO_2	0.09	g X_{NOB}.g S_{NO2}^{-1}
$Y_{AMX,NO2}$	Yield of AMX on NO_2	1.32	unitless
$Y_{AMX,NO3}$	Yield of AMX on NO_3	0.26	unitless
Y_{AMETO}	Yield of AMETOs on VFA	0.10	g X_{AMETO}.g S_{VFA}^{-1}
Y_{HMETO}	Yield of HMETOs on H_2	0.10	g X_{HMETO}.g S_{H2}^{-1}